

EUROPEAN LUNAR SYMPOSIUM

2016
18-19 MAY



VRIJE
UNIVERSITEIT
AMSTERDAM



els2016.arc.nasa.gov

AMSTERDAM THE NETHERLANDS

SCIENCE ORGANIZING COMMITTEE

Wim van Westrenen, VU University, Amsterdam, NL (Chair)

Mahesh Anand, Open University, UK (Co-Chair)

Jessica Barnes, Open University, UK

James Carpenter, ESA

Doris Daou, NASA, USA

Simone Dell'Agnello, INFN, Italy

Ralf Jaumann, DLR, Germany

Maxim Litvak, RAS, Russia

Patrick Pinet, IRAP, France

Katie Robinson, Open University, UK

Greg Schmidt, SSERVI, USA



**Program for ELS 2016,
the Fourth European Lunar Symposium**

<http://els2016.arc.nasa.gov/>

Venue

**Royal Netherlands Academy of Arts and Sciences (KNAW)
The Trippenhuis
Kloveniersburgwal 29
1011 JV Amsterdam, the Netherlands**

Science Organizing Committee

- Wim van Westrenen - VU Univ. Amsterdam, NL (Chair)
 - Mahesh Anand - Open University, UK (Co-Chair)
 - Jessica Barnes - Open University, UK
 - James Carpenter - ESA
 - Doris Daou - NASA, PSD
 - Simone Dell'Agnello - INFN, Italy
 - Ralf Jaumann - DLR, Germany
 - Maxim Litvak - Space Research Institute, RAS, Moscow
 - Patrick Pinet - IRAP, France
 - Katharine Robinson - Open University, UK
 - Greg Schmidt - SSERVI, USA

Tuesday 17th May 2016	
ELS 2016 Onsite Registration	
18:00 - 19:00	Registration (Tea/Coffee/refreshments)
19:00 - 20:00	Inaugural lecture (Prof. Harry Hiesinger , University of Muenster and Prof. Mark Robinson , University of Arizona) – Seven Years Exploring the Moon: Highlights from Lunar Reconnaissance Orbiter (LRO) Mission; Chair – Prof. Ralf Jaumann
20:00 - 21:00	Welcome Reception with drinks and snacks

Note: Names in bold are invited speakers.

Wednesday 18th May 2016				
08:15	Registration (Tea/Coffee/Refreshments)			
08:45	Welcome/Housekeeping			
All talks: 10 mins (10 minutes for Q&A at the end of each session for all speakers in that session)				
Session 1: Exploration and Future Missions 1 Chair: Wim van Westrenen				
SN	Time	Abstract #	Author	Title
1	09:00	017	Messina, P.	Moon Village
2	09:10	076	Bussey, D.B.J.	The ISECG Science White Paper – A Scientific Perspective on the Global Exploration Roadmap
3	09:20	051	Carpenter, J. (Houdou, B.)	Building ESA's Lunar Exploration Mission Capabilities
4	09:30	050	Wong, N.P.	Status of the Google Lunar XPRIZE
5	09:40	040	Zou, Y.L.	An Introduction: Scientific Objectives and its Possible Instruments of CE-4 Mission
	09:50 – 10:05	Q&As		
6	10:05	066	Savoia, M.	Prospect: Key Aspects of Drilling and Collecting Samples at Moon South Pole for Luna Resurs Mission
7	10:15	047	Barber, S.J.	ProSPA: the Chemical Laboratory for In-Situ Assessment of Lunar Volatile Resources within ESA's Prospect Package
8	10:25	060	Reiss, P.	In-Situ thermal Extraction and Analysis of Lunar Volatiles with the Lunar Volatiles Scouting Instrument
9	10:35	033	Lavagna, M.	Drill-Terrain Energy Exchange Model to Assess Moon Subsurface Icy Samples Specimen thermo-Physical Properties Preservation During the Acquisition Phases
	10:45 – 10:55	Q&As		
Tea/coffee break (11:00-11:15)				
Session 2: Exploration and Future Missions 2; Chair: Jessica Barnes				
10	11:20	080	Ferri, A.	Lunar Polar Sample Return Mission
11	11:30	079	Biggio, A.	Lunar Volatile Prospector Mission
12	11:40	031	Diedrich, T.	Prospecting and Returning Lunar Surface Samples with Volatiles.
13	11:50	048	Allouis, E.	Lunar Volatile Prospector Rover – Exploring the Lunar South Pole and the Permanently Shaded Regions
14	12:00	012	Zeigler, R. A.	MOONRISE: Sampling the South Pole-Aitken Basin to Address Problems of Solar System Significance
	12:10 – 12:25	Q&As		
Lunch (12:30-13:40)				
Session 3: Mapping and Landing Sites; Chair: Greg Schmidt				
15	13:45	003	Mitrofanov, I. G.	Landing Sites Selection for the Russian Polar Lander Luna-25
16	13:55	004	Flahaut, J.	Candidate Landing Sites Near the Lunar Poles: A European Perspective
17	14:05	009	Rommel, D.	Petrological Map of the South Pole-Aitken Basin
18	14:15	041	Day, B.H.	Extending NASA's Lunar Mapping and Modelling Portal: Enhancements for a New Era of Lunar Exploration

Note: Names in bold are invited speakers.

	14:25 – 14:35	Q&As		
Session 4: Small Missions, Instruments and Simulants; Chair: Simone Dell'Agnello				
19	14:35	081	Saunders, C.	Solving Communications and Navigation Requirements for Small Lunar Missions
20	14:45	044	Ghafoor, N.	Small Mission Challenges and Developments in Advance of a Lunar Village
21	14:55	006	Pike, W.T.	A Silicon Seismic Package (SSP) for Lunar Seismology
22	15:05	039	Czelusckke, A.	Re-examination of Apollo 17 Lunar Seismic Profiling Experiment Data.
	15:15 – 15:25	Q&As		
Tea/coffee break (15:30 – 15:45)				
23	15:50	045	Currie, D.G.	Science, Design and Flight Status of the Next Generation Retroreflector for Lunar Laser Ranging
24	16:00	077	Taylor, L.A.	Complexities of Lunar Soil: Need for Proper Simulants
25	16:10	023	Meurisse, A.	Solar 3D Printing of Lunar Regolith
26	16:20	026	Schlacht, I.L.	Walking on the Moon
	16:30 – 16:40	Q&As		
Session 5: Remote sensing and Geological Implications; Chair: Katharine Robinson				
27	16:40	015	Klima, R.L.	Integrating Remote Sensing Observations to Assess the Diversity of Intrusive Magmatism on the Moon
28	16:50	065	Martinot, M.	Characterizing the Lunar Crust-Mantle Transition with the Moon Mineralogy Mapper (M ³)
29	17:00	068	Nahm, A.L.	Relative Ages of Graben and Wrinkle Ridges on the Nearside of the Moon Reveal Contradictory Relationships
30	17:10	053	Donaldson-Hanna, K.	Investigation of Young (<100 Million Years) Lunar Surface Features: Evidence for Outgassing or Basaltic Volcanism?
	17:20 – 17:30	Q&As		
Session 6: Posters; Chair: Greg Schmidt				
	17:30	Poster intros		1 minute each presenter
<i>Poster session from ~17:45 to 20:30 with drinks and finger food.</i>				

Note: Names in bold are invited speakers.

Thursday 19th May 2016				
	08:45	Registration (Tea/Coffee/Refreshments)		
All talks: 10 mins (10 minutes for Q&A at the end of each session for all speakers in that session)				
Session 7: Remote sensing and Physical Implications; Chair: Patrick Pinet				
31	09:10	057	Robinson, M.S.	Lunar Reconnaissance Orbiter Camera: Exploring the Moon.
32	09:20	059	Greenhagen B.T.	The Diviner Lunar Radiometer: Cornerstone to thermal Infrared Studies of Airless Bodies.
33	09:30	073	Denevi, B.W.	Exploring the Effects of Space Weathering at Ultraviolet Wavelengths with the LROC Wide Angle Camera
34	09:40	067	Meyer, H.M.	The Origins of Lunar Light Plains: Implications for Exploration
	09:50 – 10:00	Q&As		
35	10:00	028	Arnold, J.A.	Modelling Thermal Infrared Spectra in a Lunar-Like Environment
36	10:10	064	Litvak, M.L.	Search for Lunar Water: From Current Lunar Reconnaissance Orbiter Global Mapping to the Sample Analysis at Surface onboard future Russian Lunar Landers
37	10:20	069	Patterson, G.W.	Mini-RF On LRO and Arecibo Observatory Bistatic Radar Observations of the Moon
38	10:30	071	Povilaitis, R.Z.	Global Crater Density: Equilibrium in the Lunar Highlands
	10:40 – 10:50	Q&As		
Tea/coffee break (10:55-11:10)				
Session 8: Lunar Volatiles and Laboratory Experiments; Chair: Mahesh Anand				
39	11:15	018	Visscher, C. (Canup, R.M.)	Incomplete Lunar Accretion and the Depletion of Volatile Elements in the Moon
40	11:25	075	Steenstra, E.S.	Metal-Silicate Partitioning of Volatile Siderophile Elements suggests Volatiles were not lost during Lunar Formation
41	11:35	034	Barnes, J.J.	Determining the Source(S) of H ₂ O in the Lunar Interior
42	11:45	035	Lin, Y.H.	Hydrous Early Moon? Constraints from Hydrous Lunar Magma Ocean Solidification Experiments
	11.55 – 12:05	Q&As		
43	12:05	054	Robinson, K.L.	Connecting Hydrogen and Chlorine Isotopes in Evolved Lunar Rocks
44	12:15	030	Greenwood, J.P.	Water and Volatiles in Apollo Rocks: New Results from Sapporo and Connecticut
45	12:25	070	Potts, N.J.	Experimental Constraints on Volatile Partitioning Between Apatite and Silicate Melt under Lunar Conditions
46	12:35	052	Kelderman, E.	Compressibility and Density of Hydrous High-Ti Lunar Red and Black Glass
	12:45 – 12:55	Q&As		
Lunch (13:00-14:10)				
Session 9 starts at 14:15 (see next page)				

Note: Names in bold are invited speakers.

Session 9: Differentiation and Evolution of the Moon. Chair: Maxim Litvak				
47	14:15	016	Kruijer, T.S.	Constraining the Origin and Differentiation of the Moon Using Tungsten Isotopes
48	14:25	072	Snape, J.F.	Pb Isotope Analyses of Lunar Samples: Implications for the Evolution of Major Lunar Silicate Reservoirs
49	14:35	061	Zhao, Y.	Influence of Variable thermal Conductivity On the thermal Evolution of the Moon.
50	14:45	022	Alexander, L.	Examining the History of the Solar System and the Galaxy through Cosmogenic Isotopes in Lunar Samples
	14:55 – 15:05	Q&As		
Tea/coffee break (15:10-15:25)				
Session 10: Impacts and Cratering on the Moon. Chair: James Carpenter				
51	15:30	020	Oberst, J.	Lunar Geodesy, Cartography, and Current Coordinate Knowledge
52	15:40	002	Hiesinger, H.	Recent Advancements in Lunar Impact Cratering
53	15:50	056	Kring, D	An Impact-Generated Lunar Magmatism Hypothesis
54	16:00	005	Morbidelli, A.	The Timeline of the Lunar Bombardment
	16:10 – 16:20	Q&As		
Closing remarks (16:20 – 16.30) Announcement of awards and 2017 ELS Finish				

Note: Names in bold are invited speakers.

Posters: ~17:45 – 20:30 Wednesday 18th May.				
<i>Presenters note that posters can be pinned up from pre-registration on Tuesday, 17th May; posters should be up to A0 in size (poster boards are 120 x 120 cm; pins/velcro/scotch tape will be provided).</i>				
S. No.	Poster No.	Abs#	Presenter	Title
55	1	042	Carpenter, J.	Challenges and Opportunities of Lunar Resource Prospecting
56	2	038	Chevrel, S.D.	Challenges in Robotic and Human Geological Field Work in Lunar Craters
57	3	013	Cowley, A.	Spaceship EAC – Enabling Activities Relevant to Lunar Exploration and 3D Printing ISRU
58	4	043	Crockett, M.	Metal-Silicate Partitioning of Siderophile Elements in the Moon: the effects of Oxygen Fugacity and Carbon.
59	5	062	de Vera J.-P.	Astrobiology and Life Sciences on the Moon
60	6	010	Durst, S.M.	International Lunar Observatory Association: 21st Century Education, Exploration and Enterprise
61	7	046	Foing, B.	Highlights From Moon Village Workshops and Studies
62	8	032	Glaser, P.	Lunar Polar Illumination and Implications for Future Landing Sites
63	9	001	Guinet, V.	Preparation of Human-Telerobotics Operations Using EAC & ESTEC Facilities
64	10	024	Hausmann, G.	Moon-Based Plasma, Dust and Radio Science: Essentials for Preparation of Future Exploration and Scientific Breakthroughs
65	11	037	Jonglez, C.	Mineral Spectrometry & Remote Control of Exogeolab Lander Instruments
66	12	014	Kamps, O.M.	Exogeolab Moon Analogue Field Activities In Eifel, Germany
67	13	019	Maccone, C.	Protected Antipode Circle (PAC) with a “Moon Village” to its South
68	14	029	Makaya, A.	3D Printing Technologies for Enabling Human Exploration and Human Settlement on the Moon: The Viewpoint of ESA Materials Scientists
69	15	025	Marco Figuera, R.	Water Ice Characterization near Candidate Landing Sites at the Lunar South Pole.
70	16	083	Offringa, M.S.	UV-VIS, NIR and FTIR Spectroscopy of Moon Analogues
71	17	074	Pendleton, Y.J.	NASA’s Solar System Exploration Research Virtual Institute: Merging Science and Exploration
72	18	036	Pinet, P.C.	MGM Deconvolution of Rock Slab Spectra with Plagioclase/Olivine Mineral Assemblages
73	19	007	Ping, J. S.	Promoting a Low Frequency Radio Observatory on the Farside of the Moon
74	20	008	Richter, Lutz	Development of Sample Handling Systems at OHB Munich
75	21	055	Robinson, K.L.	The Lynch 002 Lunar Meteorite Revisited
76	22	058	Robinson, M.S.	Flexible to Focused: the Path to Extend Human Presence Beyond Low Earth Orbit.
77	23	082	Schmidt, G.	The Desert Fireball Network
78	24	011	Wang, M.Y.	Initial Observation of the Lunar Ionosphere from Radio Occultation based on the Service Module of the Circumlunar Return and Re-entry Spacecraft
79	25	078	Wüsthoff, M.	How does Obliquity affect Diurnal Tidal Stresses on the Moon?

Note: Names in bold are invited speakers.

MOON VILLAGE. P. Messina, European Space Agency (ESA Headquarters, Paris, France, pie-ro.mesina@esa.int).

Space exploration is anchored in the International Space Station and in the current and future automatic and planetary automatic and robotic missions that pave the way for future long-term exploration objectives. The Moon represents a prime choice for scientific, operational and programmatic reasons and could be the enterprise that federates virtually all interested Nations.

On these considerations ESA is currently elaborating the concept of a Moon Village as an ensemble where multiple users can carry out multiple activities.

The Moon Village has the ambition to serve a number of objectives that have proven to be of interest (including astronomy, fundamental research, resources management, moon science, etc.) to the space community and should be the catalysts of new alliances between public and private entities and with non-space industries. Additionally the Moon Village should provide a strong inspirational and education tool for the younger generations. The Moon Village will rely both on automatic, robotic and human-tended structures to achieve sustainable moon surface operations serving multiple purposes on an open-architecture basis.

This Europe-inspired initiative should rally all communities (across scientific disciplines, nations, industries) and make it to the top of the political agendas as a the scientific and technological but also political and inspiration endeavour of the XXI century.

The current reflections are of course based on the current activities and plans on board the ISS and the discussion held in international fora such as the ISECG.

The paper will present the status of these reflections, also in view of the ESA Council at Ministerial Level 2016, and will give an overview of the ongoing activities being carried out to enable the vision of a Moon Village.

THE ISECG SCIENCE WHITE PAPER – A SCIENTIFIC PERSPECTIVE ON THE GLOBAL EXPLORATION ROADMAP. D.B.J. Bussey¹, J.C. Worms², J. Schlutz³, and F. Spiero⁴. 1. NASA, Washington D.C., USA; 2. European Science Foundation, Strasbourg, France; 3. DLR, Bonn, Germany; 4. CNES, Paris, France.

Future space exploration goals call for sending humans and robots beyond low Earth orbit and establishing sustained access to destinations such as the Moon, asteroids and Mars. Space agencies participating in the International Space Exploration Coordination Group (ISECG) are discussing an international approach for achieving these goals, documented in ISECG's Global Exploration Roadmap (GER). The GER reference scenario reflects a step-wise evolution of critical capabilities from ISS to missions on and around the Moon in preparation for the journey of humans to Mars.

As an element of this road mapping effort, the ISECG agencies are soliciting input and coordinated discussion with the scientific community to better articulate and promote the scientific opportunities of the proposed mission themes. An improved understanding of the scientific drivers and the requirements to address priority science questions that can be addressed by near-term human exploration in to the solar system (i.e. lunar surface, a deep space habitat in the lunar vicinity, or an asteroid). The output of this interaction is the development of a Science White Paper to

- Identify and highlight the scientific opportunities in early exploration missions as the GER reference architecture matures,
- Communicate overarching science themes and their relevance in the GER destinations,
- Ensure international science communities' perspectives inform the future evolution of mission concepts considered in the GER

The paper aims to capture the opportunities offered by the missions in the GER for a broad range of scientific disciplines. These include planetary and space sciences, astrobiology, life sciences, physical sciences, astronomy and Earth science. The paper is structured around grand science themes that draw together and connect research in the various disciplines, and it will focus on opportunities created by the near-term mission themes in the GER centered around 1) extended duration crew missions to an exploration habitat in cislunar space, 2) crew mission(s) to an asteroid, and 3) crew missions to the lunar surface.

The preparation of that Science White Paper has been coordinated and led by an external Science Advisory Group composed of scientists from a variety of nations. A dedicated working meeting was held in May 2015 at the European Lunar Symposium in Frascati to incorporate inputs and recommendations from international scientists. The

first draft of this White Paper was then discussed at a COSPAR-ISECG-ESF workshop in Paris on 10-11 February 2016. The recommendations developed at the workshop provide further input that is being incorporated in to the final version of the ISECG Science White Paper, expected to be published in the autumn of 2016. The authors aim to present the rationale, contents and progress of this White Paper at ELS.

BUILDING ESA'S LUNAR EXPLORATION MISSION CAPABILITIES. B. Houdou, J. Carpenter, D. De Rosa, R. Fisackerly, D. Guyomard, B. Hufenbach, B. Patti, J. Schiemann, Directorate of Human Spaceflight and Robotic Exploration, ESA ESTEC, Noordwijk, The Netherlands (berengere.houdou@esa.int).

Exploration of the Moon is the next step for human spaceflight, building on the experience of the International Space Station, which has seen human spaceflight restricted to Low Earth Orbit (LEO). This transition from LEO to Moon requires the development of new technologies, new capabilities and new knowledge across multiple domains and the progression of international partnerships exemplified through the ISS. The progression to lunar surface will be achieved through a combination of developments in robotic and human spaceflight systems and missions.

Human spaceflight capabilities: In the area of human spaceflight capabilities ESA is continuing the development of the Service Module of NASA's Multi-Purpose Crew Vehicle. This will be the vehicle that brings humans beyond LEO in the years to come. In parallel consensus is emerging around the development of an infrastructure for extended human missions in space around the Moon. This element can be an important increment towards an infrastructure enabling sustainable human lunar exploration, and a key part of future surface mission architectures.

Robotic precursor missions: In advance of human surface missions robotic missions to the surface provide an opportunity to drive up the technology and system maturities of key elements for the future, to generate relevant operational experience, to build partnerships and to generate knowledge.

To this end ESA is investing in robotic precursor missions. The first mission in this campaign is the Russian Luna-25 lander mission in 2018. ESA will provide an imaging system for this mission as a precursor to a complete precision landing and hazard avoidance system, PILOT, which will be deployed on the Luna-27 lander mission in 2021. The Precise Intelligent Landing using On-board Technology system, PILOT, is a generic exploration product, which will be available as a European contribution to future missions to enable pin-point landing.

The Russian Luna-27 mission also includes the Package for Resource Observation and in-Situ Prospecting for Exploration Commercial exploitation and Transportation, PROSPECT. This system will be used to investigate the presence, provenance and viability of lunar resources at the Luna-27 landing site. This mission also provides the basis for future deployments of PROSPECT as a system for comprehensive resource evaluation across the lunar surface. PROSPECT emphasises cold trapped polar volatiles but is intended to provide a broader investigatory capability, which could be deployed more broadly across the lunar surface.

Following these flights ESA is looking to build on the demonstrated capabilities and further support the definition of Europe's path to the lunar surface. To this end a number of mission studies are on-going including sample return and mobile surface exploration. It is important that these next steps address key knowledge and capability gaps for human exploration, build strong partnerships and build the user base for the exploration missions that will follow.

Partnerships: International partnerships have been and continue to be an essential element in ESA's approach to exploration. This is enabling for missions as it allows the pooling of resources and capabilities. The ability to work and operate together in space also represents one of the key benefits delivered by exploration; as we consistently demonstrate that diverse countries and cultures can work together to achieve the extraordinary.

A new partnership model with the private sector is also being explored. In this case ESA is investigating how it can support private sector driven exploration initiatives in such a way that the initiatives are enabled and ESA generates benefits for its stakeholders and advances its own exploration ambitions.

Conclusions: We will present the current activities in ESA to prepare for future human exploration to the surface. Emphasis will be placed on the development activities for PILOT and PROSPECT, mission studies which are on-going with European industry and on the development of partnerships.

STATUS OF THE GOOGLE LUNAR XPRIZE. N. P. Wong¹ and A. C. Barton¹, ¹XPRIZE Foundation (800 Corporate Pointe, Suite 350 Culver City, CA 90230, Nathan.Wong@xprize.org), ²XPRIZE Foundation (800 Corporate Pointe, Suite 350 Culver City, CA 90230, Andrew.Barton@xprize.org).

Launched in September 2007, the Google Lunar XPRIZE offers a total purse of US\$30 Million as an incentive based prize for international teams to create a new era of affordable access to the Moon and beyond. The US\$20 Million Grand Prize will be awarded to the first privately funded team to land on the Moon, move 500 meters and broadcast back high definition video, referred to as Mooncast. In addition to the Grand Prize, there is also second place prize money and money available for completing scientific and technical objectives on the lunar surface after completing the Grand or Second Place Prize requirements as Bonus Prizes, such as finding evidence of water or moving five kilometers across the lunar surface. All this must be complete before the competition deadline of December 31, 2017.

Teams are continueing to make both financial and technical progress as was seen in the Terrestrial Milestone Prizes, where in January 2015 \$US 6.25 Million was awarded across five teams (Astrobotic (US), Moon Express (US), Part-Time Scientists (DE), Indus (IN), and Hakuto (JP)) for significant technical progress achieved on Earth in Landing, Mobility, and Imaging Subsystems. The technical validation by the Google Lunar XPRIZE Judging Panel helped teams secure more funding and sponsorships commitments such as the Part-Time Scientists partnership with Audi, Astrobotic continuing to sign on new payloads to their mission.

To date two teams have provided verified launch contracts to XPRIZE, SpaceIL from Israel has a verified launch contract with Spaceflight Inc. on a Falcon 9 and Moon Express from the United States has a verified launch contract with Rocket Labs on an Electron rocket. Both of these missions are scheduled for sometime in 2017. All other teams must provide verified launch contract by December 31, 2016 to remain in the competition.

AN INTRODUCTION: SCIENTIFIC OBJECTIVES AND ITS POSSIBLE INSTRUMENTS OF CE-4 MISSION. Y. L. Zou¹, C. L. Li¹, H. B. Zhang¹, J. J. Liu¹ and Y. Su¹, ¹ Key Laboratory of Lunar and Deep Space Exploration, National Astronomical Observatories, Chinese Academy of Sciences, Beijing, China, 100012, ylzou@nao.cas.cn, licl@nao.cas.cn, zhanghb@nao.cas.cn, liujj@nao.cas.cn, suyan@nao.cas.cn.

Introduction: Since Chang'e-3(CE-3) lander and rover successfully landed on the moon in 2013, Chang'e-4(CE-4) has been given a new mission. The Chinese Lunar Exploration Program (CLEP) has finally confirmed the plan of sending CE-4 to the far side of the moon by 2020. The CE-4 scientific objectives are based on the following main background or constrains.

- “A Lander + a Rover + a Telecommunication Relay” in which the Lander and the Rover is the backup of the CE-3 probe meaning its overall structure and main technology design will not be changed greatly, and the Telecommunication Relay will be sent to the Earth–Moon L2 Lagrange point.
- Landing site: far side of lunar surface.
- Launching Time: about 2018 (consider the lifetime of some products of CE-3 probe, and so on).
- The weight of payloads: about 35 kg onboard the Lander and 17 kg onboard the Rover.

CE-4 Mission Scientific Objectives: The scientific objectives of CE-3 include lunar surface topography and geology survey, lunar surface material composition and resource survey, Sun-Earth-Moon space environment detection, and lunar-based astronomical observation. Based on CE-3 mission, CE-4 mission will utilize the specific local environment of lunar far side to carry out the following scientific exploration:

(1) To study the characteristics and its formation mechanism of lunar surface floating dust

- To measure the flux, charge, quality, velocity and its orientation of dust particles
- To analyze the distribution of lunar surface floating dust with different time, height, the geographic location
- To measure and study the physical properties and movement state of lunar surface floating dust

(2) To detect lunar surface temperature and radiation environment and study their characteristics, distribution and change

- To measure lunar surface temperature, analyze its change with time and different light condition
- To monitor the LET of cosmic ray and study its change with time

(3) To detect and study the lunar regional geological characteristics

- To obtain three-dimensional imaging with high resolution and study its geological structure and impact crater

- To measure chemical compositions of rocks and soils and study its distribution
- To detect and study the thickness of regolith and its structure of super layer of lunar crust

(4) Lunar surface low-frequency radio astronomical observation and research

- To identify the “knee” structure of cosmic rays, and to find the possible original position for these cosmic rays by using interfering method of two observation units working at HF frequency.
- To observe the independent kilometer wave burst event from the high layer of the solar corona, investigate its radiation characteristics and mechanism, and to explore CME and CME transporting, accelerating and evolving between SUN-Earth space.

CE-4 Mission Propositional Payloads: There are 6 propositional payloads on Lander, 5 payloads on Rover, and 1 payload on the Telecommunication Relay Orbiter.

Lander	Rover	Orbiter
1 Cameras		
2 Dust-analyzer		
3 Particle radiation detector	1 Cameras	
4 LET-detector	2 Temperature-instrument	
5 Temperature-instrument	3 Electric field analyzer	Cameras
6 Wide Band Low Frequency Digital Radio Astronomical Station for Lunar Farside Surface LF-MF-HF Astronomy	4 Infrared imaging spectrometer	
	5 Penetrating Radar	

References:

- [1] Li C. L. et al.(2015)Space Sci. Rev.,190,85-101. [2]Zarka P. et al.(2012)Planet. Space Sci., 74, 156-166. [3] Klein-Wolt M. et al. (2012)Planet. Space Sci., 74, 167-178. [4] Mimoun D. et al.(2012) *Exp. Astron.*, **33**, 529-585.

PROSPECT: KEY ASPECTS OF DRILLING AND COLLECTING SAMPLES AT MOON SOUTH POLE FOR LUNA RESURS MISSION. M. Savoia¹, A. Rusconi¹, F. Rizzi¹, A. Fumagalli¹, S. Barber², R. Fisackerly³, J. Carpenter³, M. Lavagna⁴. ¹Finmeccanica (matteo.savoia.ext@finmeccanica.com), ²Open University, ³ESA-ESTEC, ⁴Politecnico di Milano.

Introduction: ESA is working together with ROSCOSMOS to establish a cooperative program of lunar exploration. Part of the European contribution for the Luna-27 mission, a major element of such collaboration, planned to fly in 2020, is the PROSPECT drilling and sample analysis package. PROSPECT (Package for Resource Observation, in-Situ analysis and Prospecting for Exploration Commercial exploitation and Transportation) is built upon important experience gained by European industries and institutes in particular on drilling, sample handling and sample analysis. PROSPECT is made up of two main elements: the ProSEED (PROSPECT Sample Excavation and Extraction Drill) and the ProSPA (PROSPECT Processing and Analysis) sample analysis instrument. ProSEED is the next step in Finmeccanica's development of planetary drilling and sampling robots and it is specifically designed to cope with lunar icy soil specimens. ProSEED baseline design is being developed at the time this abstract has been written. It is being defined based on experience and data collected by Finmeccanica during phase A of the Lunar Drill Development project, funded by ESA. Objectives of this phase of the project were: (1) the development of a 2m drill breadboard equipped with rotation and hammering actuator in the mandrel; (2) the development of a sampling tool mechanism compatible with the Lunar Drill Breadboard and its roto-hammering functionalities; (3) the characterization of lunar highland soil simulant (NU-LHT-2M) uniaxial compressive strength, with different amounts of water ice (up to saturation) at low temperature conditions; (4) testing of the integrated LDD breadboard on the lunar simulant conditioned at very low temperatures (up to -170°C) and ambient pressure; (5) testing and comparison of different sampling tool concepts including micro-corers and tools deriving from Finmeccanica's heritage in interplanetary drilling; (6) the development of a Thermal Exchange Model (in collaboration with Politecnico di Milano) with the aim of predicting the drilling impact on soil characteristics (temperature increase) in order to define a proper mission operation profile. The proposed paper will present and discuss some important results achieved in the above mentioned activities and how those results will support the selection and definition of the PROSPECT technical baseline.

ProSPA: THE CHEMICAL LABORATORY FOR IN-SITU ASSESSMENT OF LUNAR VOLATILE RESOURCES WITHIN ESA'S PROSPECT PACKAGE. S.J. Barber¹, J.D. Carpenter², F. Rizzi³, I.P. Wright¹, F.A.J. Abernethy¹, M.R. Leese¹, G.H. Morgan¹, A.D. Morse¹, S. Sheridan¹, A. Verchovsky¹, E.K. Gibson Jr.⁴, C. Howe⁵, P. Reiss⁶, F. Goesmann⁷, G. Bianucci⁸, S. Cleaver⁹, R. Fisackerly², B. Houdou². ¹The Open University, Milton Keynes, MK7 6AA, UK, ²ESA ESTEC, The Netherlands, ³Finmeccanica S.p.A., Italy, ⁴ARES, NASA Johnson Space Center, USA, ⁵RAL Space, UK, ⁶Technical University of Munich, Germany, ⁷Max Planck Institute for Solar System Research, Germany, ⁸Media Lario Technologies, Italy, ⁹Airbus Defence and Space Ltd., UK.
simeon.barber@open.ac.uk

Introduction: Establishing the utilisation potential of resources found in-situ on the Moon may be key to enabling future sustainable exploration. A Package for Resource Observation and in-Situ Prospecting for Exploration, Commercial exploitation and Transportation (PROSPECT) is in development by ESA for application at the lunar surface as part of international lunar exploration missions in the coming decade, including the Russian Luna-27 mission planned for ~2021.

PROSPECT will support the identification of potential resources, assess the utilisation potential of those resources at a given location and provide information to help establish the broader distribution. PROSPECT will also perform investigations into resource extraction methodologies that may be applied at larger scales in the future and provide data with important implications for fundamental scientific investigations on the Moon.

PROSPECT comprises two main elements: a drill system named ProSEED designed to access samples from depths up to 1.2 to 2 m, and ProSPA (Figure 1), a miniature chemical laboratory for the extraction and characterisation of volatiles within those samples.

Objectives: ProSPA aims to extract, identify and quantify the volatile species present within samples extracted from up to 1.2 to 2 m depth. Isotopic characterisation will be performed such that the origins, emplacement processes and evolution of volatiles on the Moon can be established. An additional objective is to demonstrate the feasibility of extractions relevant to in-situ resource utilisation (ISRU) on the lunar surface.

Operational description: The ProSEED drill will obtain and handle samples and transfer these to the ProSPA sample oven and carousel assembly (Figure 1). The samples may be at temperatures of 120 K or lower, and must be handled carefully to avoid loss of the more volatile components. The samples are then sealed in ovens, derived with heritage from those developed for Rosetta [1] and activities performed through the German LUISE [2] programme. The samples are imaged within the oven to provide geological context and estimation of sample size, thus enabling the quantities of volatiles subsequently released to be expressed in terms of volumetric concentration in the source regolith.

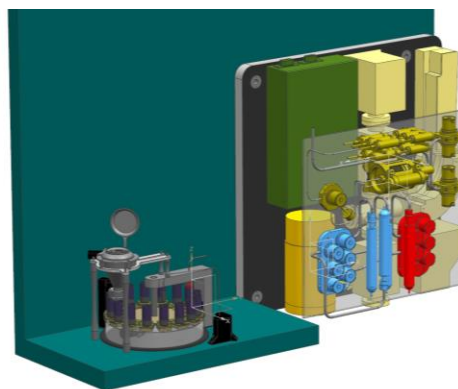


Figure 1. Conceptual representation of ProSPA. The main unit (right) containing the chemical laboratory and the electronics is housed separately from the sample ovens and carousel (left) which must be maintained cold prior to sample introduction to prevent loss of volatiles.

Samples can then be heated to temperatures as high as 1000°C or more. Heating may be performed in one of three ways (Figure 2), as described in the following.

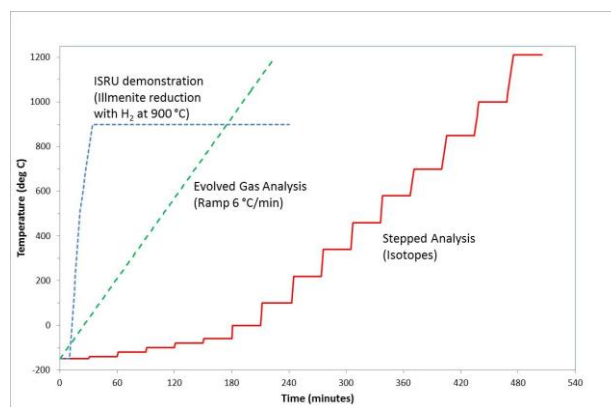


Figure 2. Indicative ProSPA sample heating profiles for extraction of volatiles. Temperature-time profiles are to be confirmed.

Evolved gas analysis ramp: By using a continuous heating ramp the evolved gases can be monitored in real time, using an ion trap mass spectrometer based upon that recently operating in the Rosetta mission [3]. This gives a qualitative measure of the composition,

and provides an indication of the overall concentrations of volatiles within the sample, allowing subsequent analysis steps to be tailored accordingly. This mode is well-established as a means of detecting a range of released volatiles and the release temperature is diagnostic of the nature of the starting material in the sample (Figure 3, left). An additional goal is to detect phase changes taking place during the heating process.

Stepped Analysis: Alternatively the heating may be undertaken in steps: in vacuum i.e. stepped pyrolysis (Figure 3, right) or in oxygen i.e. stepped combustion. The gases evolved in each step are purified or subjected to certain pre-preparations [3], before isotopic determination in a magnetic sector mass spectrometer derived from the Beagle 2 Gas Analysis Package. This utilizes on-board calibration to yield results with sufficient accuracy and precision to enable comparison with laboratory measurements on Earth of meteorites and returned samples.

ISRU Demonstrations: Reagent gases may also be introduced to the ovens to effect additional chemistry of interest, usually at a fixed reaction temperature. A number of techniques are under investigation, based on a combination of flight heritage and laboratory investigations. These include combustion with pure oxygen [4], oxidation using fluorine [5] and reduction using hydrogen and methane [6].

Challenges: The samples provided by the ProSEED drill may contain a wide range of volatiles in a variety of chemical and physical forms, and thus

ProSPA is required to have wide dynamic range to determine both trace and more abundant species. In the case of a polar mission such as Luna-27, a key target species is water which may conceivably be present in concentrations that range from ppm to percent levels. In samples at an expected temperature of 120 K, the water may be present in a variety of forms, all of which should be preserved in the sample extraction and handling chain to enable their measurement by ProSPA. This is expected to require the development of an end-to-end volatile preservation model, informed by dedicated testing on representative analogues in a representative environment.

Conclusions: PROSPECT is a package for the investigation of lunar volatiles and other potential resources with potential applications for both exploration and fundamental science. The ProSPA element builds on extensive flight heritage and capabilities developed over decades by a number of groups across Europe. PROSPECT is funded by the European Space Agency.

References: [1] Finzi et al. (2007) *Space Science Reviews* 128: 281–299 [2] Reiss P. et al. (2014) *ELS*, 65-66. [3] Wright I.P. et al., (2015), *Science*, Vol. 349, Issue 6247 [4] Wright I.P. et al. (2012) *Planetary & Space Science*, 74, 1, 254-263. [5] Sebolt W. et al, (1993) in *Resources of Near Earth Space*, University of Arizona Press, 129. [6] Schwandt et al., (2012) *Planetary & Space Science*, 74, 1, 49-56. [7] Gibson E.K., Jr. et al. (1972) *Proc. Lunar Sci. Conf.* 2029-2040.

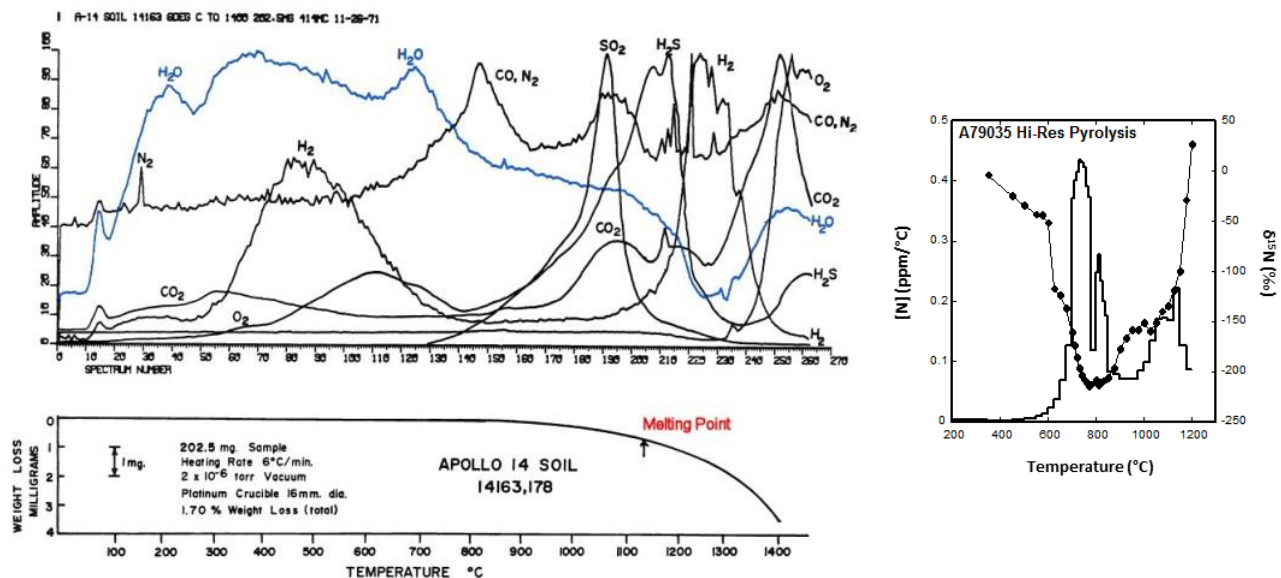


Figure 3. Left: Evolved gas release from Apollo 14 lunar soil 14163 during heating at 6°C/min from room temperature to 1400°C. [7]. Gas releases are normalized to 100% at the temperatures of greatest abundance. Right: Stepped extraction of nitrogen by pyrolysis of lunar breccia 79035. Credit: CT Pillingner

IN-SITU THERMAL EXTRACTION AND ANALYSIS OF LUNAR VOLATILES WITH THE LUNAR VOLATILES SCOUTING INSTRUMENT. P. Reiss¹, A. Hoehn¹, L. Richter², J. Biswas², O. Angerer³, N. Henn³, S. Sheridan⁴, ¹Institute of Astronautics, Technical University of Munich, Boltzmannstr. 15, 85748 Garching, Germany, (p.reiss@tum.de), ²OHB System AG, Manfred-Fuchs-Str. 1, 82234 Weßling, ³German Aerospace Center (DLR) - Space Administration, Königswinterer Str. 522-524, 53227 Bonn, Germany, ⁴The Open University, Milton Keynes, MK7 6AA, UK.

Introduction: We present the evolution of the lunar volatiles scout (LVS), a novel instrument to access and characterize lunar volatiles in-situ on a mobile platform or a lander. The instrument concept was developed through the research project LUISE (funded by the German Aerospace Center DLR), in collaboration between the Institute of Astronautics at Technical University of Munich (TUM) and the company OHB System AG, with support of the Open University.

The idea of the LVS is to enable mobile prospecting through repeated sampling of regolith and analysis for lunar volatiles to assess their variation over depth, space, and time. Operating the instrument on a mobile platform has multiple advantages over having it mounted on a static lander, as pointed out by [1]. Hence the instrument design is tailored to fit on mobile rovers, meaning that it is lightweight, compact, and simple. Different from most other sampling instruments, it eliminates the usual manipulation of the sample to reduce the risk of losing temperature-sensitive volatiles during sampling and transport.

Instrument Concept: The instrument comprises two main sections, the hollow-boring sampler and the attached volatile analyser. The hollow-boring sampler part consists of a central cylindrical heating element that is surrounded by a larger diameter auger tube. The sampler is driven into the lunar subsurface to a depth of 100-150 mm, so that a regolith sample is, more or less undisturbed, enclosed by the hollow auger. Volatiles that are bound to the regolith are released in-situ by heating the sample from the inside out. Released volatiles will then diffuse through the sample either up or downwards. Those volatiles traveling upwards to the top end of the instrument are guided through a mass spectrometer for gas analysis. The latter is the miniaturised Evolved Volatiles Ion Trap Analyzer (EVITA) provided by the Open University [2,3]. Figure 1 shows a drawing of the overall instrument design.

Two mechanisms were initially developed to drive the lower part of the instrument into the lunar subsurface. The current baseline design includes an icescrew-like mechanism, which is especially capable of penetrating icy regolith. The rotational velocity of the auger is chosen slow enough to prevent heating the sample through friction during drilling. The second considered mechanism uses a smooth sampling tube that is pushed into the subsurface with the help of vibration. However, due to recent experiments on the

insertion mechanism, the vibrating sampler was shown to be ineffective, as the vibrations did not have a favourable impact on reducing the penetration resistance.

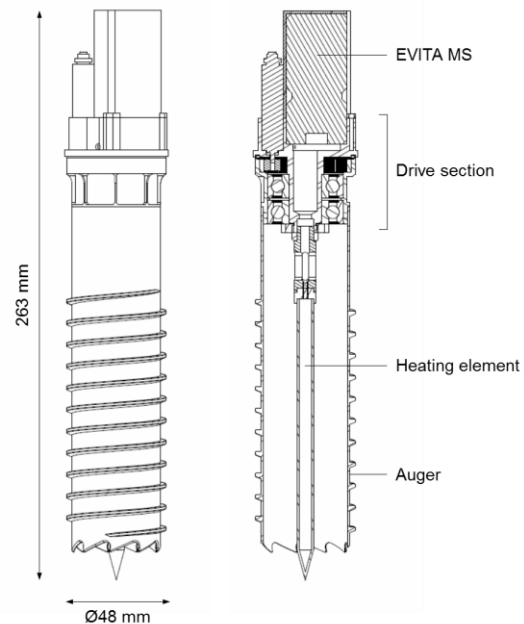


Figure 1: Dimensions and cut view of the LVS

Subsurface Insertion: A demonstrator of the insertion mechanism was established at OHB System AG to evaluate its performance with both dry and icy regolith. The test setup allows the simultaneous measurement of both penetration force and torque for the icescrew-like mechanism and penetration force, frequency and vibration amplitude of the vibrating sampler. Several drill shell geometries with varying auger sizes have been designed and 3D-printed for the icescrew-like prototypes. Penetration tests have been conducted with both samplers in regolith beds of varying density, both dry at room temperature and with 5% moisture at -35 °C (see Figure 2).

The icescrew concept was demonstrated to achieve penetration to a depth of up to 10 cm without exceeding a normal downward force of 30 N in the laboratory experiments. A simple bearing capacity model was additionally developed to predict the influence of scaling and reduced gravity on the penetration resistance. Taking into account the reduced gravity on the lunar surface, the maximum penetration force would be even lower than in the experiments on Earth.

It was also found that vibrations successfully prevent the sample from getting stuck in the drill shell. It is therefore recommended to include the capability of vibrating the icescrew-like sampler during retraction to shake off the residual sample and hence enable multiple operations with substantially reduced risk of cross contamination.



Figure 2: Sampler during subsurface insertion tests with ice-containing lunar regolith simulant JSC-1A

Thermal Extraction of Volatiles: To characterize the temperature distribution within the sample, a thermal vacuum test setup was developed at TUM. The sample was represented by the lunar mare-type regolith simulant JSC-1A.

Through the tests it was shown that with a power budget of 10 W, a minimum temperature of 400 K can be achieved across the entire sample volume. This temperature is high enough to completely release chemisorbed water in lunar cold traps, which desorb at temperatures between 180 K and ~400 K [4,5]. For physisorbed water the desorption temperatures are even lower. Heating durations for the 400 K minimum temperature however are required to be in the range of several hours to overcome the thermal inertia of the sample. Due to the extremely low thermal conductivity of lunar regolith, heat is transferred very slowly in the sample. A high power input at the heating element can lead to local temperature extremes that could either damage the heater or lead to sintering of regolith particles. Heating power and duration are hence to be traded against a sufficiently uniform temperature distribution in the sample.

A simulation model of the instrument was additionally established in the software COMSOL Multiphysics (see Figure 3). The simulation takes into account the temperature-dependent thermal conductivity and specific heat capacity of lunar regolith. The model was correlated with the thermal-vacuum test results to enable trade studies on the basis of simulations regarding the power demand and resulting temperature distribution. It was shown that by applying a constant heating power of 10 W, the 400 K threshold can be reached after about 11 hours throughout the entire sample volume. With constant 20 W, this value

is reached after 4 hours. It is recommended to dynamically adjust the power during heating so that a more uniform temperature distribution can be reached while consuming less energy in total.

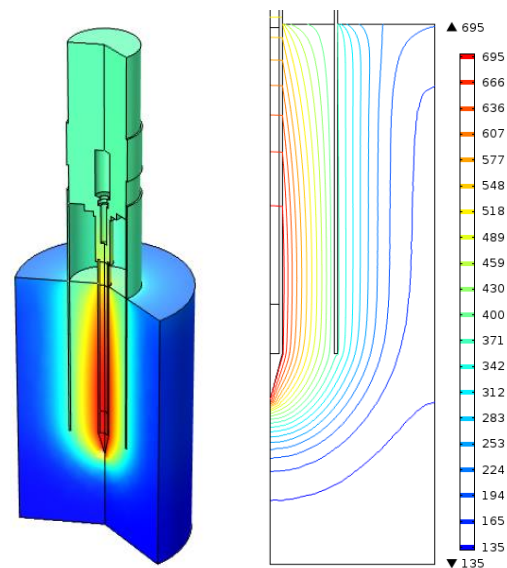


Figure 3: Thermal simulation model and exemplary analysis results showing the temperature distribution across the sample (temperatures in K)

Analysis of Released Volatiles: EVITA is an ion trap mass spectrometer based on the Ptolemy mass spectrometer on-board the Rosetta lander Philae. It is a lightweight, small and compact device that allows gas analysis in the mass range of 10 to 150 amu. EVITA uses a low power carbon nanotube ionisation source. The released volatiles will be monitored by the mass spectrometer during heating to determine their composition and indicate their quantity.

Future Work: Current and future work on the LVS includes the continuation of penetration and thermal testing as well as the combined testing of both heating element and insertion mechanism. The long term goal is to develop a full scale prototype that also contains the EVITA mass spectrometer and control electronics.

References: [1] Reiss P. et al. (2015) *ELS*, 19-20. [2] Sheridan S. (2006) *Melting Probe Review*. [3] Sheridan S. et al. (2003) *EGS/AGU/EUG Joint Assembly*. [4] Gibson E. K. and Johnson S. M. (1985) *2nd Lunar Science Conference*, Vol. 2, pp. 1351-1366. [5] Hibbitts et al (2011) *Icarus* 213, 64-72.

DRILL-TERRAIN ENERGY EXCHANGE MODEL TO ASSESS MOON SUBSURFACE ICY SAMPLES SPECIMEN THERMO-PHYSICAL PROPERTIES PRESERVATION DURING THE ACQUISITION PHASES M.Lavagna¹, C.Panza², M.Savoia², A.Fumagalli². ¹ Politecnico di Milano, Dipartimento di Scienze e Tecnologie Aerospaziali, Via La Masa 34, 20156 Milano-Italia, michelle.lavagna@polimi.it. ² Finmeccanica, Viale Europa, Nerviano-Italia, matteo.savoia@guests.selex-es.com

Abstract: In the frame of the current exploration mission studies which include in situ science, scientists are greatly interested in icy and volatiles specimen retrieval and analysis, from the Moon first, but from icy planets like Europa and Enceladus as well. Such a scientific target translates in a very challenging set of design and operational constraints on tools devoted to surface sample collection and delivery to either the scientific instrument or the preservation box to be returned to Earth. Moreover, a set of beneath surface samples are requested, to get material unmistakably representing the local chemical\physical history and not affected by exogenous factors acting on the surface. The combination of the beneath surface sampling and volatile\ice preservation translates into the development of soil penetrating tools with low energy exchange with the surrounding soil during perforation, coring, collection, delivery, to ensure the sample to keep its few tenths of Kelvin temperature to preserve its volatiles and icy structure.

Several exploration missions would benefit from icy sample collection capabilities, some of those may be part of a Moon focused space program. Volatiles search and analysis in the Moon Polar Regions is already a matter of scientific research and the technology is mature to seriously discuss on low temperature sample retrieval feasibility.

Politecnico di Milano developed an experimentally validated Energy Exchange Model (EEM) tool to support the design and operation definitions of the icy soil penetrators. In particular, the penetrator mechanical energy transferred to the soil and the sample during the whole tool operations is modelled, taking into account the detailed drill geometry and the thermo\physical soil characteristics; radiation, conduction and convection mechanisms occurring among the tool, the free space and the soil are modelled, as well as the sublimation of the icy volatiles. The penetration velocity and power, the drill geometry and materials are kept as parameters to run the sensitivity analyses and drive the design; the soil thermo-physical properties are treated as parameters as well and tuned through the experimental campaign run at Finmeccanica premise, which is responsible for the penetrator development for the PROSPECT package. The experimental campaign, still on going, was a fundamental step to calibrate the numerical tool and to identify criticalities and drivers in the analogue selection to be representative of the icy lunar regolith.

The PROSPECT is an ESA proposed set of scientific instruments fed by lunar polar samples collect-

ed by a 1,5m drill, to be embarked on the future Moon surface mission. The ESA led PROSPECT User Group is currently working to drive the samples scientific requirements and support the on-ground PROSPECT sample chain breadboarding, fundamental to ensure a successful science whenever on the Moon surface.

The EEM tool offers - as output - the 3D temperature profile along the whole penetrator operational window for each domain involved in the process: the cored specimen inside the tool, the tool, the surrounding soil.

The paper presents the EEM tool in details highlighting its flexibility and beneficial exploitation to support the PROSPECT drill design requirements verification, the icy soil sample thermal history simulation to avoid unacceptable volatiles sublimation along the whole specimen acquisition phases, from coring to deposition into the analysis boxes, and drive the tool design accordingly. The calibration phase through experimental data correlation is also presented.

To briefly show the EEM effectiveness Figure 1 is reported: it shows one of the possible EEM tool outputs: the temperature profile of the soil sample along the whole drilling phase, from the perforation, to the coring up to the transportation up to the deposition in the experiment boxes; the analysis is parametrized according to the different power input in the mechanical tool.

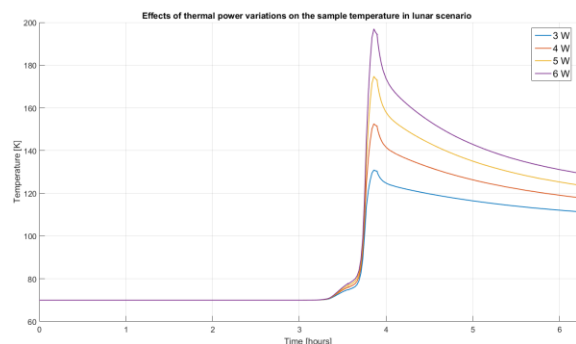


Figure 1 Lunar sample temperature evolution in the coring chamber wrt drilling power

LUNAR POLAR SAMPLE RETURN MISSION. A.Ferri⁽¹⁾, S.Pelle⁽¹⁾ antonella.ferri@thalesaleniaspace.com, stewart.pelle@thalesaleniaspace.com Thales Alenia Space Italy

Introduction: In the last years, the interest in the Lunar South Polar region has grown significantly within the international exploration and science community, fuelled by the abundance of new data acquired by the fleet of orbiter missions which have been sent to the Moon in the past decade.

The next step in exploration of this important region requires direct investigation of the surface and the material there, both through in-situ measurements and via a sample return.

The retrieved samples would enable scientist to address a number of high level science topics ranging from origin of the Earth Moon system, to the moon surface chemistry, from the prebiotic chemistry to origin of terrestrial volatiles, from the dating of the inner Solar system to the planetary differentiation and many others. The sample return mission is also a scientific and technological precursor for Human mission to our Moon.

Thales Alenia Space is leading an ESA study to design a Lunar Polar Sample Return (LPSR) mission as a joint ESA-ROSCOMOS exploration mission.

The scope of the mission is the retrieval of water ice samples from the lunar South Pole and return them back to Earth still in a solid state.

The principal objective of this activity is the definition of a feasible mission scenario and assess the European system elements of the Lunar Polar Sample Return (LPSR) mission architecture with particular regard to the sampling & return phases, including: Sample Handling & preservation of water ice from the lunar surface to retrieval on Earth, Lunar Ascent Vehicle, In-orbit Rendezvous and Capture, Orbiter Module, Earth Return Vehicle and the Earth Return Capsule.

The results of the flight segment study will be presented.

LUNAR VOLATILE PROSPECTOR MISSION. A. Biggio¹, S. Pelle¹, A. Ferri¹ Thales Alenia Space-Italy
andrea.biggio@thalesaleniaspace.com, stewart.pelle@thalesaleniaspace.com,
antonella.ferri@thalesaleniaspace.com

Introduction: Robotic technologies are playing a key role in enabling the achievement of more and more demanding mission requirements. Searching and mapping volatile elements at Moon South Pole is an example of ambitious science objectives that are going to be achieved by means of exploration rovers carrying complex payloads.

Lunar Volatiles Prospector rover mission aims at the mapping of volatiles at Moon south pole region with a medium class rover (mass below 250kg). Surface operations may endure more than two years, implying a mobility range in the order of 50km. Very precise localization will be needed to map the volatiles distribution on Moon south pole surface including Permanent Shaded Regions. The peculiarity of this mission is given by the environment in which it is going to operate. Specific challenges are given by rover perception in complete darkness, stray lights due to sun inclination and long shadows, while the entire system will need to survive the extreme low temperatures of the region with very limited power available and limited view of the Earth for communication

The ESA founded study foresees a cooperation scenario with Russian space agency that would be responsible for the delivery of the Lunar Prospecting Rover on the Lunar South Pole. The objective of the study is the definition of a feasible mission and rover conceptual design able to throughout the identified waypoints operating the scientific payloads.

This article will describe the preliminary results of the European side of the mission.

PROSPECTING AND RETURNING LUNAR SURFACE SAMPLES WITH VOLATILES. T. Diedrich¹, R. Buchwald¹, J. Bolz¹, U. Soppa¹, J. Sommer¹, E. Allouis¹, E. Monchieri¹, B. Dobke¹, S. Howarth¹, M. Musset¹, S. Battendier¹, K. Engel¹, F. Härtel¹, S. Vanden Bussche², J. Gancet³, R. Fisackerly⁴, J. Hüsing⁴, W. Martens⁴. ¹Airbus Defence and Space (mailto: robert.buchwald@airbus.com), ²QinetiQ Space, ³Space Applications Services, ⁴European Space Agency

Introduction: In the recent years, lunar exploration has returned into the focus of the space exploration community - either as stepping stone towards Mars for implementing and demonstrating key technologies, capabilities and operations which support future robotic and human exploration missions or as standalone goal of high scientific interest.

As next step in the context of the cooperation between ESA and ROSCOSMOS for the Russian Luna Glob and Luna Resurs Missions, the possibility of a joint Lunar Polar Sample Return (LPSR) mission is investigated, which shall allow in-situ measurements on the lunar surface and the return of samples in original conditions. The principal objective of the currently running mission and system assessment study is to define and assess specific system elements of the Lunar Polar Sample Return (LPSR) mission architecture that could be contributed by ESA, to support preparations for the next stages of design on those elements, to provide inputs to the technology development approach and to support ESA's interactions with ROSCOSMOS on the planning of a joint LPSR mission.

As part of the ESA Lunar Exploration feasibility assessment, a parallel study, the Lunar Volatile Prospector (LVP) study has been initiated. The Lunar Volatile Prospector is a self-contained element implemented as a mobile rover platform to support the exploration of the South Pole of the Moon and possibly a Lunar Sample Return Mission. The major goal is to determine the distribution of water and other volatiles on a local scale in the lunar polar regions at a location where a general enhancement of water is expected on the basis of orbital and other data sets. Target sites are at a location which receives less than average solar illumination (~7 days per month) and thus presents reduced surface & sub-surface temperatures. These lower regolith temperatures increase the likelihood of obtaining samples containing volatile ices.

In the frame of the currently running LPSR-MSA study, LPSR and LVP are investigated as standalone scenarios in the frame of a common endeavour - to return icy samples with volatiles from the southpole of the Moon.

LPSR mission scenario: In the reference mission architecture two main space segments are defined: the Lander Module (LM) and the Orbiter-Return Module (ORM).

The LM includes all elements required for landing and operating on the lunar surface, and for delivering

the sample to the hand-over point with the Orbiter-Return Module.

The Orbiter-Return Module itself consists of all elements required for arriving and operating in lunar orbit, for rendezvousing with the sample and for returning the sample to Earth. One part of the Orbiter-Return Module, the Orbiting Vehicle (OV) remains in a polar orbit around the Moon for providing data relay functionality for further surface activities.

Major challenges for the demonstration of mission feasibility are the challenging mass constraints for the lunar ascent vehicle, the need for implementing an effective handover and short transfer duration and the thermal control of the frozen payload for returning the samples in the best conditions possible.

LVP mission scenario: The LVP mission architecture consists principally of 2 main phases:

Launch, transfer, landing and delivery of a mobile platform (Lunar Prospecting Rover (LPR)) to the lunar surface and surface operations of the LPR.

The current early study work on the LVP mission is concentrating on the second phase, i.e. on the surface operations carried out by the LPR and on the definition of the LPR itself.

Special focus is set on sampling and operating in permanently shaded regions which imposes demanding requirements on hardware and operational concepts.

Scope of the presentation: Airbus Defence and Space as industrial prime contractor is leading a European team focusing on consolidating the first system and mission assumptions of LPSR and LVP and support the implementation of the future mission. The presentation will provide first insights in the performed investigations and the achieved results.

LUNAR VOLATILE PROSPECTOR ROVER – EXPLORING THE LUNAR SOUTH POLE AND THE PERMANENTLY SHADED REGIONS. E.Allouis¹ and E.Monchieri¹, ¹Airbus Defence and Space Ltd, Future Programmes, Gunnels Wood Road, Stevenage SG1 2AS, Elie.Allouis@airbus.com

Introduction: As part of the ESA Lunar Polar Sample Return feasibility assessment, the Lunar Volatile Prospector (LVP) is a mission concept focussing on the development of the Lunar Prospecting Rover (LPR) a mobile platform to support the exploration of the South Pole of the Moon. The 2-year mission is aimed at the 2022 to 2024 timeframe and focuses currently on the exploration of a variety of locations between the Shoemaker and Faustini craters. The purpose of a Lunar Prospecting Rover (LPR) is to determine the distribution of water and other volatiles on a local scale in the lunar polar regions at locations identified as presenting higher concentration of water in orbital datasets. The rover therefore provide an accurate ground truth to reduce the uncertainty of the orbital data and provide higher spatial resolution.

The LVP scenario. The rover platform must cover some 50km on the surface and will carry a versatile suite of payload to characterise the environment during the traverse. It consists of remote sensing instrument including a panoramic multispectral camera, a ground penetrating radar, and a set of Gamma-Ray, Neutron and IR spectrometers. In addition, the rover carries a large drill (PROSPECT) similar to the ExoMars drill and a miniaturised chemical laboratory (ProsPA) to acquire regolith samples and investigate the level and composition of volatiles. One of the key challenges for the rover however, will not only be the 2-year operation with extended hibernation during the long lunar nights, but the robust and safe exploration of Permanently Shaded Regions (PSR) where volatiles are thought to be more accessible, making the PSRs prime targets for the scientific community. The rover will therefore perform a number of incursions into PSRs over the course of the mission to acquire and analyse sub-surface samples at varying depth.

The LPR platform. As a platform of extremes, the design of the rover needs to accommodate a wide range of temperature and environmental conditions, from the full view of the sun to the darkest regions in the PSR. As such, the thermal management and energy generation capabilities are critical. The mechanical and thermal designs will be introduced, building upon current rover designs such as ExoMars and identifying key differences between a Mars and Moon designs. To facilitate the traverses in varying surface conditions, a number of teleoperation modes are introduced, highlighting the benefits of onboard autonomy to enhance the safety of the platform throughout the mission.

Linking Operations, Science and Design. The operation of the platform, the selection of specific

sites of interests and the traverse waypoints are functions of a range of scientific, operational and engineering variables that will be discussed here. This highlights the need to consider, at the planning and design stages, both the location of a specific science site and the pacing of the traverse of the platform on the surface to maximise both the illumination of the site (to supply enough energy to the rover) as well as good communication windows with Earth (to provide robust teleoperation). Accessibility map can then be derived throughout the year to select the most appropriate route, and time, to explore as many science targets in the mission timeframe.

MOONRISE: SAMPLING THE SOUTH POLE-AITKEN BASIN TO ADDRESS PROBLEMS OF SOLAR SYSTEM SIGNIFICANCE. R. A. Zeigler¹ B. L. Jolliff², R. L. Korotev², and C. K. Shearer³, ¹NASA Johnson Space Center, 2101 NASA Rd 1, Mail Code XI2, Houston, TX 77058; ²Washington University in St. Louis, 1 Brookings Dr. Campus Box 1169, St. Louis MO, 63130; ³Institute of Meteoritics and Department of Earth and Planetary Sciences, University of New Mexico, Albuquerque, N 87131. (ryan.a.zeigler@nasa.gov)

Introduction: A mission to land in the giant South Pole-Aitken (SPA) Basin on the Moon's southern far-side and return a sample to Earth for analysis is a high priority for Solar System Science [e.g., 1,2]. Such a sample would be used to determine the age of the SPA impact; the chronology of the basin, including the ages of basins and large impacts within SPA, with implications for early Solar System dynamics and the magmatic history of the Moon [3]; the age and composition of volcanic rocks within SPA; the origin of the thorium signature of SPA with implications for the origin of exposed materials and thermal evolution of the Moon [4,5]; and possibly the magnetization that forms a strong anomaly especially evident in the northern parts of the SPA basin [6].

It is well known from studies of the Apollo regolith that rock fragments found in the regolith form a representative collection of many different rock types delivered to the site by the impact process (Fig. 1) [7-9]. Such samples are well documented to contain a broad suite of materials that reflect both the local major rock formations, as well as some exotic materials from far distant sources. Within the SPA basin, modeling of the impact ejection process indicates that regolith would be dominated by SPA substrate, formed at the time of the SPA basin-forming impact and for the most part moved around by subsequent impacts [10,11]. Consistent with GRAIL data, the SPA impact likely formed a vast melt body tens of km thick [12,13] that took perhaps several million years to cool, but that nonetheless represents barely an instant in geologic time that should be readily apparent through integrated geochronologic studies involving multiple chronometers. It is anticipated that a statistically significant number of age determinations would yield not only the age of SPA but also the age of several prominent nearby basins and large craters within SPA. This chronology would provide a contrast to the Imbrium-dominated chronology of the nearside Apollo samples and an independent test of the timing of the lunar cataclysm.

The Desired Sample: Owing to the variety of landing sites and sample stations encountered during Apollo missions, we have a very good idea of what to expect to find in regolith from locations of different maturity on the Moon, with many examples among the Apollo samples. All regolith samples are dominated by fine material but contain some proportion of rock fragments, and the abundance of such rock fragments generally increases with depth, even within the upper few tens of cm. Rock

materials are needed to determine impact ages as well as ages of volcanic rocks. Ages can be determined using bulk methods, mineral separates, and in-situ microbeam methods. In some cases, for example crystalline basalts or crystalline impact-melt breccias, SIMS analyses to determine U-Pb ages of Zr-bearing and phosphate minerals will be used [14-16]. For rocks with sufficient grain size, mineral separates can be used for Sm-Nd and Rb-Sr, methods [17]. Rock subsamples can be analyzed using ⁴⁰Ar-³⁹Ar and (U-Th)/He methods [18,19].

Coherent, crystalline rock material is best suited for these types of analyses, thus we plan to sieve the regolith, which in effect increases the scientific content of the sample many-fold. Sieving to collect rock fragments in the ~4-20 mm size range will produce thousands of rock fragments in a kilogram of material, although much more than a kg might need to be sieved to obtain this quantity of rock fragments.

Preliminary Examination (PE): A critical aspect of any sample return mission is the PE. The purpose of the PE is to document the collection and to provide sufficient initial characterization to enable appropriate distribution of sample materials for analyses that will address mission science objectives. Modern methods that provide petrographic, mineralogical, and compositional information using non-invasive methods can be done with modern technology (e.g., micro-CT scanning and micro-XRF [20]). A subset of representative samples should be sectioned for micro-beam characterization. Following PE, samples would be allocated to the mission science team, which includes international partners, as well as to the broader science community for analysis according to established Curatorial procedures.

Curation and Allocation: In addition to PE, long-term curation of the sample-return materials would be done in a manner similar to the way Apollo samples and other more recent returns have been curated. Controlled atmospheric conditions for handling and storage are critical for preservation of a portion of the collection for future research as new scientific questions and analytical methods are developed. As is done now, samples would be carefully monitored for allocations of requested materials of a type and amount that is appropriate for a given scientific investigation, with review of sample requests by NASA's Curation and Analysis Planning Team for Extraterrestrial Materials (CAPTEM), working with the sample Curator, handling and distribution by the Curatorial Facility (JSC), and oversight by NASA.

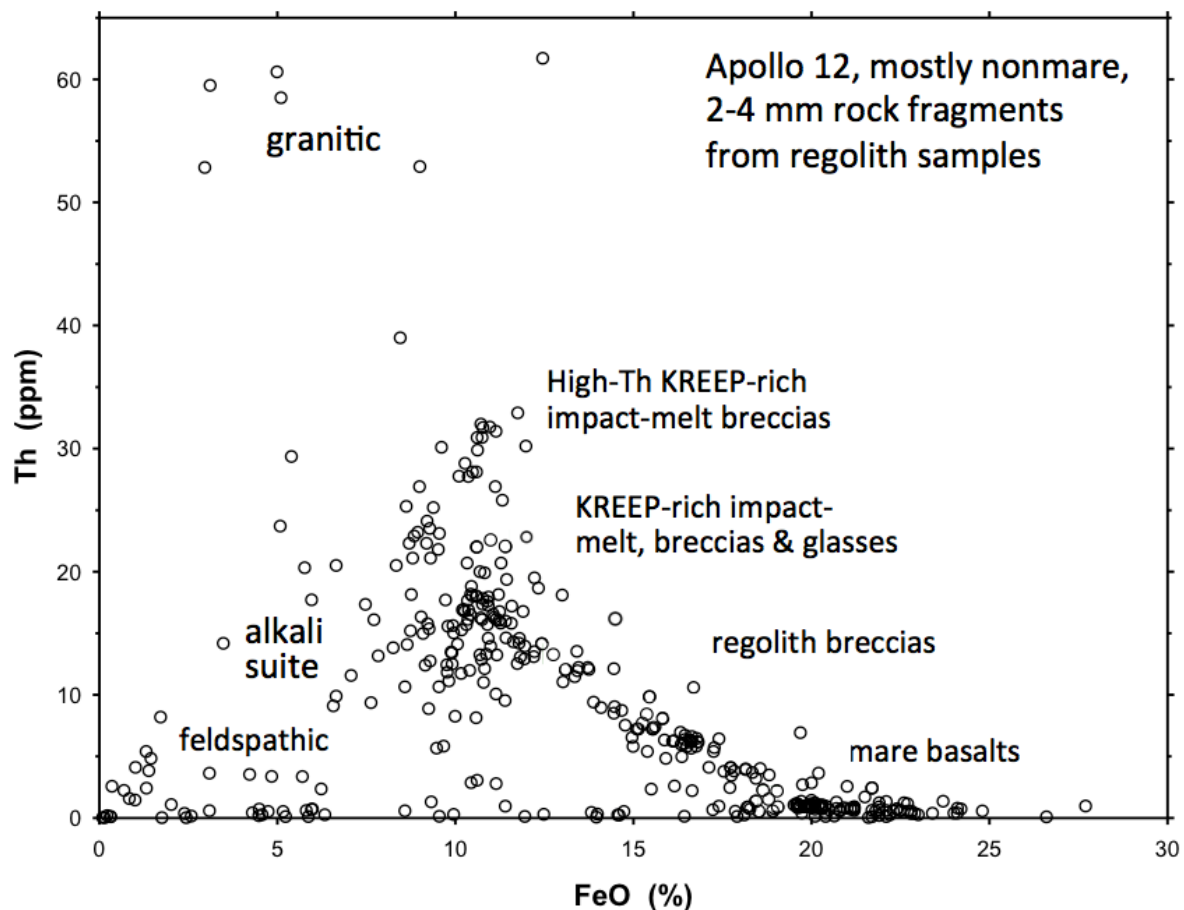


Figure 1. At the Apollo 12 landing site, rocks and regolith are dominated by the basalts that underlie the landing site. However, all of the soils contain rock components from the surrounding region, as well, delivered to the site by nearby impacts. At Apollo 12, the nonmare fraction contains an abundance of mafic, KREEP-rich impact-melt breccia that was produced by one or more large craters or basin-sized impacts into the Procellarum KREEP Terrane. A predominant age of 3.9 Ga, as found through the analysis of zircon grains crystallized from the impact melt of high-Th impact-melt breccias [16] most likely reflects the age of the Imbrium event (see also [21]).

References: [1] NRC (2003) *New Frontiers in the Solar System: An Integrated Exploration Strategy*. Natl. Acad. Press [2] NRC (2011) *Vision and Voyages for Planetary Science in the Decade 2013-2022*, Natl. Acad. Press. [3] Jolliff et al. (2016) *Lunar Planet. Sci.* **47**, #2818. [4] Garrick-Bethel and Zuber (2005) *GRL* **32**, L13203. [5] Hagerty et al. (2011) *JGR* **116**, E06001. [6] Wieczorek (2009) *Lunar Planet. Sci.* **47**, #2009. [7] Korotev et al. (2011) *GCA* **75**, 1540-1573. [8] Jolliff et al. (1991) *Proc. Lunar Planet. Sci.* **21**, 193-219. [9] Jolliff et al. (1996) *MAPS* **31**, 116-145. [10] Haskin et al. (2003) *Lunar Planet. Sci.* **34**, #1434. [11] Petro and Pieters (2004) *J. Geophys. Res.* **109**, E06004. [12] Vaughan and Head (2013) *Planet. Space Sci.* **91**, 101-106. [13] Hurwitz, D. and Kring, D. (2014) *J. Geophys. Res.* **119**, 1110-1133. [14] Grange et al. (2011) *GCA* **75**, 2213-2232. [15] Nemchin et al. (2012) *Australian J. Earth Sci.*, 277-290. [16] Liu et al. (2012) *EPSL* **319-320**, 277-286. [17] Shearer and Borg (2006) *Chemie der Erde* **66**, 163-185. [18] Cassata (2016) *Lunar Planet. Sci.* **47**,

#2118. [19] Young, K. et al. (2016) *Lunar Planet. Sci.* **47**, #1754. [20] Zeigler (2014) *Lunar Planet. Sci.* **45**, #2665. [21] Snape et al. (2016) *GCA* **174**, 13-29.

LANDING SITES SELECTION FOR THE RUSSIAN POLAR LANDER LUNA-25. I. G. Mitrofanov¹, A. B. Sanin¹, M. L. Litvak¹ and M. V. Dyachkova¹, ¹Institute for Space Research, Profsojuznaja str. 84/32, Moscow, Russia, imitrofa@space.ru.

Introduction: The lunar robotic mission Luna-25 is currently under development in Russia [1]. It is the first one in the sequence of missions to study the southern polar region of the Moon. No one spacecraft had landed at lunar poles before, while they are very attractive for exploration because of potentially rich volatiles deposits in the shallow subsurface. The proper landing sites selection is the important part of the mission implementation, which has to balance properly the redundancy of soft landing with the expectations for science investigations.

Criteria for Sites Selection: The surface flatness and roughness are the most important engineering criteria for selection of landing sites. The third one is the reliable radio link with the Earth. The longest possible solar illumination is the fourth engineering requirement for the site selection.

The scientific criteria are mainly associated with the predictable content of volatiles in the regolith. For Luna-25, as the very first polar lander, one should not request the most abundant volatiles, as might be predicted by the orbital data, but the moderate abundance would be desirable. It is agreed, that for this mission, the engineering requirements for landing site selection should prevail the criteria of science.

Candidate Sites: Luna-25 is the lander with the passive landing capabilities, which result to rather large ellipse of landing accuracy, 15 x 30 km. The short list of candidate landing sites for such landing accuracy will be presented, which is based on the analysis of LOLA digital elevation models (DEM) [2] for surface steepness and flatness. Also the local lines of horizon were produced from the LOLA DEM, which allows to determine the local conditions of the solar illumination and of the radio link with the Earth.

Durations of active time periods: Durations for active time periods of each lunation along the years 2018 – 2020 will be presented for each of candidate landing sites, which correspond to two coincident conditions: the lander should have the solar illumination and also its radio link with the ground stations should be secured. It will be shown that there are more and less favourable seasons for the science operations, when the lander active time varies from zero up to 352 hours per one lunation, respectively. The duration of the active time is the most important for the very first lunation from the time of landing till the time of Sun set, because the payload commissioning and the minimal science measurements have to be done during this time.

Conclusions: Using these data, the best landing sites together with the most favourable date for the launch will be considered for the Luna-25.

References: [1] Mitrofanov, I. G. et al. (2014), "Luna-Glob" and "Luna-Resurs": science goals, payload and status, EGU General Assembly Conference Abstracts, 16, 6696. [2] Neumann, G. A. et al. (2011), Lunar Reconnaissance Orbiter Lunar Orbiter Laser Altimeter Reduced Data Record and Derived Products Software Interface Specification, version 2.42. Url: <http://imbrium.mit.edu/DOCUMENT/RDRSIS.PDF>.

CANDIDATE LANDING SITES NEAR THE LUNAR POLES: A EUROPEAN PERSPECTIVE. J. Flahaut¹, J. Carpenter², M. Anand³, W. van Westrenen⁴, R. Fisackerly², J.-P. Williams⁵, I. Crawford⁶, N. Potts^{3,4}, S. Besse⁷ and the ESA Topical Team on the Exploitation of Local Planetary Material (ESA TT-ELPM). ¹LGL, TPE, CNRS/Université Lyon 1, 69622 Villeurbanne Cedex, France (jessica.flahaut@ens-lyon.org), ²ESA-ESTEC, Noordwijk, The Netherlands, ³Dept of Physical Sciences, The Open University, Milton Keynes, UK, ⁴Faculty of Earth and Life Sciences, VU University Amsterdam, The Netherlands, ⁵Dept of Earth and Space Sciences, University of California, USA, ⁶Dept of Earth and Planetary Sciences, Birbeck University of London, UK, ⁷ESA-ESAC, Madrid, Spain.

Introduction: In December 2014, the LEAG Volatiles Special Action Team (VSAT) produced a report in which they highlight three lunar polar areas (Cabeus/Shoemaker/Peary) of significant extent that fulfill the VSAT charter to identify regions “where NASA and international / commercial partners could operate on the lunar surface in a cooperative manner to further understand the size, distribution, form, and resource potential of deposits of water ice and other volatiles” [1]. Their initial criteria for site selection included: H content > 150 ppm, average temperature <110°K, direct-to-Earth communication potential, slope < 10°, outside of PSR. In September 2015, ESA’s Topical Team on the Exploitation of Local Planetary Material (TT-ELPM) provided a review of this report [2,3]. In its response, ESA’s TT-ELPM agrees with substantial parts of the LEAG VSAT report. However, the ESA team recommended that additional work should be carried out regarding potential landing sites, taking into account an enlarged/relaxed set of parameters + potential additional science benefits.

ESA’s TT-ELPM main recommendation is to pursue investigations of landing sites suitable for combined volatile and geological studies [3,4]. First steps towards the identification of Regions Of Interest (ROI) at both poles are presented hereafter. Further site selection work is highly mission dependent (based on objectives and requirements); an example is presented in the case of the ESA’s Lunar Prospecting Rover (LPR) mission. Two sites which meet the LPR mission requirements are proposed in the south pole vicinity. Potential traverses are also presented for site 1, located on a topographic high between Shoemaker and Faustini, and at a geologic triple point. Site 1 has good illumination conditions for the south pole area and straddles a H-rich and H-poor region as suggested by the LEND data [5]; it, therefore, represents an excellent candidate for future lander or rover missions which aim to investigate lunar polar volatiles.

Dataset and method: All available datasets were combined in a Geographic Information System (GIS) for both poles. The data collection includes: Lunar Prospector H content maps (and derived contours at 100, 125 and 150 ppm), LROC WAC and NAC polar mosaics, LOLA 20 m and 120 m DEM and

derived slope maps, LOLA average illumination, Earth visibility and PSR distribution [6], Diviner bolometric temperature maps (average, minimum and maximum) and predicted ice depth stability [7], USGS geological maps [8 and references therein], and previous mineralogic detections as compiled by [9].

Candidate landing sites near the North and South poles: Decreasing the H content threshold to >125 ppm or relaxing the direct-to-Earth and illumination constraints significantly increases the number of available sites in both polar regions. Although the H content might not be as high at those sites, there could be additional science interests (e.g., sampling of a young geological unit) that justifies the selection of those sites over a site with H>150 ppm. Examples of ROI are given below, downselection was not performed as the choice of one of several final candidate sites is highly mission dependent.

North Polar Sites. ROI (H-rich regions) extend beyond 80° in latitude near the north pole, however, at such latitudes there is a high average temperature (>110°K). Relaxing the direct-to-Earth communication constraint significantly increases the number of potential ROI, as most ROI are located on the farside.

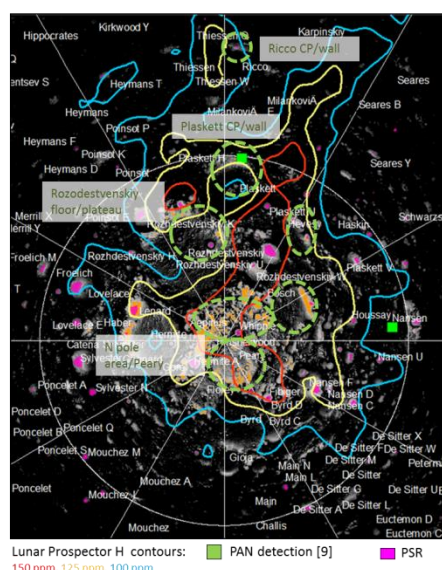


Figure 1: N pole ROI for volatile investigations (green circles). Background: Diviner average T map (white = low). Blackened areas = Diviner avg T>110K, Orange areas = Diviner average T<54K, N Pole stereographic projection.

We find that additional science benefits are possible at many of those ROI sites (e.g., sampling of Erastosthenian material on the Rozodestvenskiy plateau, ground-truthing an orbital detection of pure anorthosite in the rim of Plaskett crater [9]). Some of these sites present better slope and illumination conditions than the floor of Peary crater, and locations with average temperature $<54^{\circ}\text{K}$ (stability of CO_2 ice) (Figure 1).

South Polar Sites. There is a large area of interest around the SP with $\text{H} > 125$ ppm and $\text{avg T} < 110^{\circ}\text{K}$, which includes Amundsen crater. In addition, this area offers the unique opportunity to investigate the South Pole Aitken (SPA) basin which is the largest known impact basin in the Solar System. Slopes can be however high, limiting accessibility to PSR, and illumination conditions can be poor, which will influence further downselecting processes (Figure 2).

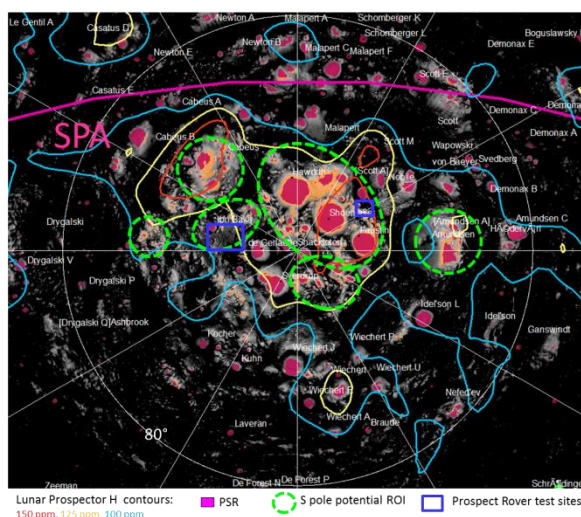


Figure 2: S pole ROI for volatile investigations (green circles). Background: Diviner average T map (white = low). Blackened areas = Diviner avg $T > 110\text{K}$, Orange areas = Diviner avg $T < 54\text{K}$, S Pole stereographic projection. Blue boxes indicate the location of the two LPR candidate sites.

The ESA Lunar Prospecting Rover (LPR) case study: The LPR is a ESA study into a mission consisting of a rover mission to the south pole of the Moon, whose objective is to determine the distribution of water and other volatiles on a local scale [10]. Mission requirements include a mobile range of 50 km, an illumination fraction >0.25 , and a direct-to-Earth communication potential. Illumination conditions are found to be the main driver for the site selection here, as most areas around the south pole do not meet the >0.25 criteria. Two potential sites were identified with the use of our GIS: Site 1 is a topographic high between Shoemaker and Faustini craters, Site 2 is an Imbrian plain south of Ibn Bajja (Figure 2, 3). Site 1 is found to be particularly interesting because, in addition to fulfilling both sci-

entific constraints and mission requirements, this site is:

- located at a geologic triple point,
- straddled at the limit of a high and low LEND H detection,
- located within an area where various ice stability depths are predicted/ Diviner Temperature is spatially variable.

Potential traverses are developed at site 1 based on high resolution observations and other available dataset. Way-Points (WP) were defined in order to prepare for complex traverses that will take hourly Earth visibility and illumination variation into account. The WP selection was defined in order to encompass:

- The contact between the three geological units (1 WP),
- At least 2 WP per geological units,
- at least 3 WP in different PSR,
- At least 2 WP in areas where the maximum T does not exceed 110°K ,
- At least 2 WP in areas where ice stability depth is predicted to be = 0, between 0.01 - 0.25 m, 0.25 - 0.5 m,
- At least 1 WP in areas where ice stability depth is predicted to be between 0.5 - 1 m, > 1 m.

Conclusions and Perspectives: We have identified a large number of potential ROI for lunar volatile investigations at both the north and south poles. Some of these ROI could allow additional geologic studies, however, further site selection is highly mission dependent and no additional exclusion of ROI can be made at this stage. Two sites were identified in the south pole vicinity as suitable for a landed mission such as the ESA LPR. We found that in the case of the LPR (solar-powered rover), illumination constraints (>0.25) are the main driver for site selection, as other requirements are met at many locations. Potential traverses are developed at site 1, located on a topographic high between Shoemaker and Faustini, which appears to be a promising site for future south pole landed missions.

References: [1,2] Available at <http://lunarvolatiles.nasa.gov/> [3] Anand, M. et al. (2015) *International Symposium on Moon 2020-2030*. [4] Flahaut, J. et al. (2016) *ISECG Lunar Polar Volatiles Virtual Workshop #2*. [5] Mitrofanov, I. et al. (2010) *Science*, 330. [6] Mazarico, E. et al. (2011) *Icarus* 211. [7] Paige, D. et al. (2010) *Science* 330. [8] Fortezzo C. M. and T. M. Hare (2013) *LPSC44th*, #2114. [9] Flahaut, J. et al. (2012) *ASR*, 53. [10] Ohtake, M. et al. (2010), *Nature*, 461. [11] Carpenter J. et al. (2015), LEAG meeting, #2027.

PETROLOGICAL MAP OF THE SOUTH POLE-AITKEN BASIN. D. Rommel¹, A. Grumpe¹, C. Wöhler¹, H. Hiesinger², A. A. Berezhnoy³, K. J. Kim⁴. ¹Image Analysis Group, TU Dortmund, Otto-Hahn-Str. 4, D-44227 Dortmund, Germany. ²Institut für Planetologie, Westfälische Wilhelms-Universität Münster, D-48149 Münster, Germany. ³Sternberg Astronomical Institute, Moscow State University, Universitetskij pr. 13, Moscow, Russia. ⁴Planetary Geology Department, Geological Research Division, Korea Institute of Geosciences & Mineral Resources, 124 Gwahang-ro, Yuseong-gu, Dajeon, 305-350, Republic of Korea.

Introduction: A giant impact on the southern lunar farside formed a basin structure of about 2500 km diameter, the South Pole-Aitken basin [1]. In this study, we construct and discuss elemental abundance and petrological maps of SPA from Moon Mineralogy Mapper (M³) data [2] and Lunar Prospector Gamma-Ray Spectrometer (LP GRS) measurements [3].

Methods and Dataset: The near-global M³ mosaic at a spatial resolution of 20 pixels per degree derived in [4] is extended towards a latitudinal range of $\pm 75^\circ$ using the same methods as [4]. Spectral parameters inferred from M³ reflectance spectra are related to the LP GRS elemental abundance measurement maps [3, 6] using a polynomial regression at a spatial resolution of 0.2 pixels per degree.

Spectral parameters. We adopt the spectral parameters from [7] to describe the spectral absorption features. These spectral parameters are the depth, width, position and continuum slope of the absorption band near 1 μm and the continuum slope and depth of the absorption band near 2 μm .

Regression. We apply a polynomial regression model [7-9] to capture the correlation between the spectral parameters and the LP GRS derived elemental abundance maps of low spatial resolution. The regression parameters are then applied to the full resolution near-global M³ mosaic, resulting in maps of the elemental abundances of Ca, Al, Fe, Mg, Ti and O. From the Fe and Mg maps (Fig. 1) we derive a petrological map based on the model suggested in [10], which is defined by the endmembers mare basalt (18 wt% Fe, 6.5 wt% Mg), Mg-rich rock (4 wt% Fe, 13 wt% Mg, e.g. troctolite or orthopyroxene-rich norite) and feldspathic rock (0.5 wt% Fe, 1 wt% Mg, especially ferroan anorthosite). The relative fractions are read from a ternary diagram in Fe-Mg space and visualised in Fig. 2.

Results and Discussion: In the SPA region, surface materials with a clearly basaltic spectral signature (red-orange in Fig. 2) occur only as relatively small patches with typical diameters around 100 km and less. These patches generally correspond to lava-flooded basins and crater floors. Examples are the partially flooded floors of Mare Ingenii (320 km diameter, MI), Apollo (535 km, Ap), Poincaré (320 km, P), and Minkowski (115 km, M) as well as the fully flooded craters Chrétien and Chrétien C (85 and 65 km, C), Hopmann (90 km, Ho), von Karman, von Karman M (180 and 225 km, K), Hess, Hess Z

(90 and 75 km, He), Leeuwenhoek (125 km, Lee), Karrer (50 km, Ka), Baldet (55 km, Ba) and Antoniadi (145 km, An). The distribution of these structures matches the map of mare basalts in [11]. In addition, high concentrations of basaltic material are found on and around the rims of craters Zeeman Y (35 km, ZY) and Eijkman D (25 km, ED) which might be associated to impact melt [8] or ejecta.

Material of high ferroan anorthosite content (blue in Fig. 2) is found in the southern farside highlands all around SPA and matches the distribution of anorthositic regions in [11]. In addition, there are small spots inside SPA, especially in the region between the inner and the main ring of the Apollo basin, a structure in the northern part of Poincaré that appears to be related to ejecta from the small fresh crater Poincaré X (20 km, PX), a structure extending from the southern floor of crater Alder (75 km, Al) outside the crater in southeastern direction, and a patch on the western wall of crater Antoniadi.

On the floor and wall of the craters Dryden (50 km, Dr) located in the northwestern part of the Apollo basin, Antoniadi and Lyman (84 km, Ly) and the central peaks of Bhabha (65 km, B) and Birke-land (80 km, Bi), Mg-rich rocks (green in Fig. 2) are found in high concentrations between 60% and 80%, also around the northern wall of Leibnitz (245 km, Lei) and in the region east of Poincaré X. Additionally, Eijkman (54 km, E), Fitzeau (110 km, F), and many more smaller deposits of Mg-rich rock, usually corresponding to small impact craters with diameters below 20 km and their ejecta, can be found in SPA in Fig. 2. This presence of Mg-rich rock was also noted in [7] and suggests that the Mg-rich rock was excavated to the surface by impacts, which would indicate the composition of the crust at least down to a few km depth being dominated by Mg-rich rock. This finding is consistent with the anomalously high crustal density in the SPA region [13] and might also be related to its relatively low crustal thickness found in [13].

The other parts of SPA are compositionally characterised by mixtures between basalt and Mg-rich rock in variable fractions with usually minor (<25%) components of ferroan anorthosite.

References: [1] Kim, K. J. et al. (2012) *Adv. Space Res.* 50, 1629-1637. [2] Pieters, C. M. et al. (2009) *Curr. Sci.*, 96(4), 500-505. [3] Lawrence, D. J. et al. (1998) *Science*, 281(5382), 1484-1489. [4] Grumpe, A. and Wöhler, C. (2014) *Proc. European Lunar Symposium 2014, Lon-*

don, 97–98. [5] Pieters, C. M. (1999) *Proc. Workshop on New Views of the Moon II*, Abstract #8025. [6] <http://www.mapaplanet.org/explorer/moon.html> [7] Wöhler, C. et al. (2011) *Planet. Space Sci.* 59, 92–110. [8] Wöhler, C. et al. (2014) *Icarus* 235, 86–122. [9] Bhatt,

M. U. et al. (2015) *Icarus* 248, 72–88. [10] Berezhnoy, A. A. et al. (2005) *Planet. Space Sci.* 53, 1097–1108. [11] Pieters et al. (2011) *J. Geophys. Res.* 106, 28,001–28,022. [13] Wieczorek et al. (2013) *Science* 339, 671–675.

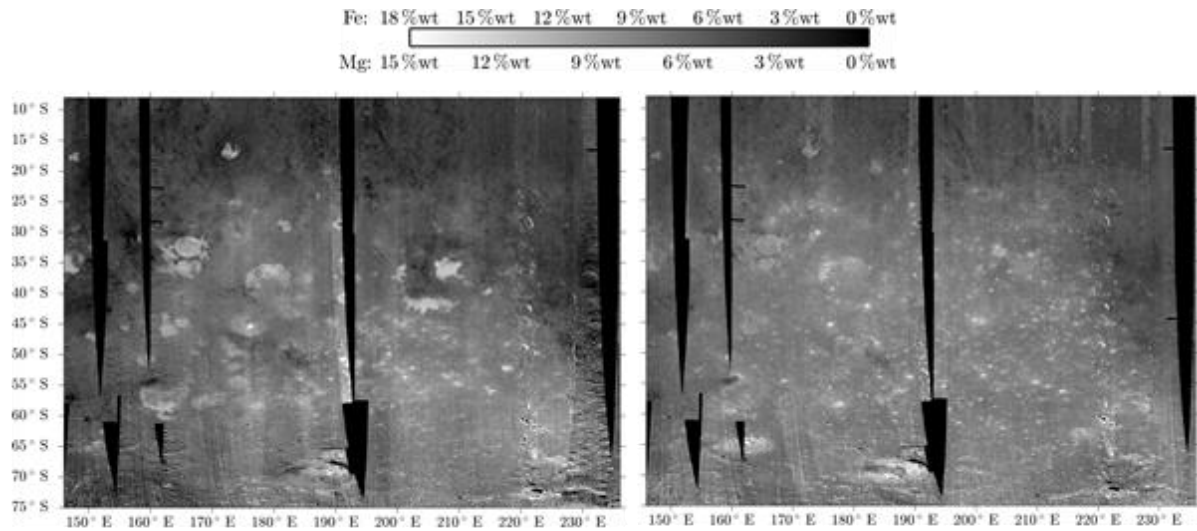


Figure 1: Fe abundance map (left) and Mg abundance map (right). Black denotes missing data.

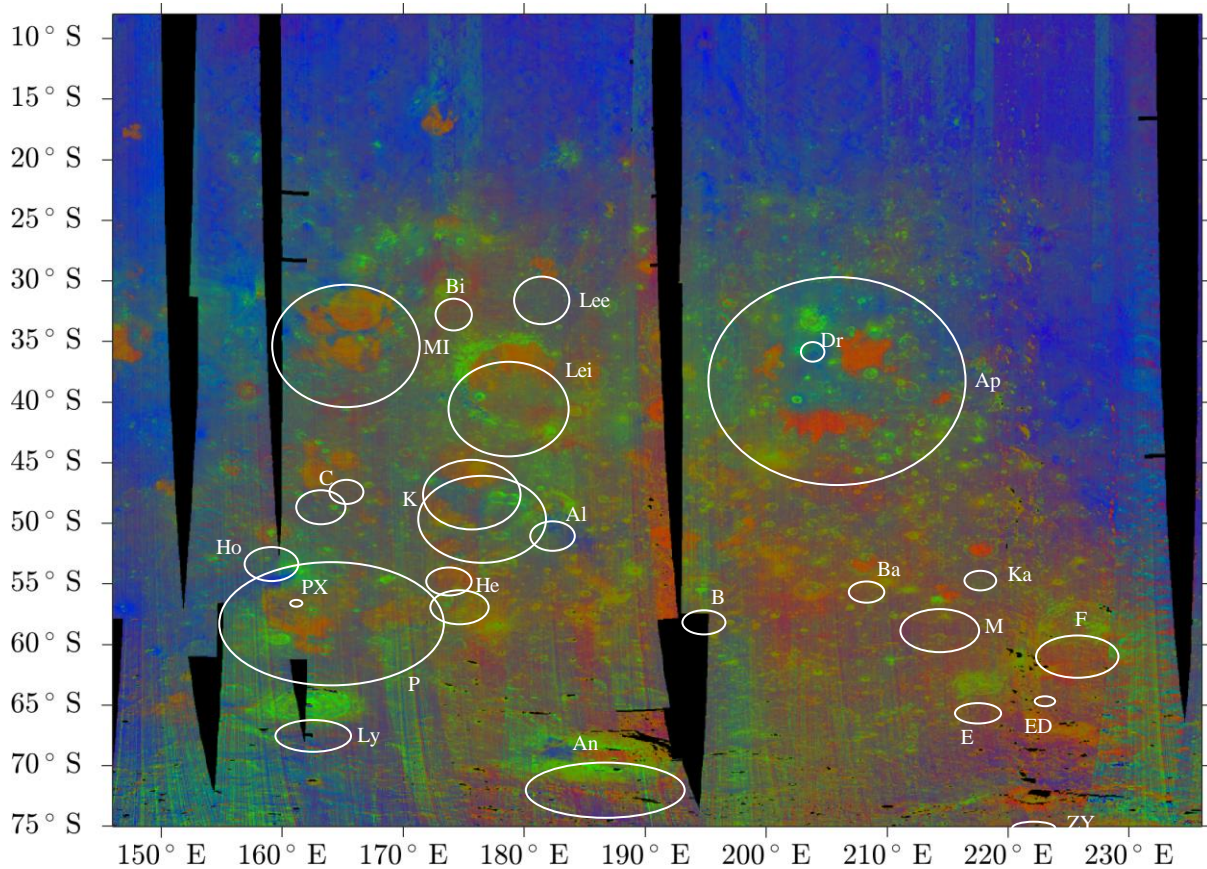


Figure 1: Petrographic map of the SPA. The relative fractions of the three endmembers in terms of the petrographic model by [9] are read from a ternary diagram in Fe-Mg space. The red channel is assigned to the mare basalt (or pyroxene) fraction, the green channel to the Mg-rich rock fraction, and the blue channel to the feldspathic rock (ferroan anorthosite, FAN) fraction. Letters denote structures described in the text and the white ellipsoids approximate their shape in the cylindrical projection. Black denotes missing data and shadowed regions.

EXTENDING NASA'S LUNAR MAPPING AND MODELING PORTAL: ENHANCEMENTS FOR A NEW ERA OF LUNAR EXPLORATION. B. H. Day¹ and E. S. Law², ¹ NASA Solar System Exploration Research Virtual Institute. NASA Ames Research Center. M/S 17-1. Moffett Field, CA, USA. 94035. (Brian.H.Day@nasa.gov), ² Jet Propulsion Laboratory, California Institute of Technology. M/S 168-200. 4800 Oak Grove Dr. Pasadena, CA, USA 91109. (Emily.S.Law@jpl.nasa.gov).

Introduction: Multiple nations and agencies are planning exciting new missions to the Moon. These missions include orbiters, landers, and rovers. In addition, Lunar CubeSat technology holds the promise to significantly lower previous barriers to lunar missions. NASA's Lunar Mapping and Modeling Portal is evolving to meet the needs of mission planners in this new era of lunar exploration.

NASA's Lunar Mapping and Modeling Portal integrates a suite of interactive tools that incorporate observations from past and current lunar missions, creating a comprehensive lunar research Web portal. The online Web portal allows anyone with access to a computer to search through and view a vast number of lunar images and other digital products. As a web-based toolset, LMMP does not require users to purchase or install any software beyond current web browsers. The portal provides easy-to-use tools for browsing, data layering and feature search, including detailed information on the source of each assembled data product and links to NASA's Planetary Data System. Using LMMP, many hundreds of lunar data products can be both visualized and downloaded. Detailed metadata for each data product is also made available to the user.

This presentation will provide an overview of LMMP uses and capabilities, highlight new features, and preview coming enhancements. This will be an interactive presentation in which members of the lunar community are specifically given the opportunity to share what enhancements they would like to have implemented.

An Integrated Suite of Interactive Tools: The Lunar Mapping and Modeling Portal provides a web-based Portal and a suite of interactive visualization and analysis tools enabling mission planners, lunar scientists, and engineers to access mapped lunar data products from past and current lunar missions. LMMP is an integral project of NASA's Solar System Exploration Research Virtual Institute, with development done at NASA's Jet Propulsion Laboratory. While emphasizing mission planning, LMMP also addresses the lunar science community, the lunar commercial community, education and public outreach (E/PO), and anyone else interested in accessing or utilizing lunar data. Its visualization and analysis tools allow users to perform analysis such as lighting and local hazard assessments including slope, surface roughness and crater/boulder distribution. Originally designed as a mission planning tool for the Constellation Program, LMMP has grown into a generalized

suite of tools facilitating a wide range of activities including the planning, design, development, test and operations associated with lunar sortie missions; robotic (and potentially crewed) operations on the surface; planning tasks in the areas of landing site evaluation and selection; design and placement of landers and other stationary assets; design of rovers and other mobile assets; developing terrain-relative navigation (TRN) capabilities; deorbit/impact site visualization; and assessment and planning of science traverses.

Significant advantages are afforded by LMMP's features facilitating collaboration among members of distributed teams (e.g., mission planning team, mission proposal team). Team members can share visualizations and add new data to be shared either with the entire LMMP community or only with members of their own team. Sharing of multi-layered visualizations is made easy with the ability to create and distribute LMMP's digital bookmarks.

Current data products include image mosaics, digital elevation models, local hazard assessment tools (such as maps of slope, surface roughness and crater/boulder distribution), lighting assessment tools, gravity models, and resource maps such as soil maturity and hydrogen abundance.

LMMP fosters outreach, education, and exploration of the Moon by educators, students, amateur astronomers, and the general public. It has been designated by NASA as a component of its Science Education Infrastructure. While great utility is provided by LMMP's interface and tools, it also provides particular value through its ability to serve data to a variety of other applications. In the outreach realm, this has been demonstrated with data served to planetariums and NASA's Eyes on the Solar System.

New Features and Coming Enhancements: A number of new products have been added. From LRO's LOLA instrument, we have added a Polar 10m/p DEM, Slope Map, Roughness Map, and Permanently Shadowed Regions Map. From LRO's Diviner instrument, we have added the CF Composition Map (updated from the previous 2011 version), Thermal Map, and Rock Abundance Map. From LRO's Mini-RF comes the new North and South Polar Mosaics including CPR, Colorized CPR, and First Stokes Parameter. Data from Kaguya includes TC Ortho Mosaic as well as the LOLA and TC Stereo DEM Merge. New data products, particularly for polar regions, will continue to be added.

Users can now draw a bounding box around any surface feature and generate an STL file for use with 3D printers. New enhancements are also being made to hazard analysis tools. Looking further ahead, we are working on automated traverse planning tools, developing plans to facilitate examining surface temperatures as a function of time, and are collaborating with Bill Farrell and the DREAM2 SSERVI team to plan a Surface Potential Analysis Tool. We will collaborate with the NASA Astromaterials Acquisition and Curation Office to integrate with their Lunar Apollo Sample database in order to help better visualize the geographic contexts from which samples were retrieved. All of this will be done within the framework of a new user interface which, among other improvements, will provide significantly enhanced 3D visualizations and navigation.

Summary and Conclusions: NASA's Lunar Mapping and Modeling Portal has grown considerably over the past year. Its new features make it especially useful for the planning of a new generation of lunar exploration missions, conducting a wide range of lunar science research, and facilitating exciting visualizations and exploration in the realms of education and outreach. The user community is invited to provide suggestions and requests as the development team continues to expand the capabilities of LMMP and the range of data products that it provides.

Acknowledgements: The authors would like to thank the the Planetary Science Division of NASA's Science Mission Directorate and the Advanced Explorations Systems Program of NASA's Human Exploration Operations Directorate for their support and guidance in the continuing development of LMMP.

SOLVING COMMUNICATIONS AND NAVIGATION REQUIREMENTS FOR SMALL LUNAR MISSIONS. C. Saunders¹, J. Friend¹, M. Cosby², B. Hufenbach³, R. Fisackerly³, J. Carpenter³, ¹Surrey Satellite Technology Limited, Tycho House, 20 Stephenson Road, Surrey Research Park, Guildford GU2 7YE, United Kingdom, ²Goonhilly Earth Station Limited, Goonhilly Downs, Helston Cornwall, TR12 6LQ, United Kingdom, ³European Space Agency, Keplerlaan 1, 2201 AZ Noordwijk, Netherlands

Abstract: There is a growing need for space exploration to be performed at the lowest possible cost, and at the highest efficiency. The important supporting infrastructure of exploration can be performed by commercial industry, allowing space agencies to focus their budgets in cutting edge technology development and science. Surrey Satellite Technology Limited (SSTL) and Goonhilly Earth Station (GES) – in partnership with the European Space Agency (ESA) - are currently planning the implementation of a commercial service partnership that will provide future lunar missions (both orbiting and landed on the surface) with communications relay and navigation signals. This will enable greater utilization of missions, reduction in mission costs, enable exploration of the far side of the moon and increase the safety of future manned missions. Nano satellites, and other small assets deployed in-situ, will, in particular, benefit from a provided communications service as it will allow their on-board systems to be minimized and data throughput to be maximized.

An initial Lunar Communications Pathfinder Mission is proposed that will demonstrate the technologies, operations and preliminary services that will be a first step towards a fully operational lunar communications and navigation system. The pathfinder spacecraft will deliver a host of customer assets (e.g. Nano satellites to lunar orbit, micro-penetrators to the lunar surface) where they will form an initial user base for the communications system. The communications element of the satellite will provide data relay services between a dedicated ground segment and multiple lunar assets. Users will be able to command and receive data from their lunar assets via an internet based interface removing the need to set up their own ground station. Opportunities to demonstrate critical technologies for exploration will be available.

The system is being designed to be compatible with other planned lunar assets (e.g. space agency missions and Google Lunar X-prize) with a view to offering back-up or supplementary communications services. International communications protocols (e.g. Consultative Committee on Space Data Systems (CCSDS) “Proximity-1”) will be used to enable interoperability and cross-support between different assets.

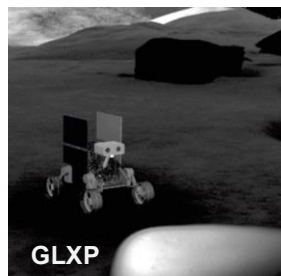
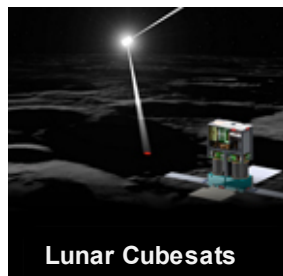
The pathfinder mission is based around flight systems currently being built by SSTL for terrestrial

communications companies, and existing large communications antenna owned and managed by GES. This approach minimises risk and non-recurring costs. The mission will be financed by selling customer payload ‘slots’ to parties around the world, and aims to bring lunar missions within budget levels of emerging space nations, universities consortia and small companies. This mission will provide a service that will be open to any customers with missions in cis-lunar space so that the progress of lunar science and exploration can be accelerated.

SMALL MISSION CHALLENGES AND DEVELOPMENTS IN ADVANCE OF A LUNAR VILLAGE.N.Ghafoor¹, H.Jones¹, J.Hackett¹, J.Newman¹, L.Stras¹, P.Visscher², D.Wooley², P.Edmunson², M.Picard³.¹ Canadensys Aerospace Corporation (Toronto, ON, Canada, nadeem.ghafoor@canadensys.com), ² Ontario Drive & Gear (New Hamburg, ON, Canada), ³ Canadian Space Agency (St-Hubert, QC, Canada)

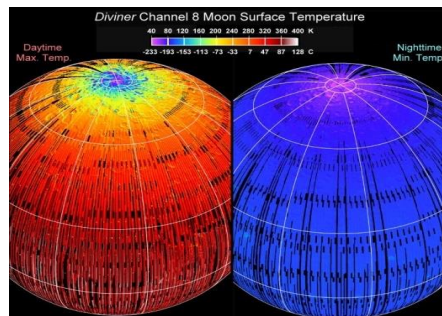
Overview: This presentation reflects on key challenges facing small mission elements within a future lunar polar surface architecture (or so called Moon Village), and summarizes a number of Canadian development activities aimed at addressing these issues.

A new exploration era: The world is changing rapidly and recent years have witnessed marked growth in global efforts to extend some of the micro-space approaches and technologies that have so transformed EO and Sat Com, to missions beyond earth orbit and similarly revolutionize space exploration. With spacecraft technologies available in ever smaller packages and hosted payload options ever more prevalent, small platforms may make an increasing contribution to exploration architectures – scientifically, technologically and commercially. The first wave of small spacecraft exploration missions are already in the build phase for orbital destinations (e.g. NASA’s cubesats) while the first private initiatives are targeting short-duration surface missions (e.g. GLXP). As plans for a lunar surface architecture (or so called Moon Village) unfold over the coming decade, small mission elements will likely have matured to the point of being valuable contributors in a number of areas.



Small missions, big challenges: At the same time, significant challenges remain. Next generation small missions target more remote destinations, more challenging environments, greater unknowns, longer durations and / or more ambitious in situ capabilities than ever before, all under the tighter resource constraints associated with smaller, lower cost missions. Success will likely demand a combination of state of the art technology advancement, close consideration of the target environment and careful, clever system design to eke out the maximum possible performance from subsystem combinations pushed to their limit.

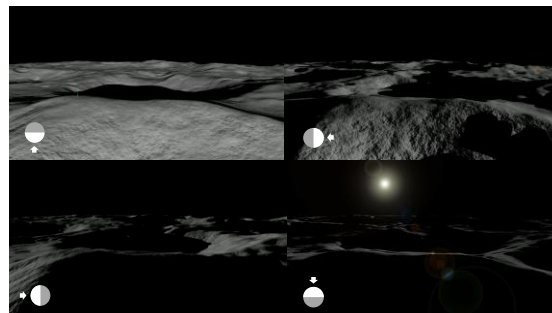
Technology preparations: This presentation reflects on key challenges facing micro and nano missions to the lunar polar region, and summarizes several development activities currently underway at Canadensys Aerospace in Toronto, Canada, in collaboration with the CSA and a number of partners.



Testing at Canadensys of a range of path-to-flight technologies under lunar thermal conditions is discussed, from lunar rover thermal control and energy storage devices for extended mission duration and/or lunar night survival, as well as a lunar rover drivetrain in collaboration with partner Ontario Drive & Gear.



Dynamic polar environment: Illumination at the lunar south pole is also a complex and dynamic environmental factor which strongly drives thermal, power and communications design, particularly for small systems. Modeling of these illumination conditions yields sobering insights into the challenge ahead, not only for these engineering parameters but also some of the more “social” elements of commercially targeted lunar initiatives.



Examples are presented, along with areas of ongoing development for the year ahead, and opportunities are highlighted for international collaboration.

A SILICON SEISMIC PACKAGE (SSP) FOR LUNAR SEISMOLOGY. W. T. Pike¹, S. Calcutt², I. M. Standley³, A. G. Mukherjee¹, J. Temple², T. Warren², C. Charalambous¹, Huafeng Liu¹, A. Stott¹ and J. B. McClean¹, ¹Department of Electrical and Electronic Engineering, Imperial College London, SW7 2AZ, United Kingdom. ²Atmospheric, Oceanic and Planetary Physics, Oxford University, OX1 3PU, United Kingdom. ³Kinematics Inc., 222 Vista Ave., Pasadena CA 91107, USA. w.t.pike@imperial.ac.uk.

Introduction: As part of the seismic payload for the InSight mission to Mars, a three-axis set of microseismometers, known as SP, was successfully delivered for launch in 2016 [1]. The three micromachined sensors are shown in fig. 1 prior to integration. These sensors are micromachined from single-crystal silicon by through-wafer deep reactive-ion etching to produce a suspension and proof mass with a fundamental vibrational mode of 6 Hz [2]. Bumpers resulting from the reflow of solder balls in cavities formed during the through-wafer etching protect the suspension from damage. The motion of the proof mass is sensed capacitively between an array of parallel electrodes on the proof mass and a matching fixed array on a glass strip separated by a fixed gap from the proof mass. The proof-mass electrodes are protected from damage by shock and vibration through a protective surface dielectric. The seismometer is robust to high shock (> 1000 g) and vibration (> 30 g rms), and the sensor is functional down to 77K, allowing deployment under much harsher conditions than expected for InSight. In addition, all three axes of the microseismometer deliver full performance over a tilt range of ± 15 degrees on Mars, allowing operation after deployment without levelling. The sensors are contained in three separate single-axis packages with a total mass of 460g, including cabling. The sensors operate in feedback with a separate associated electronics board located on the InSight lander with the feedback automatically initiated with power on of the electronics. The feedback-electronics board has a mass of 175g, giving a total mass of 635g for the three-axis SP delivery of packaged sensor heads, electronics board and associated connectors and cabling. The power requirement is 360 mW of which 30 mW is consumed in each sensor head. The performance of the vertical-axis InSight microseismometer is shown in fig. 2.

Development of SSP for lunar seismology: Following delivery, further development of microseismometer is being undertaken to further improve the performance for lunar deployment while maintaining the ease of deployment in terms of a both robustness and allowable tilt range. The lower gravity compared to Mars allows a lower resonant frequency to be employed. To achieve a noise floor at $1E-10m/s^2/rtHz$ the resonant frequency of the horizontal and vertical suspensions can be lowered from 6 to just over 1.5 Hz, improving the electronics displacement noise by a factor of 16 to 0.05 pm/rtHz.



25 mm

Figure 1 The microseismometer sensor set delivered for the InSight mission

For Mars the microseismometers were not evacuated. This greatly reduced risk and the stability of performance during the two-year nominal InSight mission duration. However, the ultimate performance of the current microseismometers is set by the thermal noise floor from gas damping within the package. The lunar environment reduces the risk of any leaks causing long-term degradation, and allows the SSP to take advantage of the much lower damping of an evacuated enclosure. The noise floor is now set by the intrinsic damping within the silicon suspension, increasing the Q factor of the suspension from 300 to more than 20,000, as measured by vibration measurements in an SEM [3].

With the reductions in the displacement transducer noise, as well as the thermal noise, our current noise model based on the achieved performance of the InSight microseismometers gives a predicted noise floor shown in fig. 2. This figure also shows the spectral amplitude of the seismic signals recorded by the Apollo seismometers [4]. With current performance we are already able to resolve larger marsquakes and meteorite impacts. With the SSP we aim to match the performance of the Apollo LP and SP seismometers in a single compact instrument.

In terms of mission architecture, the SSPs offer a number of advantages for a lunar deployment, either as a geophysics contribution to a single lander

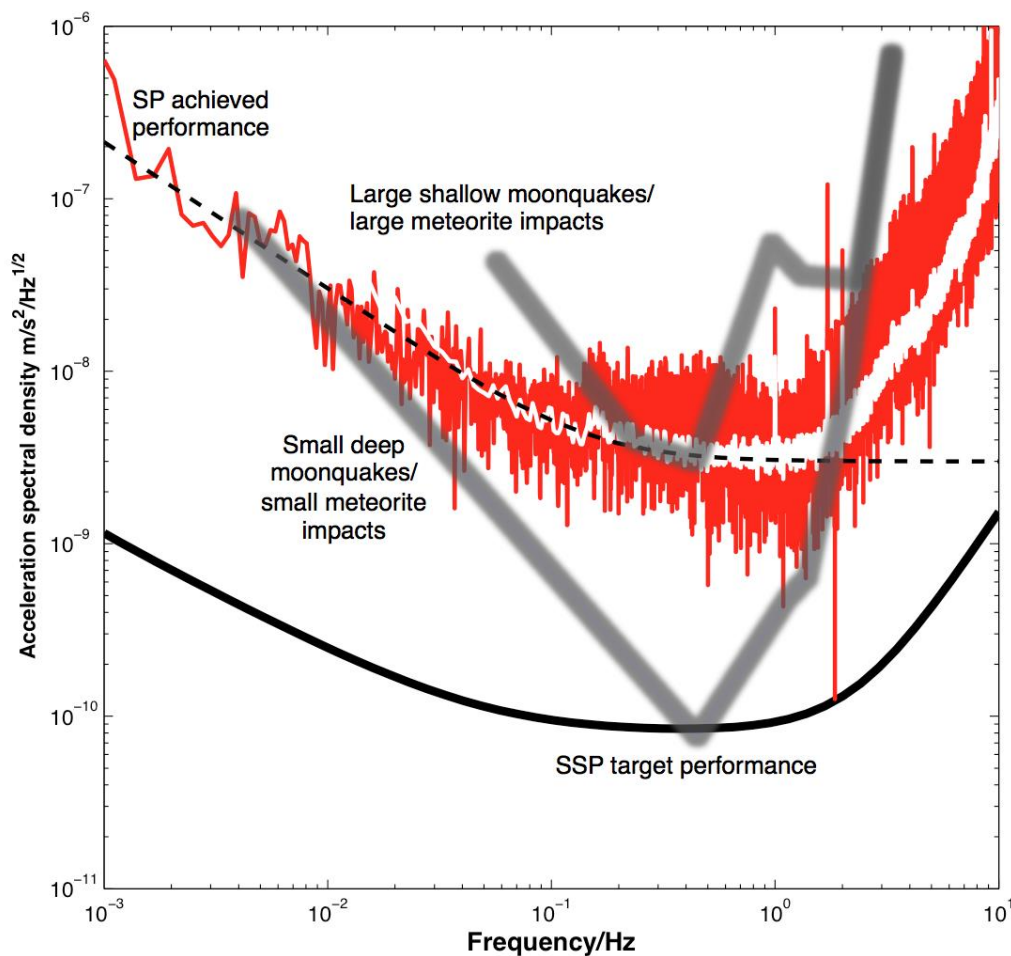


Figure 2 The measured spectral amplitude of the lunar seismic signals measured by Apollo compared to the performance of the InSight SP microseismometer, and the SSP target performance.

mission or as part of a network deployment. As the SSPs can operate over a large tilt range, no additional levelling mechanism is required. Their robustness allows sub-surface installation in high-shock deployments, reducing the need for thermal shielding. The large temperature range of operation obviates the need for keep-alive heating during the lunar night. In addition the microseismometers incorporate thermal compensation within their suspensions, allowing performance to be maintained in the presence of a varying temperature environment.

Conclusion: The microseismometers delivered to InSight have demonstrated that micromachined sensors are capable of achieving sub nano-g performance in a compact package. Development of this approach with an SSP offers new mission architectures for lunar seismology with no compromise in overall performance.

References:

- [1] The mission is now scheduled for a 2018 launch
- [2] Pike et al., IEEE Sensors 2014, pp1599-1602, 2014
- [3] Pike and Standley, J. Micromech. Microeng. **15** (2005) S82–S88
- [4] Nakamura et al. JGR. 87 (Supplement), 1982 A117–A123

RE-EXAMINATION OF APOLLO 17 LUNAR SEISMIC PROFILING EXPERIMENT DATA.

A. Czeluschke (alexandra.czeluschke@dlr.de)¹, M. Knapmeyer (martin.knapmeyer@dlr.de)¹, J. Oberst (juergen.oberst@dlr.de)^{1,2} and I. Haase (isabel.haase@tu-berlin.de)², ¹German Aerospace Center (DLR), Inst. of Planetary Research, Berlin, Germany), ²Technical University Berlin, Inst. for Geodesy and Geoinformation Sciences, Germany

Introduction: We use restored seismic data streams of the Apollo 17 Lunar Seismic Profiling Experiment (LSPE) and a Wiener filtering approach to take new travel time readings for seismic p-waves. The combined use of the new travel times readings and geometrically accurate positions of the seismic equipment derived from high-resolution pictures taken by the Lunar Reconnaissance Orbiter Camera (LROC) [1] leads to new estimates for the velocity-depth profiles beneath the Apollo 17 landing site in Taurus-Littrow valley.

Until now, only the positions of six of the eight Explosive Packages (EP) could be determined in the LROC-data. Hence, we limit our evaluations to the reduced data set of six detonations each recorded at four geophones, leading to an analysis of 24 individual seismograms in this study.

Evaluation of the data leads to either two- or three-layer models. Data points of the four closest detonations represent the uppermost layer in both cases. But depending on whether one fits the remaining two detonations together in one layer or separated in two layers leads to two- or three-layer models, respectively. We solve for thickness and seismic p-wave velocities of the layers.

Two-Layer Model: When using the old point distances published by Cooper et al. [2], the velocity of the uppermost layer can be calculated to 275 m/s and 790 m/s for the p-wave velocity of the layer below. The transition zone between the two layers is observed at a depth of 169 m.

When using the new LROC-derived coordinates, the results change slightly. The p-wave velocity of the uppermost layer rises to 285 m/s. In contrast, the velocity of the layer below decreases to a value of 775 m/s. The boundary between the two layers is almost at the same depth namely at 170 m.

Three-Layer Models: When we use the old Cooper point distances and solve for a three-layer model, we get p-wave velocities of 275, 876, and 2074 m/s for the uppermost, second, and third layer, respectively. The layer boundaries can be found at depths of 188 and 986 m. When changing over to new LROC-derived coordinates, the velocity of the first layer slightly rises to 285 m/s, whereas the velocities of the layers below decrease to values of 580 and 1825 m/s. The transitions between the layers can be found at the lowered depths of 96 and 773 m.

Discussion: The uncertainties in the experiment geometry led to a significant underestimation of the velocity gradient. Comparing the two- and three-

layer models shows that we can confirm a strong increase of seismic velocity with depth. Our new models show that the uppermost layers tend to be thinner and have lower velocities when changing over from old to new LROC-derived coordinates. Whereas as layers below tend to have higher p-wave velocities. Both leading to a more drastic increase of seismic velocity with depth compared to previous anal-

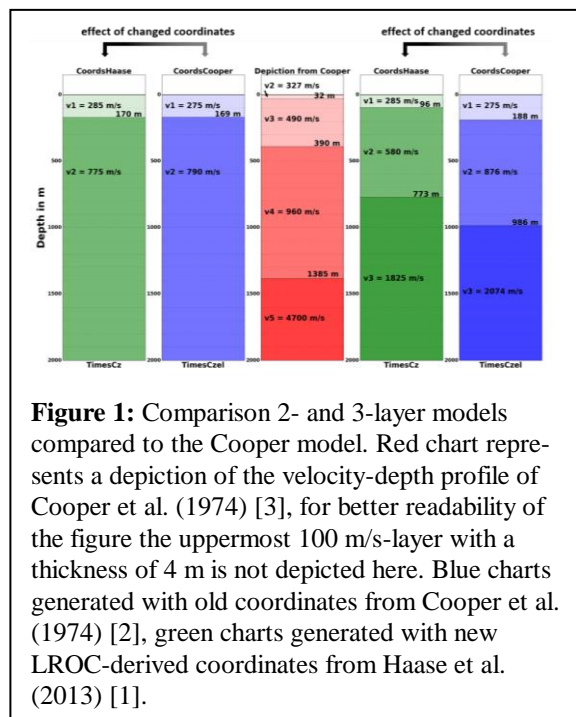


Figure 1: Comparison 2- and 3-layer models compared to the Cooper model. Red chart represents a depiction of the velocity-depth profile of Cooper et al. (1974) [3], for better readability of the figure the uppermost 100 m/s-layer with a thickness of 4 m is not depicted here. Blue charts generated with old coordinates from Cooper et al. (1974) [2], green charts generated with new LROC-derived coordinates from Haase et al. (2013) [1].

yses (Cooper et al., 1974, [3]).

The same trends can be observed when using old p-wave arrival times from Kovach [4] instead of the new p-wave arrival time readings from this study.

Acknowledgements: This study is supported by the Helmholtz Alliance “Robotic Exploration of Extreme Environments – ROBEX”, which aims at development of a new seismic experiment concept that can be conducted autonomously by robotic rovers on the Moon.

References: [1] I. Haase et al. (2013), LPSC XLIV, p. 1966 (abstract). [2] Cooper and Kovach (1975), Proc. Lunar Sci. Conf. 6th, 2863-2879. [3] Cooper and Kovach (1974) *Reviews of Geophysics and Space Physics*, Vol. 12, No. 3, 291-308. [4] R. Kovach (2015), from personal communication.

SCIENCE, DESIGN AND FLIGHT STATUS OF THE NEXT GENERATION RETROREFLECTOR

FOR LUNAR LASER RANGING: D. G. Currie^{1,2}, S. Dell'Agnello², R. D. Richards³, G. O. Delle Monache^{2,1}, B. B. Behr¹, I. Prochazka⁴, F. Hofmann⁵, J. Müller⁵, L. Biskupek⁵, M. Maiello², A. Boni², S. Berardi², C. Cantone², N. Intaglietta², C. Lops², M. Garattini², M. Martini², G. Patrizi², L. Porcelli², M. Tibuzzi², R. Vittori⁶, G. Bianco⁷, A. Coradini⁸, C. Dionisio⁹, R. March^{2, 10}, G. Bellettini^{2, 10}, R. Tauraso^{2, 10}, J. Chandler¹¹.

¹University of Maryland, John S. Toll Building, Regents Drive, College Park, MD 20742-4111, USA (currie@umd.edu), ²INFN–Laboratori Nazionali di Frascati (LNF), Via E. Fermi 40, Frascati (Rome) 00046, Italy

(simone.dellagnello@lnf.infn.it, dellemon@lnf.infn.it, Mauro.Maiello@lnf.infn.it, Alessandro.boni@lnf.infn.it, [Berardi, S.](mailto:Berardi.S@lnf.infn.it); claudio.cantone@lnf.infn.it, Nicola.Intaglietta@lnf.infn.it, Caterina.Lops@lnf.infn.it, [Garattini, M.](mailto:Garattini.M@lnf.infn.it), Manuele.Martini@lnf.infn.it, Giordano.Patrizi@lnf.infn.it, luca.porcelli@lnf.infn.it, mattia.tibuzzi@lnf.infn.it, Stefania.Contessa@lnf.infn.it, chiara.mondaini@lnf.infn.it, lorenzo.salvatori@lnf.infn.it, luca.porcelli@lnf.infn.it, Emanuele.Ciocci@lnf.infn.it, paolo.tuscano@lnf.infn.it, jchandler@cfa.harvard.edu)

³Moon Express, Inc. NASA Research Park PO Box 309. Moffett Field, CA 94035. (bob@moonexpress.com),

⁴Czech Technical University in Prague, Czech Republic (ivan.prochazka@fjfi.cvut.cz), ⁵Institut fuer Erdmessung, Leibniz Universitaet Hannover, Hannover, Germany (hofmann@ife.uni-hannover.de, mueller@mbox.ife.uni-hannover.de, biskupek@ife.uni-hannover.de)

⁶Aeronautica Militare Italiana (AMI), Rome, Italy), (roberto.vittori@esteri.it)

⁷ASI-Centro di Geodesia Spaziale, Matera, Italy, (giuseppe.bianco@asi.it)

⁸INAF-Istituto di Fisica dello Spazio Interplanetario (IFSI), Via Fosso del Cavaliere 100, 00133 Rome, Italy), G.;

Coradini ⁹INFN-LNF and CNR-Istituto per le Applicazioni del Calcolo (IAC), Viale del Policlinico 137, 00161 Rome, Italy), . Dionisio, C ¹⁰Department of Mathematics, University of Rome 'Tor Vergata', Via della Ricerca Scientifica, 00133 Rome, Italy, (riccardo.march@gmail.com, tauraso@mat.uniroma2.it, bellettini@mat.uniroma2.it)

¹¹Harvard-Smithsonian Center for Astrophysics, USA) (jchandler@cfa.harvard.edu)

Introduction: The retroreflectors deployed during the Apollo Missions [1] are still operating after 45 years. Scientific analysis [2] of this long record of ranging data has resulted in the discovery and measurement of the liquid core of the moon about 15 years ago [3]. This lunar laser ranging (LLR) program has also produced most of the best tests of Gravitation and General Relativity [4]. However, over the years the ground stations have improved their range accuracy by a factor of ~200 so today the limit in ranging accuracy is due to the combination of the libration of the moon and the design of the Cube Corner Reflector (CCR) arrays. To address this, the University of Maryland, College Park (UMCP) and the INFN–Laboratori Nazionali di Frascati (INFN–LNF) are developing the Next Generation Retroreflectors (NGR), also known as the Lunar Laser Ranging Retroreflector for the 21st Century [5] and/or MoonLIGHT. Recently the UMCP and the INFN-LNF have signed an agreement with Moon Express, Inc. [6], a commercial company pursuing the Google Lunar X Prize [7] and a space transport business, to deploy four NGRs on the lunar surface. The first of which is expected to fly in the second quarter of 2017. A brief discussion will address the expected improvements in the understanding of Gravitational and General Relativity and the impact this may have on the multiple theories that have been proposed to explain Dark Matter and Dark Energy.

The basic objectives, requirements and design will be reviewed. In particular, in order to maintain a signal level similar to that of Apollo 15, thermal gradients within the CCR must be maintained to less than

0.2°K. Since, during lunar morning, the CCR is at about 70°K and the housing is more than 300°K, the thermal design is critical. The structure and results of the required simulation programs will be reviewed. Finally, the current design of the entire package will be addressed.

Looking toward the future, two areas look particularly interesting in extending the investigation of the theories of Gravitation, General Relativity, Dark Matter and Dark Energy. The NGRs will support even greater ranging accuracy, the addition of additional ground stations and increased coverage. The first future direction is to provide a system that is not reliant on the location and orientation of the lander. This would consist of a system that, immediately after deployment, would detect the location of the earth, point toward the proper direction and then permanently lock to that pointing. The second future direction is to ameliorate the vertical motion of the lander and regolith due to the thermal expansion from lunar night to lunar day. This would take advantage of the thermal stability found about one meter in depth in the regolith.

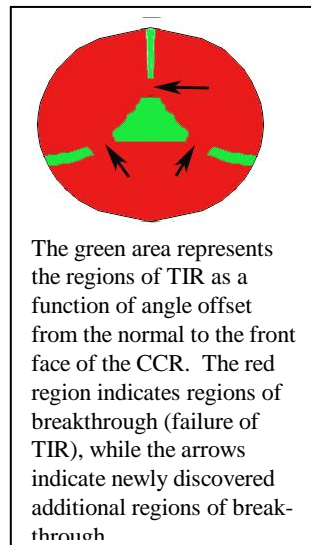
Topics to Be Addressed: Since the last discussion of the status of the NGR, there have been very significant steps in advancing to the deployment of the NGRs in the near future. The various aspects of these advances will next be briefly reviewed. In particular:

Moon Express Agreement for Deployment. In Frascati, Italy at the last meeting of the International

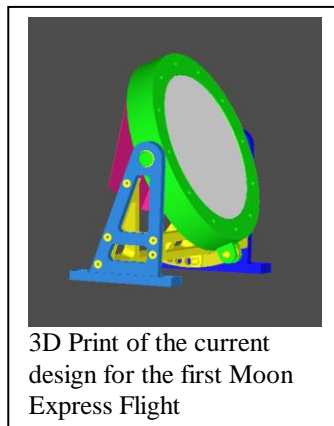
Laser Ranging Service, an agreement [8] was signed with Moon Express by the INFN-LNF of Italy and University of Maryland, College Park of the USA for the deployment of the NGRs on the first four flights of Moon Express's landers. The first of these deployments is expected in the second quarter of 2017.

Science Simulations for NGR. In particular, the effects of the improved accuracy coupled with an increased number of ground stations with limited operational conditions, the possible effects of marginal NGR designs and limited ranging opportunities has been investigated [9].

New Total Internal Reflection Break-Through. This addresses the discovery of a new CCR behaviour relating to the properties of Total Internal Reflection (TIR) [10]. There are additional portions of the lunar cycle, beyond the current understanding, during which solar radiation breaks through the TIR. This heats the housing which significantly affects thermal performance.



Current NGR De-



sign and Thermal Coatings.

Development of NGR design and thermal coatings to provide high (approximately at the Apollo 15) level of return signal through a full lunation. This has required an extensive set of programs for the simulation of

the wavelength dependent absorption of the solar radiation in the CCR, the solar input to the housing, the radiation exchanges with the regolith and space, all varying through-out the lunation. The figure illustrates the current design that has been the result.

Ultimate Ranging Accuracy Limitations. Theoretical and observational studies indicate that at the current level of modelling of the earth's atmosphere, the atmosphere will limit the accuracy of the range measurements to a level of 1 or 2 millimetres [11].

Plans for NGR Pointed System. The current design relies upon the lander achieving the specified azimuthal orientation and landing on a relatively level region. The "pointed" system to address this dependency will be discussed. The referenced video [12] illustrates the pointing procedure of one type of pointed system.

Plans for Next Generation Deployment. In the situation of mounting of the NGR on a lander, the temperature change from lunar day to lunar night implies that there is a vertical motion of 1 to a few millimetres, depending on the lander design. To address this, an "anchored" deployment has been investigated and a conceptual design for such a system [13] has been developed.

Conclusion: The deployment of a Next Generation Retroreflector to significantly improve our knowledge of the lunar interior, Gravitation and General Relativity seems to be achievable with a transport by the Moon Express Corporation. This will allow addressing the theories being presented to describe Dark Matter [14] and Dark Energy [15].

References:

- [1] Alley C. O. Chang R. F. Currie D. G. et al. (1970) *Science*, 167, 368-370. [2] Bender, P. L. Currie D. G. et al. (1973) *Science*, 182, 229-238. [3] Williams J.G. et al. (2001) *J. Geophys. Res. Planets* 106, 27933-27968 [4] Williams J. G. et al. (1996), *Physical Review D (Particles, Fields, Gravitation, and Cosmology)*, 53, 6730-6739. [5] Currie D. G. Dell'Agnello S. (2013) *Nuclear Physics B Proceedings Supplements*, 243, 218-228. [6] Moon Express: <http://moonexpress.com/>. [7] Google Lunar X Prize <http://lunar.xprize.org/> [8] www.physics.umd.edu/rgroups/am/Videos/Payload_Agreement_15_May_2015.pdf. [9] Hofmann F. Müller J. Biskupek L. and Currie D. EGU General Assembly (2014), 20140427 -> 20140502, ID#.3299. [10] Alley C. O. Chang R. F. Currie D. G.; et al. (1970) *Science*, 167, 368-370. [11] Currie D. G. and Ivan Prochazka (2014) *Proc. SPIE 9224, Laser Communication and Propagation through the Atmosphere and Oceans III*, [12] www.physics.umd.edu/rgroups/am/Videos/Pointing_Title_20121020.mp4. [13] Zacny K. Currie D. et al. (2012) *Planetary and Space Science*, 71, 131-141. [14] Hees, A. Famaey B. Angus G. W. Gentile, G. (2016) *MNRAS*, 455, 449-461 [15] Dvali G. Gruzinov, A. Zaldarriaga M. (2003) *Phys. Rev. D*, 68, ID. 024012

COMPLEXITIES OF LUNAR SOIL: NEED FOR PROPER SIMULANTS. Lawrence A. Taylor¹, Carle M. Pieters², and Daniel Britt³. ¹Planetary Geosciences Institute, Dept. of Earth and Planetary Sciences, University of Tennessee, Knoxville, TN 37996; lataylor@utk.edu; ²SSSERVI Evolution and Environment of Exploration Destinations (**SEED**); Dept. of Geological Sciences, Brown University, Providence, RI; ³Center for Lunar and Asteroid Surface Science (**CLASS**); Dept. of Physics, University of Central Florida, Orlando, FL, U.S.A.



Since man first set foot on the Moon, the desire to study the engineering properties of lunar regolith/soil has presented an enigma. With some 840 lbs of lunar samples, NASA has been reluctant to allocate much of these national treasures, in quantities suitable for the proposed studies, instead, suggesting use of lunar regolith simulants. In January 1971, enter Prof. Paul Weiblen with his Minnesota Lunar Simulant (MLS) and his key-chain lunar-simulant holders. This high-Ti diabase from Diluth, MN was the first simulant, ‘close’ in bulk composition to the high-Ti basalts and soils of Apollo 11. But, lunar soils contains some 40-50% of glassy agglutinates. Hence, the MLS simulant was dropped through a 750 K-Watt plasma furnace to melt the grains into glass, which was subsequently ground and became part of the MLS-1. This was lunar simulant No.1.

Fast-forward 40 years, to witness the use and abuse and mega-\$\$ spent making lunar simulants (Table 1) with improper physical/chemical properties and used wrongly (e.g., JSC-1A for hydrogen reduction of ilmenite). Finally in 2010, the Planetary Science Subcommittee (PSS) of the NASA Advisory Council (NAC) issued a request (Table 2) for a detailed study be performed and a report generated by the LEAG – CAPTEM Simulant Working Group.

This paper discusses and reviews the tasks put forth by the PSS, which include: 1) what is needed for lunar simulants; 2) what lunar simulants already exist; 3) protocols for their proper usage, and 4) needs for Apollo lunar samples. It is the unique properties that are most important.

Table 1.

LEAG-CAPTEM Simulant Working Group: **Larry Taylor**, (Chair), Univ. of Tenn., LADTAG, Lunar Soil Expert; **Jennifer Edmunson**, MSFC, Simulant Engr.; **Bob Ferl**, Univ. of FL, Bio Expert; **Bob Gustafson**, ORBITEC, Simulant Engr.; **Yang Liu**, Univ. of Tenn., Lunar Soil & Simulant Expert; **Gary Lofgren**, JSC, Lunar Sample Curator; **Carole McLemore**, MSFC, ISRU/Dust Project Mgr.; **Dave McKay**, JSC, LADTAG, Lunar Soil Expert (Dust/Biomedical); **Doug Rickman**, MSFC, Simulant developer and tester; **Jerry Sanders**, JSC, ISRU Head Honcho; **Mini Wadhwa**, CAPTEM Chair; **Chip Shearer**, Ex-Officio; Chair of LEAG.

REFERENCES

- Kanamori, H. et al., 1998, Proc., Int. Symp. Space 98, ASCE, Reston, Va., 462–468.
- Li, Y., et al., 2008, J. Aerospace Engr., 22, 53-57.
- McKay, D. S., et al., 1994, in Engineering, Construc-tion, and Operations in Space IV, vol. 1, 857–866.
- Rahmatian, L., and Metzger, P., 2010, Earth Space 2010, p.239-253. doi: 10.1061/41096(366)25.
- Richard, J., et al., 2007, Lunar Dust/Regolith Simulant, MSFC Workshop.
- Stoeser, D., & Wilson, S., 2007, Lunar Dust/Regolith Simulant Workshop, http://isru.msfc.nasa.gov/2007wksp_docs.html.
- Taylor, L.A., Pieters, C.M., and Britt, D., 2016, Evaluation of Lunar Regolith Simulants. Planet. Space Sci., in press.
- Taylor, P.T., 2008, LPI Contr. 1415, Abstr. 2054.
- Weiblen, P.W., et al., 1990, Space II, ASCE, 98 – 106.
- Zheng, Y., et al., 2008, Advances in Space Research, 43, 448-454.

Table 1. List of Lunar Regolith (Soil) Simulants and their purposes (up to 2011).

LUNAR REGOLITH SIMULANTS WORLDWIDE	Type
MLS-1* <u>M</u>innesota <u>L</u>unar <u>S</u>imulant Weiblen et al., 1990	High-Ilmenite mare (general use)
MLS-1P* Weiblen et al., 1990	High-Ti mare (exper., not in bulk)
MLS-2*	Highlands (general use)
ALS Arizona Lunar Simulant	Low-Ti Mare (geotechnical)
JSC-1* <u>J</u>ohnson <u>S</u>pace <u>C</u>enter, McKay et al., 1994	Low-Ti mare (general use)
FJS-1 (type 1) <u>F</u>uji Japanese <u>S</u>imulant Kanamori et al., 1998	Low-Ti mare
FJS-1 (type 2)	Low-Ti mare
FJS-1 (type 3)	High-Ti mare
MKS-1 MSFC	Low-Ti mare (intended use unknown)
JSC-1A, -1AF anonymous, undated, http://www.orbitec.com/store JSC-1A-Bulk-Data-Characterization.pdf	Low-Ti mare (general use) (JSC-1A produced from same source)
OB-1 Olivine-Bytownite Richard et al., 2007	Highlands (general use geotechnical)
CHENOBI undocumented, see http://www.evcltd.com/ index.html	Highlands (geotechnical)
CAS-1 Zheng et al., 2008	Low-Ti mare (general use)
GCA-1 Goddard Space Center Taylor et al., 2008	Low-Ti mare (geotechnical)
NU-LHT-1M & 1D NASA/USGS-Lunar Highlands Stoesser 2007	Highlands (general use)
NU-LHT-2M & 2C Stoesser et al., 2007	Highlands (general use)
Oshima base simulant	High-Ti mare (general use)
Kohyama base simulant	Intermediate; highlands & mare
NAO-1 Li et al., 2008	Highlands (general use)
CLRS-1 Chinese Lunar Reg. Sim., Chinese Acad. of Sciences	Low-Ti mare (general use?)
CLRS-2 Chinese Academy of Sciences	High-Ti mare (general use?)
CUG-1 Chinese Academy of Sciences	Low-Ti mare (geotechnical)
GRC-1 & -3 Glenn Research Center	Geotech. std. vehicle mobility simulant
TJ-1 Tongji University	Low-Ti mare (geotechnical)
TJ-2	
KOHL-1 Koh Lunar Simulant	Low-Ti mare (geotechnical)
BP-1 Black Point, Rahmatian & Metzger, 2010	Low-Ti mare (geotechnical)
CSM-CL Colorado School of Mines – Colorado Lava -	Geotechnical

SOLAR 3D PRINTING OF LUNAR REGOLITH. Alexandre Meurisse¹, Aidan Cowley², Samantha Cristoforetti², Advenit Makaya³, Laurent Pambaguian³ and Matthias Sperl¹, ¹Institut für Materialphysik im Weltraum, Deutsches Zentrum für Luft- und Raumfahrt, 51170 Köln, Germany (alexandre.meurisse@dlr.de), ²ESA-EAC, 51170 Köln, Germany, ³ESA-ESTEC, 2201 AZ Noordwijk, Netherlands.

Introduction: In-Situ Resource Utilization (ISRU) has become in the last decades one of the most prominent approaches for the building of a settlement on the Moon. The use of local resources to reduce up-mass, cost and risk of mission is now an essential consideration in future exploration scenarios. Within this trend, lunar regolith, the loose layer of crushed rock covering the Moon surface, has a key role to play. Its high metallic oxides content could offer a sustainable way of producing oxygen and it could also be used as a construction material via, for instance, a sintering process. By means of solar concentration [1], microwaves [2] or radial heating elements [3], this process would create solid building elements that could be used for roads, launch pads or habitats.

Additive manufacturing (AM) technology, commonly called 3D-printing, is widely used on Earth. Building parts layer by layer allows the realization of complex shapes, does not create wasted material and requires low post-processing work. The shift from casting to AM in aerospace and automotive industries shows the leading place given today to such technology. AM in microgravity has already been used in space since 2014 with a first polymer 3D printer on-board the International Space Station (ISS).

Combining AM with ISRU offers a way of building-up a permanent lunar outpost with a limited amount of upload from Earth. Proof of concepts using lunar regolith as main building material were given with the contour crafting [4] and D-shape approaches[5]. Both technologies create a mixture similar to concrete with the lunar soil and terrestrial consumable materials. Making any large-scale construction is therefore dependent on Earth shipments which is not viable for long term missions. In this work we demonstrate how, only using concentrated sunlight, we can 3D print a solid material from lunar regolith.

Background: Potential landing sites for first, lunar landers and then, the settlement of a Moon village are located at the lunar South Pole region, near the Shackleton crater, where continuous illumination during several months exists [6]. Long-term missions are indeed essentially limited to locations with favourable illumination for power generation thus adding interest to the use of the numerous hours of sunshine for other purposes.

Results: In the DLR solar oven, a custom solar 3D printer was constructed capable of sintering building elements using only lunar regolith simulants and concentrated sunlight. The realisation of a brick, Figure 1, has proven the concept, opening the path to further improvements and more challenging constructions designs.



Figure 1: Brick of size 240mm x 120mm x 30 mm produced from custom 3D printing protocol at DLR's solar oven in Cologne. Support is made from a porous silica brick and JSC-2A is used as lunar simulant.

References:

- [1] Hintze P. et al. (2009), *47th AIAA ASM*, 1015.
- [2] Taylor L. A. and Meek T. T. (2005) *JAE*, 18, 3, 188–196.
- [3] Gualtieri T., and Bandyopadhyay A. (2015) *ML*, 143, 276–278.
- [4] Khoshnevis, Behrokh, et al. (2005), *43rd AIAA ASM*.
- [5] Cesaretti G. et al. (2014), *Acta Astronautica*, 93, 430–450.
- [6] Diego DeRosa et al. (2012), *Planetary and Space Science*, 74, 224–246.

WALKING ON THE MOON. I.L. Schlacht¹, J. Rittweger², B. Foing³, M. Daumer⁴, M. Masali⁵. ¹Politecnico di Milano and Karlsruhe Institute of Technology (irene.schlacht@polimi.it; Kandelstr.8, Karlsruhe, Germany), ² German Aerospace Center (DLR) (joern.rittweger@dlr.de, Kologne, Germany), ³ILEWG&ESA ESTEC (bernard.foing@esa.int; Noordwijk, The Netherlands), ⁴Human Motion Institute (daumer@slcmr.org; Munchen, Germany), ⁵Università di Torino (melchiorre.masali@gmail.com; Turin, Italy).

Introduction: A specific aspect of interaction on the Moon here approached is how the crew will walk inside and outside the habitat.

Mission Simulation: How high do we jump on the Moon? Should we build architecture with steps or should we support climbing? The hypogravity will lead to vestibular system malfunction, loss of muscular mass, and stiffness of the legs, negatively affecting a person's balance: Yes, we can climb, but we can also easily lose our balance and trip up.



Fig. 1. Apollo astronaut tripping © NASA (Image elaboration Schlacht and Umhof)

To avoid all of this, we need to better understand gait and balance on the Moon. This research will investigate a methodology that focuses on the collection of basic anthropometrical and postural data needed to develop interfaces for the Moon and Mars gravity environments and habitat.

The experiment: Walking on the Moon is an experiment that aims to measure the walking pattern of astronauts during EVA (Extra vehicular activity) and IVA (Intra-Vehicular Activity). It is developed with the support of German Aerospace Center (DLR), International Lunar Exploration Working Group (ILEWG), Politecnico di Milano (POLIMI) and Karlsruhe Institute of Technology (KIT).

On the Moon, it is very important to avoid tripping by increasing one's balance in order to assure the safety required in those extreme contexts. Balance is a factor that depends on many variables, such as: visual field, sensorimotor system, vestibular system. These variables are all affected by the different environmental constraints of Moon and Mars environments [1, 2, 3, 4].

Methods: The Walking on the Moon experiment will address the walking pattern and balance by measuring the biomechanical variables of the gait that impact an astronaut's balance during Moon and Mars missions.

To simulate the same conditions of a Moon/Mars mission, we need: partial gravity achieved with a vertical treadmill, deconditioning achieved with bedrest, and artificial gravity (AG) as physiological countermeasures.

Subjects who will undergo three different conditions will be compared (parallel-group design): sixty days of -6° head down tilt bedrest only (Control group), 60-day head down tilt with continuous AG, and with intermittent AG. The data collected will be kinematographic and biomechanical data during walking and running in simulated hypogravity with a vertical treadmill.

On the vertical treadmill, the subjects will be suspended by a belt system to simulate different degrees of hypogravity. An accelerometer will measure speed, step extent, direction of movement, variation of altitude, typology of walk, and balance. The recording of video data will support the research of the line of sight to derive the vestibular plane direction.

The data will be collected three times: at the baseline, a few days after 60d of bedrest, and after recovery. Finally with a debriefing the all crew together will discuss problem and solution, this will produce qualitative data for the improvement of walk pattern and balance.

Additional research: Another methodology that will be analyzed consists of the utilization of the swimming pool of the Neutral Buoyancy Facility at the European Astronaut Centre (ESA). By using a combination of distributed mechanical loads on different parts of a subject's body (and, possibly, floaters to optimize the application point of the resultant force), a realistic reduced gravity effect can be obtained to simulate and analyze Moon and Mars walking pattern.

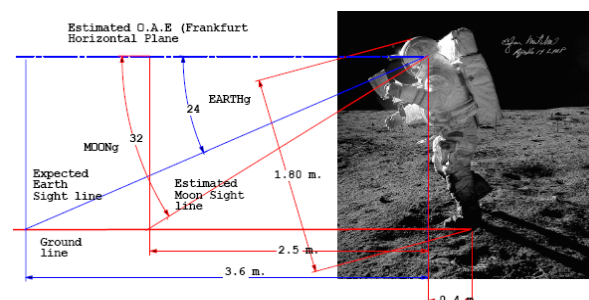


Fig. 2. Interpretation of Moon walking posture and sight-line image. Apollo 14, 1971 © NASA & M. Masali.

Conclusion: This research will address balance and deconditioning, for the first time getting much closer to the real conditions that will affect astronauts during Moon and Mars missions.

Authors. Dr. Schlacht, principal investigator and human factors field expert and coordinator of ex-

treme-design research group; Prof. Rittweger, head of the Space Physiology division of the German Aerospace Center and manager of the vertical treadmill; Prof. Foing, director of the International Lunar Exploration Working Group and scientific reviewer of the project; Prof. Daumer (and team), scientific director of the Human Motion Institute and coordinator of the data collection and analysis of the accelerometer, and Prof. Masali (and team), who has 50 years of field specialization in space anthropometry and who will support the video data analysis of the walking patterns and vestibular visual guidance.

References:

- [1] NASA (2004). Vestibular System in Space.
http://www.nasa.gov/audience/forstudents/9-12/features/F_Human_Vestibular_System_in_Space.html
- [2] Kanas N., Manzey, D., (2008). Space Psychology and Psychiatry. Springer
- [3] Clément (2005) Effects of Microgravity on the Human Organism, Springer
- [4] Rittweger, J. (2016). Communication at the Analogue Study workshop. ESA-EAC 15.2.2016

INTEGRATING REMOTE SENSING OBSERVATIONS TO ASSESS THE DIVERSITY OF INTRUSIVE MAGMATISM ON THE MOON. R. L. Klima^{1*}, J. T. S. Cahill¹, B. T. Greenhagen¹, J. J. Hagerty², P. N. Peplowski¹, D. J. Lawrence¹, ¹Johns Hopkins University Applied Physics Laboratory, Laurel, MD 20723, USA; ²USGS Astrogeology Science Center, Flagstaff, AZ, USA. *Rachel.Klima@jhuapl.edu.

Introduction: Combination of multiple remote sensing techniques affords the possibility to characterize both bulk mineralogy and abundance of some minor elements from orbit. Although in many cases there are large differences in spatial resolution between high energy analysis techniques (e.g., X-Ray, gamma ray, neutron spectroscopy) and lower energy solar reflectance and thermal emission spectroscopy, the spatial resolution of these techniques can be improved by using other data sets to forward model the lower resolution data [e.g., 1-2] or spatial deconvolution methods using the spatial response function of an instrument coupled with its statistical uncertainty [3]. Together, these data sets can provide critical insight into the geographical distribution and diversity of magmatic processes on the Moon. To explore this diversity, we use data from the Moon Mineralogy Mapper (M³), Diviner Lunar Radiometer (Diviner) and Lunar Prospector Gamma Ray Spectrometer (LPGRS) and Neutron Spectrometer (LPNS) to examine the relationships between major mineralogy and the thorium and hydroxyl (OH⁻) abundances at several locations across the Moon where plutonic rocks have been excavated.

Background and Motivation: Recent studies of water in lunar samples suggest a complicated history of water in the lunar interior. Though originally believed to be quite dry, analyses of lunar glasses [e.g., 4-5] and apatites [e.g. 6-9] suggest that at least some reservoirs may contain water at abundances similar to the mantle source of the Mid Ocean-Ridge Basalts on Earth. Because the Moon is mineralogically dominated by anorthite, olivine, and pyroxene, none of which incorporate large amounts of OH⁻ into their mineral structures, water present in the lunar magma ocean should have been concentrated with other incompatible elements urKREEP, the liquid that carried the potassium, rare earth element and phosphate (KREEP) geochemical signature measured in many lunar samples. However, the majority of analyses suggest an anticorrelation between the KREEP signature and OH⁻ abundance [e.g., 9]. This implies not only that the lunar mantle is heterogeneous but also that somehow water has been decoupled from other incompatible elements.

While clearly not of the same precision as laboratory data, orbital data can provide additional constraints about the global distribution and diversity of incompatible elements on the Moon. Characterization of absolute OH⁻ abundance from orbit is complicated by surficial adsorbed OH⁻, likely produced by interaction of solar wind hydrogen with minerals on the sur-

face [e.g., 10]. However, regions that are enhanced in OH⁻ relative to their surrounding have been reported for both intrusive [11] and extrusive [12-13] lithologies. In the case of Bullialdus crater [11] and Compton-Belkovich [12], the enhanced OH⁻ coincides with relative enhancements in thorium as detected by the Lunar Prospector (in the case of Compton-Belkovich, thorium levels may be the highest on all of the Moon)[1]. These findings suggest that the rocks within Bullialdus crater and Compton Belkovich likely contain a large amount of potassium, rare earth elements, and phosphorus (KREEP) [11-12], contrary to what has been observed in OH⁻-enriched returned lunar samples.

M³ Data Analysis: The M³ was a visible-near infrared imaging spectrometer flown by NASA as a guest instrument on India's lunar mission Chandrayaan-1 [14]. In global mode, data were obtained at 140 m/pixel spatial resolution while the spacecraft was in a 100 km orbit, and at 280 m/pixel while it was in a 200 km orbit. Spectral channels in global mode are binned to a 20-40 nm spectral sampling, with higher spectral resolution covering the 1000 nm region so that mafic absorptions due to olivine and pyroxene can be more accurately measured. Unfortunately, before launch, water/hydroxyl was not anticipated to be a major component of the global lunar surface, so data in the 3000 nm range are binned to a 40 nm resolution, complicating analysis of this feature.

Regional Comparisons: We focus here on comparing the Aristarchus and Aristillus regions with Bullialdus crater, as they are both enhanced in thorium and located at moderate lunar latitudes. This comparison helps to mitigate interference with surficial hydroxyl/water adsorption.

An image matrix depicting different measurements of the Bullialdus (20.7°N, 22.2°W), Aristillus (33.9°N, 1.2°E) and Aristarchus (23.7°N, 47.4°W) craters is presented in Fig. 1. Morphologically and mineralogically, Aristillus is more similar to Bullialdus than is Aristarchus. Both Bullialdus and Aristillus central peaks are dominated by norite, though orthopyroxene at Aristillus is modeled to be more iron-rich than that at Bullialdus [15]. The thorium anomaly over Aristillus (~12ppm) is stronger than in the Bullialdus region (~6-8ppm) [1]. Unlike Bullialdus, however, there is no hydroxyl anomaly associated with Aristillus crater. This suggests that Aristillus central peak may have excavated material more similar to alkali-suite norites found in the Apollo collection. At Aristarchus, a larger variety of minerals

are excavated [16]. The southern rim of Aristarchus is slightly enhanced in hydroxyl, and this enrichment seems to be associated with predominately anorthositic and olivine-rich material. The diffuse nature of this enrichment makes it difficult to distinguish whether it is intrinsic to the local rocks, or a later accumulation of surface hydroxyl adsorbed to the southern portion of the crater.

Summary and Future Work: Combined studies of thorium abundance, mineralogy, and hydroxyl abundance provide a powerful method to probe the composition of the lunar crust. We are expanding this study and beginning to incorporate further constraints using Diviner composition data and LPNS neutron measurements.

Acknowledgements: We thank NASA/SSERVI for supporting this research. We are also grateful to

the NASA Discovery Program, LRO, ISRO, and the M³ team.

References: [1] Lawrence, D. J. et al., 2003, *JGR*, 108, 5102. [2] Hagerty, J. J. et al. (2006) *JGR*, 111, E06002. [3] Lawrence D. J. et al. (2007) *GRL*, 34, L03201. [4] A. E. Saal et al. (2008) *Nature*, 454, 192. [5] E. H. Hauri et al. (2011) *Science*, 333, 213. [6] F. M. McCubbin et al. (2010) *PNAS*, 107, 11223. [7] Anand, M. (2010) *Earth Moon Planets*, 107, 65. [8] Boyce et al. (2010) *Nature*, 466, 7536. [9] McCubbin et al. (2015) *Am. Mineral.*, 100, 1668. [10] C. M. Pieters et al. (2009) *Science*, 326, 568. [11] Klima et al. (2013) *Nat. Geosci.*, 6, 737. [12] Petro et al. (2013) *LPSC*, 44, 2688. [13] Li and Milliken (2014) *LPSC*, 45, 2012. [14] Green et al., 2011, *JGR*, 116, E00G19. [15] Klima et al., 2011, *JGR*, 116, E00G06. [16] Mustard et al., 2011, *JGR*, 116, E00G12.

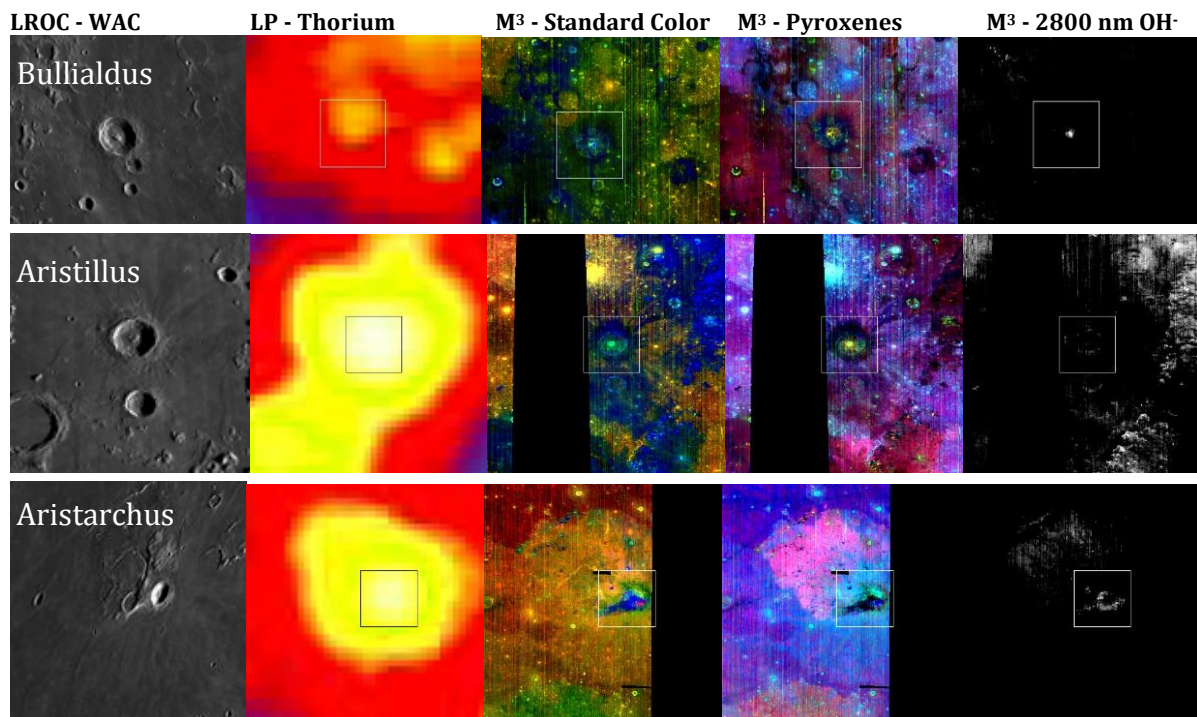


Fig. 1. Comparison of three craters with thorium anomalies (top-Bullialdus; middle-Aristillus; and bottom-Aristarchus). The left column presents a context image of the region, extracted from the Wide-Angle Camera (WAC) mosaic of the lunar nearside, produced by the Lunar Reconnaissance Orbiter Camera (LROC) team (credit: NASA/GSFC/Arizona State University). The second column presents the thorium abundance as measured by LPGRS (modified from Lawrence et al. [1]). The third column presents the standard M³ color composite, where the integrated 1000 nm band depth is displayed in the red channel, the integrated 2000 nm band depth is displayed in the green channel, and the reflectance at 1500 nm is displayed in the blue channel. In this depiction, olivine-enriched deposits appear as red or pink, orthopyroxene and noritic materials generally appear as cyan, clinopyroxenes or pyroxene mixtures appear as oranges and yellows, and anorthosite appears as blue. In the fourth column, a color composite that is designed to highlight the differences in pyroxene mineralogy is presented. The red channel displays the 1900 nm band depth, the green channel displays the integrated 2000 nm band depth, and the blue channel displays the 1000 nm band depth. In this depiction, featureless spectra (both anorthosite-dominated and very optically mature) appear as black, olivine-enriched material appears as deep blue, clinopyroxene-rich material appears as cyan, and orthopyroxene dominated material appears as yellow. Soils with a small component of orthopyroxene as well as pyroclastic glasses appear as pink. The fifth column depicts the continuum-removed 'hydroxyl' band depth at 2800 nm.

CHARACTERIZING THE LUNAR CRUST-MANTLE TRANSITION WITH THE MOON MINERALOGY MAPPER (M³). M. Martinot^{1,2}, J. Flahaut², S. Besse³, J.-F. Blanchette-Guertin⁴, C. Quantin² and W. van Westrenen¹, ¹Vrije University Amsterdam, De Boelelaan 1085, 1081 HV Amsterdam (m.martinot@vu.nl), ²Université Lyon 1, ENS-Lyon, CNRS, UMR 5276 LGL-TPE, F-69622, Villeurbanne, France, ³European Space Astronomy Centre (ESAC), P.O. Box 78, 28691 Villanueva de la Canada, Madrid, Spain, ⁴IPGP, 75013 Paris, France.

Introduction: Studies of the lunar crust composition, its lateral and vertical heterogeneities are crucial to constrain the magmatic and thermal evolution of the Moon [e.g., 1]. This survey aims to evaluate the lunar crust organisation and compositional variations around the crust-mantle boundary at a global scale. Here, the reflectance data of the Moon Mineralogy Mapper (M³) are used to study the composition of a pre-selection of 10 craters central peaks scattered on the lunar surface, which are supposed to excavate material from this region.

M³ is a hyperspectral imager that orbited the Moon between 2008 and 2009, with a spatial resolution of 140 m/pixel or 280 m/pixel, and a spectral range spanning from 430 to 3000 nm with 85 spectral channels [2].

The mineralogy of the central peaks extracted from the M³ analysis will be analysed with other datasets to provide information about the peaks' morphology (LROC images) and topography (LOLA data). This method will be applied to a wider selection of craters in the near future.

Approach: The craters were selected based on several criteria: (1) a good spectral coverage with M³ data, (2) the presence of a central peak or a peak ring, (3) a proximity value to the crust-mantle interface between +10 and -10 km, as calculated and presented in [3], using GRAIL crustal thickness models. **Table 1** shows the proximity value to the crust-mantle interface as calculated for Humboldt crater.

We have developed a custom-made routine that automatically removes a linear continuum on the M³ reflectance spectra and defines spectral parameters to allow for a mineralogical survey at a large scale (band centre, band area, band depth, etc.) as detailed in [4].

Table 1: Humboldt crater proximity value to the crust-mantle interface.

Humboldt crater	GRAIL crust thickness models			
	M1	M2	M3	M4
Proximity value (km)	-1.2	-0.4	7.4	7.3

Preliminary results: **Fig. 1-a)** shows a M³ reflectance data mosaic of Humboldt crater. The central peak is made of several mounds about 7 km wide, surrounded by floor fractures extending until the crater rim. **Fig. 1-b)** shows a RGB composite of Humboldt crater central peak with spectral parameters calculated by our custom-made routine. This

colour composite highlights plagioclase in blue, olivine in red and orange glass from pale blue to green. Fractures are highly shadowed; therefore, their reflectance signature should not be regarded. **Fig. 2** shows the spectra extracted from the central peak RGB composite. There is evidence of plagioclase (orange star in **Fig. 1-b**, orange spectrum in **Fig. 2**), and orange glass with a 1 micron absorption band shifted towards longer wavelengths compared to pyroxenes, and a 2 micron absorption band shifter to shorter wavelength [5] (white star in **Fig. 1-b**, black spectrum in **Fig. 2**).

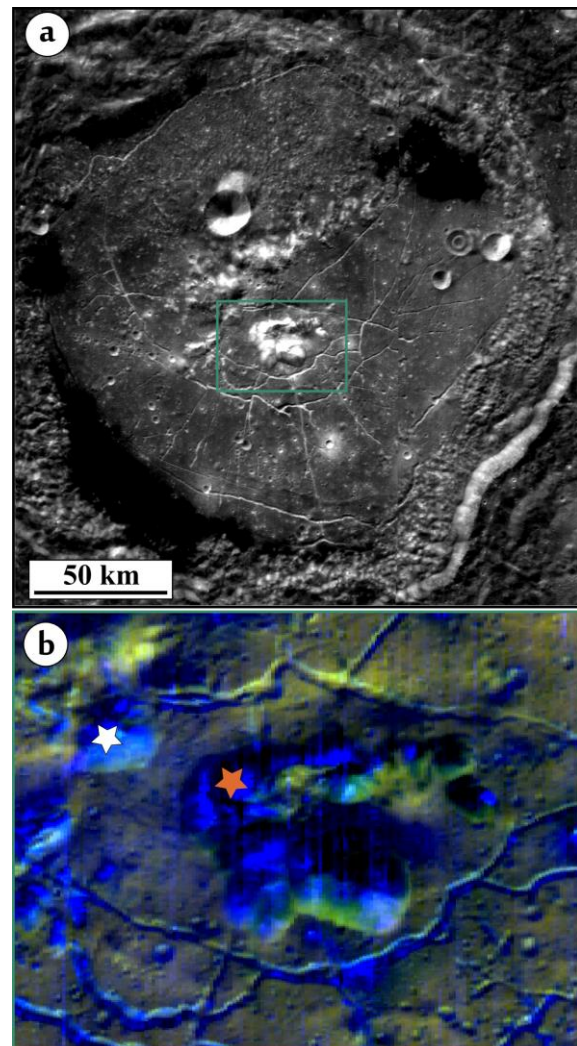


Fig. 1 : (a) M³ 1580 nm reflectance data mosaic of Humboldt crater; (b) Humboldt crater central peak RGB colour composite of M³ spectral parameters (rectangle in a). R = integrated 1 μm band depth; G = integrated 2 μm band depth; B = 1.25 μm band depth.

Discussion: According to the proximity values to the crust-mantle interface calculated from GRAIL crust thickness models 1 and 2, Humboldt crater could sample mantle material (negative value). Inversely, the proximity values calculated from GRAIL crust thickness models 3 and 4 indicate that Humboldt crater should sample only lower crust material (positive value). Humboldt crater central peak is mostly composed of plagioclase, and there are some occurrences of orange glass. The presence of abundant plagioclase corroborates a crustal origin of the central peak, consistently with models 3 and 4. Moreover, Christiansen Feature values derived from the Diviner dataset in Humboldt crater's central peak are more consistent with an anorthositic composition than with a mafic composition [6].

Perspectives: Humboldt crater displays a mineralogy that is rich in plagioclase, consistent with a crustal origin. No trend can be inferred with this observation alone. More craters around Humboldt crater should be studied in order to extract a regional and/or global pattern, if existing, but also draw conclusions on the mineralogy of the crust-mantle interface and the validity of the various GRAIL models.

References: [1] Shearer C.K. *et al.* (2006) *Reviews in Mineralogy and Geochemistry*, 60, 365–518. [2] Pieters C.M. *et al.* (2009) *Science*, 326, 568–572. [3] Martinot M. *et al.* (2015) *EPSC*, Abstract #446. [4] Martinot *et al.* (2016) *LPSC ILVII*, Abstract #1970. [5] Besse *et al.* (2014), *JGR*, 119, 1–20. [6] Song *et al.* (2013), *JGR*, 118, 689–707.

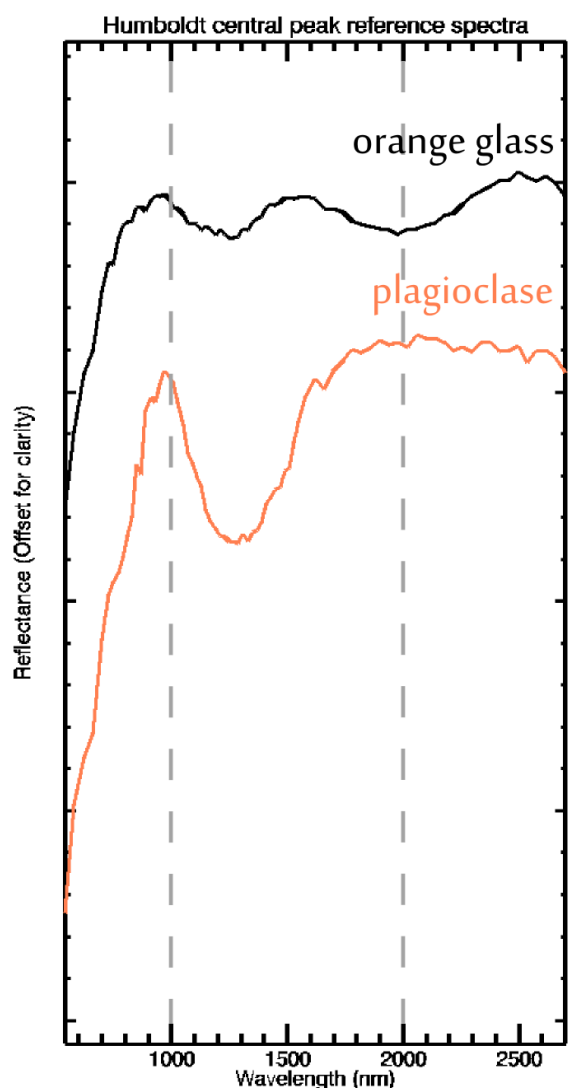


Fig. 2 : Mean spectra (7x7 pixels) are extracted from pixels of interest (star symbols in **Fig. 1**) in order to get a good mean signature. These spectra result of the automatic processing (see [3] for more details on the code).

RELATIVE AGES OF GRABEN AND WRINKLE RIDGES ON THE NEAR SIDE OF THE MOON REVEAL CONTRADICTORY RELATIONSHIPS. A. L. Nahm¹, A.-K. Dudde², and E. Hauber¹, ¹Institut für Planetenforschung, German Aerospace Center (DLR), Rutherfordst. 2, 12489 Berlin, Germany, amanda.nahm@dlr.de, ernst.hauber@dlr.de; ²Nelson Mandela School, Pfalzburger Str. 30, 10717 Berlin, annakatharinadudde@yahoo.com.

Introduction: Crosscutting relationships are used to determine the relative ages of geologic units or structures such as faults. Understanding the relative ages of events is critical to understanding the geologic history of a region or a planetary body. Understanding the tectonic history of the Moon, particularly the timing of fault formation, provides crucial constraints on the evolution and sources of stress.

Tectonic activity on the Moon is exhibited by three morphologies: graben, wrinkle ridges (WR), and lobate scarps. Contractual deformation, likely from global contraction and mare subsidence, is hypothesized to postdate extensional deformation, effectively ‘shutting off’ normal faulting on the Moon [e.g., 1, 2]. The current understanding of lunar tectonics indicates that graben formation/extensional deformation ceased around 3.6 Ga [3], though the individual normal fault known as Rupes Recta formed ≤ 3.2 Ga [4]. In contrast, contractual deformation in the form of wrinkle ridges and lobate scarps appears to have continued until ~ 1.2 Ga [2] and < 1 Ga [e.g., 2, 5, 6].

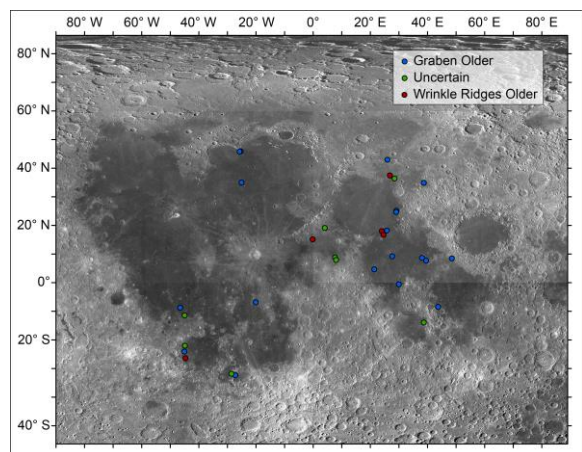


Fig. 1. Map of locations of identified crosscutting relationships listed in Table 1. Basemap is Lunar Reconnaissance Orbiter (LRO) Wide Angle Camera (WAC) mosaic, 100 m/px (http://wms.lroc.asu.edu/lroc/view_rdr/WAC_GLOBAL).

Based on this information, crosscutting relationships between wrinkle ridges and graben are expected to consistently show graben to be older than wrinkle ridges. However, rare crosscutting relationships indicate that wrinkle ridges are both older [e.g., 7] and younger than the graben [1]. Unfortunately, no list or compilation of the locations of these crosscutting relationships exists in the literature against which the timing can be compared. Thus, we have assembled locations of crosscutting relationships along with

interpretations of the sequence structural deformation (Fig. 1, Table 1).

Table 1. Catalog of observed crosscutting relationships between graben and wrinkle ridges.

Relationship Type	Approx. center long.	Approx. center lat.
Gaben older	-25.72	45.77
	-25.34	45.90
	-25.02	34.96
	26.05	42.91
	38.76	34.85
	29.07	24.66
	27.71	9.19
	38.14	8.63
	48.56	8.44
	39.53	7.68
	21.44	4.62
	-20.02	-6.88
	-46.49	-8.78
	-45.02	-24.14
	-27.18	-32.43
Uncertain	30.03	-0.60
	29.17	25.14
	25.87	18.19
	43.78	-8.53
	26.88	37.46
	28.53	36.36
	8.07	7.91
Wrinkle ridges older	7.70	8.75
	-44.91	-11.47
	-44.85	-22.06
	-28.58	-31.90
	38.76	-13.96
	4.13	19.11
-0.12	15.14	
-44.64	-26.40	
24.66	16.68	
24.04	17.98	
26.89	37.37	

Crosscutting relationship types: We have identified 3 types of crosscutting relationships: *graben older*, *wrinkle ridges older*, and *uncertain*. Examples of these relationship types are shown Fig. 2.

Discussion: The locations of 33 crosscutting interactions have been catalogued and are listed in Table 1. In general, $\sim 60\%$ of observed interactions show graben are older than wrinkle ridges, consistent with the summary given above. However, in five cas-

es, the wrinkle ridges appear to be older than the graben. Thus, graben and wrinkle ridge formation may have been contemporaneous for at least a portion of the geologic history of the Moon, or graben and wrinkle ridge formation were temporally distinct. This is supported by the timing of wrinkle ridge formation (ending ~1 Ga, but may have begun ~4 Ga [8, 9]), as well as the observations provided here. At the very least, these results indicate that the canonical view of lunar tectonics (that is, graben formed before wrinkle ridges) is overly simplistic and warrants a detailed investigation of these interesting structures.

of interactions between structures of interest. Basemap is LRO WAC mosaic, 100 m/px.

References: [1] Muehlberger, W. R. (1974) Proc. 5th Lunar Conf., 101-110. [2] Watters and Johnson (2010), in *Planetary Tectonics*, pp. 121-182, Cambridge Univ. Press. [3] Lucchitta and Watkins (1978), *Proc. Lunar Planet. Sci. Conf.* 9, 3459-3472. [4] Nahm and Schultz (2013), in: *Volcanism and Tectonism Across the Inner Solar System*, Geol. Soc., Lond., Sp. Pub. 401. [5] Watters et al. (2010) *Science*, 329, 936-940. [6] Clark et al., 2015, LPSC abstract #1730, LPSC 46. [7] Quaide, W. L. (1965), *Icarus*, 4, 374-389. [8] Hiesinger et al. (2000), *JGR*, 105, 29239-29276. [9] Hiesinger et al. (2003), *JGR*, 108, 5065.

Acknowledgements: ALN is supported by the Alexander von Humboldt Research Stiftung/Foundation. AKD performed this work at DLR during her 9th grade internship.

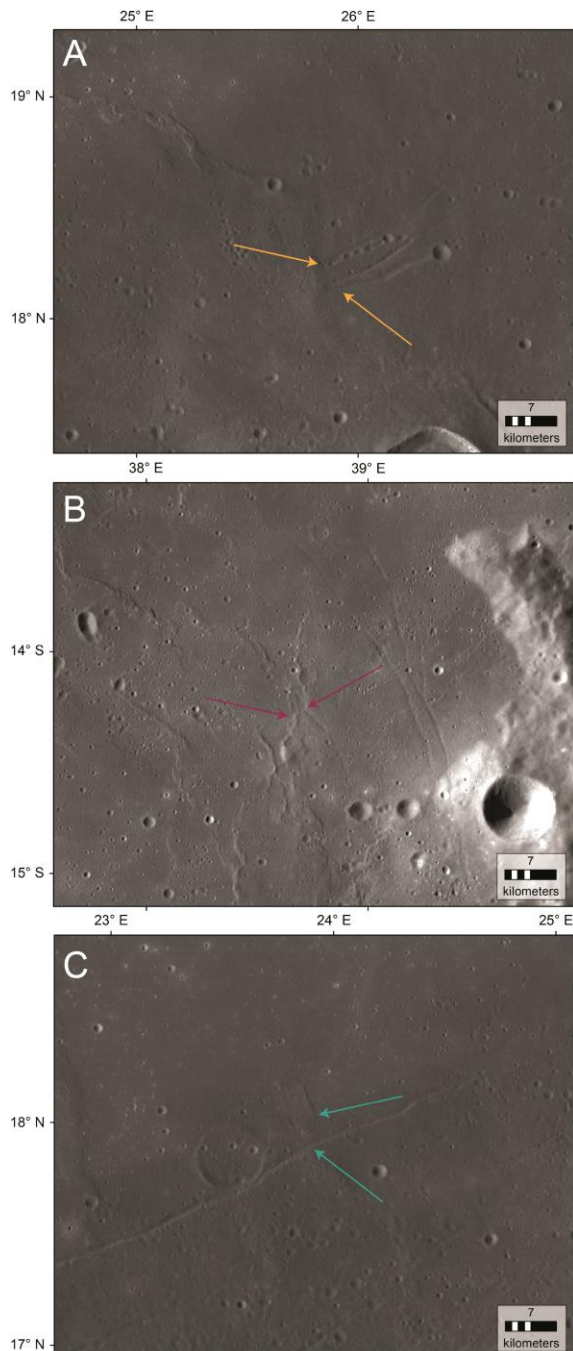


Fig. 2. Examples of crosscutting relationship types. A) Graben are older than the wrinkle ridge. B) Age relationship is uncertain. C) Graben is younger than the wrinkle ridge. Arrows denote locations

INVESTIGATION OF YOUNG (<100 MILLION YEARS) LUNAR SURFACE FEATURES: EVIDENCE FOR OUTGASSING OR BASALTIC VOLCANISM? K. L. Donaldson Hanna¹, J. Grice¹, R. Evans¹, N. E. Bowles¹, P. H. Schultz², C. M. Pieters², B. T. Greenhagen³, and K. A. Bennett⁴, ¹Atmospheric, Oceanic and Planetary Physics, University of Oxford, Clarendon Laboratory, Oxford, UK (Kerri.DonaldsonHanna@physics.ox.ac.uk), ²Dept. of Earth, Environmental and Planetary Sciences, Brown University, Providence, RI, USA, ³Johns Hopkins University Applied Physics Laboratory, Laurel, MD, USA, and ⁴School of Earth and Space Exploration, Arizona State University, Tempe, AZ, USA.

Introduction: Lunar-Orbiter/Apollo images and Clementine UVVIS observations identified four regions, including Ina, of small-scale, low relief patches of rubble with a maximum age of ~10 Ma [1]. Recent observations by the Lunar Reconnaissance Orbiter Camera (LROC) onboard NASA's Lunar Reconnaissance Orbiter (LRO) have expanded this list of unusual morphologic features by identifying similar features termed meniscus hollows [2] or irregular-bounded mare patches (IMPs) on the lunar near side with ages < 100 Ma [3]. The IMPs have two morphologically distinct deposits, uneven and smooth deposits [1-3]. The uneven deposits have a rough surface texture and contain a range of block densities, whereas the smooth deposits have a fairly uniform surface texture and almost no blocks. Most importantly, the boundary scarps have very low relief indicating recent formation. Two hypotheses for the origin of the irregular mare patches (IMPs) have been suggested: (1) recent, episodic outgassing from deep within the lunar interior [1] and (2) small basaltic eruptions that occurred after mare volcanism had ended [3].

These young morphologic features have implications for the cooling and volatile content of the lunar interior and/or may provide insight into the compositional evolution of magmatic materials over time. In this study we investigate the composition of the irregular mare patches in an effort to better understand the origin of these features. Compositional differences across each IMP as well as differences with surrounding mare materials are investigated using visible to near infrared (VNIR) observations from the Moon Mineralogy Mapper (M³) instrument and thermal infrared (TIR) observations from the Diviner Lunar Radiometer Experiment (Diviner).

Data and Methods: The focus of this initial

analysis is on the four largest IMPs, Sosigenes, Ina, Cauchy-5, and Maskelyne, as they are easily detected within the spatial footprints of M³ and Diviner. M³, an imaging spectrometer on-board the Chandrayaan-1 spacecraft, mapped the lunar surface across the VNIR (0.43-3.0 μ m) in 85 bands [4]. VNIR reflectance spectra of the lunar surface are typically dominated by absorption features near 1 and 2 μ m owing to the mafic minerals pyroxene and olivine. To investigate compositional differences between the IMPs and surrounding mare materials, spectral band parameters (band depths at 0.95 μ m and 2.3 μ m) were examined and reflectance spectra were extracted.

Diviner is a nine channel infrared filter radiometer with three narrow bands near 8 μ m used for mapping mineralogy (composition) [5,6]. Radiance data for Diviner bands 3, 4 and 5 are binned and averaged at 128 pixels per degree and then converted to three point emissivity spectra as described by Greenhagen et al. [6]. Diviner radiance data of the IMPs have been limited to lunar midday (10:00 to 14:00 local time) and emission angles < 5°. Diviner emissivity values are then corrected for local lunar time, latitude and topography to account for the effects of anisothermality [7]. The Christiansen feature (CF), an emissivity maximum indicative of composition [e.g. 8], is estimated by fitting a polynomial to each three point emissivity spectrum and identifying the wavelength of the maximum polynomial value. CF maps are made of each IMP region and 3-point emissivity spectra are extracted from the IMPs and surrounding mare materials.

Results: The M³ and Diviner observations of Ina are shown in Figures 1 and 2, respectively. The uneven deposits, the higher albedo regions around the edge of Ina, are less mature than the smooth deposits and surrounding mare and have stronger 1 and 2 μ m

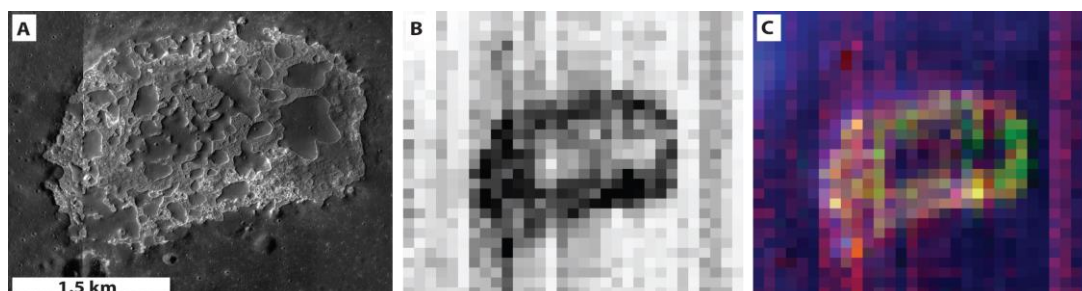


Figure 1. (A) LROC WAC and NAC mosaic of Ina. (B) M³ OMAT band parameter where black pixels indicate low values. (C) M³ band parameter map where red = 0.95 μ m BD, blue = 2.3 μ m BD, and green = reflectance at 1.578 μ m.

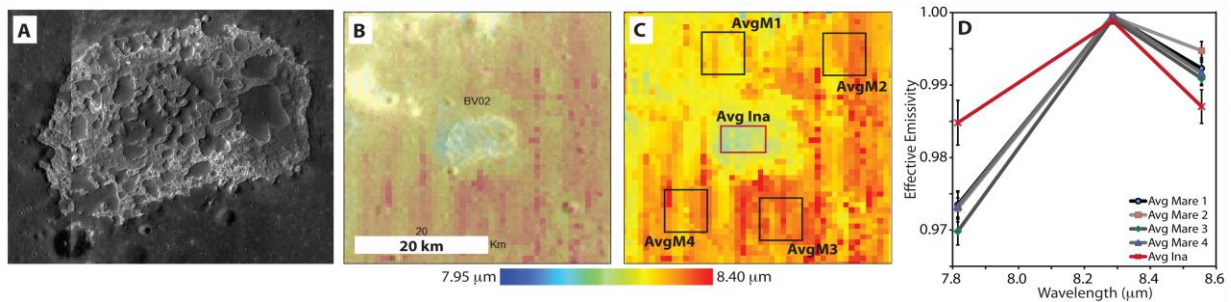


Figure 2. (A) LROC WAC and NAC mosaic of Ina. (B) Diviner CF map overlain on LROC WAC. (C) Diviner CF map indicating regions where spectra were extracted. (D) Average emissivity spectra for Ina as well as surrounding mare. The standard deviation is expressed as the y-error bars.

absorptions than the smooth deposits as seen in the M^3 band parameter map in Figure 1. Ina's smooth and uneven deposits are not similar in composition to mature soils and fresh craters in the surrounding mare except for one crater to the northwest of Ina. These results corroborate earlier spectral analyses of the uneven and smooth deposits in Ina [6,9,10].

Since the uneven and smooth deposits of Ina are difficult to uniquely distinguish from one another in the Diviner TIR observations (see Figure 2), an average Ina spectrum (including both uneven and smooth deposits) is compared to average spectra of the surrounding mare. Ina (uneven and smooth deposits combined) has a shorter CF position ($8.20 \pm 0.03 \mu\text{m}$) than the surrounding mare ($8.31 \pm 0.02 \mu\text{m}$) and has a flatter spectral slope between Diviner bands 3 and 4.

Discussion and Future Work: The VNIR investigation of the smooth and uneven deposits in Ina indicate that both units in each IMP have similar compositions, but with different degrees of space weathering. These spectral differences are likely due to the blockiness and exposure of fresh materials on the uneven deposits and the smooth surface texture and lack of boulders on the smooth deposits. Differences are seen in the spectral signatures of the Ina uneven and smooth deposits with surrounding mare material suggesting either (1) a change in magma composition over time or (2) the exposure of a mare flow below the most recent flow [1,9].

The TIR investigation of the smooth and uneven deposits in Ina indicates these units have CF positions at shorter wavelengths than the surrounding mare materials. This difference in CF position could be related to a change in composition [6,8], the degree of space weathering [11,12] and/or surface roughness effects. TIR laboratory measurements of augite (a high-Ca pyroxene found in basalts) under simulated lunar conditions found that the CF position was $8.46 \pm 0.02 \mu\text{m}$, which is longer than the $7.84 \pm 0.02 \mu\text{m}$ CF position for anorthite (a high-Ca plagioclase feldspar found in several lunar rock types) [13]. Thus the addition of more feldspathic material would shift the CF position to shorter wavelengths. Lucey et al. [11,12] has demonstrated that the Diviner TIR ob-

servations of immature locations like crater ejecta rays have CF positions at shorter wavelengths (by as much as $0.2 \mu\text{m}$) than the more mature surface locations the ejecta deposits are emplaced on. Thus, immature surface materials are expected to have CF positions at shorter wavelengths than mature surface materials of the same composition. The effects of large- and small-scale surface roughness on the CF position have yet to be quantified.

Future work will include more detailed spectral analyses on IMPs large enough to spatially resolve within the M^3 and Diviner datasets. This will allow us to better characterize the VNIR and TIR compositional trends within these features and constrain any compositional differences between the IMPs and their surrounding mare units. Combining VNIR and TIR data analyses will enable us to better constrain the origin and evolution of these young lunar features.

References: [1] Schultz P. H. et al. (2006) *Science*, 444, 184-186. [2] Stooke, P. J. (2012) *LPS XLIII*, Abstract # 1011. [3] Braden S. E. et al. (2014) *Nature Geosci.*, 7, doi:10.1038/NGEO2252. [4] Pieters C. M. et al. (2009) *Curr. Sci.*, 96, 500-505. [5] Paige D. A. et al. (2010) *Space Sci. Rev.*, 150, doi:10.1007/s11214-009-9529-2. [6] Greenhagen B. T. et al. (2010) *Science*, 329, doi:10.1126/science.1192196. [7] Greenhagen B. T. et al. (2011) *LPS XLII*, Abstract #2679. [8] Conel J. E. (1969) *JGR*, 74, 1614-1634. [9] Staid M. et al. (2011) *LPS XLII*, Abstract #2499. [10] Bennett K. A. et al. (2015) *LPS XLVI*, Abstract # 2646. [11] Lucey P. G. et al. (2010) *LPS XLI*, Abstract #1600. [12] Lucey P. G. et al. (2013) *LPS XLIV*, Abstract #2890. [13] Donaldson Hanna K. L. et al. (2012) *JGR*, 117, doi:10.1029/2011JE003862.

LUNAR RECONNAISSANCE ORBITER CAMERA: EXPLORING THE MOON. M. S. Robinson, Arizona State University, School of Earth and Space Exploration, Tempe AZ, USA, robinson@ser.asu.edu

Introduction: The Lunar Reconnaissance Orbiter (LRO) was conceived and designed to support a human return to the Moon [1]. That lofty goal required that the spacecraft acquire a diverse set of measurements to provide high-resolution maps of potential landing sites, an assessment of potentially valuable lunar resources, and a deeper understanding of radiation hazards future astronauts will face. In 2004 NASA requested proposals for instruments that could fill in the existing knowledge gaps enabling a safe and productive return to the Moon. After a competitive process, NASA selected six instruments for the LRO. During development a synthetic aperture radar system was added to the spacecraft [2].

The Lunar Reconnaissance Orbiter Camera (LROC) was selected as part of the payload and is composed of three cameras: two identical Narrow Angle Cameras (NAC), and one Wide Angle Camera (WAC) [3]. The three cameras are controlled with a small electronics assembly known as the Sequence and Compressor System (SCS). The LROC hardware was all designed and built by Malin Space Science Systems (MSSS), located in San Diego.

The original goals of the WAC were to map lighting conditions at the poles over a year and provide an accurate global cartographic base. It also was to map out color differences due to compositional variation across the globe, at moderate resolution. The original goals of the NAC were to investigate potential landing sites — both in terms of science return and engineering constraints — and to identify new impacts with before/after imaging [3].

The LRO was designed and built by the human exploration side of NASA (at the time Exploration Systems Management Directorate) and after the original Exploration Mission was completed LRO was turned over to the Science Management Directorate (SMD). This partnership between two directorates turned out to be highly beneficial to both sides and the LROC team understood the synergy from the beginning; “Scientia Facultas Explorationis, Exploratio Facultas Scientiae” (Science Enables Exploration, Exploration Enables Science) was adopted as the LROC operating motto [4] early in the development phase.

Wide Angle Camera: The WAC [3] acquires images in two ultraviolet (UV) colors (321 and 360 nm) and five visible colors (415 nm corresponding to violet-blue, 566 nm to green-yellow, 604 nm to orange, and 643 nm and 689 nm at the red end of the spectrum). The resolution is moderate, with 400 meter pixel scale in the UV and 100 meter pixel scale in the visible (from an altitude of 50 km). This softball-size camera maps the whole Moon every month, in stereo. These observations are the foundation for extremely accurate new global maps, a necessary tool for future explorers. These maps include monochrome versions at high Sun and low Sun, and 7-color renderings. Each global map requires mosaicking together about

10,000 individual WAC images, a complex task undertaken by the LROC team at the ASU Science Operations Center. Since the WAC field-of-view is 90°, there is quite a bit of distortion, especially at the edges of the images — a meticulous inflight characterization of the camera distortion from thousands of images near the poles (looking at areas of overlap) allowed for a geometric correction precise to one-tenth of a pixel (or better) [5]. The geometric correction and very accurate spacecraft tracking results in maps that are accurate to better than a half pixel (164 feet, or 50 meters).

A global WAC mosaic every month may seem repetitive or excessive. However, the data are not redundant — each month the lighting is different, so the WAC is building up the most comprehensive record of how varying light affects surface brightness ever acquired for any body in the solar system (outside of the Earth). From these multi-temporal observations photometric properties were derived leading to new insights into aspects of surface roughness and composition [6,7]. This advance translates not only to a better understanding of the lunar surface, but also to airless rocky bodies anywhere.

The repeat observations are more frequent near the poles, since LRO is in a low polar orbit it passes over each pole every 2 hours. From those passes, the LROC team created a time-lapse sequence showing regions that are in permanent shadow and other regions that are illuminated for extreme periods of time (such as mountain peaks near the poles). Both lighting extremes are potentially valuable to future explorers. Permanent shadows are extremely cold (<40K) and likely harbor deposits of ice. Areas in near-permanent illumination have stable temperatures and ready access to solar power [8].

Finally, this small camera enabled a near global topographic map of the Moon — with the exception of shadowed areas very near the poles — at a scale of 100 meters [9]. The fine pixel scale is possible because the topography is measured many times at each pixel. Since the uncertainties in the measurements are mostly random we can take the average of many estimates (on average more than 80) at that one pixel and derive a precise estimate of the elevation. Despite its diminutive size, the WAC can certainly be considered the little camera that can!

Narrow Angle Camera: The heart of each NAC [3] is a single row, or line array, of 4996 imaging pixels. The NACs build up a complete 2D image by taking advantage of the 1600 meter-per-second orbital velocity of the spacecraft. That single row of pixels is read out every 0.34 milliseconds 52,224 times (taking a total of about 18 seconds) to form a 4996 by 52,224 pixel image. Each “readout” results in one line of the image. Since the NACs almost always image simultaneously and their fields-of-view overlap about 100 pixels, we actually obtain a 9900

by 52,224 pixel image mosaic. Having two cameras also provides redundancy; if one failed we could still meet our requirements.

The NAC images reveal startling detail; hardware and astronaut tracks are discernible at all six Apollo landing sites. Due to variations in spacecraft altitude (25 km to 220 km), the nadir-observing NAC images have pixel scales ranging from 0.25 meters to 2.20 meters. In addition to the small pixel footprint, the NACs have an extended gray-scale dynamic range, recording more than 3200 shades of gray for each pixel. This extended range captures subtle changes in bright and dark areas within the same image, a critical consideration because the lunar surface has very high contrast in many areas. The combination of small pixel scale and extended dynamic range results in the exquisite detail seen in all the NAC images.

Conclusion: The LROC experiment is an overwhelming success. Its three cameras accomplished much more than the original objectives, and are still

enabling groundbreaking science as it continues mapping the Moon.

Scientific discoveries from the LROC images include new insights into the physics of impact-crater formation, discovery of very young volcanic features, confirmation that the Moon is shrinking, discovery of silicic volcanoes, a new understanding of how light interacts with the surface and much more.

References: [1] Mendell (2010), *Space Sci. Revs.* 150, pp. 3-6. [2] Vondrak et al (2010), *Space Sci. Revs.* 150, pp. 7-22. [3] Robinson et al., (2010) *Space Sci. Revs.* 150, pp. 81-124. [4] <http://lroc.sese.asu.edu/about/patch> [5] Speyerer et al. (2014) *Space Sci. Revs.*, doi:10.1007/s11214-014-0073-3. [6] Mahanti et al. (2015) *Space Sci. Revs.*, doi:10.1007/s11214-015-0197-0 [7] Sato et al. (2014) *JGR*, doi:10.1002/2013JE004580 [8] Speyerer et al. (2013) *Icarus*, doi:10.1016/j.icarus.2012.10.010 [9] Scholten et al. (2012), *JGR*, doi:10.1029/2011JE003926.

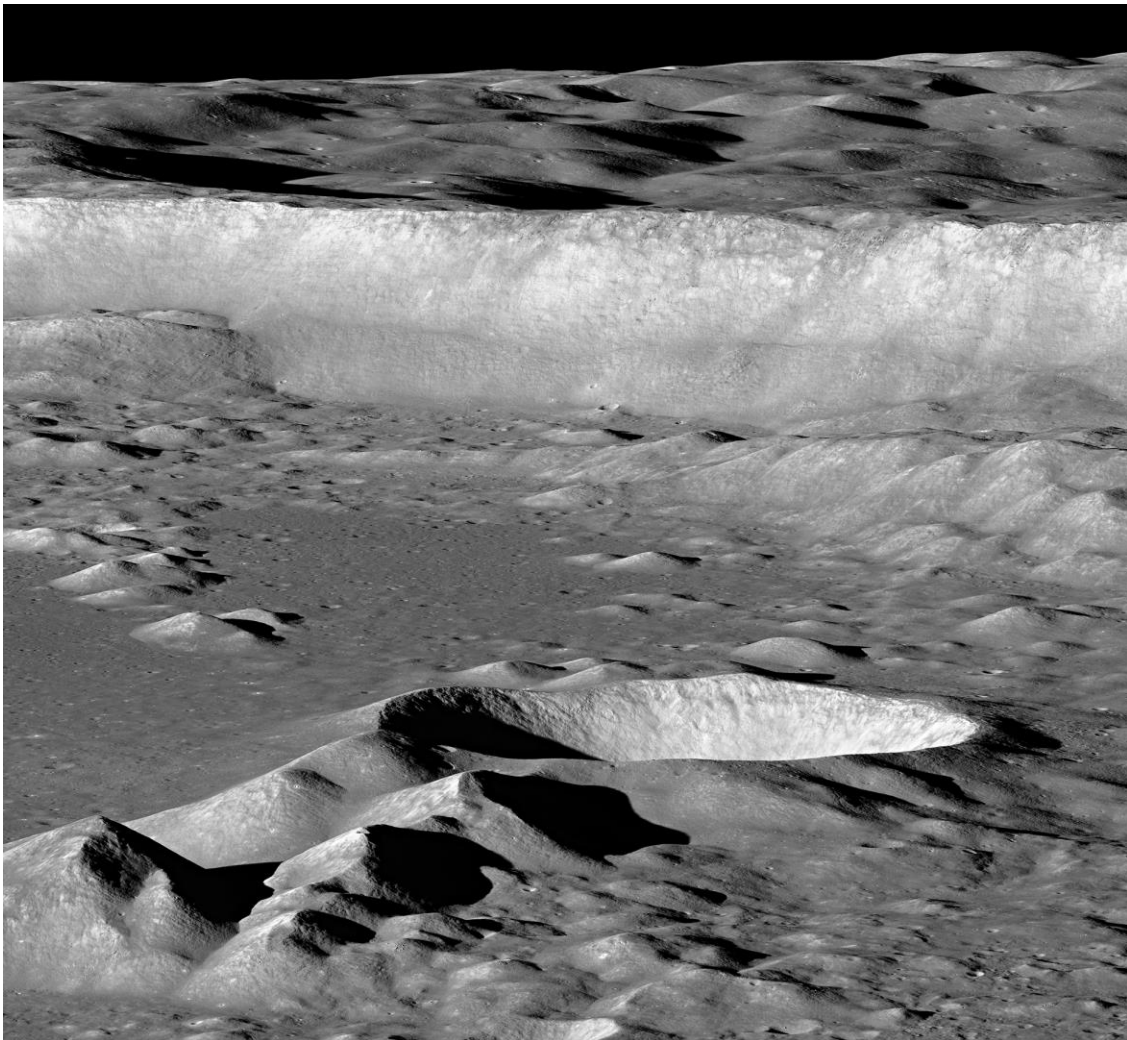


Figure 1: The 4000 m tall cliff in the background is the east wall of Antoniadi crater (140 km diameter). The bottom of the small bowl shaped crater (12 km diameter) tucked behind peaks in the center ground is the lowest point on the Moon; more than 9 km below the mean radius (*M1146021973LR*).

THE DIVINER LUNAR RADIOMETER: CORNERSTONE TO THERMAL INFRARED STUDIES OF AIRLESS BODIES. B.T. Greenhagen¹, P.O. Hayne², J.L. Bandfield³, K.L. Donaldson Hanna⁴, N.E. Bowles⁴, D.A. Paige⁵, and the Diviner Science Team. ¹Johns Hopkins University Applied Physics Laboratory, Laurel, MD USA, ²Jet Propulsion Laboratory, California Institute of Technology, Pasadena, CA USA, ³Space Science Institute, Boulder, CO USA, ⁴University of Oxford, UK, ⁵University of California, Los Angeles, CA USA.

Introduction: After nearly seven years in operation, and well into its 2nd Extended Science Mission (ESM2), the Diviner Lunar Radiometer (Diviner) continues to reveal the extreme nature of the Moon's thermal environments, thermophysical properties, and surface composition. Diviner is the first multispectral thermal infrared instrument to globally map the surface of the airless body with relatively high spatial and temporal resolution. Thus Diviner observations form the cornerstone of thermal infrared studies of airless bodies and provide critical validation for studies supported by the Volatiles Regolith Thermal Investigations Consortium for Exploration and Science (VORTICES) node of SSERVI.

Diviner Lunar Radiometer: To date, Diviner has acquired observations over twelve complete diurnal cycles and six partial seasonal cycles. Diviner daytime and nighttime observations (12 hour time bins) have essentially global coverage, and more than 80% of the surface has been measured with at least 7 different local times. The spatial resolution during the mapping orbit was ~200 m and now ranges from 150 m to 1300 m in the current elliptical "frozen" orbit. Calibrated Diviner data and global maps of visible brightness temperature, bolometric temperature, rock abundance, nighttime soil temperature, and silicate mineralogy are available through NASA's Planetary Data System (PDS) Geosciences Node.

Results: Diviner was designed to accurately measure temperatures across a broad range from midday equatorial regions such as the Apollo landing sites (around 400K), typical nighttime temperatures of less than 100K, and extreme permanent shadowed regions colder than 50K. The coldest multiply-shadowed polar craters may have temperatures low enough constrain lunar heat flow [1]. Nighttime temperatures are driven by the thermophysical properties of the lunar surface, including rock abundance and soil thermal inertia, which are used to investigate impact crater formation and evolution processes [2]. Multichannel thermal infrared spectroscopy can constrain silicate mineralogy, including compositional heterogeneity in the lunar crust [3]. In addition to lunar-specific properties, Diviner data is also used to characterize thermal emission behaviour that is fundamental to airless bodies with fine-particulate surfaces, including epiregolith thermal gradients and thermal-scale surface roughness.

Epiregolith Thermal Gradients. The uppermost portion of regolith on airless bodies represents the boundary layer between the surface and space. This

epiregolith layer is typically less than 1 mm in thickness and is characterized by significant thermal gradients (~60K / 100 μ m) that complicate the interpretation of spectral thermal emission remote sensing data [4]. These thermal gradients exist within the optical skin depth and infrared emitting layer and make thermal emission from airless bodies wholly different from Earth and Mars. Diviner observations during short thermal pulses, such as lunar eclipse, and laboratory experiments in simulated lunar environment [5] are used to investigate spectral thermal emission and disentangle intrinsic emissivity.

Thermal-scale Surface Roughness. The lunar surface is both very rough and highly insulating on scales of mm to cm, which produces range of temperatures (anisothermality) within any scene [6]. To fully characterize this behaviour requires multiple wavelength thermal infrared observations with systematically varying viewing and illumination geometries. With a vast dataset of nadir-pointing diurnal data on hand, the Diviner team now looks to use Diviner's independent gimbaling capabilities to make regional and global observations with a variety of illumination and viewing angles. This improved understanding of the emission phase function will feed directly into models of heat transfer on airless bodies, such as VORTICES SHERMAN, to study orbit drift due to differential heating and cooling (Yarkovsky effect) and volatile transport and sequestration.

Summary: This presentation will focus on recent Diviner results addressing a diverse range of scientific questions relevant to studies of airless bodies and will highlight exciting new observations proposed for LRO's third extended science mission, the Cornerstone Mission (CM). This presentation will also describe VORTICES-supported models and laboratory experiments that apply Diviner data and techniques to broader studies of the Moon, near Earth asteroids, and the moons of Mars.

Acknowledgements: Diviner observations and data analysis were supported by the LRO Project. VORTICES models and laboratory experiments were supported by SSERVI.

References: [1] Paige & Siegler (2016) LPS XLVII, Abstract #2753. [2] Ghent et al. (2014) *Geology*, 42, 1059-1062. [3] Greenhagen et al. (2010) *Science*, 329, 1507-1509. [4] Henderson & Jakosky (1994) *JGR*, 99, 19063. [5] Greenhagen et al. (2015) *NESF 2015*, #94. [6] Bandfield et al. (2014) *Icarus*, 248, 357-372.

EXPLORING THE EFFECTS OF SPACE WEATHERING AT ULTRAVIOLET WAVELENGTHS WITH THE LROC WIDE ANGLE CAMERA. B. W. Denevi¹, M. S. Robinson², H. Sato², and A. K. Boyd².

¹Johns Hopkins University Applied Physics Laboratory, Laurel, MD 20723, USA (brett.denevi@jhuapl.edu),

²School of Earth and Space Exploration, Arizona State University, Tempe, AZ 85251, USA.

Introduction: The effects of space weathering on the spectral properties of lunar soils provide an opportunity to understand the evolution of the lunar regolith, surface–space interactions, and the relative rates and consequences of the various processes that progressively alter the soil with time. The spectral effects of space weathering have been most thoroughly investigated at visible and near-infrared wavelengths, though measurements from the Lunar Reconnaissance Orbiter (LRO) provide new insights in the far-ultraviolet [1,2], near-ultraviolet [3,4], and thermal infrared [5,6]. Here we focus on how near-ultraviolet observations from the Lunar Reconnaissance Orbiter Camera (LROC) Wide Angle Camera (WAC) contribute to our understanding of space weathering.

WAC Color: The WAC provides an unprecedented dataset to assess reflectance at seven wavelengths in the ultraviolet (UV; 321, 360 nm) and visible (415, 566, 604, 643, and 689 nm) across the Moon’s surface. The WAC is a push-frame imager, with filter strips mounted on the CCD [7], and on-chip binning is performed for the UV filters to increase signal-to-noise ratio, resulting in pixel scales of ~400 and 100 m for the UV and visible, respectively. Near-global coverage is acquired each month, and this repeat coverage over a wide variety of illumination and viewing conditions allows for the development of highly accurate functions to describe the photometric variation of the surface [8,9]. Seamless photometrically normalized color mosaics have been produced by compiling many months of observations and taking the value of each pixel as the median of all observations (typically >100) at that point, which substantially increases the signal-to-noise ratio of the mosaic.

Maturity at Ultraviolet Wavelengths: Silicates exhibit a steep decrease in reflectance toward ultraviolet wavelengths due to strong charge-transfer absorption bands below ~300 nm [e.g., 10]; the wavelength at which this decrease begins is compositionally dependent. This absorption is weaker in mature soils, so the steep UV slope shallows with exposure to space weathering processes [1,3,11]. Variations in composition also have strong controls on UV reflectance, particularly the abundance of ilmenite [12], and the presence of glass, whether pyroclastic or impact-produced [3,10].

Spectral Properties of Fresh Impact Craters: Using the LROC WAC data, changes in UV slope are explored with a ratio of 321/415 nm, where a low value is consistent with a steep UV slope. As ex-

pected, low UV ratio values are observed in association with the ejecta and rays of Copernican craters throughout the maria. The observed 321/415 nm ratio values for fresh mare crater materials do not reach the low values seen for fresh endmembers (powdered rock) in laboratory spectra, but are consistent with immature to submature ($I_s/FeO \sim 10\text{--}40$) soils. The absence of observations of truly “fresh” material may be due to rapid early space weathering, mixing of immature and mature materials during the

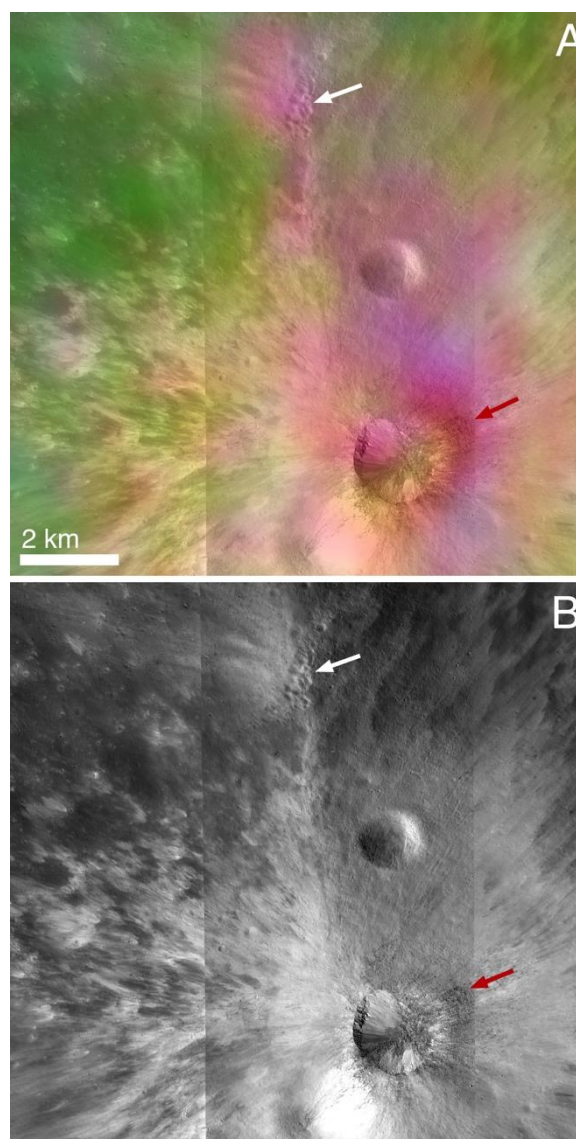


Fig. 1. Unnamed highland crater (19.377°N, 166.634°E). A) WAC color composite, with 415 nm, 321/415 nm, and 321/360 nm in red, green, and blue. In this color scheme, mature material appears green, glassy material pink, and immature soil yellow. Scene overlaid on LROC Narrow Angle Camera image mosaic seen in B). Red arrow indicates region of impact melt, white arrow indicates shocked material associated with secondary craters.

ejecta emplacement process, or an artifact of the WAC pixel scale [3].

In the highlands, the picture is more complicated. Instead of a simple relationship between maturity and 321/415 nm ratio as seen in the maria, fresh ejecta at highland craters have UV ratio values both lower (within ~one crater radius) and higher (distal ejecta and rays) than for mature soils (Fig. 1). Laboratory spectra of fresh endmember highland materials (powdered highland rocks) and soils of varying degrees of maturity show that for materials with less than ~5 wt% FeO, little change is observed in the 321/415 nm ratio except for an increase at the lowest levels of maturity ($I_S/FeO < \sim 20$). However, moderate shock pressures result in the solid-state transformation of plagioclase to a diaplectic glass, maskelynite [13]. Rather than a minimal downturn toward short wavelengths (~360 nm), maskelynite and low-iron glass have a strong downturn at ~415 nm. This feature is likely the result of broadening of the plagioclase UV absorption due to vitrification, indicating the low 321/415 nm ratio values near to crater rims are likely due to the effects of shock. WAC observations of highland materials are thus relevant for both studies of maturity and shock and melting, and can be an effective tool for locating melt samples for radiometric dating of key impact events [14].

Observations of Lunar Swirls: Swirls, high albedo features associated with crustal magnetic anomalies, are also found to be distinct in WAC color [4], as well as at far-UV wavelengths observed by the Lyman Alpha Mapping Project (LAMP) instrument on LRO [2]. Similar to fresh craters, swirls have low 321/415 nm ratios and elevated reflectance, and this distinguishing characteristic allowed for the creation of a comprehensive map of their distribution across

the surface [4] (Fig. 2). Though the reflectance of swirls is higher than nearby mature regions, it is typically not as high as that of immature craters. In some cases, it appears that swirl reflectance is higher when near to Eratosthenian craters, suggesting fresh material may be preserved longer within swirls than in non-swirl regions. The visible–near-infrared reflectance properties of swirls are generally consistent with the presence of immature material, but in some cases swirls are found to have low 321/415 nm ratios even when other indicators of immaturity are not found. These low ratio values could indicate the presence of fresh silicates or a glassy component that does not have a substantial abundance of embedded large submicroscopic iron grains (i.e., a difference in the agglutinate fraction of the soil).

References: [1] Hendrix A.R. et al. (2012) *JGRP*, 117, E12001. [2] Hendrix A.R. et al. (2016) *Icarus*, in press, doi: 10.1016/j.icarus.2016.01.003. [3] Denevi B.W. et al. (2014) *JGRP*, 119, 2013JE004527. [4] Denevi B.W. et al. (2016) *Icarus*, in press, doi: 10.1016/j.icarus.2016.01.017. [5] Glotch T.D. et al. (2015) *Nat. Commun.*, 6, 6189. [6] Lucey P.G. et al. (2013) *LPSC 44*, Abs. 2890. [7] Robinson M.S. et al. (2010) *Space Sci Rev*, 150, 81–124. [8] Sato H. et al. (2014) *JGRP*, 119, 1775–1805. [9] Boyd A.K. et al. (2012) *LPSC 43*, Abs. 2795. [10] Wells E. and Hapke B. (1977) *Science*, 195, 977–979. [11] Hendrix A.R. and Vilas F. (2006) *Astron J*, 132, 1396–1404. [12] Sato H. et al. (2015) *LPSC 46*, Abs. 1111. [13] Milton D.J. and de Carli P.S. (1963) *Science*, 140, 670–671. [14] Cohen B.A. et al. (2016) *LPSC 47*, Abs. 1389.

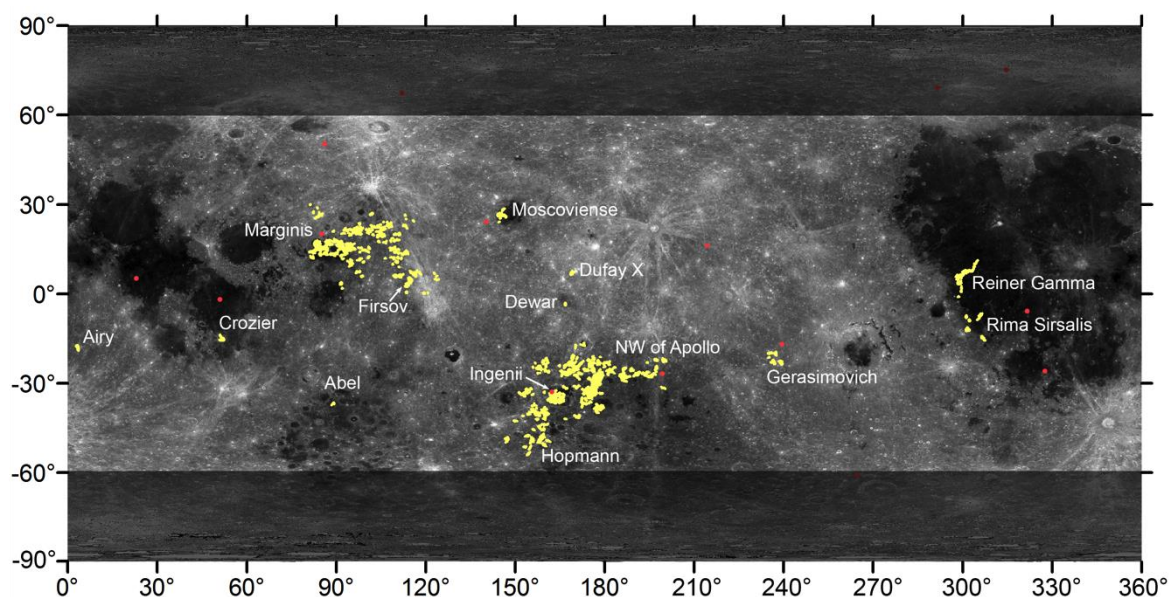


Fig. 2. LROC WAC-based map of the distribution of swirls (yellow) [4]. WAC color has more favorable phase angles between $\pm 60^\circ$; latitudes outside this range are shaded. Note that the outlines of swirls are shown in bold to make them visible at this scale, which slightly exaggerates their size.

THE ORIGINS OF LUNAR LIGHT PLAINS: IMPLICATIONS FOR EXPLORATION. H. M. Meyer¹, M. S. Robinson¹, and R. Z. Povilaitis¹, ¹School of Earth and Space Exploration, Arizona State University, Tempe, AZ, Heather.M.Meyer@asu.edu.

Introduction: Light plains are smooth to gently rolling, relatively flat deposits that occur in topographic lows, such as crater floors, in the lunar highlands and exhibit reflectance values comparable to the surrounding highland terrain [e.g. 1,2]. Due to their resemblance to the maria (See **Fig. 1**), the light plains were originally thought to be volcanic deposits. Apollo 16 visited the type region for light plains, the Cayley Formation, where they found no evidence for volcanism, but rather a thick deposit of impact breccia [1,3,4]. From this discovery, the light plains were reinterpreted as products of the deposition of fluidized basin ejecta [e.g. 1,2]. Conflicting relative age estimates suggest that the light plains originated with the Orientale and Imbrium basins [5], or from a larger number of impact events combined with possible volcanic eruptions [2,6]. Because our understanding of lunar geologic history hinges on our understanding of large basin stratigraphy, it is critical to determine if the light plains are in fact basin deposits extending beyond the traditional zone of surface modification, i.e. the continuous ejecta. Further, the physical characteristics of light plains make them excellent highland landing sites, in which case a detailed understanding of their formation is essential to provide geologic context for any in-situ operations and sample return.

Oriente Pilot Study: The light plains, as defined by [1] and [2], were mapped (**Fig. 1**) using LROC Wide Angle Camera (WAC) [7] monochrome mosaics of opposite illuminations and an RGB roughness map [8] within two study areas encompassing ~10.5 million sq. km, located to the north-northwest and west-southwest of the Orientale basin (full methods detailed in [9]). The areas around Orientale were chosen because the light plains in these regions display morphologic relationships to the Orientale basin, specifically at the edge of the continuous ejecta, and because they allow an analysis of the areal distribution with respect to Orientale and Imbrium.

Morphologic and spatial relationships were sought in the study areas between the light plains and the continuous ejecta of Orientale. The areal distribution with respect to Orientale and Imbrium basins was measured and plotted against distance from the basin rim. The vertical distribution was assessed using the elevation of the light plains from the Global Lunar Digital Terrain Model (DTM) GLD 100 [10] and was compared to the vertical distribution of the highlands and the maria. The composition of the light plains in terms of UV ratio (TiO_2), FeO abundance from Clementine [11], and the location of the

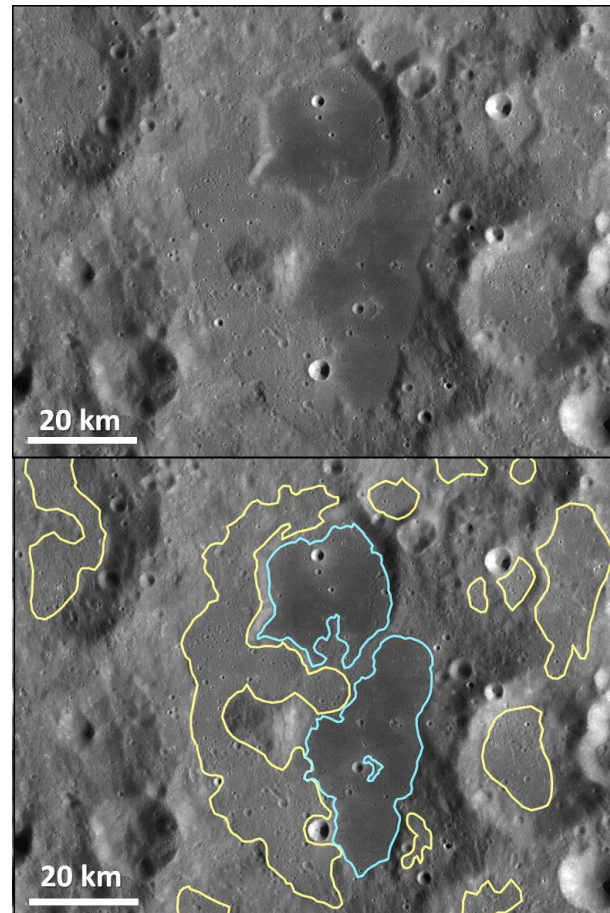


Figure 1. The top panel shows the LROC WAC monochrome basemap centered at 16°N 263°E, and the bottom panel shows the same basemap with the mapped light plains unit (yellow) [9] and a farside mare pond (blue) outlined for comparison [14].

Christiansen Feature [12] were compared to the respective compositions of the highlands, maria, and red spots.

Age estimates were derived using crater measurements for eleven light plains areas and three areas on the continuous ejecta of Orientale for comparison to the basin-forming impact. Finally, observations of the degree of crater fill by light plains deposits was made to determine to a first order (using the relationships derived by [13]) if the thickness of the light plains varies with increasing distance from Orientale.

Results & Interpretation: Consistent with previous work, both gradational and sharp embayment relationships were identified between the continuous ejecta and the light plains, which suggests that the two deposits formed concurrently. Flow features are common within the light plains and suggest that the ejecta flowed over topography and ponded in

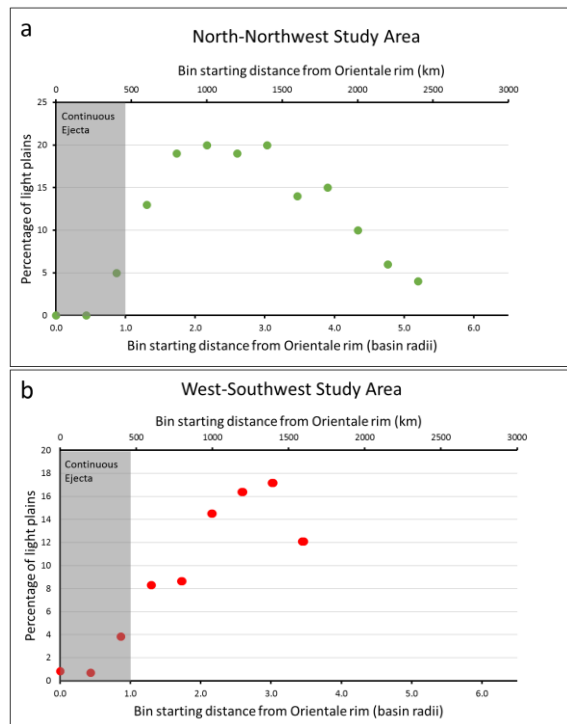


Figure 1. The areal distribution of light plains in the (a) north-northwest region from [9] and (b) the west-southwest region with respect to the Orientale basin.

topographic lows forming the light plains. The areal distribution of light plains in both the north-northwest and the west-southwest study areas suggests that the primary source of the light plains is the Orientale basin (**Fig. 2**), with some minor contribution from Imbrium. The vertical distribution of light plains covers a wide range of elevations, indicating that the ejecta was emplaced as a high energy, ground-hugging flow. Compositionally, the light plains are indistinguishable from the highlands, consistent with a common origin.

Because the light plains deposits are small and display few craters, the uncertainty associated with the absolute model ages (i.e. the error bars) does not reflect the true uncertainty of the measurements [15]. When the light plains regions are merged, the resulting absolute model age is indistinguishable from the absolute model age of Orientale. Because of the uncertainty associated with crater counting on small light plains deposits, we conclude that the combined statistics for the light plains are more reliable, so the light plains could be the same age as Orientale, which is consistent with an origin with the formation of Orientale. Crater fill estimates suggest that the light plains thin with increasing distance from the rim of Orientale. Overall, we conclude that the majority of the light plains within the study areas likely formed with the Orientale basin-forming impact. In this case, the basin-forming impact profoundly modified the lunar surface to at least four basin radii from the rim.

Ongoing Work: We are currently expanding the light plains map globally in order to assess the current distribution of light plains with respect to all large basins. The light plains in many cases likely reflect multiple generations of large basin-forming impacts, so we are also creating a global map of the initial post-formation zones of surface modification, extrapolated from the Orientale study [9], to determine if any changes to the current interpretation of lunar stratigraphy are warranted and to aid in the interpretation of any returned samples.

Implications for Exploration: This work significantly expands the zone of surface modification for large lunar basins. This means that the surface modification due to basin impacts needs to be reconsidered when assessing highlands regions for exploration. Regions that previously were thought to have escaped modification by large basins may in fact fall within the expanded zone of surface modification. Any future sample return mission will require a detailed understanding of the target landing site, meaning that the sequence of nearby basin impacts must be understood in order to provide geologic context for the analysis of any samples returned.

References: [1] Eggleton R. E. and G. G. Schaber (1972) NASA Apollo 16 Prelim. Sci. Rep., 29-7-29-16. [2] Scott et al. (1977) Geologic Map of the West Side of the Moon, USGS, Denver, CO. [3] Young J. W. (1972) NASA Apollo 16 Prelim. Sci. Rep., 5-1 -5-6. [4] Muehlberger W. et al. (1972). NASA Apollo 16 Prelim. Sci. Rep., 6-1 - 6-81. [5] Boyce J. M. et al. (1974) Proc. Fifth Lunar Sci. Conf., 11 -23. [6] Neukum G. (1977) The Moon 17, 383-393. [7] Robinson M. S. et al. (2010) Space Sci. Rev. 150, 81 -124. [8] Boyd A.K. et al. (2012) EPSC 7, abstract #854. [9] Meyer et al. (2016) doi:10.1016/j.icarus.2016.02.014. [10] Scholten F. et al. (2011) JGR, 117, doi:10.1029/2011JE003926. [11] Lucey P. G. et al. (2000) J. Geophys. Res., 105 (E8), 20297-20305. [12] Greenhagen B. T. et al. (2010) Science, 329, 1507-1509, doi:10.1126/science.1192196. [13] Pike R. J. (1977) Size-dependence of fresh lunar craters on the Moon, in Impact and Explosion Cratering, pp. 489-509. [14] Nelson et al. (2014) LPSC 45, #2861. [15] van der Bogert et al. (2015) Cratering Workshop, 9023.

MODELLING THERMAL INFRARED SPECTRA IN A LUNAR-LIKE ENVIRONMENT. J. A. Arnold¹, R. Schröpfer², K. L. Donaldson Hanna¹, N. E. Bowles¹ and J. Blum² ¹University of Oxford (AOPP, Clarendon Lab, Parks Rd, Oxford, OX1 3PU; jessica.arnold@physics.ox.ac.uk), ²Technische Universität Braunschweig

Introduction: Mid-infrared (MIR), 2.5-100 μm or 100-4000 cm^{-1} , spectroscopy is useful for understanding regolith properties of airless bodies. However, MIR emissivity is controlled by many factors such as: composition; grain size distribution, shape, and packing; as well as atmospheric pressure and the thermal environment [1,2,3]. Moreover, low gravitational acceleration and small particle sizes result in a high-porosity regolith surface [4,5,6]. Accurately modeling spectral changes due to these factors is particularly challenging for the very fine-grained regolith ($d \sim < 60 \mu\text{m}$) typical of the lunar surface.

We started with a currently existing, layered, plane-parallel radiative transfer model [7]. This model couples Mie scattering with the DISORT radiative transfer code. To test and validate this code, we compared modeled emissivity spectra with laboratory measurements of two different size separates of the mineral olivine. Then, the model was extended to account for regolith porosity and include several compositions. Additionally, individual layers may now have different properties and layers may be composed of mineral mixtures.

Methods and Samples: Gem-quality millimeter-sized San Carlos olivine grains were crushed and dry sieved to obtain five different size separates ($< 45 \mu\text{m}$, $45-75 \mu\text{m}$, $75-125 \mu\text{m}$, $125-250 \mu\text{m}$). The largest and smallest of these size fractions were measured under both ambient (1 bar N_2 with sample heated from below) and simulated lunar conditions (cooled chamber under vacuum with sample heated from above and below) using facilities within the Planetary Spectroscopy Facility at the University of Oxford.

Porosity. To gain a better understanding of the effects of porosity on emissivity we collected spectra of mono-disperse smooth, spherical SiO_2 grains of known packing density profiles [6] under ambient conditions. As demonstrated by [8], the single scattering albedo and asymmetry parameters derived from Mie theory are not suitable for densely packed media. A few different approaches been developed to deal with this issue. To test these various methods, we have built a choice of packing corrections into our model.

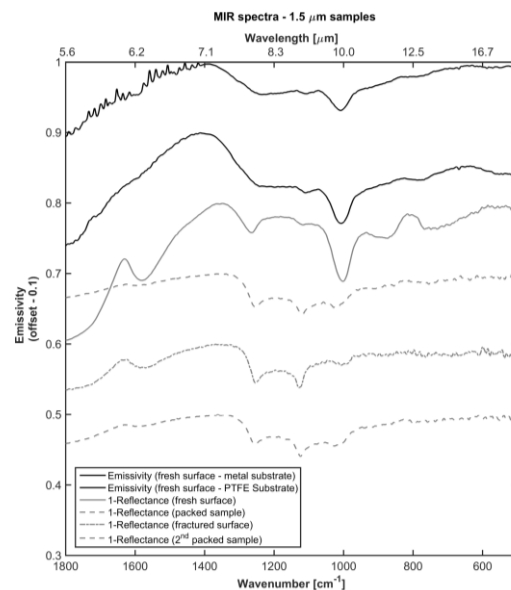


Figure 1: Emissivity and diffuse reflectance measurements of silica, with offset of 0.1 for clarity. Diffuse reflectance is presented as $\epsilon = 1-R$ for comparison with emissivity measurements.

Space weathering. Space weathered materials have reduced visible albedo and this causes a shift in the Christiansen feature, an emissivity maximum that is can be used to infer silicate composition [9]. We examine the impact of space weathering on MIR spectra by comparing lunar environment laboratory spectra of quartz-carbon mixtures to two different types of models: 1) quartz-carbon mixtures and quartz-iron mixtures and 2) simply reducing the visible single scattering albedo of quartz.

Results: Modeled spectra suggest that the responses of the reststrahlen bands (RB), Christiansen feature, and shorter wavelengths to grain size under cold, airless conditions differ substantially from those observed in an ambient or Earth-like environment. In ambient conditions, as particle size decreases, so does the spectral contrast of the RB, and our models are able to replicate this effect.

Both measurements and models show that porosity influences the width of the CF, but has little effect on the CF position, and has a significant impact on the transparency features. However, the increase in the RB depth for packed materials observed in laboratory emissivity spectra is not present in the modelled spectra.

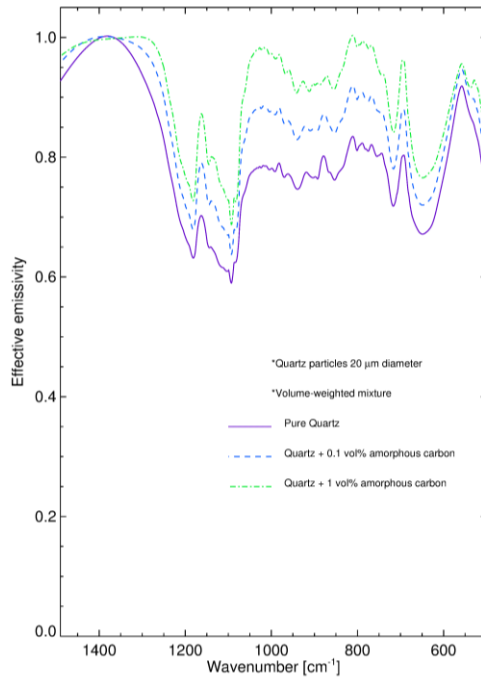


Figure 2: “Space weathered” quartz modeled as a mixture with 100nm carbon black.

The modeled spectra of quartz mixed with darkening material and quartz with reduced visible albedo show a shift of the CF to longer wavelengths compared to pure quartz. This matches the direction of the shift of this feature observed in laboratory measurements of quartz-carbon mixtures and quartz irradiated to simulate space weathering [9].

References: [1] Logan L.M. et al. (1973) *JGR*, 78, 23, 4983–5003. [2] Salisbury J.W. and Eastes J.W. (1985) *Icarus*, 64, 586-588. [3] Donaldson Hanna K.L. et al. (2014) *ELS*, p. 91. [4] Hapke B. (1993) *Theory of Reflectance and Emittance Spectroscopy*, 224. [5] Carrier W.D. et al. (1991) In *Lunar Sourcebook* (Heiken G.H., Vaniman D.T., and French B.M., Eds.), pp. 475–594. [6] Blum J. et al. (2006) *Astrophys. J.*, 652, 1768–1781. [7] Milan L. et al. (2011) *JGR*, 116, E12003. [8] Mishchenko M.I. (1994) *J. Quant. Spec.*, 52, 1, 95–110. [9] Lucey P.G. et al. (2013) *LPS XLIV*, #2890.

SEARCH FOR LUNAR WATER: FROM CURRENT LUNAR RECONNAISSANCE ORBITER GLOBAL MAPPING TO THE SAMPLE ANALYSIS AT SURFACE ONBOARD FUTURE RUSSIAN LUNAR LANDERS. M.L. Litvak¹, I.G. Mitrofanov¹, ¹Space Research Institute, RAS, Moscow, 117997, Russia, litvak@mx.iki.rssi.ru

Introduction: The NASA Lunar Reconnaissance Orbiter (LRO) mission successfully continues from 2009 providing global mapping of lunar surface using different instrumentation onboard. One of the requirements is to perform high spatial resolution mapping of hydrogen deposits at the Moon's poles and to perform reconnaissance of the putative near-surface water ice deposits. LRO integrates such instruments as collimated neutron spectrometer LEND (global mapping of subsurface Hydrogen with spatial resolution 10 km), UV spectrometer LAMP (search for surficial ice layer using UV radiation from stars and the Sun's Lyman- α emission), lunar radiometer DIVINER (measurements of subsurface temperature and identification areas with ice preservation). Each instrument provides its own piece of puzzle how water ice could be distributed in the polar regions.

In our study we summarize these data and tried to connect it with the investigations and experiments planned onboard future Russian polar lander missions.

Landers will be launched in 2018-2020 and will be landed at Moon southern high latitudes. They will conduct remote sensing experiments (active neutron and gamma spectroscopy, IR observations) together with sampling analysis of lunar regolith properties to detect volatiles and first of all – subsurface water ice. These studies will be implemented through close international cooperation between Russian Federal Space Agency (Roscosmos) and European Space Agency (ESA).

MINI-RF ON LRO AND ARECIBO OBSERVATORY BISTATIC RADAR OBSERVATIONS OF THE MOON. G. W. Patterson¹, D. B. J. Bussey¹, A. M. Stickle¹, F. S. Turner¹, J. R. Jensen¹, M. Nolan², D. A. Yocky³, D. E. Wahl³, and the Mini-RF Team. ¹Johns Hopkins University Applied Physics Laboratory, Laurel, MD (Wes.Patterson@jhuapl.edu), ²University of Arizona, Tucson AZ, ³Sandia National Laboratory, Albuquerque NM.

Introduction: NASA's Mini-RF instrument on the Lunar Reconnaissance Orbiter (LRO) and the Arecibo Observatory (AO) in Puerto Rico have been operating in a bistatic architecture (AO serves as the transmitter and Mini-RF serves as the receiver) over approx. a 2.5 year period in an effort to understand the scattering properties of lunar terrains as a function of bistatic (phase) angle. In that time, 28 observations of the surface have been acquired for the lunar nearside and poles. These observations include mare materials, highland materials, pyroclastic deposits, and a variety of craters (polar and non-polar). The primary motivation for acquiring these data is to characterize the opposition response of lunar terrains at S-band wavelengths (12.6 cm) to differentiate the Circular Polarization Ratio (CPR) response of materials that are rough from surfaces that harbor water ice.

Background: The transmitter for Mini-RF bistatic observations is the 305 m Arecibo Observatory radio telescope in Puerto Rico. For each observation, the antenna is pointed at a target location on the moon and illuminates the lunar surface around that location with a circularly polarized, S-band (2380 MHz) chirped signal that has a fixed peak power of 200 kw and tracked the Mini-RF antenna boresight intercept on the surface of the Moon. The data returned provide information on the structure (i.e., roughness) and dielectric properties of surface and buried materials within the penetration depth of the system (meter(s) for Mini-RF) [1-4]. The bistatic architecture allows examination of the scattering properties of a target surface for a variety of bistatic (phase) angles.

Laboratory data and analog experiments, at optical wavelengths, have shown that the scattering properties of lunar materials can be sensitive to variations in bistatic angle [5]. This sensitivity manifests as an opposition effect. Analog experiments and theoretical work have shown that water ice is also sensitive to variations in phase angle, with an opposition effect that it is tied primarily to coherent backscatter [6,7]. Differences in the character of the opposition response of these materials offer an opportunity to differentiate between them, an issue that has been problematic for radar studies of the Moon that use a monostatic architecture [8].

Observations: CPR information is commonly used in analyses of planetary radar data [1-4], and is a representation of surface roughness at the wavelength scale of the radar (i.e., surfaces that are

smoother at the wavelength scale will have lower CPR values and surfaces that are rougher will have higher CPR values). High CPR values can also serve as an indicator of the presence of water ice [9]. We use CPR as a function of bistatic angle to explore the opposition response of lunar materials at S-band wavelengths.

Data of mare materials, highland materials, pyroclastic deposits, and a variety of craters (polar and non-polar) have been acquired over the course of Mini-RF bistatic operations. Observations of mare materials and pyroclastic deposits show a uniform CPR response for bistatic angles $< 10^\circ$. Observations of crater ejecta show variations in CPR, as a function of bistatic angle, that are not uniform for Kepler and Byrgius A or consistent from crater-to-crater. The response of Kepler and Byrgius A is suggestive of an opposition effect. The inconsistency from crater-to-crater may be related to the age of the deposit and/or target material properties. Observations of the floor of Cabeus crater show variations in CPR, as a function of bistatic angle, that are also indicative of an opposition response.

Results: Mini-RF has acquired a significant amount of bistatic radar data of the lunar surface in an effort to understand the scattering properties of lunar terrains as a function of phase angle at S-band wavelengths (12.6 cm). Observations that include mare materials, highland materials, and pyroclastic deposits have not shown an opposition response over for bistatic angles of $\sim 0.1^\circ$ to 10° . In contrast, observations of the ejecta blankets of young, fresh craters have shown an opposition response but the character of the response varies for each crater. Observations of portions of the floor of the south polar crater Cabeus also show an opposition response. The character of the radar response from the crater, as a function of bistatic angle, appears unique with respect to all other lunar terrains observed. Analysis of data for this region suggests that the unique nature of the response may indicate the presence of near-surface deposits of water ice.

References: [1] Campbell et al. (2010), *Icarus*, 208, 565-573; [2] Raney et al. (2012), *JGR*, 117, E00H21; [3] Carter et al. (2012), *JGR*, 117, E00H09; [4] Campbell (2012), *JGR*, 117, E06008; [5] Hapke et al. (1998), *Icarus*, 133, 89-97; [6] Hapke and Blewett (1991), *Nature*, 352, 46-47; [7] Mishchenko (1992), *Astrophysics and Space Science*, 194, 327-333; [8] Spudis et al. (2013), *JGR* 118, 1-14; [9] Black et al. (2001), *Icarus*, 151, 167-180.

GLOBAL CRATER DENSITY: EQUILIBRIUM IN THE LUNAR HIGHLANDS. R. Z. Povilaitis¹, M. S. Robinson¹, C. H. van der Bogert², H. Hiesinger², H. Meyer¹, P. Thomas³, L. R. Ostrach⁴, ¹School of Earth and Space Exploration, Arizona State University, Tempe, AZ 85287 USA (rpovilaitis@ser.asu.edu), ²Institut für Planetologie, Westfälische Wilhelms-Universität, Münster, Germany, ³Center for Astrophysics and Planetary Science, Cornell University, Ithaca, NY 14853, USA, ⁴NASA Goddard Space Flight Center, Greenbelt, MD 20771, USA

Introduction: Impact crater density has long been used as an indicator of the relative age of surface units on the Moon [1]. Crater density also provides direct evidence of resurfacing events that have locally altered the crater population. Basin-forming impacts played a large role in regional resurfacing on the Moon, as well as contributing to the currently preserved crater population. The oldest areas of the Moon should contain crater populations at or approaching saturation equilibrium - the condition in which on average the formation of a new impact crater erases a similarly sized existing crater.

The global population of lunar craters >20 km diameter was analyzed by Head et al. [2010] to correlate crater distribution with resurfacing events and multiple impactor populations. The work presented here extends the global crater distribution analysis to smaller craters (5-20 km diameters, n=22,746). Smaller craters form at a faster rate than larger craters and thus add granularity to age estimates of larger units, enable more accurate age estimates for smaller younger units, and reveal areas of resurfacing. This new dataset reveals regional deficiencies of 5-20 km diameter craters interpreted to be due to major events such as resurfacing by Orientale ejecta, fewer basin secondaries in the central nearside highlands, and partial mare flooding of the Australe basin. Chains of 5-13 km secondaries NW of Orientale and possible 5-10 km basin secondaries on the farside highlands are also evident.

Determining the diameter range of saturation equilibrium is important for understanding the nature of the crater population and the effect of resurfacing events and/or secondary bombardment. Our data show that many areas within the highlands are at saturation equilibrium with diameters between 57 and 160 km.

Crater Counts: All craters between 5 km and 20 km in diameter were digitized at a scale between 1:250,000 and 1:500,000 in ArcGIS. Basemaps used included: 1) a 100 m/pixel scale WAC monochrome (643 nm) mosaic with an average solar incidence of 60°, and 2) a shaded relief map based on 100 m/pixel LROC WAC Digital Elevation Model (GLD100 [3]) to help demarcate craters in shadowed regions at the poles and/or subdued craters. An existing database of >20 km craters supplemented this dataset [4].

Crater Density: We determined areal crater density for each diameter range (5-20 km and >20 km) independently using a moving neighborhood method with a radius of 500 km and an output cell size of 15 km (Fig. 1). Density magnitude values for each map

were divided into 10 equal-interval bins and reclassified with a ranking of 1 to 10 (1 being lowest density and 10 being highest). The resulting 5-20 km density map (Fig. 1) was subtracted from the >20 km density map to produce a crater density difference map (Fig. 2). Output cell values of the difference map range from -4 to +5. Positive difference values represent a high density (red) of >20 km craters relative to 5-20 km craters, and negative values represent low density (blue) of >20 km craters relative to 5-20 km craters.

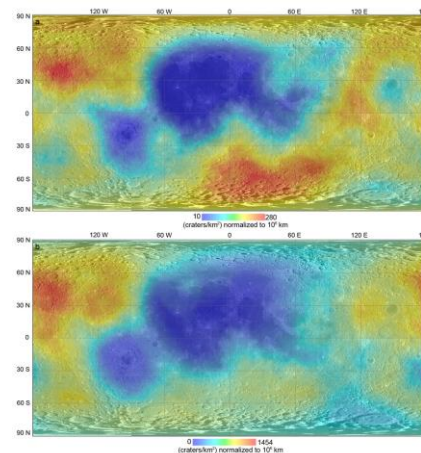


Figure 1. Areal crater density for >20 km (a) and 5-20 km (b) craters.

Crater Saturation Equilibrium: A total of 17 crater size bins were populated with all craters within a 500 km radius of the center of each 15x15 km output cell. Relative density (R) values were calculated for each bin using the method outlined in [5]. Global crater density equilibrium maps (Figure 3) were then created showing those areas having $R \geq 0.3$ for each crater bin. This measure conservatively restricts the condition for equilibrium to ~10% of geometric saturation - the upper end of published estimates. The maps show areas where crater density equilibrium for a particular crater size range may exist or begin to develop first (Fig. 3).

Basin Ejecta Zones: Ejecta zones extending 4 and 5 radii from the centers of 13 post-Nectarian basins (Orientale, Schroedinger, Imbrium, Bailly, Sikorsky-Rittenhouse, Hertzprung, Crisium, Humorum, Humboldtianum, Mendeleev, Korolev, Moscoviense, and Mendel-Rydberg) were plotted over the 5-20 vs >20 km crater density difference map (Fig. 4). The maps delineate areas more likely to contain basin secondaries.

Results: Areal crater density difference (Figure 2) provides a comprehensive view of the extent and degree of regional and global variations in the densi-

ties of mid- to large-scale craters (5-20 km) relative to the larger diameter population (>20 km) [2]. The difference map highlights several notable features with one of the most prominent being a large zero difference area encompassing the mare and several large impact basins on the nearside (Fig. 2a). Observing such similar behavior between mare and some highlands is consistent with a production function that is constant in time, rather than temporally changing proportions of different impactor types [6]. A positive difference area surrounding the Orientale basin (Fig. 2b) indicates that this area has retained a greater number of >20 km craters relative to 5-20 km craters, which is expected for a basin that profoundly disrupted the existing crater population and whose continuous ejecta preferentially obliterated smaller craters out to 2 basin diameters from the rim [2]. To the northwest of Orientale basin, beyond this proximal affected zone, is a negative difference area peppered with chains of 5-20 km secondaries traceable back to the Orientale basin (Fig. 2c) [7]. Other anomalous areas exhibiting the most extreme relative differences include a widespread positive density difference in the southern nearside highlands (Fig. 2d) and a region of negative density difference throughout much of the farside highlands (Fig. 2e). Finally, an area in the heavily-cratered “pristine” NW farside highlands displays zero density difference (Fig. 2f).

Maps a-c of Figure 3 show the full extent of saturation equilibrium of craters in three diameter ranges for the whole Moon - expanding on previous work which has suggested saturation equilibrium may exist in parts of these areas [8-10]. Areal coverage for these bins is as follows: 27% (57-80 km), 39% (80-113 km), 12.4% (113-160 km). Saturation equilibrium of craters down to 5 km craters has also been mapped, though areal coverage of these bins is much lower (< 1% for 5-7 km craters).

Maps of post-Nectarian basin ejecta zones provide additional information about the extent of resurfacing (Fig 4). At 4 and 5 basin radii, ejecta zones cover much of the lunar surface with the exception of the majority of area d which remains exposed. The high density of >20 km craters relative to 5-20 km craters here may indicate this area is among the oldest surfaces least affected by post-Nectarian basin secondaries/ejecta and is thus the best area to retrieve samples of the ancient crust.

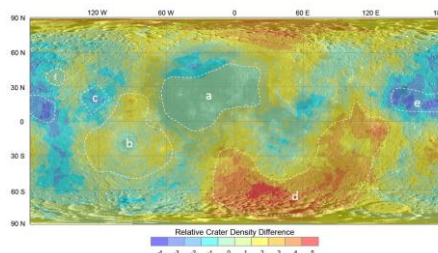


Figure 2. 5-20 km vs >20 km crater density difference.

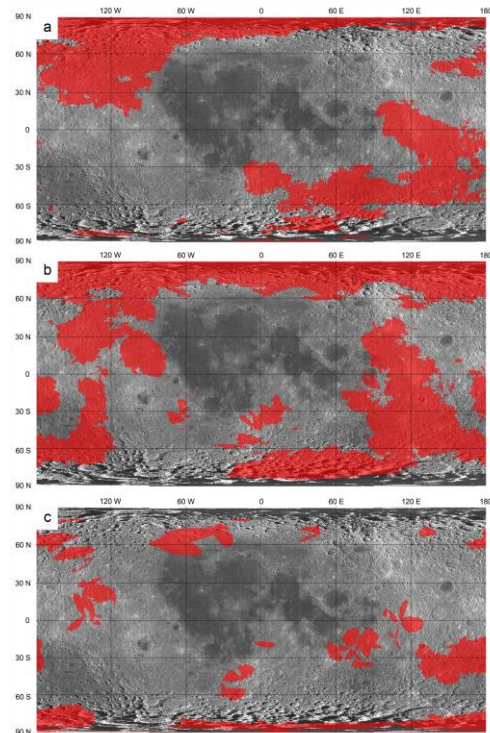


Figure 3. Crater saturation equilibrium for 57-80 km (a), 80-113 km (b), and 113-160 km (c) craters.

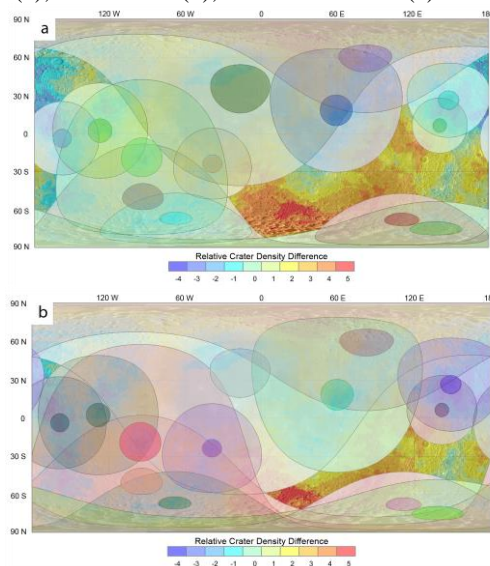


Figure 4. Ejecta zones extending 4 radii (a) and 5 radii (b) from center of 13 post-Nectarian basins.

References:

- [1] Baldwin, 1964, *Ast. Jour.*, 69, 377 [2] Head, et al., 2010, *Science* 329, 5998, 1504-1507 [3] Scholten et al., 2012, *JGR* 117, E00H17 [4] Kadish, S. J., et al. LPSC. Vol. 42. 2011. [5] Arvidson, et al., 1979, *Icarus* 37, 467-474 [6] Wilhelms, 1976, *Proc. LPSC* Vol. 7. p. 2883-2901 [7] Neukum, et al. 2001 *Space Science Reviews* 96. 1-4, 55-86. [8] Richardson, 2009, *Icarus*, 204, 697-715 [9] Hartmann, 1984, *Icarus*, 60, 56-74 [10] Fassett, 2011, *Geophys. Res. Lett.*, 38, L10202.

INCOMPLETE LUNAR ACCRETION AND THE DEPLETION OF VOLATILE ELEMENTS IN THE MOON. R. M. Canup^{1,2}, C. Visscher^{1,3}, J. Salmon^{1,2}, and B. Fegley, Jr.³. ¹SSERVI Institute for Science of Exploration Targets (ISET); ²Southwest Research Institute (1050 Walnut Street, Suite 300, Boulder, CO, 80302; robin@boulder.swri.edu); ³Dordt College; ⁴Washington University in St. Louis.

Introduction: Compared with the bulk silicate Earth (BSE), the Moon is depleted in moderately volatile elements including potassium, sodium, and zinc [e.g., 1]. It has been suggested that volatiles were evaporatively lost from an impact-generated protolunar disk prior to the Moon's accumulation [2-3], based in part on the enrichment of lunar samples in heavy Zn isotopes compared with the BSE [2]. However escape may have been minimal for expected disk conditions [4].

A depletion could also result if volatiles were preferentially accreted by the Earth rather than by the Moon [1, 4-5]. We explored this concept in [9] in the context of current models of the Moon's formation from an impact-generated disk. We combine results of lunar accretion simulations [6] with estimates of the disk's thermal state [7] and predictions from a chemical equilibrium code [8]. We find that K, Na and Zn condense late in the disk's evolution when the majority of inner disk material is scattered onto the Earth rather than being accreted by the Moon [9]. This would produce depletions in particularly the outer portions of the Moon even in the absence of escape [9].

Disk evolution: After the Moon-forming impact, the two-phase silicate disk may develop a vertically stratified structure, with a mid-plane melt layer surrounded by a silicate vapor atmosphere [7]. Clumps form in the melt due to local gravitational instability. Within the Roche limit ($a_R = 3R_\oplus$), such clumps are sheared apart by planetary tides, producing a viscosity that dissipates energy and spreads the melt [e.g., 6-7]. The balance between radiative cooling and viscous heating causes the Roche interior disk to spread over $\sim 10^2$ yr [7]. Exterior to a_R viscous heating is likely minimal, and silicate vapor condenses on a timescale $\tau \sim (\sigma_v l)/(2\sigma_{SB} T_p^4) \sim 3$ yr ($\sigma_v/10^6$ g cm⁻²)(2000 K/ T_p)⁴, where $l = 2 \times 10^{11}$ erg g⁻¹ is the silicate latent heat of vaporization, σ_{SB} is the Stefan-Boltzmann constant, T_p is the disk photospheric temperature, and σ_v is the vapor surface density. In the

outer disk, melt present after the impact (or that subsequently condenses) rapidly accretes into moonlets in < 1 yr.

Fig. 1 shows results from a lunar accretion model [6]. The Roche-interior disk is described analytically, and its total mass and outer edge evolve due to viscous spreading and resonant interactions with outer moonlets. Material outside the Roche limit is described by an N -body accretion simulation. The latter assumes that outer disk material has largely cooled so that this region may be approximated as a condensate disk. As inner disk material spreads beyond the Roche limit, mass and angular momentum are removed from the inner disk and added to the N -body portion of the model in the form of new moonlets. Such spawned moonlets can form rapidly via local gravitational instability just outside a_R .

In “phase 1”, material placed into orbits outside the Roche limit by the impact rapidly accretes into a moonlet that in this case contains $\sim 40\%$ of the Moon's mass. In phase 2, resonant torques from this moonlet confine the inner disk to within the Roche limit, and the Moon's accretion stalls. The inner disk spreads, and once its edge reaches the Roche limit it spawns moonlets just beyond a_R (phase 3). Initially these spawned moonlets are rapidly driven outward due to resonant interaction with the inner disk, and they are efficiently accreted by the Moon (Fig. 1b). However as the inner disk mass decreases, disk torques weaken, and spawned moonlets are scattered onto high-eccentricity orbits by the Moon. Most are then tidally disrupted as their perigees near the Earth's surface before they can accrete onto the Moon (Fig. 1b). The result is a transition from an accretionary regime – in which the Moon in this case gains the final $\sim 60\%$ of its mass from inner disk melt – to a non-accretionary regime – in which most inner disk melt is ultimately accreted by the Earth [6]. Inner disk elements that condense subsequent to this transition will be depleted in the Moon relative to the Earth.

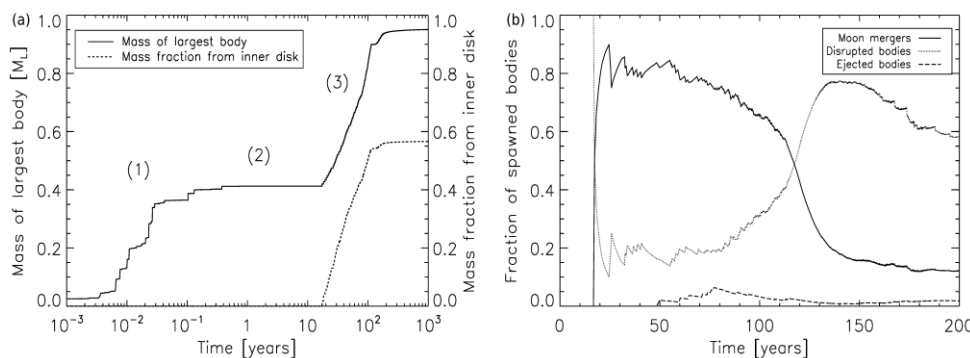


Fig. 1: Lunar accretion model [6]. (a) Moon mass in lunar masses vs. time (solid) and fraction derived from inner disk (dotted). (b) Fate of material spawned from the inner disk. Initially $\sim 80\%$ is accreted by the Moon (dark line), but a cut-off occurs at ~ 120 yr.

To approximate the formation temperature of moonlets spawned from the inner disk, we estimate the disk's mid-plane temperature at the Roche limit (T). Initially, the disk is in silicate vapor-melt equilibrium [7], with T (K) $\approx T_1(\sigma/10^7 \text{ g cm}^{-2})^\alpha$, where σ is the disk's surface density at a_R , and α and T_1 are fitting factors that are functions of x , the atmosphere's vapor fraction at the mid-plane [9]. Eventually cooling allows all the silicate vapor to condense, and the inner disk is no longer regulated by the silicate two-phase equilibrium. The remaining volatile-rich atmosphere is heated by viscous dissipation in the melt (which decreases with time as the melt spreads) and by the Earth's luminosity [9].

Condensation temperatures: We estimate the partitioning of elements between the disk's vapor vs. melt using the MAGMA chemical equilibrium code for a BSE composition disk (e.g., [8]). We derive the partial vapor pressure of each species which, in combination with the total bulk elemental inventory of the disk, is used to estimate the relative fraction of each element in the vapor vs. melt phase as a function of T and σ (Fig. 2).

Results: Fig. 3a shows the inner disk surface density vs. time for the Fig. 1 simulation. Fig. 3b shows estimated mid-plane temperatures at the Roche limit during the silicate two-phase stage and the subsequent cooling period once the inner disk's silicate vapor has condensed (dotted line). The colored curves show our estimated 50% condensation temperatures (T_{50}) for Zn (grey), Na (orange), and K (green). The formation temperature of inner disk clumps remains above T_{50} for these elements until the Moon has essentially completed its accretion (Fig. 3c) and the efficiency of inner clump accretion by the Moon has decreased to $\sim 10\%$ (Fig. 1b).

Discussion: Late-added portions of the Moon derived from the inner disk will be substantially depleted in volatile elements even in the absence of thermal escape. The equivalent depth of this volatile-depleted outer "layer" varies between 100 and 500 km, depending on the assumed initial radial distribution of

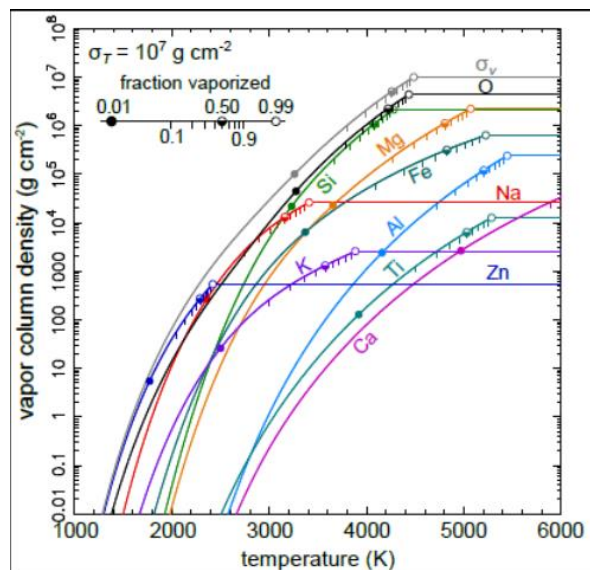


Fig. 2: Fraction of species in a BSE disk in the vapor phase as a function of T for $\sigma = 10^7 \text{ g cm}^{-2}$. Vapor surface density (g cm^{-2}) of each element and the total vapor surface density (σ_v) at the Roche limit for $\sigma_T = 10^7 \text{ g cm}^{-2}$. Vertical marks indicate mass fraction in the vapor phase from 0.1 to 0.9; symbols indicate 1% (\bullet), 50% (\circ) and 99% (\circ) vaporization.

mass in the disk. In contrast, the first portions of the Moon to accrete in "phase 1" derived from the outer disk may have retained their volatiles. This suggests a potentially heterogeneous volatile content, with volatile-poor outer layers overlying volatile-rich interior material, depending on the degree of interior mixing in the newly formed Moon.

References: [1] Taylor, S.R. et al. (2006) *Geochem Cosmo*, 70, 5904; [2] Paniello, R.C. et al. (2012) *Nature* 490, 376; [3] Desch, S. & Taylor, G.J. (2011) *42nd LPSC*; [4] Nakajima, M. & Stevenson, D.J. (2014) *45th LPSC*; [5] Stewart, S.T. et al. (2013) *44th LPSC*; [6] Salmon, J. & Canup, R. (2012) *Astrophys J*, 760; [7] Ward, W.R. (2012) *Astrophys J*, 744; [8] Visscher, C. & Fegley, B., Jr. (2013), *Astrophys. J. Let.*, 767, L12; [9] Canup, R. M., et al. (2015) *Nature Geoscience*, 8, 918.

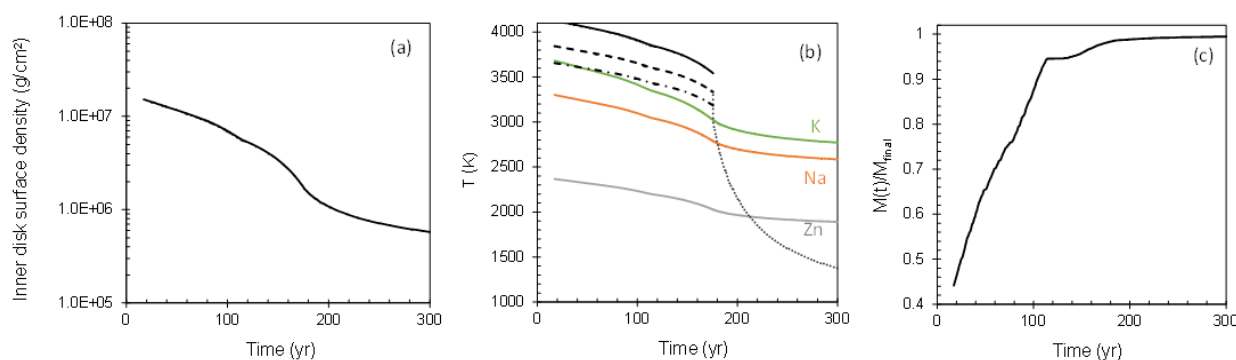


Fig. 3. For the Fig. 1 simulation: (a) Inner disk $\sigma(t)$; (b) Disk mid-plane T at a_R (black lines; solid has $x = 1$, dotted has $x = 0.1$, and dot-dashed has $x = 0.01$), and T_{50} for Zn (grey), Na (orange), and K (green) vs. time; and (c) fraction of the Moon accreted vs. time. The Moon accretes only \sim a percent of its mass after T falls substantially below T_{50} for potassium.

METAL-SILICATE PARTITIONING OF VOLATILE SIDEROPHILE ELEMENTS SUGGESTS VOLATILES WERE NOT LOST DURING LUNAR FORMATION. E. S. Steenstra¹, Y. H. Lin¹, D. Dankers¹, N. Rai^{2,3}, J. Berndt⁴, S. Matveev⁵, W. van Westrenen¹. ¹Faculty of Earth & Life Sciences, VU Amsterdam, NL (e.s.steenstra@vu.nl), ²Centre for Planetary Science, Birkbeck-UCL, UK ³Department of Earth Sciences, Mineral & Planetary Sciences Division, Natural History Museum, London, UK ⁴Department of Mineralogy, University of Münster, Germany ⁵Department of Petrology, Utrecht University, Utrecht, NL.

Introduction: The use of siderophile element depletions in planetary mantles in conjunction with their experimentally derived metal-silicate partitioning behavior has proven to be a valuable tool to constrain the pressure (P), temperature (T) and redox (fO_2) conditions during core formation in planetary bodies [1-4]. These models require adequate knowledge of the intrinsic variables that affect their metal-silicate partition coefficients (D 's). At present, the metal-silicate partitioning of a number of volatile siderophile elements (VSE) is poorly quantified, which is unfortunate because VSE abundances have the potential to provide valuable insights into the devolatilization history of planetary bodies [5]. Here we present new D 's for a number of VSE and use them to assess volatile loss during formation of the Moon. We focus on volatile siderophile elements S, Se, Te and Sb, which are believed to have been lost from the Moon due to devolatilization during the Moon-forming event [e.g., 6-8].

Methods: We used a Bristol-type end-loaded piston cylinder press to equilibrate metal-silicate mixtures within MgO capsules at 1-2.5 GPa and 1783-1883 K. We used synthetic equivalents of the Apollo green glass [9] and a lunar granite [10] obtained by mixing appropriate amounts of high-purity oxides. The metal consisted of Fe powder doped with 1 wt.% of each siderophile element, 5 wt.% Ni and 15 min [4], samples were imbedded in epoxy resin, polished for analysis and analyzed for major elements with an EMP at Utrecht University. Trace elements were measured with LA-ICPMS at Münster University.

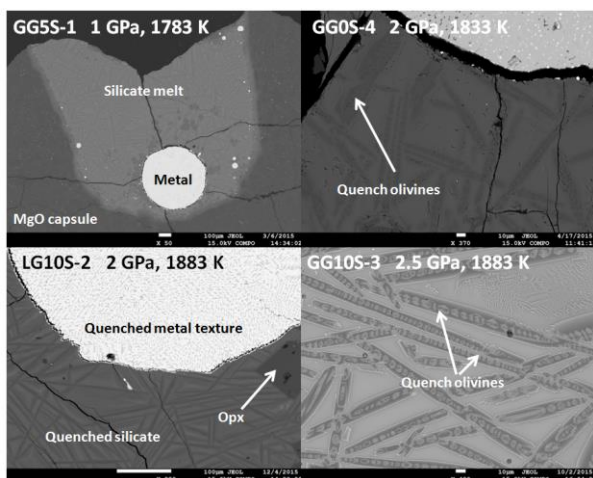


Fig. 1.: BSE images of typical run products.

Results: A typical run product is shown in Figure 1. Silicate composition varied ($nbo/t = 1-3.3$) due to variable degrees of forsterite crystallization or interaction with the capsule walls. The fO_2 was -1.2 ± 0.4 log units below the iron-wüstite buffer (ΔIW), which was calculated assuming non-ideal mixing behavior for Fe and $\gamma_{FeO} = 1.5$ [11].

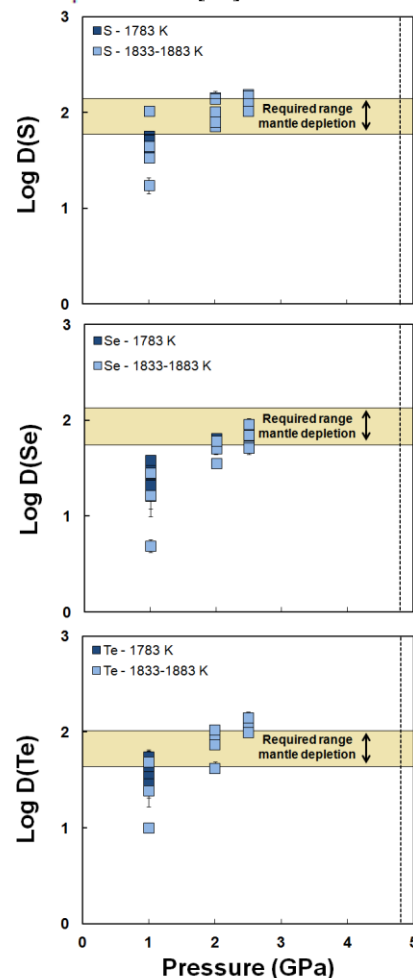


Fig. 2.: D as a function of P for low S experiments. D 's were normalized to $x_{FeO} = 0.08$. Vertical lines represent P - T conditions during lunar core formation from [2,5]. Horizontal bars represent the required D to explain their lunar mantle depletions.

The silicate melt composition varies mostly in FeO. At constant P - T and similar S contents of the metal, we observe a decrease of $D(S, Se, Te)$ with x_{FeO} . For S, this is consistent with [12]. We use these dependencies to correct for their metal-silicate partitioning when assessing other variables. $D(Sb)$ values were corrected for variable fO_2 assuming a 3+

valence state in the silicate melt [13]. Results from this study shows that $D(S, Se, Te)$ increase strongly with P (Fig. 2). No P effects for $D(Sb)$ are observed. Extrapolation of $D(Se, Te)$ with the T term of [14] to the experimental T of this study results in D 's that are much higher than observed. This suggests that [12] significantly overestimated the effect of T on $D(Se, Te)$. This agrees with the minor T effect on $D(S)$ proposed by [12].

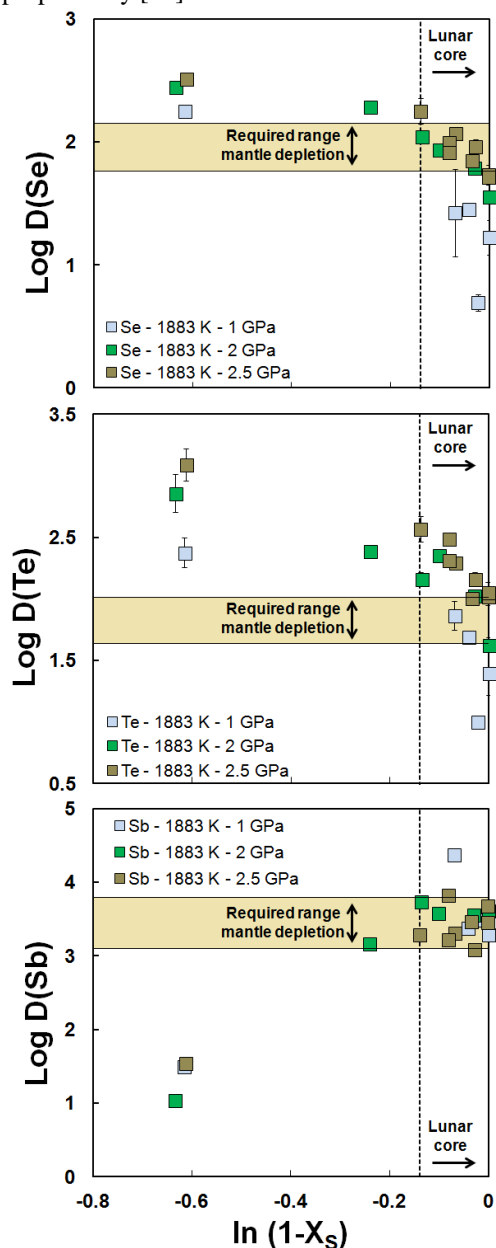


Fig. 2.: D as a function of metal S contents. D 's were normalized to $xFeO = 0.08$. Vertical line represent maximum S content in lunar core [18]. Horizontal bars are the required D to explain lunar mantle depletions by core formation assuming no volatile losses at all.

Discussion: We now asses to what extent the estimated lunar mantle depletions of $S, Se, Te,$ and Sb can be explained through their incorporation into a Fe-rich lunar core by using Eq. (1) [1-5]:

$$D_{c(i)} = \frac{C_{BM(i)} - x C_{BSM(i)}}{m(i) C_{BSM(i)} (1-x)} \quad (1)$$

where $C_{BM(i)}$ is the concentration by weight of element i in the bulk Moon (BM), $C_{BSM(i)}$ is the concentration by weight of element i in the bulk silicate Moon (BSM) and x is the mass fraction of the silicate mantle of the Moon, assumed here to be 0.975 [2,3]. The BM abundances were considered to be equal to bulk silicate Earth (BSE), validated by their identical isotope compositions for many elements, and are 250 ± 50 ppm for S , 80 ± 17 ppb for Se , 11 ± 1.7 ppb for Te and 5.5 ppb for Sb [15,16]. The BSM abundances were used from [8] and are 74.5 ± 4.5 ppm, 24 ppb, 4.1 ppb and 0.08 ppb for $S, Se, Te,$ and Sb , respectively. In other words, we assume no loss at all of S, Se, Te and Sb during Moon formation.

Figure 2 shows that the lunar mantle depletions of $S, Se,$ and Te are easily reconciled with core formation within the higher pressure range of the Moon (Fig. 2) [5]. The light element composition of the lunar core should also be taken into account, as it may drastically affect the metal-silicate partitioning of the elements considered here. Recent studies suggest that the sulfur budget of the lunar core ranges anywhere between $\sim 0 - 8$ wt% [e.g., 17-18] and in a companion abstract, we provide geochemical arguments that the lunar core is unlikely to contain appreciable amounts of S [19].

For Se and Te , addition of S to the lunar core would only further increase the feasibility of explaining their abundances in the lunar mantle, as it significantly increases their siderophile behavior (Fig. 3). Sb shows chalcophobic behavior resulting in a significant decrease with S in the metal. However, the estimated range of lunar core S is not high enough to sufficiently reduce the siderophile behavior of Sb . In addition, [3] recently showed that the lunar mantle depletions of 13 other siderophile elements do not require a S -bearing core. The lunar mantle depletion of Sb is therefore also consistent with core formation depletion only. We conclude that the Moon contains as much S, Se, Te and Sb as the silicate Earth – no devolatilization of these elements needs to have occurred during the Moon forming event.

References: [1] Rai & van Westrenen (2013) *JGR* 118 [2]

Rai & van Westrenen (2014) *EPSL* 388 [3] Steenstra et al (2016) *GCA* 177 [4] van Westrenen et al (2016) *LPSC* [5] Steenstra et al (2016) *EPSL* 441 [6] Taylor (1987) *GCA* 51 [7] Taylor (2014) *PTRS* 372 [8] Hauri et al (2015) *EPSL* 409 [9] Delano (1986) *JGR* 91 [10] Warren (1983) *EPSL* 64 [11] O'Neill & Eggins (2002) *CG* 186 [12] Boujibar et al (2014) *EPSL* 391 [13] Righter et al (2009) *GCA* 73 [14] Rose-Weston et al (2009) *GCA* 73 [15] McDonough & Sun (1995) *CG* 120 [16] Wang & Becker (2013) *Nature* 499 [17] Steenstra et al (2016) *Under review* [18] Laneville et al (2014) *EPSL* 401 [19] Steenstra et al (2016) *ELS*

DETERMINING THE SOURCE(S) OF H₂O IN THE LUNAR INTERIOR. J. J. Barnes¹, D. A. Kring², R. Tartèse³, I. A. Franchi¹, M. Anand^{1,4} and S. S. Russell⁴, ¹Planetary and Space Sciences, The Open University, Milton Keynes, MK7 6AA, UK (jessica.barnes@open.ac.uk), ²Lunar and Planetary Institute, 3600 Bay Area Boulevard, Houston, TX 77058, USA, ³IMPMC, Muséum National d'Histoire Naturelle, Sorbonne Universités, CNRS, UPMC & IRD, 75005 Paris, France. ⁴Department of Earth Sciences, Natural History Museum, London, SW7 5BD, UK.

This work is currently embargoed.

This work is currently embargoed.

HYDROUS EARLY MOON? CONSTRAINTS FROM HYDROUS LUNAR MAGMA OCEAN SOLIDIFICATION EXPERIMENTS. Y. H. Lin*, E. S. Steenstra and W. van Westrenen, Faculty of Earth and Life Sciences, VU University Amsterdam, The Netherlands (y.lin@vu.nl)

Introduction: Since ~2008, the traditional view of a dry Moon [1] has been challenged by the identification of water in lunar pyroclastic glasses [2, 3], lunar minerals including apatite [3–12] and melt inclusions in lunar olivine [3, 13, 14]. Water could therefore play an important role in the evolution of the Moon, including perhaps during the cooling and crystallization of an early lunar magma ocean (LMO). Numerical [15] and recent experimental [16, 17] models simulating solidification of the LMO were all performed under anhydrous conditions. Although some models of the effect of water on the evolution of the Moon have been published [e.g. 18], these are based on experimental data of physical and chemical rock properties obtained under anhydrous conditions. Water has been shown to greatly affect the physical and chemical properties of minerals and magmas, even at low concentrations [19]. Therefore, the presence of significant amounts of water in the ancient lunar interior requires a reassessment of lunar evolution models.

This study: Here, we show results of a ~95% crystallization sequence of a wet LMO using experiments at pressure-temperature (*P-T*) conditions that are directly relevant to the evolution of the lunar interior. A ‘two-stage’ model of magma ocean solidification is assumed, which features early efficient crystal suspension in magma and corresponding equilibrium crystallization, followed by fractional crystallization of the later residual magma ocean. The crystallization sequence and composition of the resulting concentric cumulate layers with different mineralogical assemblages are of primary importance for further understanding key events in lunar evolution, including the thickness of a plagioclase-rich crust [20]. The aim of this work is to solve two main questions: (1) What is the crystallization sequence of a hydrous LMO and how do the chemical compositions of cumulates and corresponding residual LMO vary with progressive solidification under hydrous conditions. (2) What are the quantitative differences between dry and wet LMO solidification scenarios. Answering the latter question could provide new constraints on the amount of water that can/should/might be present in the Moon during LMO crystallisation.

Experimental: Except for the water content of the experiments, we use a similar experimental approach as in our companion work focusing on the evolution of a dry LMO [17]. Hydrous experiments were performed from the fifth step of our dry LMO solidification model [17], which is the first step in

which plagioclase starts crystallizing. In the first set of experiments reported here, we simulate a hydrous LMO by adding quantitative amounts of Mg(OH)₂ to produce 2 wt.% OH (1 wt.% H₂O) upon melting from the fourth step of the dry LMO solidification series [17]. This implies a water content of 3150 ppm H₂O in the initial LMO. The water concentrations in subsequent starting materials are calculated and added based on mass-balance and the percent of the residual liquid of the previous crystallization step with removal of the corresponding crystals. Future experiments will start with different initial water concentrations.

Analytical: All experiments were analyzed with a JEOL electron microprobe at Utrecht University (15kV, 25nA for Si, Ti, Al, Fe, Mg and Ca), and checked for contamination and/or iron loss. The mineral and melt proportions were determined both by mass balance calculations and area percentage using an EDAX EDS system in imaging mode.

Results: Unsurprisingly, our results differ markedly from our companion experimental study performed on the same bulk magma ocean composition under anhydrous conditions [17]. There are obvious differences in formation conditions and the amount of crystallized minerals between the anhydrous and wet LMO [15,17] (Fig. 1). Under hydrous conditions, plagioclase first appears between 73 and 77 per cent crystallisation (PCS) (68–76 PCS for [17]). Ca-rich pyroxene starts crystallizing at 70–73 PCS, and olivine does not crystallize at >77 PCS. Plagioclase starts crystallizing at 1200 °C in our experiments, 40 °C lower than that for a dry system [17]. Subsequently, the crystallizing amounts of plagioclase are smaller than those produced at the same *P-T* conditions in a dry system (Fig. 1). From 89 to 95 PCS, spinel, ilmenite and quartz appear and coexist with plagioclase and cpx. Corresponding residual LMO compositions also differ markedly from those produced under dry conditions [17].

Discussion and conclusions: The presence of water significantly suppresses the crystallization of plagioclase [19], and results in the formation of spinel. At ~95 PCS, the anorthosite crust has a thickness of 32.2 km, which is about 26 km thinner compared to ~58 km under dry conditions [17]. This suggests that improved estimates of lunar crustal thickness [e.g. 21,22] could be used as a hygrometer for the early lunar interior.

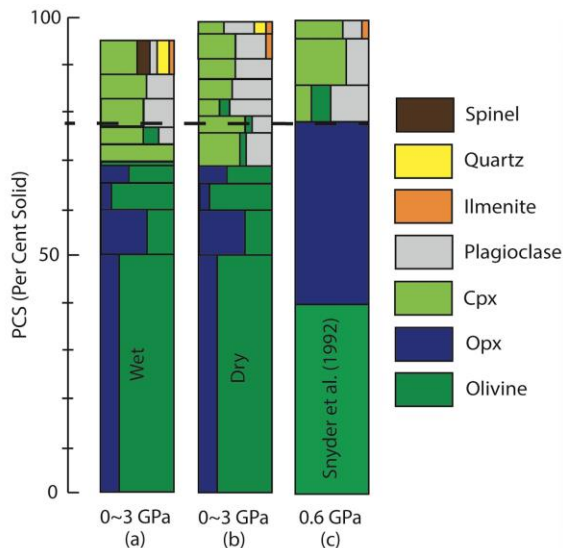


Figure 1: Comparison of experimental LMO solidification models (a) this study, wet Moon, (b) from [17], dry Moon, (c) from [15], dry Moon)

Outlook: At the meeting we plan to provide further updates on the progress of our LMO crystallisation study. Upcoming experiments will be focused on constraining estimates of the total predicted thickness of the plagioclase crust under different lunar interior water contents.

References:

- [1] Taylor S. R. et al. (2006) *Rev. Mineral. Geochem.* 60, 657–704.
 [2] Saal A. E. et al. (2008) *Nature*, 454, 192–195.
 [3] Saal A. E. et al. (2013) *Science*, 340, 1317–1320.
 [4] McCubbin F. M. et al. (2010a) *Proc. Natl. Acad. Sci. U.S.A.*, 107, 11223–11228.
 [5] McCubbin F. M. et al. (2010b) *Am. Mineral.* 95, 1141–1150.
 [6] Boyce J. W. et al. (2010) *Nature*, 466, 466–469.
 [7] Greenwood J. P. et al. (2011) *Nat. Geosci.* 4, 79–82.
 [8] Hui H. J. et al. (2013) *Nat. Geosci.* 6, 177–180.
 [9] Tartèse and Anand (2013) *Earth Planet. Sci. Lett.* 361, 480–486.
 [10] Tartèse R. et al. (2013) *Geochim. Cosmochim. Acta* 122, 58–74.
 [11] Tartèse R. et al. (2014) *Geology*, 42, 363–366.
 [12] Barnes J. J. et al. (2014) *Earth Planet. Sci. Lett.* 390, 244–252.
 [13] Hauri E. H. et al. (2011) *Science*, 333, 213–215.
 [14] Chen Y. et al. (2015) *Earth Planet. Sci. Lett.* 427, 37–46.
 [15] Snyder G. A. et al. (1992) *GCA*, 56, 3809–3823. [16] Elardo S. M. et al. (2011) *GCA*, 75, 3024–3045. [17] Lin Y. H. et al. (2016) *LPSC*.
 [18] Elkins-Tanton and Grove (2011) *Earth Planet. Sci. Lett.* 307, 173–179.

[19] Sisson T. and Grove T. (1993) *CMP*, 113, 143–166.

[20] Shearer C. K. et al. (2006) *Reviews in Mineralogy and Geochemistry*, 60, 365–518.

[21] Wiczorek M. et al. (2013) *Science*, 339, 671–675.

[22] Martinot M. et al. (2016) *LPSC*.

CONNECTING HYDROGEN AND CHLORINE ISOTOPES IN EVOLVED LUNAR ROCKS. K. L. Robinson^{1*}, J.J. Barnes¹, M. Anand^{1,2}, G.J. Taylor³, and I.A. Franchi¹. ¹Dept. of Physical Sciences, The Open University, Walton Hall, Milton Keynes MK7 6AA UK. ²Department of Earth Sciences, Natural History Museum, London, SW7 5BD, UK, ³Hawaii Institute of Geophysics and Planetology, The University of Hawaii at Manoa, 96822 USA. *katie.robinson@open.ac.uk

Introduction: Apatite [$\text{Ca}_5(\text{PO}_4)_3(\text{OH},\text{F},\text{Cl})$] is invaluable for investigating the volatile content of the Moon. Water in apatite has now been measured in most major lunar rock types [1-9]. Water (used as shorthand for OH, H, and H_2O) in the lunar interior seems to vary both by abundance (e.g. “wet” and “dry” reservoirs) and by H isotopic composition [6,10].

Chlorine is also an important lunar volatile. The range of ratios of ^{37}Cl to ^{35}Cl (usually expressed as $\delta^{37}\text{Cl}$ relative to SMOC) in the Moon has been found to be much larger than that of Earth (~ -4 to $> +30$ ‰ versus ~ 0 to $+1$ ‰ in Earth’s mantle, [9,12-16]). The isotopic variation of Cl in lunar apatites has been used to argue for an anhydrous lunar mantle [12], but could also be related to the amount of KREEP component in lunar rocks [16].

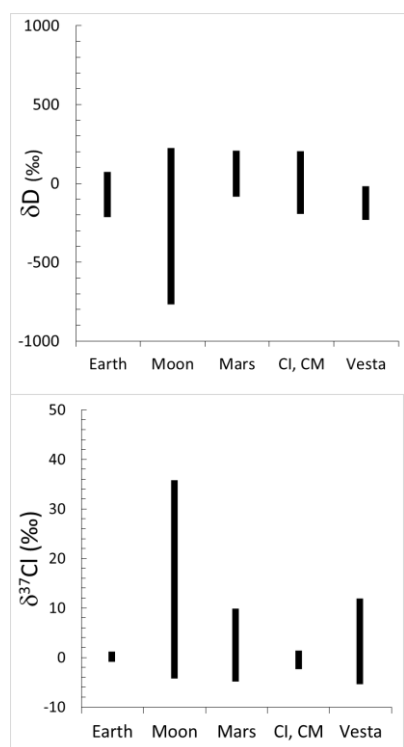


Fig. 1. δD and $\delta^{37}\text{Cl}$ range widely in the Moon compared to other bodies, though Vesta may have $\delta^{37}\text{Cl}$ as high as $+36$ [28]. Data from [6,9,12-16,22-27].

The quartz monzodiorites (QMDs) are evolved lunar rocks thought to have been formed intrusively through extensive fractional crystallization of a KREEP basaltic magma [10,17-18]. This intrusive origin makes them attractive for H_2O and H isotope

studies as intrusive rocks, formed at depth and pressure, may have undergone less magmatic degassing (which fractionates H isotopes) prior to apatite crystallization than eruptive rocks such as the mare basalts [e.g. 4-5,7-8]. Work by Robinson et al. [10-11] on a set of QMDs from Apollo 15 showed that their apatites have extremely low (D-depleted) D/H ratios, which may represent a primitive H component in the lunar interior. Here we present data for the isotopic composition of Cl in apatite in these same samples.

Samples and Methods: We studied apatite in three QMD thin sections: 15404, 51 and -,55, and 15403, 71. Apatite in these sections had been previously measured for H_2O content and δD at the Open University and Univ. of Hawaii [10-11]. All of these apatite grains have extremely low δD values (~ -440 to -750 ‰) and < 300 ppm H_2O [10-11]. Two additional apatite crystals in 15404, 55 were measured for Cl. Cl isotopes were measured using the OU Cameca NanoSIMS 50L following a similar protocol to those described in Tartèse et al. [9], and Barnes et al. [15].

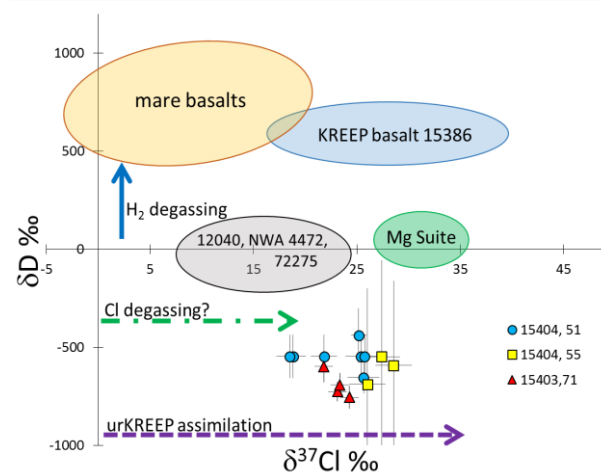


Fig. 2. δD value vs $\delta^{37}\text{Cl}$ value of lunar apatites. The data from this study are shown as points. If a δD value for a given apatite was not available, the average of all other apatite δD analyses in the same thin section was used. Literature data are represented by fields [4-5,7-9,12,15-16], and arrows indicate the effects of various processes that could have caused the observed H and Cl isotopic variations [4-5,7-8,15-16,19].

Results: Apatite grains in the QMDs studied here are very enriched in ^{37}Cl with respect to Earth’s mantle, which has a $\delta^{37}\text{Cl}$ value of ~ 0 ‰ [13] (Fig. 1,2). With respect to the Moon, they are enriched in ^{37}Cl and exhibit a relatively narrow range in $\delta^{37}\text{Cl}$ values

(Fig.2.). Uncertainties on these measurements were usually better than 2 ‰. There do not appear to be any systematic variations (such as zoning) within the grains studied here.

Discussion: Lunar samples have been shown to exhibit a wide range in $\delta^{37}\text{Cl}$ values [9,12,14-16], and a huge range in δD values (-750 to +1200 ‰) [2,4-11]. We compare the δD and $\delta^{37}\text{Cl}$ values of lunar apatites in Fig. 2. Apatite in the mare basalts have elevated δD values [2,4,5] and a large spread in $\delta^{37}\text{Cl}$ values (~-4 to +18 ‰) [15-16], while KREEP basalt 15386 contains apatite with moderately elevated δD values [8] and a large spread in $\delta^{37}\text{Cl}$ values [15]. Apatite, in mare basalt 12040, KREEP basalt 72275, and in KREEP basalt clasts from meteorite NWA 4472 have low δD values but moderately elevated $\delta^{37}\text{Cl}$ values [8-9,12,16]. In addition, rocks from the magnesian suite have apatite characterized by low δD values and elevated $\delta^{37}\text{Cl}$ values [7,15].

A number of processes may have affected the isotopic composition of H and Cl in mare magmas (Fig. 1). High δD values recorded by apatite in lunar basalts have been attributed to magmatic degassing of H_2 , which likely enriched the residual melt in D [4-5,7-8]. Degassing of Cl in the form of metal chlorides may also have enriched basaltic melts in the heavier ^{37}Cl isotope, causing isotopic fractionations of up to 20 ‰ [19].

On a wider scale, Cl degassing from the lunar magma ocean has been suggested to have caused the apparently elevated (~+30 ‰) $\delta^{37}\text{Cl}$ composition of urKREEP [15-16]. This argument is supported by the positive correlation between Cl isotopic composition and KREEP component (defined by incompatible trace element ratios) in lunar samples [15-16, 20].

If the elevated $\delta^{37}\text{Cl}$ values of apatite correspond to a greater amounts of KREEP component in the samples, then the Apollo 15 QMDs discussed here are interesting. The Cl isotopic composition of apatites in the QMDs (Fig. 2) are consistent with the compositions of apatite from other KREEP-rich samples [9,12,15]. This similarity in Cl isotopic composition makes it more difficult to reconcile the ultralow δD values of apatite in the QMDs [10-11], which are highly anomalous among lunar rocks. It seems that in the KREEPy parental melts to the QMDs, water and Cl were decoupled, and our results indicate that perhaps Cl and water were derived from different sources within the Moon.

Conclusions: The distribution in the lunar interior of both water and Cl is heterogeneous. Cl appears to be decoupled from water and related to urKREEP content, as proposed by [14]. The Apollo 15 QMDs contain very dry apatite (< 300 ppm H_2O , [10-11]) and are high in KREEP content. They have correspondingly high $\delta^{37}\text{Cl}$ values (Fig. 2). However, their anomalously low δD values (as low as -750 ‰ [11])

cannot be explained by any of the processes (degassing, etc.) discussed so far and may indicate a unique source of H in the lunar interior.

References: [1] McCubbin, F. M. et al. (2010) *PNAS*, 107, 11223-11228. [2] Greenwood, J. P. et al. (2011) *Nat. Geosci.*, 4, 79-82. [3] Boyce J. W. et al. (2010) *Nature*, 466, 466-469. [4] Barnes J. J. et al. (2013) *Chem. Geol.*, 337-338, 48-55. [5] Tartèse R. et al. (2013) *GCA*, 122, 58-74. [6] Robinson K. L. and Taylor G. J. (2014) *Nat. Geosci.*, 7, 401-408. [7] Barnes J. J. et al. (2014) *EPSL*, 390, 244-252. [8] Tartèse R. et al. (2014) *Geology*, 42, 363-366. [9] Tartèse R. et al. (2014) *MaPS*, 49, 2266-2289. [10] Robinson K. L. et al. In review, *GCA* [11] Robinson K. L. et al. (2014) *LPS XLV*, Abstract #1607. [12] Sharp Z. D. et al. (2010) *Science*, 329, 1050-1053. [13] Sharp Z. D. et al. (2013) *GCA*, 107, 189-204. [14] Treiman A. H. et al. (2014) *Am. Min.*, 99, 1860-1870. [15] Barnes J. J. et al. In review, *EPSL*. [16] Boyce J. W. et al. (2015) *Sci. Adv.*, 1 (8), 1-8. [17] Ryder G. (1976) *EPSL*, 29, 255-268. [18] Ryder G. & Martinez R. R. (1991) *LPS XXI*, 127-150. [19] Ustunisik G. et al. (2015) *Am. Min.*, 100, 1717-1727. [20] Barnes J. J. et al. (2016) *LPS XLVII*, Abstract #1439. [21] Geiss J. and Gloeckler G. (1998) *Space Sci. Rev.* 84, 239-250. [22] Hallis L.J. et al. (2012) *EPSL*, 359-360, 84-92. [23] Hallis L.J. et al., (2015) *Science* 350, 795-797. [24] Sarafian A.R. et al. (2014) *Science* 346, 623-626. [25] Roszj r J. et al. (2015) *Misasa V Abst. Vol.*, P-10, 55. [26] Sharp Z.D. et al. (2016) *Meteor. Planet. Sci.* 10.1111/maps.12591 [27] O'D Alexander, C. M. et al. *Science* 337, 721-723 (2012). [28] Barrett T.J. et al., (2016) *LPS XLVII, Abstract*

Acknowledgements: We thank NASA CAPTEM for allocation of lunar samples. This research was partially supported by grants from UK STFC (# ST/L000776/1 to M.A. and I.A.F) and the Open University.

WATER AND VOLATILES IN APOLLO ROCKS: NEW RESULTS FROM SAPPORO AND CONNECTICUT. J. P. Greenwood¹, S. Itoh², N. Sakamoto³, P. H. Warren⁴, J. A. Singer¹, M. E. Lowe¹, S. Mahmood¹, and H. Yurimoto³ ¹Dept. of Earth & Environmental Sciences, Wesleyan University, Middletown, CT 06459 USA, ²Graduate School of Science, Kyoto University, Kyoto JAPAN, ³Natural History Sciences, Hokkaido University, Sapporo, JAPAN 060-0810, ⁴Institute of Geophysics & Planetary Physics, UCLA, Los Angeles, CA 90095 USA.

Introduction: Since the discovery of water in lunar soil samples [1], there has been an explosion in research on the new field of lunar water. We have been analyzing water, D/H, and other volatile elements in Apollo rock samples since 2009, and have now conducted thousands of analyses, using SIMS spot analyses, SCAPS ion image analyses, FEG-EPMA, FEG WDS $K\alpha$ mapping, FEG-EDS, and micro-Raman spectroscopy in high titanium mare basalts, low titanium mare basalts, AI-basalts, KREEP basalts and highland rocks. This extensive analysis of Apollo rock samples allows us to understand the history and distribution of volatiles in lunar samples that cannot be attained by studying lunar soil samples alone.

High Titanium Basalts: We have now found abundant evidence for volatile-rich and water-rich glasses and melt inclusions in high-titanium basalts [2-4]. We have also found evidence for a change to more oxidizing conditions in the high-titanium basalts upon emplacement near the lunar surface, wherein we find Fe metal becoming oxidized to form hercynite (FeAl_2O_4). We have also found a new lunar volatile mineral, with the preliminary name of Ce-Chlor-Britholite, that crystallizes *after* apatite in slowly-cooled high titanium basalts. That this mineral crystallizes after apatite, and is F-,Cl-rich, shows that apatite crystallization did not deplete the melt in fluorine, as predicted by the Lunar Apatite Paradox model [5]. We predict that all high-titanium basalts were similarly enriched in volatile elements. We will present results that demonstrate that some high-titanium basalts have only an order of magnitude depletion in H_2O relative to terrestrial magmas. If high-titanium magmas underwent significant degassing [6], then this would predict at least earth-like levels of water, and possibly higher.

Low Titanium Basalts: The low-titanium basalts have proven especially fruitful for disentangling the D/H history of lunar magmas. We will present the results of a comprehensive and cohesive model to explain D/H systematics of the Moon. This model indicates a high D/H for the lunar mantle, as originally found by [7].

According to the Lunar Apatite Paradox model, OH-rich apatites are due to low overall volatile element contents of lunar magmas. OH-rich apatites are only found in low-titanium basalts, suggesting overall lower volatile contents for low-titanium basalts relative to high-titanium basalts. Conversely, chromite-

hosted melt inclusions have high F and Cl abundances [8], suggesting that water behavior may be decoupled from F and Cl in these magmas, and especially during their subsolidus history [9].

KREEP basalts: We have found the most Cl-rich extraterrestrial glasses in KREEP basalts 15382 and 15386, with up to 1000 ppm Cl [10]. Comparison of volatile/refractory elements such as F/Nd and Cl/Nb of KREEP basalts, shows an order of magnitude depletion in F and double that in chlorine relative to the Earth (Fig. 1). All lunar samples analyzed for F and Cl thus far, including 74220 water-rich olivine hosted melt inclusions, show a similar relationship (Fig. 1).

Summary: Comprehensive analyses of volatile element distributions in Apollo rock samples since 2009 have finally unveiled the history of lunar volatiles and the origins of the Moon's water. High D/H of the lunar mantle is still best explained as delivery of cometary water to the Moon after the Giant Impact.

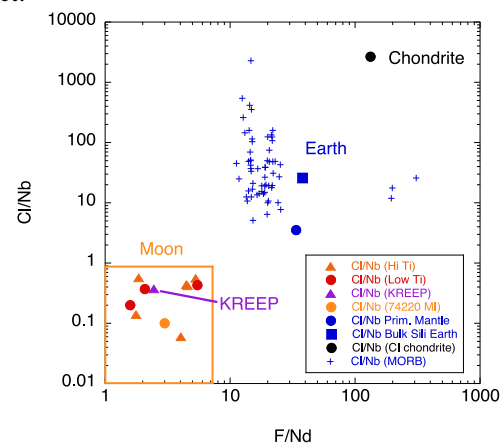


Figure 1. Cl/Nb vs. F/Nd of the Moon, Earth, and Cl.

References: [1] Saal A. E. et al. (2008) *Nature*, 454, 192-196. [2] Greenwood J. P. et al. (2016) *In submission*. [3] Lowe M. E. et al. (2016) *LPS XLVII*. [4] Mahmood S. (2016) *LPS XLVII*. [5] Boyce J. W. et al. (2014) *Science* 344, 400-402. [6] Hauri E. H., et al. (2015) *Earth Planet. Sci. Lett.* 409, 252-264. [7] Greenwood J. P. et al. (2011) *Nature Geosci.*, 4, 79-82. [8] Singer J. A. et al. (2016) *Geochem J.* in submission. [9] Treiman A. H. et al. (2016) *Am. Mineral.* In press. [10] Greenwood J. P. et al. (2016) *Nature Geosci.* In review.

EXPERIMENTAL CONSTRAINTS ON VOLATILE PARTITIONING BETWEEN APATITE AND SILICATE MELT UNDER LUNAR CONDITIONS. N. J. Potts^{1,2*}, W. van Westrenen², R. Tartèse^{1,3}, I. A. Franchi¹, J. J. Barnes¹, M. Anand^{1,4}. ¹Planetary and Space Sciences, The Open University, Walton Hall, Milton Keynes, MK7 6AA, UK. ²Faculty of Earth and Life Sciences, Vrije Universiteit Amsterdam, De Boelelaan 1085, 1081 HV Amsterdam, The Netherlands. ³Institut de Minéralogie, de Physique des Matériaux et de Cosmochimie, Muséum National d'Histoire Naturelle, Sorbonne Universités, CNRS, UPMC & IRD, 75005 Paris, France. ⁴Department of Earth Sciences, The Natural History Museum, Cromwell Road, London, SW7 5BD, UK. *Corresponding author: nicola.potts@ed.ac.uk

Introduction: Apatite is the main volatile-bearing phase in lunar samples and is widespread throughout the lunar rock collection, making it an ideal candidate to serve as a probe to reconstruct the volatile content of the interior of the Moon [1]. Translating measurements of volatiles (F, Cl, OH) in apatite to volatile abundances in the parent melt from which it crystallised, however, remains a major challenge. Previous experiments [2,3,4,5,6] have attempted to constrain volatile partitioning between apatite and silicate melt, yet none have been performed with bulk compositions directly relevant to the Moon. Additionally, synthesis of fluorapatite has been a lower priority in experimental investigations, with no study detailing F, Cl, OH partitioning in fluorine-rich apatite. In most lunar basalts, apatites are Cl-poor and have volatile compositions extending along the F-OH join of the F-Cl-OH apatite ternary diagram, with the majority of analyses clustering close to the F-rich fluorapatite end-member [1].

We measured the volatile contents of magmatic fluorapatite, containing variable amounts of Cl and OH, and co-existing silicate melt under lunar high-pressure, high-temperature conditions. Apatite crystals were grown from a silicate melt similar in composition to reconstructed melt compositions from mesostasis regions in which apatite is most commonly found in lunar basalts [7].

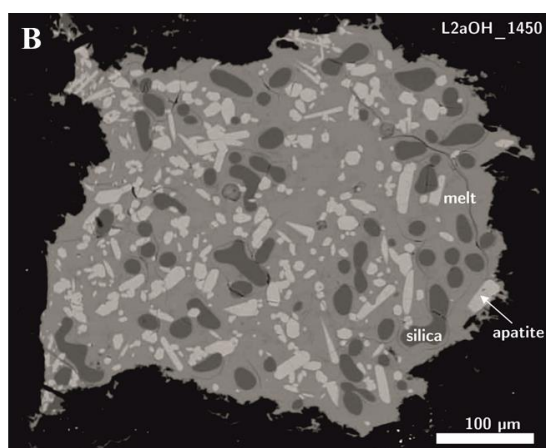


Fig. 1: Back-scattered electron image of a representative experiment in this study.

Methods: *Experimental methods.* Experiments were conducted in an end-loaded piston cylinder at

Vrije Universiteit Amsterdam using a talc-pyrex assembly and a double capsule of Pt and graphite. Each mixture was heated to 1550 °C (super liquidus) at 100 °C/minute, dwelled for 10 minutes, and subsequently cooled to final experimental temperatures at 50 °C/hr. During the heating cycle pressure was kept low, ~300 psi until the final T was reached and then increased to ~715 psi (equivalent to 1GPa). Experiments were left to dwell for 21 hrs at final T. Runs were quenched by turning off the power. Experiments were conducted for 7, 18, 46, and 72 hrs to assess equilibrium.

NanoSIMS methods: Volatiles were measured with the Cameca NanoSIMS 50L at the Open University. Apatite and glass targets were identified using real time imaging of Si and F ions. Once identified an 8 × 8 μm area was rastered using a 110 pA beam for 1 minute. For analysis, secondary ions of ¹⁶O ¹H, ¹⁸O, ²⁸Si, ¹⁹F, ³¹P, and ³⁵Cl were collected simultaneously from the central area of a 4 × 4 μm area using a 30 pA beam current for 3 minutes. F, OH, and Cl abundances were calibrated using ¹⁹F/¹⁸O, ¹⁶O¹H/¹⁸O, and ³⁵Cl/¹⁸O ratios measured on apatite [9] and glass [10,11] standards with known volatile abundances.

Results: In each experiment, we observed apatite and quenched silicate melt. In addition, crystalline silica formed in some experiments (Fig.1). All the melts in these experiments range between dacitic and basaltic-andesite. This is similar to calculated compositions of apatite-forming melts in Apollo mare basalts [7].

In experiments, run at temperatures between 1500 and 1350 °C and a pressure of 1 GPa, simple Nernst partition coefficients were calculated from Eq. 1, where C is the concentration of an element (i) in apatite (a) or melt (b);

$$D = C_i^a / C_i^b \quad (\text{Eq.1})$$

These D values in this study range from:

- $D_{\text{OH}} = 0.24 \pm 0.004$ to 1.02 ± 0.009 ,
- $D_{\text{Cl}} = 0.23 \pm 0.020$ to 8.00 ± 0.002 ,
- $D_{\text{F}} = 1.80 \pm 0.06$ to 7.7 ± 0.039 .

$$K_D^{F-Cl} = \frac{X_F^{\text{Ap}} X_{\text{Cl}}^{\text{melt}}}{X_{\text{Cl}}^{\text{Ap}} X_F^{\text{melt}}} \quad (\text{Eq.2})$$

The $K_D^{\text{F-Cl}}$, $K_D^{\text{F-OH}}$, and $K_D^{\text{Cl-OH}}$ values from this study are calculated using Eq.2 where X_F is the mole fraction of F in apatite or melt, respectively (F is in-

terchangeable for Cl or OH). This method differs from studies where D values, calculated from wt.%, have been used to calculate K_D 's.

The K_D values in this study range as follows;

- $K_D^{F-Cl} = 0.8 \pm 0.5$ to 2.7 ± 0.1
- $K_D^{F-OH} = 2.7 \pm 0.1$ to 12.5 ± 0.6
- $K_D^{Cl-OH} = 1.4 \pm 0.03$ to 8.9 ± 0.01

Discussion: *Apatite-melt partitioning of volatiles:* Similar to previous studies, our experiments show a clear preference for partitioning of $F \gg Cl \gg OH$ into the apatite structure. K_D values calculated from this study are compared with those from literature studies [2,3,4,5,6] in Fig. 2. In the fractional crystallization model of [12] Cl and OH do not begin to partition into apatite until F becomes depleted in the melt. Our experiments, however, demonstrate that apatite can incorporate significant amounts of Cl and OH even when the melt still contains appreciable amounts of F.

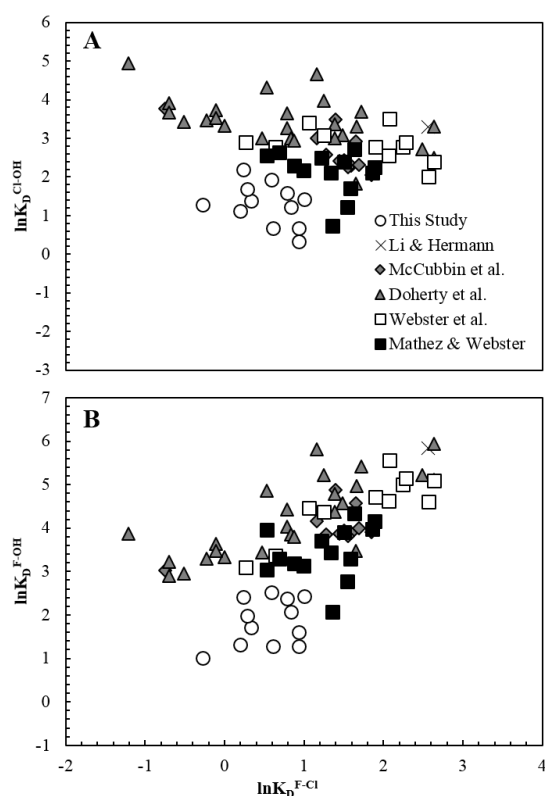


Fig.2: $\ln K_D^{F-Cl}$ plotted against (A) $\ln K_D^{Cl-OH}$ and (B) against $\ln K_D^{F-OH}$ for values obtained in this study and those of the literature [2,3,4,5,6].

Overall the K_D values we calculated here are clearly different from the recently proposed constant values of [3]. Compared to the experiments of [3], our experiments were performed with different silicate bulk compositions, at different temperatures, and with a different bulk volatile inventory. Rough trends between increasing temperature and decreasing K_D are observed; stronger trends between melt SiO_2 and total volatile content are seen in experiments here and

[3]. The overall current experimental database for apatite-melt partitioning of volatile compounds is not extensive enough to be able to specifically link the variability in K_D values exhibited in Fig. 2 to one or more specific parameters.

The results of this study highlight how apatite with similar compositions can form from melts with different volatile contents. We conclude that intrinsic parameters, including temperature and silica content of the melt, could exert a greater control on apatite-melt volatile partitioning than the relative proportions of volatiles F, Cl and OH or the total volatile abundance in the system.

Acknowledgements: This work was funded to an STFC studentship awarded to NJP, a STFC research grant to MA (Grant no. ST/I001298/1) and a NOW Vici grant to WvW. NanoSIMS machine time was allocated through UKCAN (Grant no. ST/I001964/1 to IAF).

References: [1] McCubbin et al. (2015) *Am. Min.* 100, 1668-1707. [2] Li and Hermann (2015) *GCA*, 166, 267-297. [3] McCubbin et al. (2015) *Am. Min.*, 100, 1790-1802. [4] Doherty et al. *Chem. Geol.*, 384, 94-111. [5] Webster et al. (2009) *GCA*, 73, 559-581. [6] Mathez and Webster (2005) *GCA*, 69, 1275-1286. [7] Potts et al. (*in review*), *MaPS*. [8] McCubbin et al. (2012) *Geology*, 40, 683-686. [9] MacDonald et al. (2010) *U.S.G.S Prof. Paper*, 1523, 214. [10] Jochum et al. (2011) *Geostds & Geoanal. Res.*, 35, 397-429. [11] MacDonald et al., (2010) *U.S.G.S. Paper*, 1523, 214. [12] Boyce et al. (2014) *Science*, 344, 400-2.

COMPRESSIBILITY AND DENSITY OF HYDROUS HIGH-TI LUNAR RED AND BLACK GLASS.

Eva Kelderman¹, Bart Davids¹, Yanhao Lin¹, Nachiketa Rai², Wim van Westrenen¹ and Edgar S. Steenstra¹. ¹Faculty of Earth and Life Sciences, VU University Amsterdam, The Netherlands, ²Department of Earth and Planetary Sciences, Birkbeck University of London, United Kingdom. (e.s.steenstra@vu.nl).

Introduction: The Apollo high-Ti red and black glasses are thought to represent a partial melting product of high-Ti cumulates in the deeper lunar mantle [e.g., 1] and are among the densest magmas known in our solar system. Previous studies determined the density of the black glass at high pressure (P) and temperature (T) using sink/float experiments [1] and synchrotron experiments [2,3]. A major outcome of this work was that the black glass is neutrally buoyant at the lunar-core mantle boundary and may be present there as a stable partial melt [3,4]. These measurements were all based on dry compositions. However, recent studies have suggested the presence of significant amounts of volatiles in lunar glasses, up to 1400 ppm H₂O [5-8]. Volatiles may drastically affect melt physical properties such as density and viscosity. In addition, a recent study [9] suggests significant (>2.5 wt% H₂O) water contamination of previously published sink/float experimental data, but the degree of contamination is not known. Finally, no experimental density data exists for the Apollo 15 red glass. Here, we explore the density of the Apollo 14 black and Apollo 15 red glass under hydrous conditions.

Approach: We bracket the density of high-Ti lunar melts by using the sink/float technique [10] and for this purpose we use natural San Carlos Fo₉₀ and synthetic Fo₁₀₀ spheres (200-500 μ m) obtained by abrading gem-quality crystals in a Bond air mill [11]. Starting compositions were obtained by mixing the appropriate amounts of high-purity oxides under ethanol. Al(OH)₃ was added in hydrous experiments to generate 2 wt% H₂O. Starting compositions were packed with two spheres in Mo capsules and subjected to high P-T in a non-endloaded Depths of the Earth Quickpress. Mo capsules were welded shut to minimize the ex- or infiltration of volatiles [9]. Experimental run durations were kept short (<45s) to minimize capsule-melt and sphere-melt interaction [1,9,10]. Samples were held at T slightly above the liquidus [1] to prevent dissolution of Fo spheres and crystallization. We explore a P range of 0.5 – 2.5 GPa because it is directly applicable to the lunar interior and because melt compressibility curves are largely determined in the low-P regime [e.g., 1].

Results: Run products quenched to a combination of metastable quench crystals and interstitial glass (Fig. 1) [1,12]. Runs show a highly porous texture, which may reflect degassing of H₂O upon quenching [12], implying H₂O was retained during the experiments

[13]. Spheres show a limited reaction rim due to the contrasting melt-sphere composition, but this does not significantly affect sphere density [1]. EPMA analysis confirmed the molten state of the melt and showed that some FeO loss and MoO₃ infiltration occurred, common in Mo-capsule experiments [1,9].

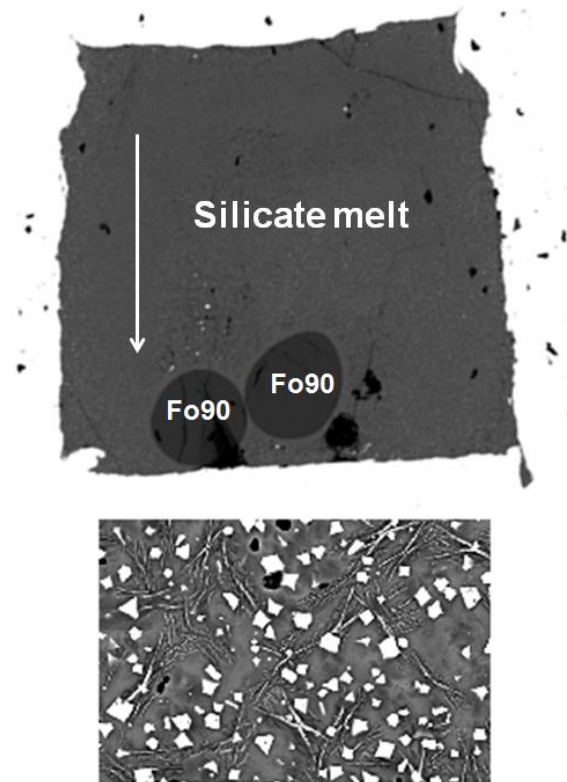


Fig. 1: Backscattered electron image of run BD-2 showing a sink with and close up of quench texture

Run	BD1	BD2	BD3	BD4.2	BD5
P (GPa)	0.5	0.75	1	1.25	1.5
T (K)	1648	1668	1688	1698	1713
Sphere	Fo ₉₀	Fo ₉₀	Fo ₉₀	Fo ₉₀	Fo ₉₀
Sphere density (g/cm ³)	3.20	3.21	3.21	3.22	3.22
Result	Sink	Sink	Sink	Sink	Sink
Run	BD6	BD7	BD8	BDE-1	BDE-3
P (GPa)	1.75	2.0	2.5	0.5	1.25
T (K)	1723	1738	1758	1648	1698
Sphere	Fo ₉₀	Fo ₉₀	Fo ₉₀	Fo ₁₀₀	Fo ₁₀₀
Sphere density (g/cm ³)	3.23	3.24	3.24	3.07	3.09
Result	Sink	Sink	NB	NB	Float

Table 1: Results for the Apollo 14 black glass (BD) NB stands for Neutral Buoyancy

Sphere densities at high P and T were calculated according to [14] and their reported sources of parameter input.

The Fo_{100} spheres were neutrally buoyant at 0.5 GPa, bracketing the hydrous Apollo 14 black glass melt density to $3.07 \pm 0.02 \text{ g/cm}^3$ at 0.5 GPa. This is increased to $3.24 \pm 0.03 \text{ g/cm}^3$ at 2.5 GPa, where Fo_{90} is neutrally buoyant with respect to the silicate melt.

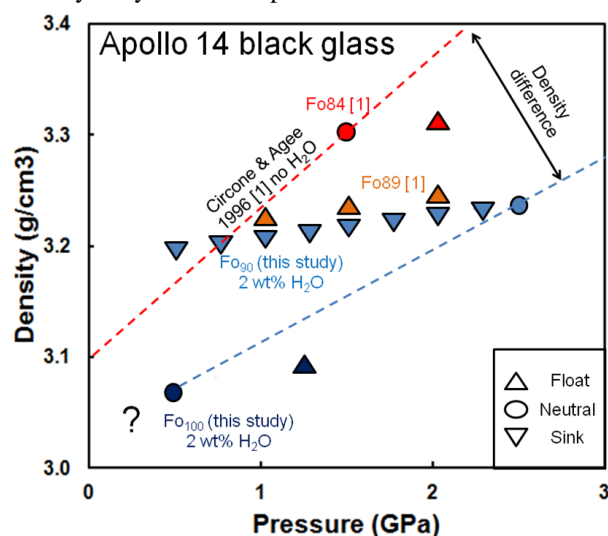


Fig. 2 Summary of experiments on synthetic molten Apollo 14 black glass from this study and [1] at T slightly above the liquidus (Table 1). Y-axis intersect of [1] is based on 1 bar density of 3.10 g/cm^3 [1,9].

Discussion: When comparing our results to those of [1], we observe a distinctly lower density of the Apollo 14 black glass. Densities are $>0.07 \text{ g/cm}^3$ lower at 0.5 GPa, and $\sim 0.16 \text{ g/cm}^3$ lower at 2.5 GPa, relative to the ‘‘anhydrous’’ experiments of [1]. The increase of density difference with P is opposite to previously reported effects of H_2O on the compressibility of Ti-poor liquids [12]. However, it is unclear to which extents the experiments of [1] were H_2O -free [9], which could explain the apparent increase of density difference with P . The significantly lower density of Apollo 14 black glass with 2 wt% H_2O derived here, suggests water contamination in the experiments [1] cannot have exceeded $>2 \text{ wt}\%$, as proposed by [9], and is probably far less. This therefore questions the feasibility of water content corrections that were recently done on sink/float data for a wide range of lunar glasses [9].

This study suggests that addition of 1 wt% H_2O results in an density decrease of at least $>0.035 \text{ g/cm}^3$ (and probably far more), which is significantly higher than 0.03 and 0.04 g/cm^3 for a ultramafic lower mantle liquid and a 50% komatiite – 50% fayalite liquid with 5 wt% H_2O , respectively [12, 13].

Work is ongoing to further constrain the dependence of lunar high-Ti melt densities as a function of

H_2O content. Additional results for the Apollo 14 black glass and first results for the Apollo 15 red glass will be reported at the meeting.

References: [1] Circone and Agee (1996) *GCA* 14, 2709-2720 [2] Sakamaki et al. (2010) *EPSL* 299, 285-289 [3] van Kan Parker et al. (2012) *Nat. Geosci.* 5, 186-189 [4] Weber et al. (2011) *Science* 331, 309-312 [5] Saal et al. (2008) *Nature* 454, 192-196 [6] Saal et al. (2013) *Science* 340, 1317-1320 [7] Hauri et al. (2011) *Science* 333, 213-215 [8] Hauri et al. (2015) *EPSL* 409, 252-264 [9] vander Kaaden et al. (2015) *GCA* 149, 1-20 [10] Agee and Walker (1988) *JGR* 93, 3437-3449 [11] Bond (1951) *Rev. Sci. Instr.* 22, 344-345 [12] Agee (2008) [13] Jing et al. (2012) *GCA* 85, 357-372 [14] van Kan Parker et al. (2011) *GCA* 75, 1161-1172

CONSTRAINING THE ORIGIN AND DIFFERENTIATION OF THE MOON USING TUNGSTEN ISOTOPES. T.S. Kruijer & T. Kleine. Institut für Planetologie, University of Münster, Wilhelm-Klemm-Str. 10, 48149 Münster, Germany. (thomas.kruijer@wwu.de).

Introduction: The Moon likely formed from hot debris produced in a giant impact on the proto-Earth [e.g., 1]. After this event, the Moon underwent large-scale differentiation, which probably involved the crystallisation of a lunar magma ocean [e.g., 2,3]. These processes can be studied using the short-lived ^{182}Hf - ^{182}W system ($t_{1/2} = 8.9$ Myr), because (i) the Moon may exhibit an ^{182}W anomaly inherited from the impactor, and (ii) early crystallisation of the lunar magma ocean would have led to ^{182}W heterogeneities within the Moon [e.g., 5-8]. However, precisely determining ^{182}W compositions of lunar samples is complicated by cosmic ray-induced neutron capture on Ta, leading to the production of ^{182}W and large cosmogenic ^{182}W variations among lunar samples [e.g., 9]. Two recent studies have precisely determined the pre-exposure ^{182}W value of KREEP-rich samples by analysing specimens devoid of neutron capture effects. These studies showed that KREEP has a 27 ± 4 ppm ^{182}W excess over the modern bulk silicate Earth (BSE) [7,8]. This finding raises the question as to whether other lunar reservoirs—such as the mare basalt sources—exhibit similar or larger ^{182}W excesses. Addressing this question is important not only for deducing the timescales of lunar differentiation but also for precisely determining the ^{182}W value of the bulk Moon.

Determining the ^{182}W signatures of mare basalts is challenging, because due to their high Ta/W, neutron capture effects may be significant even for weakly irradiated samples. One way to overcome this problem would be to analyse metal samples [5,6], but given the low abundance of metals in mare basalts, large sample masses must be processed to obtain sufficient W for precise isotope analysis. Here we use a different approach and utilize high-precision Hf isotope and Ta/W ratio measurements to empirically quantify the effects of secondary neutron capture on measured ^{182}W compositions. We report results for several low-Ti and high-Ti mare basalts, as well as for Mg-suite sample 77215, and lunar meteorite Kalahari 009.

Methods: After digestion of the lunar samples (~0.5 g) in HF-HNO₃ (2:1), and taking aliquots for determining Ta/W ratios, Hf and W were separated by ion exchange chromatography [7]. The Hf and W isotope compositions were measured on a ThermoScientific Neptune Plus MC-ICPMS at Münster [7], and reported in ϵ -units as the parts per 10⁴ deviation from terrestrial standard values.

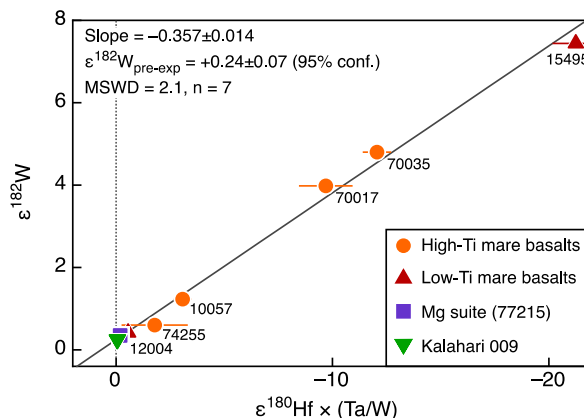


Fig. 1: $\epsilon^{182}\text{W}$ vs. $\epsilon^{180}\text{Hf} \times (\text{Ta}/\text{W})$ for lunar samples, with Ta/W ratios from [5,12].

Results: All investigated samples exhibit $\epsilon^{182}\text{W}$ distinctly higher than the terrestrial value (Fig. 1,2), consistent with [7,8]. Consistent with its very low exposure age (~230 yr) [10], Kalahari 009 shows no resolvable Hf isotope anomaly, and its $\epsilon^{182}\text{W}$ is in good agreement with the value previously obtained for KREEP [7,8]. The low- and high-Ti mare basalts, as well as Mg-suite sample 77215, have variably elevated $\epsilon^{182}\text{W}$ (Fig. 1), but also show Hf isotope variations, indicative of neutron capture effects (Fig. 1).

Discussion: *Homogeneous $\epsilon^{182}\text{W}$ in the bulk silicate Moon.* Due to neutron capture, lunar samples exhibit a positive correlation between $\epsilon^{182}\text{W}$ and $\epsilon^{180}\text{Hf} \times (\text{Ta}/\text{W})$. Samples having the same pre-exposure $\epsilon^{182}\text{W}$ should then plot on one single correlation line, whose intercept defines the pre-exposure $\epsilon^{182}\text{W}$ of this suite of samples. Fig. 1 shows that all investigated samples—including all mare basalts, Mg-suite sample 77215, and lunar meteorite Kalahari 009—plot on a single, well-

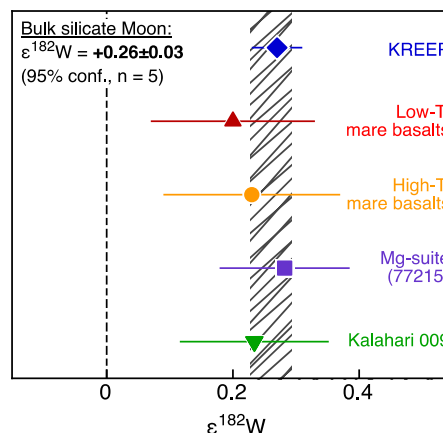


Fig. 2: Pre-exposure $\epsilon^{182}\text{W}$ data of lunar source lithologies. Data for KREEP are from [7].

defined $\epsilon^{182}\text{W}$ and $\epsilon^{180}\text{Hf} \times (\text{Ta}/\text{W})$ correlation. These samples are, therefore, characterised by a common pre-exposure $\epsilon^{182}\text{W}$ of $+0.24 \pm 0.07$ (95% conf.) as obtained from the intercept of the correlation line. After correcting the $\epsilon^{182}\text{W}$ of individual samples for neutron capture using the slope of this correlation line, all lunar source lithologies exhibit indistinguishable $\epsilon^{182}\text{W}$ (Fig. 2). Thus, our data do not reveal a resolvable ^{182}W difference between lunar basalts and KREEP, implying that the weighted mean $\epsilon^{182}\text{W}$ value of $+0.26 \pm 0.03$ (95% conf.) is representative for the bulk silicate Moon.

Timing of lunar magma ocean differentiation. Crystallisation of the lunar magma ocean led to mantle reservoirs with markedly distinct Hf/W [5,6,11-13]. Hence, if magma ocean crystallisation occurred within the lifetime of ^{182}Hf , then these reservoirs should have evolved to distinct $\epsilon^{182}\text{W}$ over time. However, our results demonstrate that, despite the variable Hf/W inferred for their sources [5,6,10-12], low-Ti and high-Ti mare basalts as well as KREEP have a homogeneous $\epsilon^{182}\text{W}$ (Fig. 3). Constraining the source Hf/W of Kalahari 009 and 77215 is not straightforward, but the radiogenic initial Hf isotopic composition and old age of ~ 4.2 Ga of Kalahari 009 [14] point to a mantle source that had undergone strong incompatible element depletion early in lunar history. Such a mantle source would likely have had a high Hf/W, but the $\epsilon^{182}\text{W}$ of Kalahari 009 is indistinguishable from KREEP, which is characterised by the lowest Hf/W among the lunar sample suite. Our results, therefore, demonstrate that the sources of KREEP, the mare basalts and Kalahari 009 must have been established after ^{182}Hf extinction, most likely later than ~ 80 Myr after solar system formation (Fig. 3). Such a late time of magma ocean differentiation is consistent with the ‘young’ ages of ~ 4.4 Ga inferred for lunar mantle sources using other isotope systems [e.g., 15].

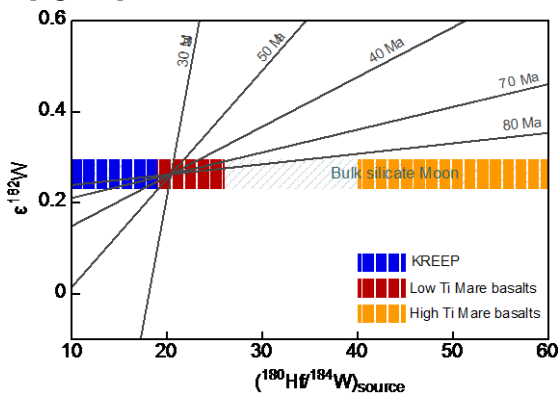


Fig. 3: $\epsilon^{182}\text{W}$ vs. the $^{180}\text{Hf}/^{184}\text{W}$ of lunar mantle sources. Shown are the pre-exposure $\epsilon^{182}\text{W}$ of the Moon from this study (hashed area), ranges in the Hf/W estimated for different lunar mantle reservoirs [5,6,11-13] (shaded areas), and reference isochrons for differentiation at different times after the start of the solar system (solid lines).

Constraints on the origin of the Moon. Our results demonstrate that the Moon shows an excess in $\epsilon^{182}\text{W}$ of $\sim 26 \pm 3$ ppm over the modern BSE. This excess agrees

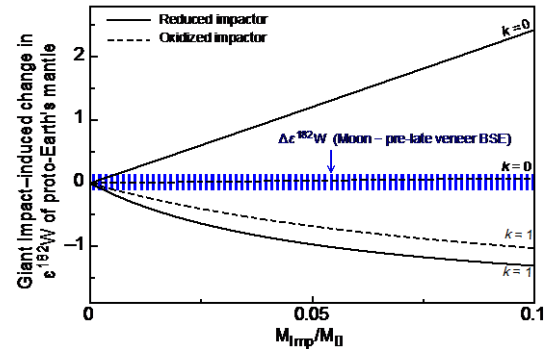


Fig. 4: Effect on the $\epsilon^{182}\text{W}$ of the proto-Earth after mixing variable amounts ($M_{\text{imp}}/M_{\oplus}$) of impactor mantle and core material. The effects are shown for two impactor compositions and for no ($k=0$) or full ($k=1$) equilibration of the impactor core with the proto-Earth mantle.

with the predicted ^{182}W change resulting from disproportional late accretion to the Earth and Moon after Earth’s core had fully formed [7,8]. Hence, the pre-late-veneer BSE and the Moon were indistinguishable in ^{182}W . However, the giant impact itself should have caused a notable Earth–Moon ^{182}W difference by (1) changing the $\epsilon^{182}\text{W}$ of the proto-Earth mantle by adding impactor mantle and (partially) equilibrating impactor core material (Fig. 4), both carrying distinct $\epsilon^{182}\text{W}$ anomalies, and (2) by supplying W-rich but ^{182}W -depleted impactor core material into the lunar accretion disk. Thus, the Earth–Moon ^{182}W homogeneity is an unexpected outcome of the giant impact. Unlike for Ti and O isotopes, the $\epsilon^{182}\text{W}$ homogeneity is difficult to explain by accretion of impactor and proto-Earth from a homogeneous inner disk reservoir [16] or by making the Moon fully from proto-Earth mantle [17,18]. Thus, the ^{182}W results require a post-giant impact state that facilitated efficient isotopic equilibration of the BSE and the Moon.

Acknowledgement: We thank CAPTEM, NASA, and Ryan Zeigler for generously providing the Apollo lunar samples for this study.

References: [1] Canup RM & Asphaug E. (2001) *Nature* 412, 708–12. [2] Shearer C.K. & Papike J.J. (1999) *Am. Min.* 84, 1464–1494. [3] Wood J. A. et al. (1970) *Proc. Apollo 11 Lunar Sci. Conf.* 965–988. [4] Zhang J. et al. (2012) *Nature GeoSc.* 5, 251–255. [5] Kleine T. et al. (2005) *Science* 310, 1671–1673. [6] Touboul M. et al. (2007) *Nature* 450, 1206–1209. [7] Kruijer T.S. et al. (2015) *Nature* 520, 523–537. [8] Touboul M. et al. (2015) *Nature* 520, 530–533. [9] Leya I. et al. (2000) *EPSL* 175, 1–12. [10] Nishiizumi K. et al. (2005) *MetSoc abstract* #5270. [11] Righter K. & Shearer C.K. (2003) *GCA* 67, 2497–2507. [12] Münker C. et al. (2010) *GCA* 74, 7340–7361 [13] Fonseca R.O.C. (2014) *EPSL* 404, 1–13. [14] Sokol A.K. et al. (2008) *GCA* 72, 4845–4873. [15] Gaffney A.M. & Borg L.E. (2014) *GCA* 140:227–240 [16] Dauphas N. et al. (2014) *Phil Trans R Soc A.*, 372. [17] Čuk M. & Stewart S.T. (2012) *Science* 338, 1047–1052. [18] Canup R.M. (2012) *Science* 338, 1052–1055.

PB ISOTOPE ANALYSES OF LUNAR SAMPLES: IMPLICATIONS FOR THE EVOLUTION OF MAJOR LUNAR SILICATE RESERVOIRS. J. F. Snape¹, A. A. Nemchin², J. J. Bellucci¹, M. J. Whitehouse¹, ¹Department of Geosciences, Swedish Museum of Natural History, SE-104 05 Stockholm, Sweden (Joshua.snape@nrm.se), ²Department of Applied Geology, Curtin University, Perth, WA 6845, Australia.

Introduction: Studies of Pb isotopes in lunar rocks are problematic, primarily due to their characteristically low bulk Pb concentrations [1]. Through *in situ* Secondary Ion Mass Spectrometry (SIMS) analyses of the Pb isotopic compositions in individual minerals, we have been able to circumvent some of the problems that have previously hindered measurements of Pb isotope compositions of lunar samples [2]. Using this method we have obtained precise crystallisation ages (2σ errors typically within ± 10 Ma) for several mare basalts and KREEP-rich basalts (those enriched in K, Rare Earth Elements and P; [3]). We have also applied this method to the Apollo 16 polymict impact melt breccia, 66095. Furthermore, by assuming that the least radiogenic compositions measured in several of these samples represent initial Pb isotope compositions, we have begun to construct a multiple stage Pb isotope evolution model to describe the development of major lunar silicate reservoirs [2].

Methods: Backscattered electron (BSE) and element mapping of the sample was performed with a Quanta 650 FEGSEM. These maps were then used to identify phases for SIMS analysis. Prior to the SIMS analyses, the sample was thoroughly cleaned with distilled water and ethanol using an ultrasonic bath and was then gold coated. The Pb systematics of the grains were analysed with a CAMECA IMS 1280 ion microprobe at the NordSIMS facility in the Swedish Museum of Natural History, Stockholm, using a methodology similar to that outlined in previous studies [4-6]. The analyses were made spot sizes of between 10-30 μm . A 20-35 μm area around each grain was pre-sputtered for 60 seconds in order to remove the gold coating and minimize surface contamination. Analyses of the USGS basaltic glass reference material, BCR-2G, were used for mass fractionation and gain calibration corrections [7].

Results: The crystallization ages determined for the mare basalts range from ~ 3.1 - 3.2 Ga for the low-Ti (where bulk rock $\text{TiO}_2 = 1$ - 6 wt%) Apollo 12 basalts, 3200-3300 Ma for the low-Ti Apollo 15 basalts, 3700 Ma for the single high-Ti Apollo 11 basalt analysed so far, while the two analysed KREEP-rich basalts (14072 and 15386) both have ages of ~ 3900 Ma. Furthermore, there is an indication of resolvable differences in both the crystallisation ages and initial Pb isotope compositions between the different basaltic suites sampled at individual landing sites (Fig. 1).

The Pb isotope compositions measured in the Apollo 16 breccia (66095), yield a Pb/Pb isochron age of 3909 ± 17 Ma (2σ). Taking the work of previ-

ous studies into account [8-9], this is interpreted as representing the formation of breccia, shortly followed by the introduction of volatile material (including Pb) during fumarolic activity, initiated by the degassing of the ejecta blanket within which the rock was emplaced. An initial Pb composition was also determined from these data (Fig. 2).

Evolution of basalt sources: The ages and initial Pb isotope compositions of all the samples analysed necessitate that source reservoirs with high μ -values (the ratio of $^{238}\text{U}/^{204}\text{Pb}$), compared to those determined for terrestrial mantle reservoirs, were established sufficiently early (>4400 Ma) in order for such radiogenic Pb isotope compositions to have evolved. A two-stage Pb evolution model indicates that the data from the basaltic samples can be explained with a primordial lunar reservoir forming by ~ 4500 Ma with a μ -value of 462 ± 46 (2σ). This would have evolved until 4376 ± 18 Ma (2σ), at which point the sources differentiated and evolved separately with μ -values of ~ 370 - 640 for the mare basalts, and ~ 2600 - 3700 for the KREEP-rich samples (Fig. 2). Note, this model calculation makes a simplistic assumption that both the mare basalt and KREEP reservoirs differentiated from a single primordial lunar reservoir at approximately the same time. Given the very high μ -values predicted for the sources of the KREEP-rich samples relative to the primordial lunar reservoir, the 4376 ± 18 Ma age most likely provides an estimate for the time of separation of the KREEP reservoir (urKREEP; [3]).

Interpretation of the 66095 age: The Pb/Pb age determined for 66095 is consistent with recent estimates for the age of the Imbrium basin forming impact, based on U-Pb analyses of zircons and phosphates in Apollo 12 and Apollo 14 impact melt breccias, as well as the lunar meteorite SaU 169 (3926 ± 2 Ma; [10-12]). An Imbrium origin is consistent with the classification of 66095 as one of the Apollo 16 "Mafic Impact-Melt Breccias" [13], which have been demonstrated as most likely representing ejecta from the Imbrium basin [14], as well as the variety of clasts in the breccia, which include highland lithologies (e.g. anorthosite) that would be expected to occur in the Apollo 16 region, and KREEP-rich material (e.g. Fra Mauro "Basalt") most likely sourced from within the Procellarum KREEP Terrane, where Imbrium is located [15-17]. This KREEP connection is also supported by the trace element compositions determined for 66095 and other polymict Apollo 16 impact breccias [18].

Origin of 66095 Pb component: A single stage model for the evolution of the Pb component in 66095 indicates that it originated from a source reservoir that was established by 4433 ± 16 Ma (2σ) with a μ -value = 943 ± 32 (2σ). If the initial Pb isotope composition and age obtained for the breccia are included in the two-stage model generated for the basalts, then the Pb component can be explained by a source reservoir that formed at a similar time to the mare basalt and KREEP reservoirs (4376 ± 18 Ma), with a μ -value of 936 ± 33 (2σ).

In the case of 66095, modelling the Pb component as having evolved in a single reservoir is likely incorrect. Given the mechanism by which Pb and other volatiles are thought to have been introduced to the breccia (i.e. fumarolic degassing of an ejecta blanket), as well as the range of materials that were present in the breccia and the surrounding Imbrium ejecta blanket, it is probable that the initial Pb isotope composition measured in 66095 represents a homogenised mixture of Pb that originated from both lunar highland lithologies and KREEP-rich material. The uncertainty in typical μ -values for the sources of different lunar lithologies [5,19] means that it is extremely hard to quantify the constituents of such a mixture. However, if the high μ -values determined for the KREEP-rich basalt sources ($\mu = 2600$ -3700) are taken as being typical of other KREEP-rich materials, then the remaining constituents (e.g. the highland lithologies) in the mixture must have originated from sources with μ -values less than ~ 900 in order to explain the measured Pb isotope composition in the breccia.

References: [1] Tatsumoto M. (1970) *LPS II*, 1595-1612. [2] Snape J. F. et al. (2015) *Proc. 78th Ann. Met. Soc.*, Abstract #5236. [3] Warren P. H. and Wasson J. T. (1979) *Rev. Geophys. Space Phys.*, 17, 73-88. [4] Whitehouse M. J. et al. (2005) *Chemical Geology*, 222, 112-131. [5] Nemchin A. A. et al. (2011) *GCA*, 75, 2940-2964. [6] Bellucci J. J. et al. (2015) *JGR*, 120, 2224-2240. [7] Woodhead J. D. and Hergt J. M. (2000) *Geostand. Geoanal. Res.*, 24, 33-38. [8] Nunes P. D. and Tatsumoto M. (1973) *Science*, 182, 916-920. [9] Shearer C. et al. (2014) *GCA*, 139, 411-433. [10] Gnos E. et al. (2004) *Science*, 305, 657-660. [11] Liu D. et al. (2012) *EPSL*, 319, 277-286. [12] Snape J. F. et al. (2016) *GCA*, 174, 13-29. [13] Korotev R. L. (1994) *GCA*, 58, 3931-3969. [14] Korotev R. L. (1997) *MAPS*, 32, 447-478. [15] Garrison J. R. and Taylor L. A. (1980) *Proc. Conf. Lunar Highlands Crust*, 395-417. [16] Hunter R. H. and Taylor L. A. (1981) *LPS XII*, 261-280. [17] Jolliff B. L. et al. (2000) *JGR*, 105, 4197-4216. [18] Ebihara M. et al. (1992) *LPS XXII*, 417-426. [19] Premo W. R. et al. (1999) *Int. Geol. Rev.*, 41, 95-128. [20] Göpel C. et al. (1985) *GCA*, 49, 1681-1695.

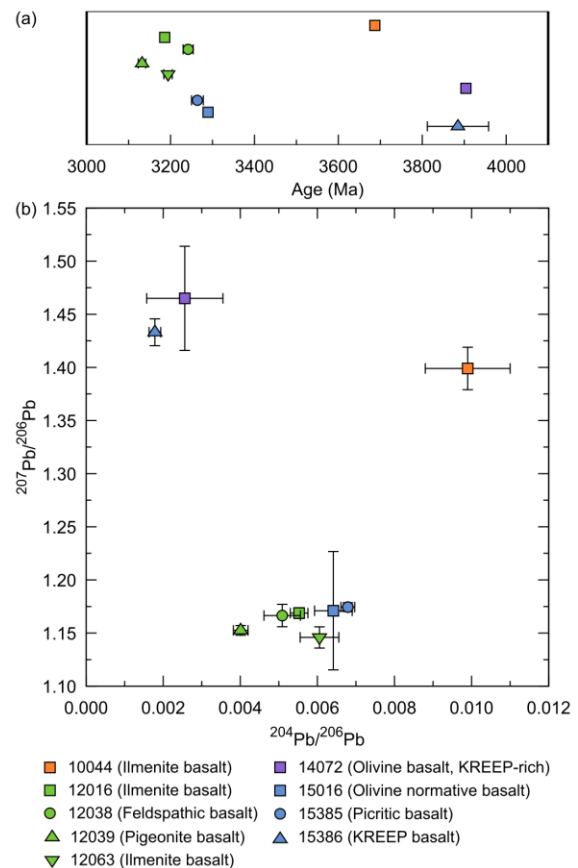


Fig. 1 - (a) Ages and (b) initial Pb isotope compositions determined for a range of lunar basalts. Error bars show 2σ uncertainties.

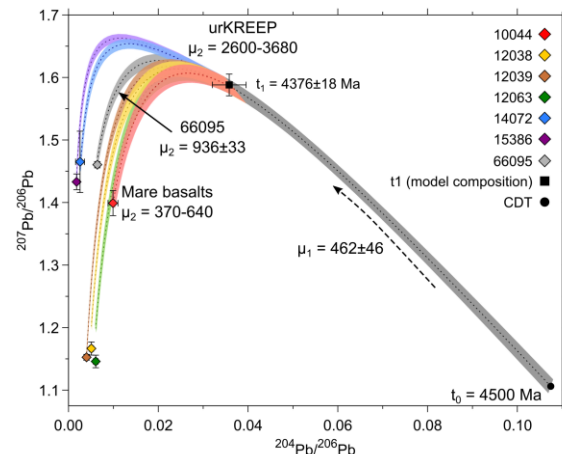


Fig. 2 - $^{207}\text{Pb}/^{206}\text{Pb}$ vs. $^{204}\text{Pb}/^{206}\text{Pb}$ plot illustrating the two-stage Pb isotopic growth model with t_0 set at 4500 Ma, and starting with Canyon Diablo Troilite (CDT) composition [20]. Dashed curves indicate the growth curves constructed with the mean model values, while the surrounding fields indicate 2σ uncertainties of these values. The initial Pb compositions determined for each sample are plotted as diamonds, colour coded to the model growth curves. Error bars indicate 2σ uncertainties.

INFLUENCE OF VARIABLE THERMAL CONDUCTIVITY ON THE THERMAL EVOLUTION OF THE MOON. Y. Zhao¹, A. P. van den Berg¹ and W. van Westrenen¹, ¹Faculty of Earth and Life Sciences, VU University Amsterdam, the Netherlands, email y.zhao@vu.nl.

Introduction: The Moon is a relatively small planetary body. Its high surface-to-volume ratio suggests that it is expected to have cooled relatively rapidly. However, recent observations suggest that it may still maintain a high temperature in its present-day interior [1, 2], raising questions about the mechanism(s) behind a delayed cooling. Temperature-dependent viscosity has been studied as a first-order factor [3] in controlling the rate of planetary cooling. The effect of variable thermal conductivity has been studied before for other planetary bodies [4, 5], but not the Moon.

The lunar crust is mainly composed of anorthositic plagioclase [6], with a small volume of mare basalt on parts of the surface. Both of these phases have a thermal conductivity of around 2 W/m/K [5, 7]. This study considers the effect of variable thermal conductivity in the lunar interior, including a low value in the crust, and assesses how it influences cooling history. This is in contrast to the uniform mantle value of 4 W/m/K commonly assumed in previous studies [4, 5, 8, 9].

An updated conductivity profile: To arrive at a more refined conductivity profile for the Moon, Hofmeister's [10] temperature- and pressure-dependent conductivity model for average mantle material is applied under lunar conditions. Temperature is obtained from the mantle convection models of [8]. Pressure is obtained from a depth-dependent gravity profile calculated from uniform mantle density and assuming an Fe-rich core radius of 350 km. Thermal expansivity decreases with depth and has a negative effect on conductivity. Results obtained from the GRAIL mission show that the lunar crust is 34-43 km thick [11]. In this study, we assume the crust has a thickness of 40 km, and a thermal conductivity of 2 W/m/K.

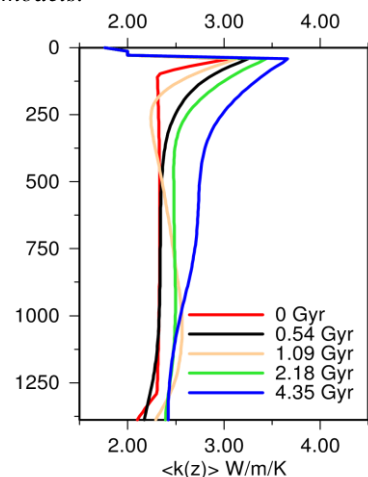
The resulting temperature- and pressure-dependent thermal conductivity profile changes during secular cooling. A few snapshots from model H1 (Table 1) are shown in Figure 1. As van den Berg et al. have calculated for the Earth [4, 9] and exoplanets [12], due to strong temperature dependence, conductivity in the thermal boundary layers (e.g. the lithosphere) decreases rapidly with increasing temperature. For the above-mentioned planets, conductivity increases with depth in the convective mantle, due to the dominance of pressure dependence over temperature dependence in the deeper mantle. This creates a low-conductivity zone (LCZ) at the base of the lithosphere [4, 9, 12], which affects the style and efficiency of planetary cooling. On the contrary, in the Moon, the positive effect of pressure is significantly

smaller due to the low gravity, decreasing with increasing depth. The negative effect of temperature almost cancels the positive effect of pressure in the bulk mantle. Although a sharp change of gradient is observed at the bottom of the lithosphere, it does not represent a clear minimum.

In our preliminary studies, we verify that the main influence of variable thermal conductivity on planetary cooling comes from the thermal boundary layers. The low conductivity in the lunar crust leads to overall high thermal resistance of the lithosphere, which acts as a strong resistor to the heat flow caused by the temperature contrast between the mantle and the surface.

Model setup: Convection equations are solved for an incompressible, infinite Prandtl number fluid, using the extended Boussinesq approximation. Modeling experiments are performed using a cylindrical finite element mesh with a total of 20000 elements.

Figure 1. Evolution through time of the variable thermal conductivity in the lunar mantle in model H1. The initial conductivity profile (red) is identical in the H models.



Our models start from the end of lunar magma ocean (LMO) solidification [13]. Density and the internal distribution of heat-producing elements are based on the stratified structure of the cumulates [13]. The initial temperature distribution follows a laterally homogeneous profile that increases linearly in the convective part of the bulk mantle. The rate of increase with depth is obtained from a linear approximation of a convecting lunar mantle in previous model results [8]. In our preliminary studies, the viscosity scale value is 1×10^{23} Pa s. This results in a Rayleigh number of 1.005×10^4 .

A set of four models is used, summarized in Table 1. H1 and H2 use the variable conductivity model. They are compared to U1 and U2 which use a uniform conductivity of 4 W/m/K. H1 and U1 assume that the heat-producing elements of the KREEP layer remain in the lunar crust, whereas H2 and U2 assume they follow the ilmenite-bearing cumulates (IBC) in the mantle overturn after solidification of the LMO.

Table 1. Models used in this study. Unit of thermal conductivity is W/m/K.

Models	H1	H2	U1	U2
Conductivity model	$k=k(z)$	$k=k(z)$	$k=4$	$k=4$
Location of KREEP layer heat producing elements	crust	IBC layer	crust	IBC layer

Results and discussion:

Figure 2. Evolution of average mantle temperatures.

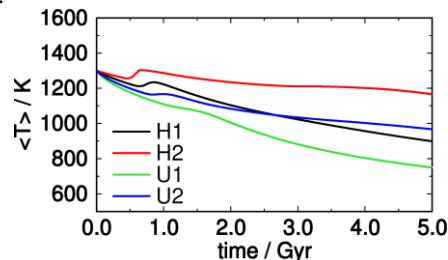
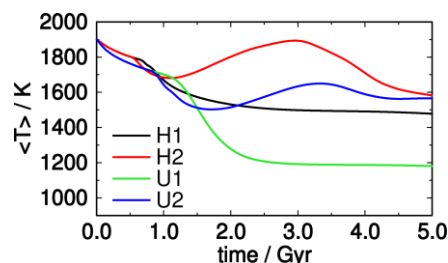


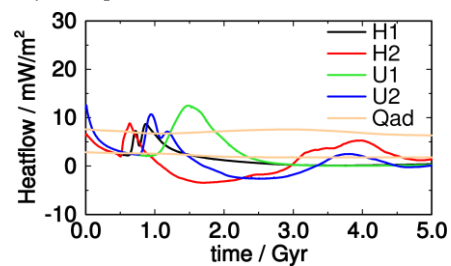
Figure 3. Evolution of average core temperatures.



The effect of variable conductivity can be seen by comparing the H models to the corresponding U models. The different conductivity models result in differences in present-day average mantle temperature of more than 100 K. This corresponds to a delay of cooling of 2 Gyr or more, for the H models to reach the same present-day mantle temperature. This means that variable thermal conductivity, including low values in the crust, is a significant controlling factor in the thermal evolution of the Moon.

Core temperature evolution is sensitive to both variable thermal conductivity and the location of the KREEP layer heat production. Variable thermal conductivity moves the onset of mantle overturn back in time by more than 0.5 Gyr.

Figure 4. Heat flux across the core-mantle boundary, compared to the Q_{ad} criterion.



A variable conductivity does not result in significant differences in present-day surface heat flux. CMB heat flux is compared to a necessary condition of lunar dynamo, which computes the minimum amount of heat flow (Q_{ad}) out of the core to sustain an adiabat in the outer core [14]. The timing of dynamo existence is a complex result of competing factors. A variable thermal conductivity results in faster mantle overturn after solidification of the LMO. The subsequent evolution of the ilmenite-bearing material from the CMB depends on both the timing of the mantle overturn, and the thermal conductivity of the CMB thermal boundary layer.

Conclusion: For small planetary bodies with a high surface-to-volume ratio, including the Moon, thermal conductivity in the lithosphere can be a strong limiting factor in their thermal evolution. The high concentrations of plagioclase in the lunar crust significantly increase thermal resistance of the lithosphere, and therefore insulate the convecting mantle.

Our results show that a variable conductivity profile predicts higher present-day mantle temperatures by more than 100 K, an early mantle overturn, and may influence the predicted time range of dynamo existence.

References: [1] Weber R. C. et al. (2011) *Science*, 331, 309-312. [2] Khan A. et al. (2014) *J. Geophys. Res. Planets*, 119, 2197-2221. [3] Tozer D. C. (1972) *Phys. Earth Planet. Interiors*, 6, 182-197. [4] van den Berg A. P. and Yuen D. A. (2002) *Earth Planet. Sci. Lett.*, 199, 403-413. [5] Schumacher S. and Breuer D. (2006) *JGR*, 111, E02006. [6] Tompkins S. and Pieters C. M. (1999) *Meteorit. Planet. Sci.*, 34, 25-41. [7] Branlund J. M. and Hofmeister A. M. (2012) *Am. Mineral.*, 97, 1145-1154. [8] de Vries J. et al. (2010) *Earth Planet. Sci. Lett.*, 292, 139-147. [9] van den Berg A. P. et al. (2005) *Phys. Earth Planet. In.*, 149, 259-278. [10] Hofmeister A. M. (1999) *Science*, 283, 1699-1706. [11] Wiczorek M. A. et al. (2013) *Science*, 339, 671-675. [12] van den Berg A. P. et al. (2010) *Phys. Earth Planet. In.*, 178, 136-154. [13] de Vries J. et al. (2011) *LPS XLII*, Abstract #1745. [14] Stegman D. R. et al. (2003) *Nature*, 421, 143-146.

EXAMINING THE HISTORY OF THE SOLAR SYSTEM AND THE GALAXY THROUGH COSMOGENIC ISOTOPES IN LUNAR SAMPLES. L.Alexander^[1,2], I. A. Crawford^[1,2], J. Schwanethal^[3], K. H. Joy^[4], P. Vermeesch^[3], and N. M. Curran^[4]. 1. Birkbeck, University of London (l.alexander@bbk.ac.uk) 2. Centre for Planetary Sciences at UCL-Birkbeck 3. Department of Earth Sciences, UCL. 4. SEAES, University of Manchester.

Introduction: Since the formation of the Sun ~ 4.6 billion years ago, the Solar System has orbited the Galaxy approximately 20 times and been exposed to a wide range of galactic environments as it passes through the spiral arms and star-forming regions. Supernova explosions and associated supernova remnants will result in an enhanced galactic cosmic ray (GCR) flux which may be recorded in the lunar geological record [1, 2]. Measuring concentrations of cosmogenic isotopes (^3He , ^{21}Ne and ^{38}Ar) in lunar samples of known ages may record variations in the GCR flux over time which will provide valuable information about the structure and evolution of the galaxy [3].

Methods and project outline: Cosmogenic isotopes are formed in rocks and soils by GCRs when they strike the lunar surface. The rate of production of cosmogenic nuclides depends on the GCR flux, the target elements and also the shielding depth, which can be difficult to unravel. However, the $^3\text{He}/^{21}\text{Ne}$ and $^{38}\text{Ar}/^{21}\text{Ne}$ ratios in rocks provide information to constrain the shielding history of the samples (e.g. [2]; [4]). We hope to analyse impact melt coats from the ejecta of young (<100 Ma) lunar craters in order to obtain the crystallisation age of the impact melt and the concentration of cosmogenic nuclides in order to examine variations in the GCR flux.

The concentrations of cosmogenic ^3He , ^{21}Ne and ^{38}Ar will be measured at Birkbeck/UCL using a Nu Instruments Noblesse multi-collector noble gas mass spectrometer and a CO_2 laser for bulk release and analysis. Crystallisation ages and ^{38}Ar argon exposure ages will be analysed using a step-heating approach on an Argus multi-collector noble gas mass spectrometer coupled to a CO_2 laser at the University of Manchester.

The results from this project will enable us to assess the feasibility of extracting the galactic record from existing lunar samples returned by the Apollo missions. One of the aims of this project is also to help develop criteria for selecting future lunar samples which may be better suited for this research [1]. For example, layers of ancient regolith (or 'paleoregolith'); formed as lava flows cover existing regolith in a repeated process would be especially useful since they contain material from different dateable horizons (Fig. 1) with potentially different cosmic ray histories [3].

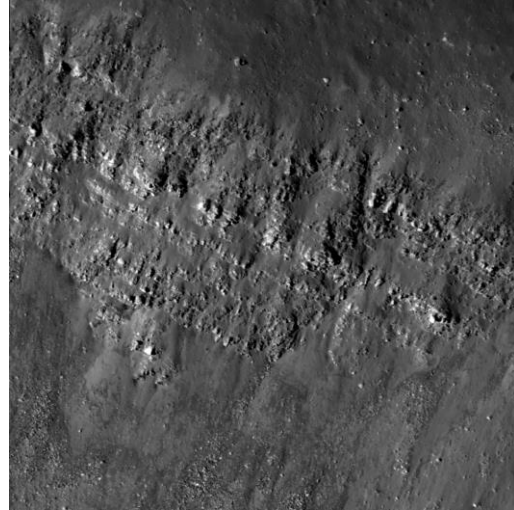


Figure 1. LROC NAC image MI35073175R showing examples of layering in Bessel crater. Image is 500 meters across. Credit NASA/GSFC/Arizona State University. Each layer in this image potentially provides a step back in time and sampling of these layers would allow a more complete picture of Solar System history to be revealed.

Future applications: The study of cosmogenic isotopes in lunar samples illustrates the potential to obtain information not only about the Moon and the cosmic ray exposure history of the lunar regolith, but also about the Earth, the early Solar System and the Galaxy. In particular, it can provide us with information about the amounts of radiation in the early Solar system which will also have impacted on the Earth at the time that life originated [3]. Accessing appropriate samples for future lunar missions will require advanced drilling and sample return capabilities in order to access the sub-surface and return a diverse range of samples to Earth for analysis. This would be facilitated by the presence of human explorers on the lunar surface.

References: [1] Crawford and Joy (2014) Phil. Trans. R. Soc. A 372. [2] Wieler, R. (2002) Rev. Mineral. Geochem., 47, 125-170. [3] Crawford, I.A. et al. (2010) Earth, Moon and Planets, 107, 75-85. [4] Lorenzetti, S et al. (2005) Meteoritic. Planet. Sci., 40, 315-327.

LUNAR GEODESY, CARTOGRAPHY, AND CURRENT COORDINATE KNOWLEDGE. J. Oberst (Juergen.Oberst@dlr.de)^{1,2}, P. Gläser (Philipp.Glaeser@tu-berlin.de) and I. Haase (Isabel.Haase@tu-berlin.de)², ¹German Aerospace Center (DLR), Institute of Planetary Research, Berlin, Germany, ²Technical University Berlin, Institute for Geodesy and Geoinformation Sciences, Germany

Abstract: For the Moon, two surface-fixed coordinate systems are in use. The ME (Mean Earth) system is based on the Moon's mean geometric orientation parameters– the PA (Principle Axis) system is based on the orientations of the moment-of-inertia axes. Both systems are basically defined through the coordinates of the Laser Reflectors deployed by the astronauts or those on the Lunokhod vehicles. Hence, landing sites constitute important landmarks. Earth-Moon ranges, Lunar motion and orientation models, and associated reflector coordinates are known to centimeter level. Using high-resolution LRO images, maps for wider areas of Lunar landing sites have been produced, accurately tied to this Lunar-fixed coordinate system. Positions of resolvable small-scale features near the landing sites, e.g. rover tracks, or astronaut equipment, can be recovered within an accuracy of meters, respectively. While coordinate knowledge is excellent near the landing sites, knowledge deteriorates rapidly at greater distances. It is data from LOLA (Lunar Orbiting Laser Altimeter) on LRO (Lunar Reconnaissance Orbiter), which provides global surface control. Benefitting from improved gravity field models by the GRAIL spacecraft and updated LRO orbit models, ground features (at the resolution limit of the LOLA shot of approx. 20 meters; LOLA spot size: approx. 5 m) can be positioned within tens of meters, as has been verified against the Laser reflector coordinates. However, outliers among LOLA tracks must be identified and removed. More recently, coordinate knowledge has greatly improved for both polar areas, where LOLA tracks converge. Using 7 years of LOLA data, involving 95 Million and 115 Million LOLA shots for north and south polar areas, respectively, 400 x 400 sqkm terrain models have been produced at effective resolutions of 20 m, which represent critical base maps. Catalogs of Laser altimeter tracks extending across both hemispheres and co-registered to North and South polar base maps are currently being prepared, which are intended to represent a stable reference grid for any place on the Moon with expected positional accuracy of meters.

RECENT ADVANCEMENTS IN LUNAR IMPACT CRATERING. H. Hiesinger¹, C.H. van der Bogert¹, J.H. Pasckert¹, ¹Institut für Planetologie, Westfälische Wilhelms-Universität Münster, Wilhelm-Klemm-Str. 10, 48149 Münster, hiesinger@uni-muenster.de

Introduction: The Lunar Reconnaissance Orbiter mission was launched in 2009 and carries a suite of cameras, including two narrow angle cameras (NAC) and a wide-angle camera (WAC) that comprise the Lunar Reconnaissance Orbiter Camera (LROC) [1]. The images of the WAC have pixel scales of about 100 m; the NACs acquire images with about 0.5 m pixel scales. Both data sets, in combination with SELENE Terrain Camera (TC) images with about 10 m pixel scales [2], allow us to investigate the lunar cratering process and the determination of absolute model ages (AMAs) based on crater size-frequency distribution (CSFD) measurements in unprecedented detail. To derive AMAs across the lunar surface and throughout the inner Solar System, accurate knowledge of the lunar cratering chronology (LCC) is a prerequisite [e.g., 3]. Unfortunately, there are only a few data points at ages younger than about 3 Ga, and no data points at ages older than 3.9 Ga to constrain the LCC. In the last few years, we systematically performed CSFD measurements for Copernicus, Tycho, North Ray, Cone, and Autolycus craters to test and improve the LCC. The first four craters are important anchor points, because they are the only craters with absolute sample ages used to constrain the LCC over the last 1 Ga. On the basis of these four data points, a constant lunar impact rate for the last 3 Ga was postulated [e.g., 4,5]. Hence Copernicus, Tycho, North Ray, and Cone craters are crucial for the determination of an accurate LCC and our understanding of the impact rate in the inner Solar System (including Earth) over the last 1 Ga. In addition, it has been proposed that some Apollo 15 rocks date Autolycus crater. If correct, that would allow us to further constrain the LCC and to potentially improve its accuracy by giving us an additional calibration point between 1 and 3 Ga [6]. Although LROC images allow us to map and count small craters, it became obvious that at these small crater sizes various factors influence the cratering process that were negligible at larger crater diameters on which the CSFD technique is mostly based. Thus, in the last few years we also studied whether our technique can be reliably used for these observations. For example, for CSFDs based on small craters, effects of count area size, target properties, self-secondary cratering, and illumination geometry become increasingly important and have to be understood. Thus, in addition to our efforts to test and improve the LCC, we have also performed extensive tests of our dating technique [e.g., 7].

Data and Method: We used LROC NAC and WAC images, as well as SELENE TC images to perform CSFD measurements. The images were calibrated and map-projected with ISIS 3 and imported into ArcGIS. Within ArcGIS, we used CraterTools [8] to perform our CSFD measurements. The CSFDs were then plotted with CraterStats [9], using the lunar production and chronology functions of [5]. The technique of CSFD measurements has been described extensively elsewhere [e.g., 5, 10-12].

Results: Methodology: Target properties/self secondary cratering: At several craters we found discrepancies between small crater CSFDs of two contemporaneous units, i.e., melt pools and the ejecta blanket, which can be explained by either self-secondary cratering [13] or by target properties [14]. We counted craters with diameters through the transition from strength- to gravity-scaling on two large impact melt deposits at Tycho and King craters, and we modeled the effects of differing target properties on final crater diameters for five different lunar targets [7]. The new CSFD for the large King

melt pond bridges the gap between the discrepant CSFDs within a single geologic unit. Thus, the observed trends in the impact melt CSFDs support the occurrence of target property effects, rather than self-secondary and/or secondary contamination. The CSFDs generated from our models show that targets with higher density and effective strength yield smaller crater diameters than porous, weaker targets, such that their relative and absolute ages will be lower relative to the latter. Consequently, coeval impact melt and ejecta units will have discrepant apparent ages [7].

Effects of count area sizes: We performed a systematic study to investigate the effects of small count area sizes on the accuracy and precision of CSFD measurements. We found that with decreasing count area sizes the precision and accuracy of CSFDs decreases. The percent errors for 100 Ma old surfaces are larger than for older surfaces. Young surfaces of 100 Ma may have 50-100% percent errors, while old surfaces (e.g., 4 Ga) have percent errors typically <5%. Thus, even with these inaccuracies for young surfaces, the very young ages of irregular mare patches, for example, can be confidently interpreted to be late Copernican in age [15].

Testing the LCC: Cone crater: Exposure ages of Apollo 14 samples were used to date the formation of Cone crater. Although there is a wide range in exposure ages [e.g., 16,17], several studies agree on a formation age of ~25-26 Ma [e.g., 6,18,19]. Derived from nine count areas around Cone crater, our absolute model age (AMA) is ~39 Ma, similar to previous AMA results that vary from ~24 Ma [20] to ~73 Ma [21]. Thus, the AMAs are consistent with the exposure ages.

North Ray crater: Cosmic ray exposure indicates an age of 48.9 ± 1.7 to 50.3 ± 0.8 Ma of North Ray crater [22-24], similar to the ⁸¹Kr-Kr age of 50.6 ± 3.8 Ma [25], and similar to ²²Na-Ne ages and particle track ages. Microcrater frequencies suggest that North Ray formed more than 20 Ma ago [26] and ³⁸Ar-³⁷Ar cosmic-ray exposure ages are between 30 and 50 Ma [27]. Thus, [6] concluded that North Ray was formed 50.3 ± 0.8 Ma ago. For North Ray, four individual count areas, as specified by [4], were counted independently by two counters, yielding ages of 46 and 47 Ma, respectively [3].

Tycho crater: Analyses of samples returned from the landslide at the Apollo 17 landing site, which was presumably triggered by Tycho secondaries [27,28], revealed exposure ages of about ~100 Ma, interpreted to represent the formation age of Tycho crater [e.g., 23,28-30]. In particular, [23,30] concluded that Tycho is 109 ± 4 Ma old, similar to an exposure age of 96 ± 5 Ma for the landslide derived by [29]. NAC CSFD measurements of four areas on the continuous ejecta blanket yielded a combined AMA of 85 Ma – identical to our combined AMA of three count areas on the landslide, but slightly younger than the WAC CSFD-derived AMA of the ejecta blanket (124 Ma). CSFDs of [31] yielded an AMA of 75 Ma for the ejecta blanket.

Copernicus crater: A faint ray of Copernicus material crosses the Apollo 12 landing site, which led [32] to propose that KREEPy glass in the samples (from Head crater) was ejected by the Copernicus event, and could be used to date the impact. Exposure ages of the glass have an age of 800-850 Ma [33-37]. Radiometric ages, including degassing ages of felsite clasts within the ropy glasses, also support an age of 800 ± 15 Ma [36,38-39]. Analyses of 21 regolith samples show degassing ages of 700-800 Ma, which give an estimated 782 ± 21 Ma age for the Copernicus impact event [40]. At Copernicus

crater we used NAC images to count 9 areas on the ejecta blanket, which revealed an AMA of 797 Ma. CSFD measurements for three ejecta blanket areas on WAC images yielded a similar age of 779 Ma. Our results for Copernicus crater fit the existing lunar chronology of [5] significantly better than their previous counts [5].

Autolycus crater: Rays from Autolycus and Aristillus crater cross the Apollo 15 landing site and presumably transported material to this location [e.g., 41,42]. Thus, [43,44] proposed that the ^{39}Ar - ^{40}Ar age of 2.1 Ga, derived from three petrologically distinct, shocked Apollo 15 KREEP basalt samples, date Autolycus crater. A heating event in sample 15405 at 1.29 Ga was interpreted as the age of Aristillus crater [45]. The exact timing of the two impacts, however, remains under debate because [46] interpreted newer U-Pb ages of zircon and phosphate grains of 1.4 and 1.9 Ga from sample 15405 as the formation ages of Aristillus and Autolycus. Provided Autolycus crater is indeed the source of the dated exotic material at the Apollo 15 landing site, CSFD measurements on the ejecta blanket of Autolycus crater offer a new calibration point to the lunar chronology, particularly in an age range that was previously poorly constrained. NAC CSFD measurements for 6 areas inside and on the ejecta blanket of Autolycus crater yielded widely variable AMAs. None of our CSFDs yielded AMAs that correspond either to the 2.1 Ga [43,44] or 1.9 Ga [46] sample ages. This either implies that the dated samples are not related to Autolycus or that the CSFD measurements are so heavily affected by resurfacing and secondaries from the younger Aristillus event that they do not reflect the formation age of Autolycus crater. In either case, because of these uncertainties Autolycus can not be used as a reliable calibration point for the LCC.

Landing Sites: Another independent test for the LCC is comparing CSFD measurements for the lunar landing sites with radiometric ages from returned samples. Recently, [47] re-measured crater densities at all chronology tie sites and reported that there is a disagreement between the new CSFD estimates and those used by [5] to construct the LCC, such that if the classical Neukum chronology [5] is used, certain model ages will differ by more than 1 Ga. However, Hiesinger et al. [3,48-50] found a good agreement between the derived AMAs and the respective radiometric and exposure ages of the samples when applying the production and chronology functions of [5] to their CSFDs.

Applications: Mare Basalt Ages: In previous studies, we have dated most of the mare basalts on the lunar nearside, using Lunar Orbiter images [48-50]. Mare Crisium was not covered by suitable Lunar Orbiter images and was not included in our dating effort. However, with LROC images becoming available, we were able to derive AMAs for basalts in Mare Crisium [51]. Our absolute model ages show a range of Imbrian and Eratosthenian ages from 2.71-3.61 Ga. The Alhazan Basalt shows an age of 3.60 Ga with a resurfacing at 3.27 Ga, being consistent with the wide range of ages found by [52]. The Eimmart Basalts in the NE and the Agarum Basalt in the SE are younger than central basalts, and the Swift Basalt appears to be younger than the Shapley Basalts. We also expanded our CSFD measurements to basalts on the lunar farside [53]. Mare basalts in and around Bolyai crater show AMAs from 2.1 Ga to 3.5 Ga (two units), varying drastically within short distances. Mare areas south of Coblentz crater exhibit AMAs from 2.1 Ga to 3.8 Ga and those in Roche V crater show an AMA of 2.2 Ga. Five volcanic units in Rosseland crater show the youngest AMAs, ranging from 1.5 Ga to 2.9 Ga. Mare basalts south of Rosseland crater shows older AMAs of 3.3 Ga. Mare basalts in Pauli and Roche craters show AMAs from 1.7 Ga to 3.1 Ga and those between Eötvös and Roche craters show AMAs from 1.9 Ga to 3.1 Ga. Our

results indicate that the lunar farside was volcanically active for nearly as long as the lunar nearside (1.2 Ga ago, [49]), or at least longer than predicted by models of the ascent and eruption of lunar basalts [53].

South Pole-Aitken Basin: We also performed CSFD measurements for craters superposed on the South Pole-Aitken basin in an attempt to date the largest, deepest, and presumably oldest basin on the Moon and to investigate the plausibility of the terminal cataclysm between 3.9 and 4.0 Ga [54]. Our CSFD measurements indicate that the SPA basin is ~ 4.26 (± 0.03) Ga old ($N(1) = 3.70 \times 10^{-1}$) and, thus, is likely too old to be consistent with some models for lunar cataclysm [55]. Garrick-Bethell et al. [56] concluded that the lunar samples 63503, 76535, 60025, 67955, 78155, and 78235 all show old ages of 4.11-4.27 Ga. In addition, lunar meteorites Dhofar 489 and Yamato 86032, which are believed to come from the farside also show Ar-Ar ages of 4.23 Ga [57,58]. Because 76535 originated from a depth of 40-50 km [58], and Dhofar 489 also comes from deep crustal layers, a very large impact is required to excavate these samples. This led [56] to propose that these sample ages might represent the age of the SPA basin. Our absolute model age for SPA is indeed close to these radiometric ages, thus supporting such a model.

References: [1] Robinson et al. (2010) Space Sci. Rev. 150. [2] Haruyama et al. (2008) Earth Planets Space 60. [3] Hiesinger et al. (2012) JGR 117. [4] Neukum (1983) Habil. thesis, U. of Munich. [5] Neukum et al. (2001) Space Sci. Rev. 96. [6] Stöffler and Ryder (2001) Chronology and Evolution of Mars. [7] van der Bogert et al. Icarus submitted. [8] Kneissl et al. (2012) PSS 59. [9] Michael and Neukum, (2010) EPSL 294. [10] Hiesinger et al. (2000) JGR 105. [11] Hartmann (1966) Icarus 5. [12] Crater Analysis Working Group (1979) Icarus 37. [13] Zanetti et al., (2016) Icarus submitted. [14] van der Bogert et al. (2016) New Views 2. [15] van der Bogert et al. (2015) LPSC 46. [16] Bhandari et al. (1972) PLPSC 3. [17] Crozaz et al. (1972) PLPSC 3. [18] Arvidson et al. (1975) Moon 13. [19] Stadermann et al. (1991) GCA 55. [20] Moore et al. (1980) Moon and Planets 23. [21] Plescia and Robinson (2011) LPSC 42. [22] Drozd et al. (1974), GCA 38. [23] Drozd et al. (1977), PLPSC 8. [24] Marti et al. (1973), PLPSC 4. [25] Behrmann et al. (1973), PLPSC 4. [26] Morrison et al. (1973), PLPSC 3. [27] Wolfe et al. (1975), PLPSC 6. [28] Lucchitta (1977), Icarus, 30. [29] Arvidson et al. (1976), PLPSC 7. [30] Guinness and Arvidson (1977), PLPSC 8. [31] Krüger et al. (2016), Icarus, 10.1016/j.icarus.2016.02.018. [32] Meyer et al. (1971), PLPSC 2. [33] Eberhardt et al. (1973), The Moon 8. [34] Alexander et al. (1976) PLPSC 7. [35] Silver (1971), EOS, Trans. Am. Geophys. Union 52. [36] Bogart et al. (1994), GCA 58. [37] Korotev et al. (2000), LPS XXXI. [38] Bogard et al. (1992), Lunar Planet. Sci. Conf. 23. [39] Wentworth et al. (1994), Meteoritics 29. [40] Barra et al. (2006), GCA 70. [41] Wilhelms (1987), USGS Spec. Pub. 1348. [42] Russ et al. (1972), EPSL 15. [43] Bogard et al. (1990), GCA 54. [44] Ryder et al. (1991), Geology 19. [45] Bernatowicz et al. (1978), PLPSC 9. [46] Grange et al. (2013), JGR 118. [47] Robbins (2014), EPSL 403. [48] Hiesinger et al. (2010), JGR 115. [49] Hiesinger et al. (2003), JGR 108. [50] Hiesinger et al. (2011), Geol. Soc. Am. Spec. Pap. 477. [51] Hiesinger et al. (2011) EPSC-DPS. [52] Head et al. (1977) GCA 9. [53] Pasckert et al. (2015) Icarus 257. [54] Tera and Wasserburg (1974) LPSC V. [55] Hiesinger et al. (2012) LPSC 43. [56] Garrick-Bethell et al. (2008) Early Solar System Impact Bombardment. [57] Takeda et al. (2006) EPSL 247. [58] Nyquist et al., (2006) GCA 70.

AN IMPACT-GENERATED LUNAR MAGMATISM HYPOTHESIS. David A. Kring^{1,2}, Patrick J. McGovern^{1,2}, Ross W. K. Potter^{1,2}, Gareth S. Collins³, Marion L. Grange⁴, and Alexander A. Nemchin^{4,5}, ¹Center for Lunar Science and Exploration, USRA Lunar and Planetary Institute, 3600 Bay Area Blvd., Houston TX 77058 (kring@lpi.usra.edu), ²NASA Solar System Exploration Research Virtual Institute, ³Impacts and Astromaterials Research Centre, Dept. Earth Science and Engineering, Imperial College, London UK, ⁴Department of Applied Geology, Western Australian School of Mines, Curtin University, Western Australia, ⁵Department of Geosciences, Swedish Museum of Natural History, Stockholm, Sweden.

Introduction: A compilation (Fig. 1) of zircon analyses [1-6] indicate there was a particularly large magmatic epoch 4.30-4.36 Ga. Zircon is found in a diverse suite of magmatic lithologies (anorthosite, troctolite, gabbro-norite, quartz-monzodiorite, granites, felsites) and in impact breccias that incorporate clasts of those lithologies. The zircon crystals are derived from Apollo landing sites spanning a distance of 1758 km (Apollo 12 to Apollo 17), an area of 878,750 km², and involve impact basin deposits that were excavated from depths up to ~60 km (by the Imbrium impact) – providing extensive sampling of magmatic rocks in the nearside crust. The 4.30-4.36 Ga peak in zircon ages is similar to several other ages [7-9], including an urKREEP average model age of 4.368 ± 0.029 Ga [10]. The latter has been interpreted to represent the solidification of the lunar magma ocean, although it is difficult to reconcile that model with ancient lunar zircon ages (up to 4.417 ± 0.007 Ga) without a very complicated petrogenetic model [10].

Lunar Magmatism Hypothesis (LMH): As an alternative, we hypothesize that the magmatic epoch was triggered by the immense, 2500-km-diameter South Pole-Aitken basin impact on the lunar farside, which is the oldest, largest, and deepest impact basin on the Moon. Hydrocode simulations of the South Pole-Aitken impact [11] indicate mantle melting on the farside, leading to an immense differentiated magmatic system [12,13]. Simulations [11,14] also show the impact generated sharp pressure anomalies in the mantle beneath the lunar nearside crust and correspondingly large displacements, strains, and stress changes. Additional modeling shows that those pressure anomalies would have accelerated the ascent of mantle partial melts, producing a concentrated magmatic epoch among nearside lithologies too.

Modeling the SPA Impact and the Magmatic Response. The observed dimensions, gravity structure, and distribution of lithologies of the South Pole-Aitken basin are best fit with a hydrocode impact model using a 170 km diameter asteroid hitting the Moon vertically at 10 km/s [11], or one slightly larger for an oblique impact [14]. In this model, the pre-impact thermal structure of the Moon is such that the lower crust and upper mantle temperatures are at or very close to the solidus between a depth of ~25 and 560 km – the vestige of the Moon's magma ocean.

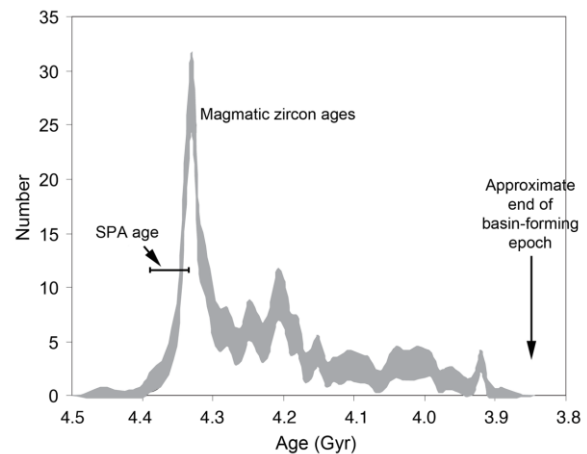


Fig. 1. Distribution of zircon crystallization ages that reflect the production of magma on the Moon [1-6]; the estimated SPA age is from [22].

Here we have extended our analysis of those hydrocode results to evaluate the consequences of the impact on the entire sphere of the Moon, including the upper mantle beneath the nearside crust. Pressure and stress waves generated by the impact event radiated around the Moon, beginning with the shock wave and followed by a train of high-amplitude surface waves. The pressure in the initial shock wave exceeded ~400 MPa (above the lithostatic load) in the upper mantle across the entire Moon; wave focusing would have increased the stress magnitude in a zone around the impact antipode by perhaps as much as an order of magnitude (Fig. 2), depending on the angle of impact [14] and asymmetries in the Moon's figure and internal structure at the time of impact [15]. The consequences of the South Pole-Aitken basin impact were felt around the Moon for hours after the initial shock wave arrived. In particular, the presence of a weak asthenosphere leads to large deformation of the crust during the formation of the basin. Oscillations of the crater floor inside the basin send a series of high-amplitude gravity waves around the Moon, causing displacements of ~1 km and shear stresses sufficient to cause pervasive fracturing of the crust.

The globally distributed dynamic stress changes would have had a profound effect on melt migration by creating new pathways and enhancing forces that drive melt ascent. In addition to pervasive large-scale fracturing [14], the impact would have cata-

lyzed melt migration at all scales. Estimates of magma ascent velocity and effective buoyancy in dikes [16,17] can be derived from vertical gradients in horizontal stresses via analysis of pressure balances across the dike [18]. For typical locations on the lunar nearside, the averaged stress state during a vertical opening event indicates positive velocities in the lower crust and negative velocities in the upper crust. These findings predict the formation of an intrusive horizon in the lower crust.

Discussion and Final Observations: Thus, we propose the South Pole-Aitken impact mobilized melt around the whole Moon, particularly beneath the antipodal lunar nearside surface that is the provenance of the Apollo sample suite, accounting for the observed spike in magmatic zircon ages. Effectively, the process has the capacity to perturb the normal ascent of partial mantle melts and accelerate them upward, creating a magmatic pulse or cluster of magmatic events over a timescale of several millions of years to produce the observed age spike (Fig. 1).

This process is distinct from the proposed concept of decompression melting beneath the floor of an impact crater [19], a process that fails to generate melt in most impact events [20], with the possible exception of the largest basin-size events. While that process and the processes described here may have enhanced the mobility of melt beneath the South Pole-Aitken impact site, only the process described here has the capacity to generate a period of enhanced magmatism on the lunar nearside.

The 10 km/s impact velocity in our hydrocode model of the South Pole-Aitken basin impact is consistent with an independent assessment of average impact velocities (9 km/s) at that time in lunar history based on the size distribution of craters [21]. A calibration of crater densities on the most ancient portions of the floor of South Pole-Aitken basin also implies an age of 4.33 to 4.39 Ga [22], consistent with the timing needed to generate the subsequent magmatic pulse (Fig. 1). Confirming an age of the South Pole-Aitken basin will be a good test of our hypothesis and is one more reason for a South Pole-Aitken basin sample return mission [23,24].

Interestingly, recent analyses of the production of impact melt within the South Pole-Aitken basin [13] suggest the basin-forming impact event occurred prior to mantle overturn on the Moon. If so, then the same mantle perturbations proposed here to produce an enhanced period of magmatism may have also provided the activation energy needed to initiate that overturn, produce adiabatic melting [25], and further enhanced the amount of magmatism.

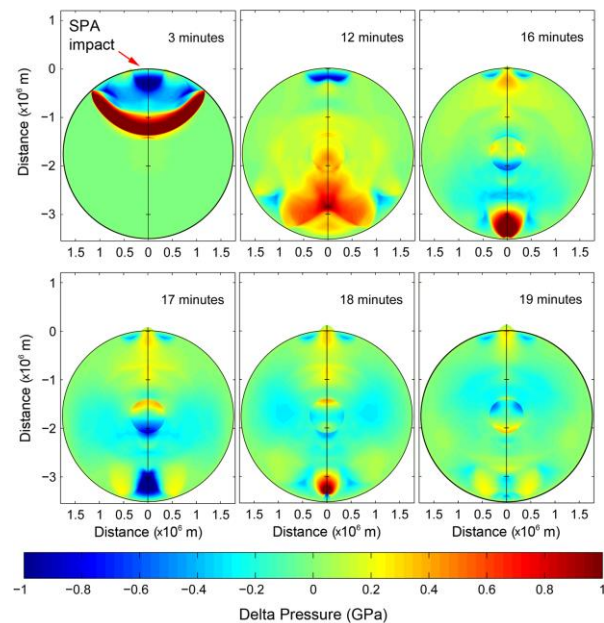


Fig. 2. Pressure variation relative to the initial lithostatic pressure at 3, 12, 16, 17, 18, and 19 minutes after impact. The nearside is at the bottom of each panel.

References: [1] Nemchin A. A. et al. (2008) *Geochim. Cosmochim. Acta*, 72, 668-689. [2] Grange M. L. et al. (2009) *Geochim. Cosmochim. Acta*, 73, 3093-3107. [3] Taylor D. J. et al. (2009) *Earth Planet. Sci. Lett.*, 279, 157-164. [4] Nemchin A. A. et al. (2011) *Austral. J. Earth Sci.*, 59-2, 277-290. [5] Liu D. et al. (2012) *Earth Planet. Sci. Lett.*, 319-320, 277-286. [6] Zhang A. C. et al. (2012) *Geochim. Cosmochim. Acta*, 95, 1-14. [7] Borg L. E. et al. (2011) *Nature*, 477, 70-73. [8] Brandon A. D. et al. (2009) *Geochim. Cosmochim. Acta*, 73, 6421-6445. [9] McLeod C. L. et al. (2014) *Earth Planet. Sci. Lett.*, 398, 179-189. [10] Gaffney A. M. and Borg L. E. (2014) *Geochim. Cosmochim. Acta*, 140, 227-240. [11] Potter R. W. K. et al. (2012) *Icarus*, 220, 730-743. [12] Vaughn W. M. and Head J.W. (2013) *Planet. Space. Sci.*, 91, 101-106. [13] Hurwitz D. M. and Kring D. A. (2014) *J. Geophys. Res.*, 119, 1110-1133. [14] Schultz P. H. and Crawford D. A. (2011) *GSA Spec. Pap.*, 477, 141-159. [15] Meschede M. A. et al. (2011) *Geophys. J. Int.*, 187, 529-537. [16] McGovern P. J. et al. (2013) *J. Geophys. Res.*, 118, doi:10.1002/2013JE004455. [17] McGovern P. J. et al. (2013) *LPS XIV*, Abstract #3055. [18] Rubin A. M. (1995) *Ann. Rev. Earth Planet. Sci.*, 23, 287-336. [19] Jones A. P. et al. (2002) *Earth Planet. Sci. Lett.*, 202, 551-561. [20] Ivanov B. A. and Melosh H. J. (2003) *Geology*, 31, 869-872. [21] Marchi S. et al. (2012) *Earth Planet. Sci. Lett.*, 325-326, 27-38. [22] Morbidelli A. et al. (2012) *Earth Planet. Sci. Lett.*, 355-356, 144-151. [23] National Research Council, *The Scientific Context for Exploration of the Moon*, 107p. [24] National Research Council, *Vision and Voyages for Planetary Sciences in the Decade 2013-2022*, 382p. [25] Elkins-Tanton L. T. et al. (2011) *Earth Planet. Sci. Lett.*, 204, 326-336.

THE TIMELINE OF THE LUNAR BOMBARDMENT. A. Morbidelli⁽¹⁾, S. Marchi⁽²⁾, W.F. Bottke⁽²⁾, D.A. Kring⁽³⁾, ¹Dep. Lagrange, UCA, CNRS, OCA, Nice, France, (Email: morby@oca.eu), ²SwRI, Boulder, CO, SA, ⁽³⁾Lunar and Planetary Institute, Houston, TX, USA.

Introduction: We revisit the early evolution of the Moon's bombardment. Our work combines modeling (based on plausible projectile sources and their dynamical decay rates) with constraints from the lunar crater record, radiometric ages of the youngest lunar basins, and the abundance of highly siderophile elements in the lunar crust and mantle. We deduce that the evolution of the impact flux did not decline exponentially over the first billion years of lunar history, but also there was no prominent and narrow impact spike ~ 3.9 Gy ago, unlike that typically envisioned in the lunar cataclysm scenario. Instead, we show the timeline of the lunar bombardment has a sawtooth-like profile, with an uptick in the impact flux near ~ 4.1 Gy ago [1]. The impact flux at the beginning of this weaker cataclysm was 5-10 times higher than the immediately preceding period. The Nectaris basin should have been one of the first basins formed at the sawtooth. We predict the bombardment rate since ~ 4.1 Gy ago declined slowly and adhered relatively close to classic crater chronology models [2]. Overall we expect that the sawtooth event accounted for about 1/4 of the total bombardment suffered by the Moon since its formation. Consequently, considering that $\sim 12-14$ basins formed during the sawtooth event, we expect that the net number of basins formed on the Moon was $\sim 45-50$, in great agreement with measurements from GRAIL [3]. From our expected bombardment timeline, we derived a new and improved lunar chronology suitable for use on Pre-Nectarian surface units. According to this chronology, a significant portion of the oldest lunar cratered terrains has an age of 4.38-4.42 Gyr. Moreover, the largest lunar basin, South Pole Aitken, is older than 4.3Gy, and therefore was not produced during the lunar cataclysm.

We also discuss the possibility of a cometary component of the late lunar bombardment.

References: [1] Morbidelli, A., Marchi, S., Bottke, W.F., & Kring, D.A. 2012, *Earth and Planetary Science Letters*, 355, 144 ; [2] Neukum, G. & Ivanov, B.A., 1994, in *Hazards due to Comets and Asteroids*, p. 359 ; [3] Neumann, G.A., Lemoine, F.G., Mazarico, E., et al. 2013, *Lunar and Planetary Science Conference*, 44, 2379

CHALLENGES AND OPPORTUNITIES OF LUNAR RESOURCE PROSPECTING. J. Carpenter¹, R. Fisackerly¹, M. Landgraf¹, the PROSPECT industrial consortium led by Finmeccanica (F. Rizzi lead) with the Open University (S. Barber lead), the PROSPECT User Group, Topical Team for Exploitation of Local Planetary Materials (M. Anand Chair), ¹ESA ESTEC, Noordwijk, The Netherlands (james.carpenter@esa.int)

Introduction: ESA is looking to the Moon as the next destination for human exploration and is working to prepare missions and capabilities that will enable this. This exploration must be affordable and sustainable delivering on-going and visible benefit and demonstrating feed forward to other destinations. One of the greatest unknowns for future exploration missions is the viability of using in situ resources. It is evident that “living off the land” is likely to be more sustainable than a scenario in which all materials and consumables have to be brought from Earth. However a major transition is required to enable the incorporation of in-situ resources into future plans. This is going to require resource prospecting followed by in-situ demonstration.

Various possible applications for in-situ resources have been and are being investigated. These include the use of regolith as a material for construction, the use of oxygen and other chemicals extracted from the minerals and glasses in regolith and the use of water and its constituents, extracted from the cold trapped ices of the lunar poles.

Of these the later provides perhaps the greatest opportunities and the greatest unknowns and several studies have illustrated the potential such a resource offers for future exploration architectures. Extensive information now exists which alludes the presence of water ice across the polar regions, with a positive detection by L-CROSS at one location.

However significant uncertainties still exist which prevent the inclusion on In-Situ Resource Utilisation on the critical path of exploration. In the case of polar ice unknowns include the form, abundance, and distribution on both regional and local scales. The answers to these questions will determine whether or not lunar polar ice and other locally resident materials will ever be considered as resources in the planning of exploration missions.

If resources are to be utilised then they must first be characterised and their viability demonstrated. While this is true for all possible resources, an emphasis is placed on polar ices for the first robotic precursor missions.

Measurements needed: While new orbital data sets are welcome and can support the evaluation of resources, assessment requires surface missions. These missions must assess the form, quantity, and lateral and vertical distribution. These quantities must be related to the local and time variable environment at the prospected locations.

Key measurements will be made on regolith samples from beneath the surface extracted from varying

thermal and illumination environments. Volatile species extracted from these samples need to be analysed and their compositions and abundance determined. Comprehensive isotopic measurements reveal the origins and emplacement processes. Such measurements should be accompanied by complimentary measurements (e.g. neutron spectroscopy and near infrared spectroscopy) which provide a broader context for measurements of samples and allow them to be related to measurements made from orbit.

PROSPECT for Luna-27 and following missions: As a first step ESA is developing PROSPECT, a package that will drill, sample and analyse potentially ice bearing material from a near polar locations. While emphasising polar ices PROSPECT shall also generate information regarding a broader suite of potential resources and important geotechnical information, regardless of the presence or otherwise of ices. The first measurements from PROSPECT will be returned from the Russian Luna-27 mission, which is currently in development for flight in 2020/2021. This flight will provide important information for both resources and fundamental scientific research and demonstrate the PROSPECT capabilities for future mobile platforms such as the Lunar Volatile Prospector mission currently under study. The experience gained can also feed forwards to missions to return frozen polar samples such as Russia’s proposed Lunar Polar Sample Return mission, which is currently the subject of an ESA industrial study.

The development of PROSPECT includes a number of activities that are providing insight into the possible nature of lunar ices, the engineering challenges that they pose and the scientific discoveries that they may yield.

Small mission opportunities: Small platforms may also provide a means to advance knowledge of potential resources through targeted orbital measurements or small surface platforms (e.g. penetrators). ESA is investigating ways to facilitate the emerging small sat industry and enable small sat exploration of the Moon by a broad community, through competitions and commercial partnerships.

Conclusion: Lunar resources could be the key to sustainable lunar exploration and exploration beyond the Moon, with polar volatiles providing perhaps the most promising avenues for investigation. Prospecting and technology development must culminate in in-situ demonstration of viability if resources are to be included in future plans.

CHALLENGES IN ROBOTIC AND HUMAN GEOLOGICAL FIELD WORK IN LUNAR CRATERS.

S. D. Chevrel^{1,2}, P. C. Pinet^{1,2} and Y. Daydou^{1,2}, ¹Université de Toulouse; UPS-OMP; IRAP; Toulouse, France, ²CNRS IRAP; 14 av. E. belin, F-31400 Toulouse, France (serge.chevrel@irap.omp.eu).

Introduction: During the last 50 years lunar exploration has been conducted both by sampling on the ground (Apollo missions, 1969-1972) and by remote sensing techniques from orbit, from Clementine (1994) to Lunar reconnaissance Orbiter (2009-present), greatly improving our knowledge about the Moon. However, many questions arised from these missions and we identified places to go for sampling and to conduct other surface geological activities, both to answer key questions (concerning the lunar crust, volcanism...) and to better interpret remote sensing data, e.g., spectral data relying on composition. However, some places to be deeper investigated by robots and humans in the future are challenging from a technical point of view. Among them are the impact craters.

Interest of study of impact craters: Impact craters, specially large craters are complex formations showing a great diversity of morphological features and compositions for their materials. They require in situ detailed investigations in order to fully understand cratering processes, from contact of the impactor with the target, to excavation and modification stage. In addition, materials excavated and deposited during crater formation give information on the composition of deep seated materials, a way to answer key questions concerning the structure, formation and evolution of the lunar crust. Remote sensing techniques such as multispectral observations, for surface composition, are presently largely employed but still need ground truth. Crater materials present large degree of melting and mixing raising issues in the interpretation of spectral data. We need also to link the compositional information to small scale morphological observations on the ground. For large craters sampling and in situ observations and measurements must be conducted in different places of the crater interior: its floor, central peak and walls (presenting terraces) in order to understand the distribution and degree of melting of the excavated materials and their origin in the target. However, the navigation across the impact craters is difficult either for automatic rovers or humans.

Investigation of North Ray crater (Apollo 16):

The largest impact crater visited by astronauts was the North Ray crater during the Apollo 16 mission. This young crater (40-60 Ma) [1] of 0.98 km in diameter, not contaminated by other crater ejecta, was a primary sampling target during the last of the three EVA made during the flight because it excavated materials 250 meters into the subsurface at the foot of Smoky Mountain. It was the best available documentation for stratigraphic investigation in the Apollo

16 traverse area at the Descartes site, in the enigmatic Cayley formation, at that time.

At about 5 km north of the lunar module (LM), John Young and Charlie Duke investigated the southern rim crest portion of North Ray (Station 11) (Figure 1) and its outer continuous ejecta blanket (Station 13) on a spot located 750 m south of the rim. The two astronauts collected light-matrix and dark-matrix breccias with clasts and inclusions of glassy to crystalline texture, the dark breccias being more coherent than the light ones, and representing the deeper horizon, near or at the bottom of the crater [1]. On the rim, they visited and sampled a spectacular boulder (25 x 20 m) named House Rock being deposited late in the ejecta sequence of North Ray (Figure 1A).

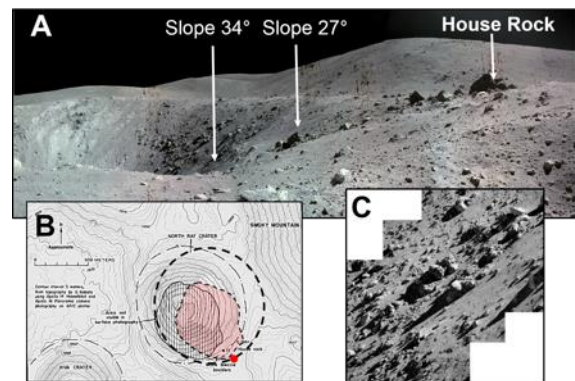


Figure 1: A: Panoramic view of the half eastern portion of North Ray crater (field of view about 500 m), taken from the south-eastern rim (at Station 11; see red spot in B); B: Sketch map (adapted from [1]) of the North Ray crater area. Red area corresponds to the part of the crater not photographed by the astronauts due to steep slopes of the walls (see A). Red spot is Station 11; C: As it has been not possible to sample inside the crater, only pictures of boulders on the walls have been taken using a 500 mm tele lens. Mosaics (A and C) assembled by S. Chevrel.

The crater shows a rounded rim but its walls rapidly fall with convex shapes ranging from 27° at the top to 34° in the lower half. These relatively steep slopes did not permit to take pictures of the lower part of the crater walls, only the upper 60%, being observable from the vantage point at Station 11 (Figure 1B). Although it was not planned, it would not have been possible for the two astronauts to venture themselves to close to the rim and into the walls. Instead of being sampled, distant boulders on the walls were photographed using a 500 mm telelens (Figure 1C).

Thus, the investigation of a relative simple crater such as North Ray proves to be a difficult task and it

has been limited in space and time during the third traverse of Apollo 16.

Investigation of a large crater: the case of Aristarchus. Aristarchus is a young impact crater (175 Ma [2]), 42 km in diameter, showing various morphologies and fresh materials (Figure 2). It excavated deep seated materials (from a depth of 3 to 4 km [3]), giving information on the composition of the lunar crust [e.g., 3, 4] which is not well exposed in this portion of the Moon, namely the Procellarum KREEP Terranes (PKT). The freshness of the morphological units and materials for the well-preserved Aristarchus crater are unique to better understand impact cratering processes, by linking morphologic features and composition.

In previous works [4,5] large areas having spectral anorthositic signatures mixed with pyroxenes (red and orange in figure 2) have been found within the crater, on the northeastern terraced wall, where the albedo is the lowest in the crater (figure 2). It corresponds to large impact melt deposits, mantling the terraces. LROC very high resolution images (0.5 m/pixel) show large ejected boulders (up to 100 m in size for some), most of them being embedded and mantled with dark melt deposits (see figure 2). Few are free of melt. In this portion of the crater, many large stratified blocks have also been identified. Thus the spectral signature may arise from these boulders and/or from partially crystallized melts. Most of materials in craters are melt materials formed and deposited during the impact event. For large craters little is known about the melt products in terms of stratigraphic origin in the target, mode of emplacement and repartition on the crater floor and terraces. Also, little is known about the amount of rocks embedded in the melts and the amount of crystallized versus amorphous materials in the units on the floor and terraces, a crucial point in the interpretation of optical spectral data (UV-Vis-NIR).

Thus, field work by astronauts and automated vehicles is strongly needed to understand impact cratering processes. Visual/photographic observations (morphology, texture, flowing features) and sampling (blocks, clasts and matrix of melt materials) of complex melt sheets within the crater would greatly contribute to understand their thickness and mode of emplacement (flowing and settling), and thus answer key questions related to impact processing.

However field work in large craters such as Aristarchus present major difficulties [6]. The central peak, with steep slopes, prevent from any ground access. On the terraced walls the trafficability is greatly reduced for long distances. The crater floor, which appears to be relatively flat, is in part made of hummocky terrains making difficult its exploration. It is also true for the crater exterior having slopes and very blocky areas forming the continuous ejecta.

Therefore, future in situ investigations of crater interior and ejecta, of high scientific value, by humans

and/or automated means, appear to be very challenging.

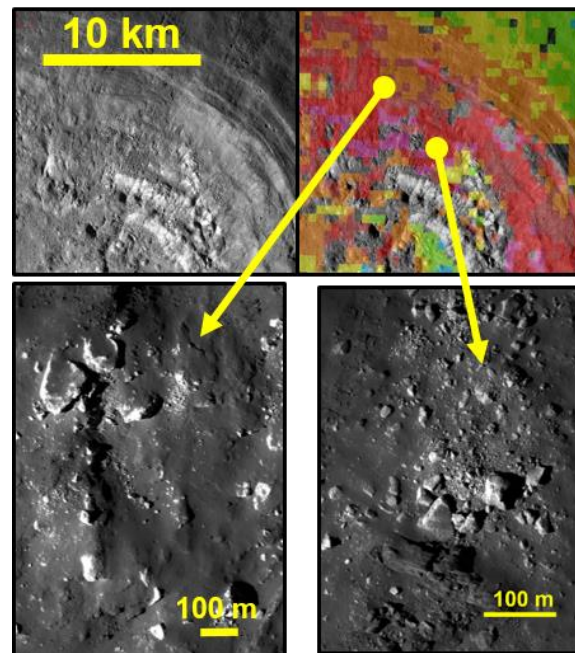


Figure 2: Morphology (upper left) and abundances from spectral data (upper right) of anorthositic rich material with pyroxenes (orange and red meaning high abundances) on the northeastern rim of Aristarchus (see [4,5]). Detailed images (lower left and right) show ejected boulders and melt deposits (images from LROC NAC M120161915LE).

Future operations for investigating large craters:

For impact craters, due to complex access and limitations in trafficability on the ground, robotic and crew exploration vehicles would necessarily have the ability to take off and land from place to place, with high capabilities in hovering to carefully select safe areas to land. Piloted unpressurized or pressurized grasshopper vehicles would ideally be employed. First, automatic vehicles would be used to select the most interesting places to send humans for further investigations. Reliable manned or unmanned grasshopper vehicle, flying from one spot to another on the lunar surface have still to be designed for detailed reconnaissance and collecting samples. Without the development of such techniques and new surface operations, lunar craters will remain poorly investigated, strongly limiting advances in lunar science. These techniques would also apply to the study of other lunar formations presenting a strong interest in lunar science but being difficult to explore, such as massifs surrounding the impact basins, volcanic domes and sinuous rilles.

References: [1] Ulrich G. E. (1981), in *Geol. Surv. Prof. Paper 1048, D2*, 45-81. [2] Zanetti M. et al. (2011), *LPSC 42nd*, Abstract#2262. [3] Mustard J. F. et al. (2011), *J. Geophys. Res.*, 116, E00G12. [4] Chevrel S. D. et al. (2009), *Icarus*, 199, 9-24. [5] Chevrel S. D. et al. (2015), abstract, European Lunar Symposium 3rd. [6] Chevrel S. D. et al (2015), abstract, Moon 2020-2030, ESA.

SPACESHIP EAC – ENABLING ACTIVITIES RELEVANT TO LUNAR EXPLORATION AND 3D PRINTING ISRU. A. Cowley¹, A. Meurisse², T. Haefner¹, S. Cristoforetti¹, M. Sperl², ¹ European Astronaut Centre EAC, European Space Agency, 51170 Köln, Germany, ² Institut für Materialphysik im Weltraum, Deutsches Zentrum für Luft- und Raumfahrt, 51170 Köln, Germany.

Introduction: The operational capabilities of the European Astronaut Centre (EAC) in terms of training and support for human spaceflight operations on the ISS are well known. With increasing attention now being given to post-ISS human spaceflight and exploration scenarios, teams at EAC and the broader ESA are collaborating on initiatives that would leverage the capabilities and experience available from EAC to further these exploration objectives.

The activities of EAC result in unique experience with respect to operations involving astronauts. “Spaceship EAC” utilises this experience and aims at developing operational concepts and low-TRL-level technologies in support of lunar human exploration scenarios. The individual concept/technology development and demonstration projects within the “Spaceship EAC” initiative are coordinated with ESTEC (mission scenarios, technology roadmaps) and exploit synergies with EAC facilities and operational competence as well as with the surrounding DLR campus and European research groups.

Two particular developments at EAC are discussed herein; the development of a lunar analogue surface operations facility, and ongoing developments relating to 3d printing using in-situ resources to enhance mission capability and autonomy.

The planned facility will comprise of a large regolith test bed area located between the existing EAC facility and DLR EnviHab building situated in Cologne, with a half spherical fully enclosing dome structure housing the testbed. The perimeter of the structure is given with a diameter of 34m – the effective surface operations area is projected to be approximately 900m², inclusive of experiment preparation areas. The testbed will comprise of a lunar regolith simulant sourced from the local Eifel region volcanic and basalt sources, which are satisfactory low cost mechanical and compositional simulant.

In collaboration with ESTEC, DLR and a number of European researchers, we will report on early studies into utilizing conventional thermal sintering approaches of simulants as well as microwave sintering of these compositions. Both techniques are candidates for developing a 3d printing methodology using Lunar regolith, following on from the successful ESA General Studies Programme project concept proposed in 2013 [1].



Fig. 1 – Processed DNA sintered simulant via conventional resistive heating oven (vacuum).

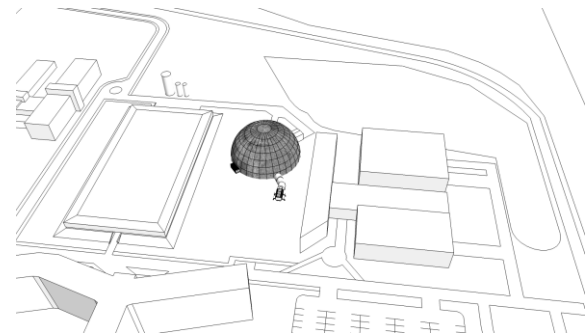


Fig. 2 – Architectural drawing illustrating the surface operations regolith testbed under development, situated between EAC (right) and DLR EnviHab (left).

References:

- [1] ESA GSP study on Lunar Base 3D printing: http://www.esa.int/Our_Activities/Space_Engineering_Technology/Building_a_lunar_base_with_3D_printing

METAL-SILICATE PARTITIONING OF SIDEROPHILE ELEMENTS IN THE MOON: THE EFFECTS OF OXYGEN FUGACITY AND CARBON. M. Crockett¹, R. Putter¹, A. Seegers¹, N. Rai^{2,3}, W. van Westrenen¹, E. S. Steenstra¹. ¹Faculty of Earth & Life Sciences, VU Amsterdam, NL (e.s.steenstra@vu.nl) ²Centre for Planetary Science, Birkbeck-UCL, UK, ³Department of Earth Sciences, Mineral and Planetary Sciences Division, Natural History Museum, London, UK.

Introduction: Linking siderophile element depletions in planetary mantles to their experimentally derived metal-silicate partitioning behavior has proven to be a valuable tool to constrain the pressure (P), temperature (T) and redox (fO_2) conditions during core formation in planetary bodies [1-4].

However, these models are particularly dependent on the quantification of the effects of fO_2 on their metal-silicate partition coefficients (D 's), which is a function of their dominant valence state in the silicate melt. Adding to the complexity, many siderophile elements undergo valence state transitions (e.g., Cr, V, Mo, W) with different fO_2 conditions [e.g., 4-6], but the exact ranges are poorly constrained and may differ as a function of melt composition [5]. It has also been shown that metal-silicate partitioning of siderophile elements may be strongly dependent on the composition of the liquid metal.

Previous studies have shown that the light element budget of the lunar core is likely dominated by S [e.g., 7] and/or C [8]. However, a C-rich lunar core may be more likely, given the low S abundance in the lunar mantle and its moderately siderophile behavior during lunar core formation [8,9]. We have previously shown that the depletions of 15 siderophile elements in the lunar mantle can be reconciled with a S-free and S-rich lunar core, but the feasibility of a C-rich lunar core can as of yet not be assessed due to lack of data in C-bearing systems for many elements=.

Here, we study the metal-silicate partitioning of a wide range of elements as a function of (1) fO_2 and (2) carbon in the metallic liquid to better constrain core formation conditions in the Moon.

Methods: We used a Bristol-type end-loaded piston cylinder press to equilibrate metal-silicate mixtures within MgO or graphite capsules at 1-2.5 GPa and 1883 K. For graphite saturated systems, a Pt outer capsule was used which was welded shut prior to experiments. Synthetic equivalents of the Apollo green glass [10] and a lunar granite [11] were used and obtained by mixing appropriate amounts of high-purity oxides. The metal consisted of Fe powder doped with 1-2 wt.% of each siderophile element and variable amounts of $Fe_{83}Si_{17}$ to generate variable redox conditions upon melting. Run times were 15-120 min, which has been previously shown to be sufficient for attaining metal-silicate equilibrium [12]. Samples were embedded in epoxy resin, polished for analysis and analyzed for major elements using EMPA.

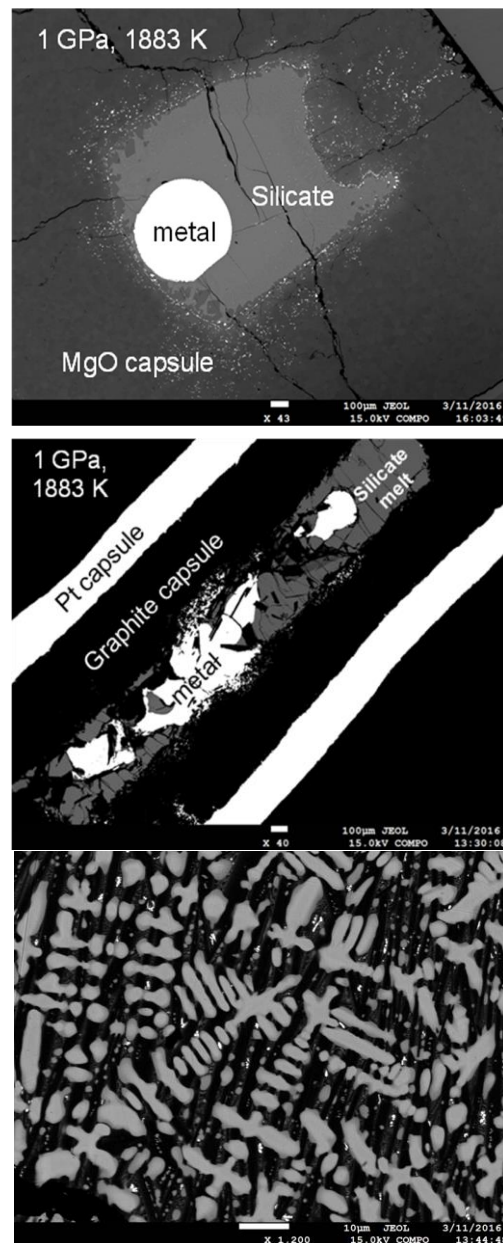


Fig. 1.: BSE images of experiments performed at 1 GPa – 1883K in (a) MgO capsule and (b-c) in graphite capsule at 1883 K and 1 GPa with close up of metal quench texture

Results: Typical run products are shown in Figure 1. Silicate melts quenched to either a glass or a heterogeneous matte of quench crystals and melt. Quenched metals showed a dendritic texture in graphite saturated experiments and metals in MgO capsules generally quenched to heterogeneous alloys without clear quench textures. The fO_2 is defined

relative to the iron-wüstite buffer and calculated using Eq. (2):

$$\Delta IW = -2 \cdot \log (a_{\text{FeO}}/a_{\text{Fe}}) \quad (\text{Eq. 2})$$

where a_{FeO} is the activity of FeO in the silicate melt and a_{Fe} is the activity of Fe in the liquid metal. The activity of Fe was calculated using the online metal activity calculator [14] and the activity coefficient of FeO was assumed to be 1.5 [12].

Electron microprobe analysis of metals from C-saturated systems showed low totals, consistent with several wt% of C partitioning into the metal. We calculated the amount of C in the metal using [14]. Several runs performed in graphite capsules also showed significant infiltration of Pt (several wt%) in the metal, which can be used for quantification of Pt metal-silicate partitioning. Preliminary results show that FeO contents in the silicate melt were significantly lower than the added amounts, due to the reducing conditions by addition of $\text{Fe}_{83}\text{Si}_{17}$. As expected, with increasingly low $f\text{O}_2$, the amount of Si partitioned into the metal is increased.

Discussion and outlook: Experimental and analytical work is ongoing to quantify the metal-silicate partitioning of siderophile elements as a function of $f\text{O}_2$ and carbon. Additional metal-silicate partitioning work and its implications for lunar core formation will be reported at the meeting.

References: [1] Rai & van Westrenen (2013) *JGR* 118 [2] Rai & van Westrenen (2014) *EPSL* 388 [3] Steenstra et al (2016) *GCA* 177 [4] van Westrenen et al (2016) *LPSC* [5] O'Neill and Eggings (2002) *CG* [6] Righter et al (2016) *EPSL* [7] Laneuville et al (2014) *EPSL* [8] Steenstra et al (2016) *Under review* [9] Boujibar et al (2014) *EPSL* 391 [10] Delano (1986) *JGR* 91 [11] Warren (1983) *EPSL* 64 [12] Steenstra et al (2016) *LPSC* [13] Mysen et al (1982) *RGSP* 20 [14] Wade and Wood (2005) *EPSL* 236

ASTROBIOLOGY AND LIFE SCIENCES ON THE MOON. J.-P. de Vera¹, M. Baqué¹, D. Billi², U. Böttger³, J. Carpenter⁴, R. de la Torre Noetzel⁵, R. Demets⁴, P. Ehrenfreund⁶, A. Elsaesser⁷, B. Foing⁴, G. Horneck⁸, N. Kozyrovska⁹, J. Meeßen¹⁰, R. Möller⁸, S. Onofri¹¹, F. Sohl¹, S. Sommer¹², U. Szewzyk¹³, D. Wagner¹⁴ and Frances Westall¹⁵, ¹German Aerospace Center (DLR), Institute of Planetary Research, Management and Infrastructure, Astrobiological Laboratories, Rutherfordstr. 2, 12489 Berlin, Germany, jean-pierre.devera@dlr.de, ²University of Rome Tor Vergata, Rome, Italy, billi@uniroma2.it, ³German Aerospace Center (DLR), Institute of Optical Sensorsystems, Rutherfordstr.2, 12489 Berlin, Germany, ute.boettger@dlr.de, ⁴ESA-ESTEC, Noordwijk, The Netherlands, James.Carpenter@esa.int, ⁵INTA, Dpo. Observación de la Tierra, Crta. Ajalvir, km. 4, Torrejón de Ardoz, 28850-Madrid, Spain, torrenr@inta.es, ⁶Space Policy Institute, George Washington University, 20052 Washington DC, USA, pehren@gwu.edu, ⁷Experimental Molecular Biophysics, Arnimallee 14, 14195 Berlin, Germany, a.elsaesser@fu-berlin.de, ⁸DLR, Institute of Aerospace Medicine, Radiation Biology Department, Research Group Astrobiology, Koeln, Germany, Ralf.Moeller@dlr.de, ⁹Institute of Molecular Biology & Genetics of NASU, Kyiv, kozyrnat@gmail.com, Ukraine, ¹⁰Institute of Botany, Heinrich-Heine-University (HHU), Düsseldorf, Germany, joachimmeessen@gmx.de, ¹¹Univ. del. Tuscia Viterbo, Italy, onofri@unitus.it, ¹²GEOMAR, FE Marine Geosysteme Forschungsbereich 2: Marine Biogeochemie, Wischhofstrasse 1-3, 24148 Kiel, Germany, ssommer@geomar.de, ¹³TU Berlin, Institute of Environmental Technology, Environmental Microbiology, Ernst-Reuter-Platz 1, Berlin, 10587 Berlin, Germany, ulrich.szewzyk@tu-berlin.de, ¹⁴GFZ German Research Centre for Geosciences, Helmholtz Centre Potsdam, Section Geomicrobiology, Telegrafenberg, 14473 Potsdam, Germany, dirk.wagner@gfz-potsdam.de, ¹⁵CNRS, CBM, UPR 4301, rue Charles Sadron, 45071 Orléans, France, frances.westall@cnrs-orleans.fr

Introduction: One important mechanism for understanding the interaction between cells and the various radiation sources in deep space is to perform laboratory analysis on microorganisms or bio-relevant molecules which have been exposed to this radiation environment. However, to date comprehensive scientific assessment of biological effects caused by the exposure to deep space environments has not been performed in reasonable extent and cannot be simulated completely in the laboratories. Many studies were performed in the past to approach “deep space exposure experiments” by using simulation facilities in terrestrial laboratories [1] and through exposure on platforms in Low Earth Orbit (LEO). Such platforms included a series of FOTON satellites (with the exposure platform BIOPAN) and the International Space Station (with the exposure platform EXPOSE-E on the Columbus module, EXPOSE-R on the Zvezda module and various exposure platforms on the KIBO-module) [2]. For all experiments in LEO however there is an intense shielding effect by the Earth’s magnetic field and therefore real “deep space” conditions cannot be tested [3]. A platform with biological samples placed on the Moon might achieve more realistic results on the effect of deep space environment because of the lower influence of the Earth’s magnetic field allowing radiation to reach the sample sites almost unhindered [4]. Such a Moon-based exposure platform can easily be integrated in the sample return hardware and is independent from complex operation modes, whereas the main analysis of the exposed samples will be conducted back on Earth.

Lunar environmental effects: The outcome of such kind of bio-relevant lunar investigations is of

great importance, because it allows estimations of the damage range of deep space effects such as UV, ionizing solar and galactic radiation. The results will promote our knowledge on the limits of terrestrial life under extraterrestrial conditions. Moreover, the results will contribute to our understanding of deleterious effects of deep space environments in future human missions, especially in regard to the human body, its dermal and intestine microbiomes as well as to other organisms present in exploration systems either by intention (e.g. use within a life support system) or not (e.g. potentially corroding, hazardous or pathogenic biofilms formed by fungi and bacteria colonizing space hardware material). The collection of lunar dust during a sample return mission and the use of such material in the laboratories back on Earth might enrich our knowledge about the effect of lunar dust on humans and microorganisms by testing selected human relevant cells and microorganisms in contact to that dust [5].



Search for bio-relevant resources: Tests with microorganisms exposed to lunar samples might also

clarify if lunar regolith can be exploited as a potential resource for the organisms. Identifying these capacities will have profound implications on what kind of resources are available on the Moon to support and sustain temporary or permanent human outposts on the Moon (e.g. the use of lunar substrates to be implemented in bio-driven life supporting systems) [6].

Stability of biomolecules: Analysis of selected biosignatures or bio-traces which were exposed to space conditions or simulated planetary conditions on the Moon might elucidate about the stability of such kind of molecules within environmental conditions which can be considered as an approach to planetary-like environments [4]. This would be an important step further to support future space exploration missions with the main goal to detect life on other planets and satellites, because due to the pre-tests on the Moon we aim to get a better understanding and hints for the search and characterization of biomolecules in planetary soils and ices. In this context instrument tests and operation modes on the Moon with payloads which are foreseen to be applied for life detection such as e.g. Raman-, IR/VIS- and fluorescence-spectroscopy might also clarify how data obtained by these instruments might look like under real space conditions.

[1] Lorek A. and Koncz A. (2013) ed. by de Vera, J.-P. and Seckbach J. *Habitability of other planets and satellites*, 147-162. [2] Rabbow E. et al. (2015) *International Journal of Astrobiology*, 14 (1), 3-16. [3] Reitz, G. et al. (2009) *Radiation Research* 171, 225–235. [4] de Vera et al. (2012) *Planetary and Space Science* 74 (1), 103-110. [5] Carpenter, J.D. et al. (2010) *Earth Moon Planets* (2010) 107:11–23. [6] Verseux C. et al. (2016). *International Journal of Astrobiology* 15 (1), 65–92.

INTERNATIONAL LUNAR OBSERVATORY ASSOCIATION: 21ST CENTURY EDUCATION, EXPLORATION AND ENTERPRISE. S. M. Durst¹, J. Sulla², P. R. Merrell³ ^{1,2,3}International Lunar Observatory Association (65-1230 Mamalahoa Hwy, D20, Kamuela, HI 96743, USA).

Space agencies and Astronomy institutions in Europe and worldwide will have the opportunity to participate and observe the Galaxy / Stars, local lunar environment and Earth in various wavelengths and to conduct a wide-range of Moon-to-Earth and Moon-to-Space communications through the ILOA four missions. Mission development and realization will enhance and be supported by the education and outreach activities of the Galaxy Forum program while helping to advance Hawaii's leadership in Astronomy for the next 100 years.

ILO-1: The flagship ILOA mission will see a multi-functional 2-meter dish observatory placed near the South Pole of the Moon. The mission (NET 2018) will conduct radio and optical astronomy, including Galaxy First Light Imaging Program; and Commercial Communications, including Space Calendar Lunar Broadcasting, while serving as a beacon for lunar base buildout. ILOA is embarking on a pioneering multi-year lunar electronics contract with Canadensys Aerospace of Canada to develop technology for the ILO-1 scientific payload. Joint venture partner Moon Express Inc. of USA is preparing to deliver the payload to the lunar surface.

ILO-X: ILOA is also working on a 7-cm optical telescope precursor mission known as ILO-X, partnering with Moon Express to ride on its Google Lunar XPrize lunar lander scheduled for launch with Rocket Lab in 2017.

LUT: ILOA signed an MoU with the National Astronomical Observatories of the Chinese Academy of Sciences (NAOC-CAS) in September 2012 allowing ILOA scientists to conduct Galaxy Observations with the UV telescope aboard the 2013 Chang'e-3 lunar lander. This was followed by an MoU with CNSA in August 2013. In exchange for use of Chang'e-3 LUT, ILOA will provide observation time to NAOC during ILO-X and ILO-1 missions. ILOA has successfully conducted observations with the Chang'e-3 LUT, including the first Spiral Galaxy (M101) observed from the lunar surface on New Year's day 2015. ILOA is looking ahead at collaboration on the Chang'e 4, 5, 6 missions.

ILO-HSM: A Human Service Mission to the future ILO at Moon South Pole is being advanced through collaboration / partnership with international organizations and private partners such as Golden Spike Company. The goal of ILOA is to participate in a Human Moon mission within the decade.

ILOA Galaxy Forum: Galaxy Forums are public events specifically geared towards high school teachers, educators, astronomers of all kinds, students and the general public. Presentations are provided by ex-

perts in the fields of astrophysics / galaxy research, space exploration and STEM education, as well as related aspects of culture and traditional knowledge. Interactive panel discussions allow for community participation and integration of local perspectives.

Almost 70 Galaxy Forums with a total of more than 300 presentations have been held in 26 locations worldwide (since Galaxy Forum USA, July 4, 2008) including Hawaii, Silicon Valley, Canada, China, India, Southeast Asia, Japan, Europe, Africa, Chile, Brazil, Kansas and New York.

HIGHLIGHTS FROM MOON VILLAGE WORKSHOPS AND STUDIES. B. Foing¹, P. Batenburg, D. Winter, A. Calzada, A. Jaime Albalat, A.M. Kleinschneider, C. Welch, D. Esser, D. Ivanov, H. Lökk, A. Kapoglou, M. Hazadi, O. Kamps, M. Offringa, S. Pieterse & participants ¹ESA/ESTEC & ILEWG (Bernard.Foing@esa.int)

Summary: We report on Moon Village workshops that gathered a multi-disciplinary group of professionals from all around the world to discuss their ideas about the concept. The workshop participants focussed on **Moon Habitat Design, science and technology potentials** of the Moon Village, and **engaging stakeholders**. We also report on technical and research studies, and activities that followed.

Introduction: The new DG of ESA, Jan Wörner, has expressed from the very beginning of his duty a clear ambition towards a Moon Village, where Europe could have a lead role. The concept of Moon Village is basically to develop a permanent station on the Moon with different countries and partners that can participate and contribute with different elements, experiments, technologies, and overall support.

ESA's DG has communicated about this programme and invited inputs from all the potential stakeholders, especially member states, engineers, industry, scientists, innovators and diverse representatives from the society. In order to fulfill this task, a series of Moon Village workshops have been organized first internally at ESA and then at international community events, and are also planned for the coming months, to gather stakeholders to present their ideas, their developments and their recommendations on how to put Moon Village into the minds of Europeans, international partners and prepare relevant actions for upcoming International Lunar Decade.

Workshop: A Moon Village Workshop in ESTEC [1-38] was organized by ILEWG & ESTEC Staff Association in conjunction with the Moon 2020-2030 Symposium. It gathered people coming from all around the world, with many young professionals involved, as well as senior experts and representatives, with a very well gender balanced and multidisciplinary group. Engineers, business experts, managers, scientists, architects, artists, students... presented their views and work done in the field of Lunar Exploration. Participants included colleagues from ESA, SGAC Space Generation Advisory Council, NASA, and industries such as OHB SE, TAS, Airbus DS, CGI, etc... and researchers or students from various Universities in Europe, America, and Asia.

In the afternoon, the Workshop participants split in three working groups: **Moon Habitat Design, Science and Technology potentials on the Moon Village, and Engaging Stakeholders**. They were tasked to discuss ideas, and pilot projects with the aim to consoli-

date visions for Moon Village stakeholders and provide some recommendations to the ESA DG, Jan Wörner.

The **Moon Habitat Design** group discussed principles and concepts for a minimum base that would start with 4-10 crew, allowing a later evolution to 50 crew and elements contributed by Moon Village partners at large. Various aspects were assessed including habitats, laboratories, EVAs, pressurized vehicles, core modules, inflatable extensions, power systems, life support systems and bioreactors, ISRU using regolith, emergency, services, medical, escape, shelters.

The **Science and Technology** group analyzed the importance and readiness level of technologies needed for lunar robotic landers and for the Moon Village. The current ESA lunar exploration activities focus on the contribution within ISS operations barter of the ESA service module to bring Orion capsule to the Moon starting with an automatic demonstration in 2018. It is encouraged to consolidate this path for using the service module for crewed missions EM2 and EM3 giving also the possibility of an ESA astronaut, together with advanced technology, operations and science utilization. They noted the interesting contribution of instruments, drill, communications, and landing in support to Russian lunar polar lander missions Luna 27.

Building on previous studies (EuroMoon, lunar polar lander) ESA should develop a **mid-class lunar lander** (affordable in cost 300 Meu class), demonstrating the expertise at system level for a platform, that could carry innovative competitive robotic payload contributed and already with advance development from member states and international or commercial partners. With teleoperations from Earth and cis-lunar orbit, this will advance progress towards the next steps of Moon Village and beyond.



Fig. 1: Moon Village Workshop participants

The **Engaging Stakeholders** working group started by identifying the main stakeholders and groups that play a role or that could play a role towards the Moon Village project. These stakeholders were classified on their influence towards the programme, and their attitude towards it. One clear conclusion was that most of the stakeholders showed a positive view towards the Moon Village programme, and that the most important step within a short term strategy should focus on the actions to be taken to engage stakeholders for the next ESA Ministerial to support the programme. Finally the group came up with some recommendations on which should be the actions to be taken by the ESA DG to engage the most direct stakeholders: ESA delegations, media, national governments, citizens, taxpayers, and to invite partners.

Recommendations: The participants encourage the design and operations of a **Moon base simulation at EAC** with facility and activities in the context of SpaceShip EAC, with the support of EAC, DLR, ESTEC, ISU and other partners, and collaborations with other Lunar Research Parks worldwide.

It was also proposed to have an **“ESTEC Moon Village pilot project”** where 20 young professional interns could be hosted to work concurrently on various aspects (technology, science, instruments platforms, Moon base design, human factors, programmatics, outreach, community events) with links and support activities from ESTEC senior experts, and interactions with colleagues in member states, academia and industries.

The workshop finalized with some **hands-on experiments**, organized with some students demonstrating their work on a lunar lander with tele-operated instruments and systems, and on the measuring spectra of Moon-Mars analogue minerals. The day ended with a refreshing lunar music session, and a networking event on ESTEC ESCAPE where the last informal conversations marked a great wrap up of such exciting day.

Follow up Moon Village events have been organised in 2016 at ESTEC, EAC and at international community venues. Also news studies and technical research have been conducted. New means of outreach, communications and social media must be developed. You can follow Moon Village tweets, using #MoonVillage, and contribute to the virtual discussions. ESA is really looking forward to engage all stakeholders into the discussion, no matter of their background, nationality or interest.

We shall report on latest activities from these 2016 events, studies and field research.

References: [1] <http://sci.esa.int/ilewg/> and <https://ildwg.wordpress.com/> [2] Foing B. *Moon exploration highlights and Moon Village introduction*. [3] Baten-

burg P. & Calzada A. *Young Lunar Explorers report on Moon exploration*. [4] Young Lunar Explorers *Report ESTEC Moon village sessions with community and young professionals*. [5] Head J. *Lunar science and human exploration from Moon Village* [6] Cowley A. *Spaceship EAC—fostering activities for lunar exploration and in-situ resource utilisation*. [7] Urbina D. *Moon walk and Luna studies*. [8] Gerzer R. *The Skolkovo Institute of Science and Technology: preparing for Moon exploration* [9] Hausmann G. *OHB activities for lunar exploration* [11] Tanier G. *CGI Space activities on habitats and operations relevant to Moon Village*. [12] Beldavs V. et al *International Lunar Decade*. [13] Kapoglou A. *Engaging stakeholders for the Moon Village* [14] Panel of international and commercial stakeholders. [15] Preparation for ESA DG's Moon Village Jam session on 11 January 2016. [16] Pieterse S. *Moon village and urban planning, social media*. [17] Hazadi M. *Robotic exploration before and assisting the manned flights*. [18] Esser D. *Human-Machine Interaction & Cognitive Artificial Intelligence for Moon Village*. [19] VU Amsterdam *A mission to explore lunar polar ices*. [20] Kamps O. *Assessment of lunar polar sites for future landers, rovers, human-assisted exploration*. [21] Paternostro S. *Mission and Trajectory analysis and Mass budget*. [22] Berquand A. *YGT/Trainees ESTEC Moon village sessions*. [23] Kleinschneider A. *Mission architecture and -elements, system engineering, ISRU*. [24] Jaime A & Calzada A. *SGAC MoonMars exploration workshops and activities*. [25] Milassin G. *Materials, processes, structures, radiation shielding, dealing with lunar dust* [26-28] *Reports from Splinter groups: 1) Moon base design; 2) Technologies, science; 3)Engaging stakeholders & Outreach/media*. [29] Kamps O. *Demo on ExoGeolab instruments and telescope*. [30] Offringa M. *Demo on visible, IR and Raman spectroscopy of Moon-Mars analogue samples* [31] Schlacht I. et al *Human factors design for a Moon station: Sustainability, affordability & performance*. [32] Schmidt G. *Nasa's SSERVI: science and technology for lunar exploration*. [33] Foing B. *Preparing for Moon Village, ILEWG/SGAC Moon village workshop, ICEUM/COSPAR*. [34] Preusterink J. *Outreach and education*. [35] Coté A. *Lunar outreach activity at Brown U. SSERVI node*. [36] Hoetjes A. *MoonVillage and space artscience film project*. [37] *Moon Village music event* [38] *Moon Telescopic Watch, Networking and Social event*. [39] Abstracts from Moon Symposium 2020-2030 organised at ESTEC

***Organisation:** Bernard Foing, ESA/ESTEC & ILEWG
ESTEC Moon Village workshop WGs co-conveners: Peter Batenburg, Andrea Jaime, Abigail Calzada, Angeliki Kapoglou, Chris Welch, Susanne Pieterse, Daniel Esser, Audrey Berquand, Daniel Winter, Dmitri Ivanov, Simone Paternostro, Matias Hazadi, Oscar Kamps

LUNAR POLAR ILLUMINATION AND IMPLICATIONS FOR FUTURE LANDING SITES.

P. Gläser¹, J. Oberst^{1,2}, G.A. Neumann³, E. Mazarico³, E.J. Speyerer⁴, M.S. Robinson⁴. ¹Technische Universität Berlin, Institute of Planetary Geodesy, Strasse Des 17. Juni 135, 10623 Berlin, Germany (philipp.glaeser@tu-berlin.de), ²German Aerospace Center, Institute of Planetary Research, Rutherfordstrasse 2, 12489 Berlin, Germany, ³NASA Goddard Space Flight Center, Code 698, Greenbelt, MD 20771, USA, ⁴Arizona State University, School of Earth and Space Exploration, Tempe, AZ 85287, USA

Abstract: We investigate the polar illumination conditions of the Moon based upon data from the Lunar Orbiter Laser Altimeter (LOLA). We simulate the received sunlight for a solar-panel of a lander or rover at a height of 2 m above the ground. Six landing sites, three near each pole, were identified with average illumination intensities ranging from 77.76-86.62%. Here, a lander could reside in sunlight for a total of 85.54-91.04% for our studied one-year period, roughly 312-332 days out of the year. Permanently Shadowed Regions (PSRs), possibly containing polar volatiles, are found within kilometre-range of the proposed sites.

Introduction: The lunar day lasts about 29.5 Earth days. As the lunar rotational axis is tilted wrt the ecliptic plane by only a small angle (1.54°), areas near the lunar equator are in sunlight for about 15 Earth-days followed by equally long nights throughout the year. However, polar illumination, is more complex. The combination of grazing sunlight and local topography leads to extreme conditions. Permanently Shadowed Regions (PSRs), for instance, exist in close proximity to regions receiving illumination for the greater part of the year [1][2][3]. Accordingly, PSRs are amongst the coldest areas on the Moon [4] and have long been suspected to harbor enhanced concentrations of hydrogen and hence possibly also water ice [5]. Landing sites in quasi-continuous illumination and close proximity to PSRs will be ideal exploration sites for robotic missions. Landing units and rovers at such sites can rely on solar power and are able to explore polar volatiles in nearby PSRs.

Data/Method: For this study consistent, large-scale and high-resolution Digital Terrain Models (DTMs) were produced. Similar to the generation of a south polar DTM using Lunar Orbiter Laser Altimeter (LOLA) data as shown in [3], a north polar LOLA DTM was created using co-registration techniques [6]. Both DTMs cover areas of 400 x 400 km at a resolution of 20 m/pixel, respectively (Fig. 1).

Based on the polar LOLA DTMs illumination conditions can, for instance, be simulated by applying the horizon method [1][3]. Here, illumination conditions at 2 m (height of a solar panel on a lander or rover) above ground were evaluated for regions near each pole.

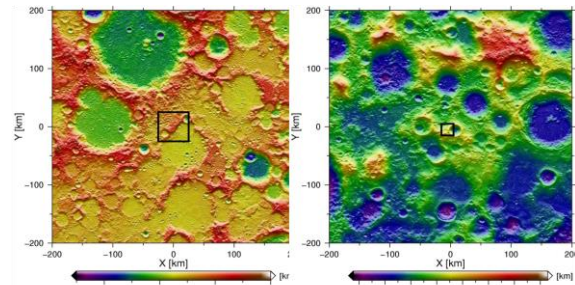


Figure 1: Lunar polar LOLA DTMs, 400 x 400 km and 20 m/pix resolution. The investigated areas are outlined in black. Left: North pole. Right: South pole.

Results: Illumination conditions were evaluated in one-hour increments over a one-year period resulting in 8760 individual illumination maps for each pole. The randomly chosen one-year periods were January, 01 2016 to January, 01 2017 for the north pole and October, 22 2018 to October, 22 2019 for the south pole. For each location in the map and each time-step, the fraction of the visible solar disk is recorded. The average of these maps are displayed as accumulated illumination maps in Fig. 2, revealing locations receiving the highest average illumination intensities. In principle, however, locations receiving the highest insolation do not necessarily need to coincide with locations residing in sunlight for the longest time. At each pole three potential landing sites with extended illumination were found. Average illumination intensities at the north pole range from 77.76-85.49% with accumulated percentages in sunlight of 85.54-91.04% during the studied one-year period (~312-332 days). At the south pole intensities range from 81.64-86.62% with accumulated percentages in sunlight from 87.03-90.93% (~318-332 days).

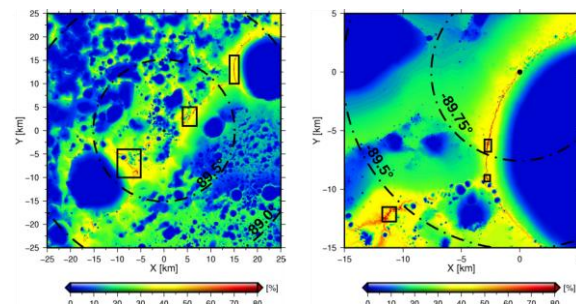


Figure 2: Accumulated illumination maps of the poles. Three potential landing sites with extended illumination are highlighted at each pole. Left: North pole, Right: South pole.

The three sites identified at the north pole are situated at the equator-facing crater rims of Hinshelwood, Peary and Whipple crater. At the south pole we find two sites located at the rim of Shackleton crater and one site residing on the ridge connecting de Gerlache and Shackleton crater. All sites are located in close proximity (km-level) to PSRs, which are excellent conditions for investigating polar volatiles while having the possibility to re-charge batteries in sunlight.

Table 1 lists the identified sites along with their illumination levels and their accumulated percentage in sunlight during our studied one-year periods.

North Pole	Max. average illumination intensities	Longitude/Latitude	Percentage in sunlight
Peary Rim	77.76%	110.3904°/ 89.8533°	85.54%
Hinshelwood Rim	82.05%	325.9908°/ 89.6551°	89.46%
Whipple Rim	85.49%	128.2630°/ 89.3679°	91.04%
South Pole			
Shackleton Rim 1	81.64%	203.8649°/ -89.7840°	87.03%
Shackleton Rim 2	83.34%	197.2137°/ -89.6869°	87.83%
Connecting Ridge	86.62%	222.8066°/ -89.4395°	90.93%

Table 1: List of identified locations with extended illumination near lunar poles. Shown are maximum average illumination intensities in percentage, the coordinates of the locations in the ME reference system and the time in sunlight given in percentage over the studied one-year period.

Conclusions We identified several potential landing sites with extended illumination levels near the lunar poles, especially interesting for missions relying on power supply through solar panels. At each site PSRs can be found within kilometre-range distances, which are prime science targets regarding the studies of polar volatiles. Future work will include thermal modeling of the polar areas based on the presented illumination maps.

Acknowledgement This project was funded by a grant of the German Research Foundation (FOR 1503, OB 124/8-1). We wish to thank the LOLA and LROC Science Team for releasing such great data products.

References

- [1] Mazarico, E., Neumann, G.A., Smith, D.E., Zuber, M.T., Torrence, M.H., 2011. Illumination conditions of the lunar polar regions using LOLA topography. *Icarus* 211, 1066–1081.
- [2] Speyerer, E.J., Robinson, M.S., 2013. Persistently illuminated regions at the lunar poles: Ideal sites for future exploration. *Icarus* 222, 122–136.
- [3] Gläser, P., Scholten, F., De Rosa, D., Marco Figuera, R., Oberst, J., Mazarico, E., Neumann, G.A., Robinson, M.S., 2014. Illumination conditions at the lunar south pole using high resolution Digital Terrain Models from LOLA. *Icarus* 243, 78–90.
- [4] Paige, D.A. et al., 2010. Diviner Lunar Radiometer Observations of Cold Traps in the Moon's South Polar Region. *Science* 330, 479.
- [5] Watson, K., Murray, B., Brown, H., 1961. On the possible presence of ice on the Moon. *Journal of Geophysical Research* 66, 1598–1600.
- [6] Gläser, P., Haase, I., Oberst, J., Neumann, G.A., 2013. Co-registration of laser altimeter tracks with digital terrain models and applications in planetary science. *Planetary and Space Science* 89, 111–117.

PREPARATION OF HUMAN-TELEROBOTICS OPERATIONS USING EAC & ESTEC FACILITIES

V. Guinet^{1,3}, M. Monnerie^{1,3}, B. Jehannin^{1,3}, A. Cowley¹, C. Jonglez^{2,3}, B. H. Foing², ¹ESA/EAC, Köln, Germany, ²ESA/ESTEC, Noordwijk, The Netherlands, ³ISAE-SUPAERO, Toulouse, France.

Introduction: As outlined in various international roadmaps and the Global Exploration Strategy [1], ESA is preparing for future missions beyond LEO and toward the Moon. Home of ESA's astronauts, the European Astronaut Center in Köln, Germany has been used for training and support of inhabited missions for more than 25 years. In this context, a lunar analogue environment is under construction at EAC to develop, test and validate the operational designs of future field missions to the Moon or other bodies. This research is focused on tele-operations of robotic assets and how to use the current and future EAC facilities to prepare the coming missions.

Use of EAC facilities for analogue missions: EAC installations have been continuously adapted to recreate the environment of Mir and now the ISS. However, with the end of the ATV program and the evolution of the needs, some facilities are no longer in regular use, like the full-sized mockups for the ATV, the work compartment of the Zvezda module and a Soyuz simulator capsule. These elements are already fitted with partly-realistic interior furniture and equipments. With some modifications, it will be possible to use them to recreate operational concepts. Due to the lack of ECLS and human-support systems, the envisioned operational scenarios are purposely focused on tele-operation of robotic assets and short-duration scenarios.



Figure 1. ATV mockup in the Training Hall at EAC, docked to the Zvezda replica

Cis-lunar habitat. With a “pressurized” volume of respectively 48m³ and 75m³ and linked by a replica of the Russian probe and drogue docking system, the ATV and Zvezda mock-ups offer similar dimensions as some early designs of evolvable Deep Space Habitat [2] described in recent papers [3, 4]. The modular internal layout eases possible modifications to sup-

port future international standards for racks and experiments, while providing power and network access. The docking system offers a passage of 800mm in diameter, which is consistent with the new International Docking System Standard [5].

Crewed vehicle. The Soyuz mock-up features a simplified version of the capsule controls along simulation equipments.



Figure 2. Soyuz mockup in opened configuration

These elements could be refurbished to simulate an Orion MPCV and especially possible experiments to be conducted on-board, although in a significantly smaller volume.

Moon dome. A lunar environment analogue is currently under construction at EAC. Featuring a test area of approximately 750m², it will enable simulations to be performed in realistic conditions.

Tele-operated rover: The first step of developing a tele-operated rover is to choose the adapted equipments. The main body of a rover is the ground vehicle with many sensors allowing the robot to move correctly and to avoid obstacles. Several commercially available models have been evaluated, corresponding to all the constraints. Once the equipments available, tele-operations and software will be developed using ROS (Robotic Operating System), an open-source operating system widely used in robotics. In the long term, other sensors or actuators could be purchased to develop even more the tele-operation. Human teleoperation is not the only goal, robot cooperation can also be experienced. The rover could also interact with an equipped lander to extract samples in order to analyse them directly on the field. This type of interaction will be testable as soon as the rover with the robotic arm is functional.

This research enables tests that directly support ESA's Moon Village endeavour, robotic precursors

being set to be extensively used for mission preparation, infrastructures and facilities deployment and crew support.

Astronomical instruments tele-operation:

Demonstrating the ability to do remote astronomical observation is one of the possible mission scenarios being investigated for future lunar missions.. The astronomical observations will be performed by a VLF antenna and a telescope which are currently in the ExoGeoLab of ESTEC [6] amid other spectrometers which can be used for sample analysis [7]. At EAC, tools will be developed to remotely control those instruments. Before their arrival at EAC, those tools will be implemented with the devices and the remote control system of ESTEC's ExoGeoLab instruments.

VLF antenna. The VLF antenna is used to perform radio astronomy observation around 20.1 MHz. The first design to be implemented is the RadioJove antenna interfaced with a SDR (software defined radio) system. The SDR system consists of an up-converter board which rise the bandwidth 0.1 / 60 MHz to 125.5 / 175 MHz and a SDR dongle which digitalize the analogical signal to send I/Q frames in a USB connection [8]. A Raspberry Pi will then be in charge of retrieving the frames from the SDR dongle and then streaming them over the network. This solution is highly portable and can be integrated in a larger scale system as needed.

Telescope. Another instrument to control is a telescope: it must be able to point a given direction, to perform control data acquisition and to send images to the user.



Figure 3. ExoGeoLab lander with a telescope

Network. The two instruments will communicate with the controller through a ROS middleware and a VPN network.

GUI. In a scenario of a remote control of the instruments by astronauts, a simple, intuitive and robust interface will be implemented. It must allow an access to the relevant information and a real time control.

Acknowledgements: We thank the Spaceship EAC Team, Samantha Cristoforetti, our colleagues at

EAC and ESTEC and professors at ISAE-SUPAERO.

References: [1] ESA website, *Exploring together: The Global Exploration Strategy*. [2] ISECG (2013) *The Global Exploration Roadmap*. [3] Smitherman D. et al. (2014), *AIAA Space 2014*, M14-3857. [4] Hopkins J. B. et al. (2014) *IAC-14-A5.1.1*. [5] International Docking Standard (2015) *IDSS IDD Revision D*. [6] Foing, B. et al. (2010) LPSC 1701, [7] Foing B. et al (2011) IJA 10, 141-160. [8] Brown J. et al (2015), *Radiojove bulletin 17*, December, 3.

MOON-BASED PLASMA, DUST AND RADIO SCIENCE: ESSENTIALS FOR PREPARATION OF FUTURE EXPLORATION AND SCIENTIFIC BREAKTHROUGHS. G. Hausmann¹, J. Bergman², H. Falcke³, M. Klein-Wolt⁴, R. Srama⁵, A. Jaime⁶, ^{1,6}OHB System AG, Gerrit.Hausmann@ohb.de, Andrea.Jaime@ohb.de, ²Swedish Space Institute of Space Physics, Sweden, jb@irfu.se, ^{3, 4}Radboud University Nijmegen, The Netherlands, h.falcke@astro.ru.nl, m.kleinwolt@astro.ru.nl, ⁵University of Stuttgart, Germany, srama@irs.uni-stuttgart.de.

Abstract: The surface of the moon is a unique observing platform for many scientifically interesting phenomena such as the solar wind, the lunar wake, earth's ionosphere, solar flares, coronal mass ejections, surface and dust charging and levitated dust. It also is an excellent location for fundamental research of the physics of complex plasma and for radio astronomy.

A particular case of interaction between these phenomena is the moon's exosphere of dusty plasma, also known as complex plasma or crystal plasma. This is a very complex state of matter of which not much is known yet. On the one hand it resembles gaseous, weakly coupled, plasma and on the other hand a strongly coupled, crystalline solid. What makes dusty plasma so interesting is that it is an example of a non-Hamiltonian system of interacting particles. It is self-organizing, as it can form filaments and structures. This has applications in astrophysics, where dusty plasmas appear frequently, for instance, in interstellar molecular clouds, in proto-planetary disks, in cometary tails and planetary rings.

Besides being of high interest to many scientific fields, the understanding of this dusty plasma exosphere is also of crucial importance to prepare for future extended missions on the moon, especially when taking the dust-related problems of the short-duration Apollo missions into account. For example, effects of lunar dust reported by astronauts then included dust sticking to clothing and gear, damaged seals and mechanisms and even respiratory problems.

In the preparation of ESA's Lunar Lander mission, a lightweight multidisciplinary instrument package has been developed for the investigation of these phenomena, dubbed the Lunar Dust Environment and Plasma Package (L-DEPP). The main elements of this package are a set of dust cameras, Langmuir probes, a radio antenna and a common electronics support package.

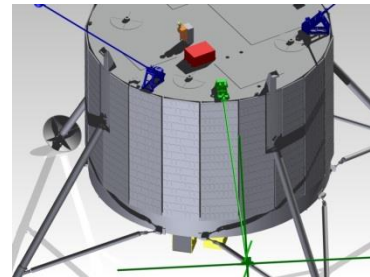


Figure 1. L-DEPP accommodation close-up

With respect to future activities, dust, plasma and radio science will be able to profit greatly from an extensive exploration of the moon's surface. Rovers could allow sensor networks to span vast areas. 3D printing could be used to manufacture larger antennas directly in-situ. In return, especially when operating on the far side of the moon, scientific breakthroughs such as the detection of the 21 cm line can be expected, showing us the universe's earliest history.

At the symposium, we will present L-DEPP main instruments, and the importance of the study of dust, y plasma study for future exploration.

MINERAL SPECTROMETRY & REMOTE CONTROL OF EXOGEOLAB LANDER INSTRUMENTS

C. Jonglez^{1,3} (clement@jonglez.space), B. H. Foing¹ (bernard.foing@esa.int), V. Guinet^{2,3}, B. Jehannin^{2,3}, M. Monnerie^{2,3}, A. Cowley², ¹ESA/ESTEC, Noordwijk, The Netherlands, ²ESA/EAC, Cologne, Germany, ³ISAE-Supaero, Toulouse, France

Introduction: The ExoGeoLab lander is a project at ESA/ESTEC initiated in collaboration with ILEWG task groups [1]. It is a structure with a rover deployment hatch, transparent windows and can be equipped with several instruments such as UV-VIS, NIR and Raman spectrometers and a telescope. Those payloads can be remotely operated using two laptops connected via a Wi-Fi network. Some improvements need to be made to improve the lander's autonomy and operational capabilities and to ease its remote control. Those tasks are performed in cooperation with a team at EAC, which works on remotely operating cameras, spectrometers, a rover, a telescope and a radioastronomy system in the 20 MHz band [2]. Furthermore, the spectrometers need to be calibrated to be able to recognize mineral samples during campaigns [3], this is why a database of mineral spectra is being established.



Figure 1 Set-up of the lander with instruments during a campaign.

Goals: In 2015, the telescope guidance has been improved [4] using a motorized focus controlled by Arduino and a computer-controlled Nikon DSLR. Further improvements still have to be made to the system, in particular on the fixation of the focus motor. What's more, the DSLR mounted on the back of the telescope currently prevents the telescope to have an elevation larger than 60 degrees. A new power system using a bigger battery and a solar panel is being studied to increase the battery life to a couple of hours. A laptop with Windows 7 mounted on the lander handles the instruments. A second laptop then controls the first one with VNC via a Wi-Fi network. A Labview program gathers all instruments in one single interface to enable an easier remote control. However, this remote control still relies heavily on

graphical interfaces and lacks robustness and modularity, and the laptop takes a significant amount of space in the lander. A more embedded solution is being studied with a smaller computer only running the backend of the acquisition software, and sending the data through the network. The Wi-Fi transmission is also being taken care of to enhance its range and reliability.

Preliminary results: The calibration of the spectrometers using mineral samples has already been started since September 2015 [5]. This database of mineral spectra is being continued. The simultaneous use of both UV-VIS and NIR spectroscopes on the same laptop has been demonstrated.



Figure 2 Test bench with NIR&UV-VIS reflectance spectrometer.

We shall present at ELS latest results from teleoperations of ExoGeLab lander and instruments from ESTEC & EAC, and prospects for their utilisation in field research campaigns in Moon-Mars analogue environments [6].

Acknowledgements: We thank Spaceship EAC, Samantha Cristoforetti, ESTEC supporting colleagues, EAC supporting colleagues, ILEWG, ISAE-Supaero.

References: [1] Foing B. et al, (2010) *LPI 41*, #1701. [2] Guinet V. et al, (2016) *ELS*, Preparation of human-telerobotics operations using EAC & ESTEC facilities. [3] Kamps, O. et al, (2016) *LPI 47*, #2508. [4] Kolmas J. et al, (2015), ESTEC internship final report. [5] Offringa M. et al, (2016) *LPI 47*, #2522. [6] Foing B. et al. (2011) *IJA 10* (3), 141-160.

EXOGEOLAB MOON ANALOGUE FIELD ACTIVITIES IN EIFEL, GERMANY O. M. Kamps¹, M. S. Offringa², B. H. Foing^{2,3}, and C. Jonglez^{3,4} ¹Faculty of Geosciences, Universiteit Utrecht, Utrecht, NL (o.m.kamps@students.uu.nl), ²Faculty of Earth & Life Sciences, Vrije Universiteit, Amsterdam, NL (marloesoffringa@hotmail.com), ³ESA/ESTEC, Noordwijk, NL (bernard.foing@esa.int), ⁴ISAE-Supaero, Toulouse, FR.

Introduction: Recent updates on the ExoGeoLab lander prepared the system for geological field campaigns which were conducted in November 2015 and February 2016. As closest volcanic area from ESTEC, we performed the campaigns in the Eifel, Germany. These campaigns tested the abilities of remote control of the lander, doing measurements with the lander instruments, and to study the interaction with astronauts or rovers [1].

ExoGeoLab: ExoGeoLab is a collaborative project between ILEWG and ESA which has started in 2008 to support research in Moon-Mars analogue field campaigns (such as EuroMoonMars campaigns [2]). The ExoGeoLab project consists of a habitat (ExoHab), laboratory (ExoLab), and prototype lander [3]. The ExoGeoLab lander is a test bench to do in-situ research and is build with the requirements of the Google Lunar X-Prize [1]. In the last years the lander has been updated with respect to the remote control and the implementation of instruments to make it suitable for geological field campaigns. Such a lander could be useful for sample analysis in a sample return mission or to assist an astronaut during manned mission. Remote control of the instruments makes it possible that experts can do analysis from Earth.



Fig. 1: Sample stage including fiber feeds to spectrometers and webcam for sample visualization.

The lander can be divided in three compartments, which have different functionalities. The lower compartment was used to store a rover. With remotely controlled ramp and panels it is possible to access this compartment. The middle compartment contains all the equipment for computers, instruments and wiring of the lander. Spectrometers and a webcam are placed in this compartment but point on the sample stage which makes it possible to measure and analyse the sample (fig. 1). The upper compartment which is the top of the lander hosts a telescope which can be used for multiple purposes. Besides astronomical research and observations it could be used to make a reconnaissance and analyse the horizon surroundings of the lander. This could be used to assess interesting exploration and sampling sites for a rover or astronaut but also to assist an astronaut during his distant EVA.

Multiple instruments are included for doing geological and possibly biological analysis in the field. Two reflection spectrometers in the UV-visible and near-infrared range are used to study the samples. A webcam is used for an optical real-time view on the sample on the sample stage (fig. 1).

Eifel as Moon-Mars analogue: The Eifel is the closest volcanic area from ESTEC Netherlands and at proximity of European Astronaut Centre which makes it a close lunar analogue terrain. Both campaigns were conducted at the Wingertsberg wall (fig. 2) which contains deposits of eruption of the Laach Lake volcano. The wall exposes proximal pyroclastic fall and surge deposits which are a result of a Plinian eruption.



Fig. 2: Wingertsbergwall near Meidinger

Eifel campaign 2015: The main goal of the Eifel campaign in November 2015 was to test the func-

tionality of instrumentation in the field. Only the top plate of the lander was used for placing the instruments (fig. 3). Below the wall samples were collected from a 2.5 meter stratigraphy and measured in-situ with the UV-VIS spectrometer. A stratigraphic log has been made and samples collected to repeat the measurements in controlled conditions. The telescope was deployed to follow the activities of the astronaut from a distance. Also a mosaic of the wall was made with the telescope to analyse after some photo editing to see if compositional differences can be recognized. [5]



Fig. 3: Instrument set-up for Eifel 2015 campaign

Eifel campaign 2016: Lessons learned from test campaign in 2015 were used as basis for the campaign in February 2016 [5]. This time the whole set-up of the lander was brought to the same location at the Wingertsberg wall (fig. 4). A large van vehicle was used for transport and functioned as pressurized remote station to control the lander by a base team and evaluate measurements. One astronaut was guided from the lander to the location chosen by the base team. Some samples were brought to the lander and placed on the sample stage for analysis with the UV-VIS and NIR spectrometers. The webcam provided a view for the support team remote from the lander.



Fig. 4: Lander including instrumentation during the Eifel 2016 campaign

Conclusion and future work: The combination of both campaigns were good tests for the lander and its instruments. In the second campaign we were able to do good measurements with the sun as light source for the spectrometers. The system must be made more robust as it should be for such a field campaign. As future work it is proposed to improve the systems and wiring connections which makes it possible to place the lander pre-assembled in the field.

Up to now the remote control works with a wireless ad-hoc network. If a solution can be found to use the laptop computer remotely via another network the system can be controlled from a larger distance.

The February campaign had a remote area to control the lander but it was still in sight. The ultimate test would be that a team is supporting the astronauts while they have not seen the surrounding of the lander in advance.

The success of the 2016 campaign was partly due to good weather conditions (e.g sunny and no rain). This made it possible to use the sun as illumination source for the spectrometers. A good artificial source should be adapted which provides sufficient light. The sun also provided enough light for the solar panel which was used for the power supply of the instruments. On a less sunny day another solution should be found which could replace the solar panels.

We are developing further the functions of remote control of instruments on ExoGeoLab to be used in future technology demonstrations and research activities with ESTEC, EAC, and collaborators [6,7], preparing for human and robotic exploration and supporting research for the Moon Village initiative [8,9].

Acknowledgment: We acknowledge the work of other interns Andrew Barton, Pooja Mahapatra, Emmanuil Detsis, Koen Langermeijer and Jan Kolmas who have improved the lander system. We thank Dominic Doyle for providing the NIR spectrometer and assistance in the work with the spectrometers. Thanks to our colleagues from EAC and ESTEC for their interest, enthusiasm and support during the 2016 Campaign.

References: [1] Foing B. H. (2010) *EGU 2010*, 13779. [2] Foing B. et al (2011) *IJA 10* (3) 141-160. [3] Foing B. et al. (2010), *LPI 41*, 1701. [4] Foing B. et al. (2009), *EGU 2009*, 13122. [5] Kamps O. et al. (2016), *LPI 47*, 2508. [6] Guinet V. et al. (2016) ELS, submitted. [7] Jonglez C. et al. (2016) ELS, submitted. [8] Foing B. et al. (2016) *LPI 47*, 2719. [9] Patenburg P. et al. (2016) *LPI 47*, 2798.

PROTECTED ANTIPODE CIRCLE (PAC) WITH A “MOON VILLAGE” TO ITS SOUTH. C. Maccone, International Academy of Astronautics (IAA) and Istituto Nazionale di Astrofisica (INAF), Via Martorelli 43, 10155 Torino (Turin), Italy, e-mail: clmaccon@libero.it.

ABSTRACT. The Moon Farside is the only place in space, and not too far from the Earth, where radio transmissions and noises produced by Humanity on Earth may not reach since the spherical body of the Moon blocks them, acting like a shield. Thus, protecting the Moon Farside from all kinds of non-scientific future exploitations (e.g. real estate, industry and military) has long been a concern for many far-sighted space scientists as well as for several IAA Academicians. We started facing this problem in the 1990s, when the French radio astronomer Jean Heidmann of the Paris Meudon Observatory first promoted an IAA Cosmic Study about which areas of the Moon Farside should be reserved for scientific uses only. But Heidmann passed away on July 2, 2000, and his work had to be continued by others. This author took over his IAA Cosmic study and a paper describing both the scientific and legal aspects of the problem was published in 2008 (see Ref. [1]), Later, on June 10, 2010, this author was the first scientist to present the case for the Moon Farside Protection at the United Nations Office of Outer Space Affairs in Vienna (see Ref. [2]) during a meeting of UN-COPUOS, the United Nations Committee on the Peaceful Uses of Outer Space.

Unfortunately, the undeclared but quite real “current, new race to the Moon” complicates matters terribly.

All the space-faring nations now keep their eyes on the Moon, and only the United Nations might have a sufficient authority to Protect the Farside and keep safe its unique “radio-noise free” environment. But time is money, and the “Moon Settlers” may well reach the Moon before the United Nations come to agree about any official decision concerning the Farside Protection.

Quite an URGENT ISSUE that we describe in this talk.

In this paper, we propose that the new “Moon Village” supported by the vision of the ESA Director General, Professor Jan Woerner, be located OUTSIDE the PAC (obviously not to interfere with the detection of radiation coming from space) but also SOUTH OF THE PAC, so as to be “close” to the South Pole as much as needed to benefit of water there.

It thus appears the best venue for the “Moon Village” would be on or around the 180 degree meridian and south to the -30 degree in latitude of the PAC, possibly much more south of that, almost at the South Pole, thus resolving once and for all the VENUE ISSUE for the Moon Village.

References:

[1] C. Maccone, Protected Antipode Circle on the Farside of the Moon, *Acta Astronautica*, 63 (2008), 110-118.

[2] C. Maccone, Official Presentation made at the United Nations Office of Outer Space Affairs (UNOOSA) on June 10, 2010, about the Moon Farside Protection and about scientifically defining the Protected Antipode Circle (PAC). It may be downloaded from the official UNOOSA site:

<http://www.unoosa.org/pdf/pres/copuos2010/tech-06E.pdf>

3D PRINTING TECHNOLOGIES FOR ENABLING HUMAN EXPLORATION AND HUMAN SETTLEMENT ON THE MOON: THE VIEWPOINT OF ESA MATERIALS SCIENTISTS A. Makaya¹, L. Pambaguian¹, A. Cowley², M. Sperl³, C. Buchner³, ¹ Materials Technology Section, European Space Research and Technology Centre ESTEC, European Space Agency, Noordwijk, The Netherlands, ² European Astronaut Centre EAC, European Space Agency, Koeln, Germany ³ Granulare Materialien, Institut fuer Materialphysik im Weltraum, DLR Deutsches Zentrum fuer Luft- und Raumfahrt, Koeln, Germany, ⁴ Aerospace Engineering, FOTEC Forschungs- und Technologietransfer GmbH, Wiener Neustadt, Austria

A consensus rises in the space community: 3D printing technologies will be instrumental to settling on the Moon (and likely on Mars as well). To this end, Materials Scientists from the European Space Agency are currently looking at sensible uses of the 3D printing techniques and defining how they should be further developed for being implemented in such a remote location. The present paper reviews the efforts made so far toward this goal, through activities funded by or conducted within ESA. These completed, running and intended activities address In Situ Resource Utilisation (ISRU) but also 3D printing technologies in a broader perspective. The reviews will cover studies in the 3D printing of Lunar base building blocks with and without binders brought from Earth, the analysis of processes for on-site hardware manufacturing with limited resources, as well as efforts to investigate how energy sources and processes can be used to process lunar regolith and other types of materials brought from Earth. All the reviewed activities will be key elements for conceiving manned moon missions at system level. Their outcome will also be valuable for development of the hardware to be transported to the moon to allow the building and the maintenance of a safe shelter for the astronauts as well as all infrastructure around.

WATER ICE CHARACTERIZATION NEAR CANDIDATE LANDING SITES AT THE LUNAR SOUTH POLE. R. Marco Figuera¹, J. Flahaut², P. Gläser³, P. Williams⁴, A. P. Rossi¹. ¹Jacobs University Bremen, Physics and Earth Sciences (Campus Ring 1, Bremen, Germany. r.marcofiguera@jacobs-university.de), ²LGL, TPE, University Lyon 1, France, ³Technical University Berlin, Department of Geodesy and Geoinformation Science, Berlin, Germany, ⁴Dept. Earth, Planetary, and Space Sciences, University of California, Los Angeles, USA.

Introduction: Volatile characterization on the Lunar south pole has been already carried out in the past, however most of the studies have focused their investigations on large craters. In these studies a combination of radar, laser altimeter and temperature data has been used [e.g.1]. Preliminary results of water ice characterization in small to mid-size craters (20 m to 5 km) near candidate landing sites at the lunar south pole are presented. Water ice characterization has been carried out in an area ranging from -80° to -90° . We have used QGIS, a Geographic Information System (GIS) open-source tool, in order to select the areas of study. The study focuses on small craters reachable by rovers near candidate landing sites from the European Lunar Lander [2].

Data: The data used in this study include:

- A co-registered Lunar Orbiter Laser Altimeter (LOLA) and Narrow Angle Camera (LROC-NAC) DTM [3] and its derived illumination, slopes and aspect.
- Circular Polarization Ratio (CPR) from the Miniature Radio Frequency (MINI-RF) [4].
- Temperature map derived from Diviner instrument data [5].

All the data has been added to a GIS system to select the areas of study. Different criteria have been taken into account:

- Permanent shadowed regions (PSR).
- Crater slopes $< 10^\circ$.
- $CPR > 1$.
- South Polar Facing slopes (SPFs) $-10^\circ < SPFs < +10^\circ$.
- Trafficability slopes $< 25^\circ$.

Candidate Landing Sites: Three candidate landing sites proposed in [2] have been selected for further analyses of water ice in their vicinity (Table 1).

Name	Lat $^\circ$	Lon $^\circ$
Connecting Ridge (CR1)	-89.4679	-137.411
Shackleton Ridge 1 (SR1)	-89.7755	-156.448
Shackleton Ridge 2 (SR2)	-89.689	-162.351

Table 1. Candidate landing sites proposed in [2] that have been analyzed in this study.

Methods: The illumination has been computed using parallel computation on a Graphics Processing Unit (GPU) [6] and converted to a GeoTiff format using GDAL. Slopes and aspects have also been derived from the DTM using GDAL. CPR data from

Mini-RF has been retrieved from PDS. The SPFs have been computed by calculating the difference between the azimuth to the south pole of each pixel and the azimuth of the aspect. All the slopes within a range of $\pm 10^\circ$ facing the south pole have been selected [7]. Temperature maps have been computed from Diviner data. The analysis was limited to areas of trafficability, e.g. with slopes $< 25^\circ$.

The selection of possible areas of study has been carried out by combining all the data into QGIS. The results presented in this abstract includes areas that fulfill all the constraints mentioned above.

Preliminary Results: Three areas of study have been selected near CR1, SR1 and SR2. Figure 1 shows the area of study. SPFs $< 10^\circ$ appear in tones of red. In green are shown the CPRs > 1 and in light-blue the PSRs. The yellow squares show the focus areas near landing sites. Given the previous constraints, we estimate that approximately 200 craters within the focus areas might harbour water ice. The minimum crater size included in this results is 20 m in diameter which corresponds to the resolution of the DTM.

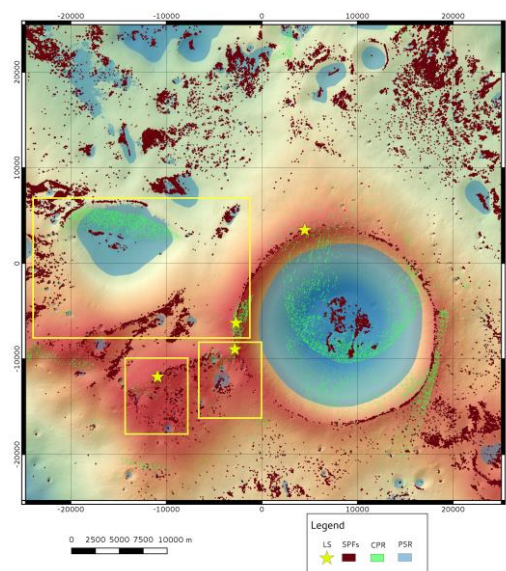


Figure 1. Global area of study in this research. In yellow the focus areas.

Future Work: An additional survey at the same sites will be carried out including 3 ranges of slopes: 6° - 10° , 10° - 13° , 13° - 16° and a global range of 6° to 16° . A volumetric estimation of water-ice will be carried out. Trafficability maps taking into account sur-

face roughness and boulder distribution will be added. The region above Shackleton crater will be further analysed.

Derived dataset will be produced and included in the PlanetServer-2 service [8]. PlanetServer-2 focuses on the visualization and analysis of space mission data on solid planets and moons, using Open Geospatial Consortium (OGC) standards on a web client based on the JavaScript version of NASA's World Wind [9].

Acknowledgements: This research is funded through the European Commission Project "EU H2020-INFRA 654367 EarthServer-2".

References: [1] Zuber, M.T. et al., (2012). *Nature*, 486(7403), pp.378–381. [2] De Rosa, D. et al., (2012) *Planetary and Space Science*, 74(1), pp.224–246. [3] Gläser, P. et al., (2013) *Planetary and Space Science*, 89, pp.111–117. [4] Fa, W. & Cai, Y., (2013) *Journal of Geophysical Research: Planets*, 118(8), pp.1582–1608. [5] Paige, D. a et al., (2010) *Science (New York, N.Y.)*, 330(6003), pp.479–482. [6] Marco Figuera, R. et al., (2014) *EPSC Abstracts*, Vol. 9, EPSC2014-476. [7] McClanahan, T.P. et al., (2015) *Icarus*, 255, pp.88–99. [8] Rossi, A.P. et al., (2016) *EGU General Assembly Conference Abstracts*, 18(EGU2016-3996, 2016). [9] Hogan, P. & Gaskins, T., (2009). In Volume XXXVIII-4/W10, 2009, ISPRS Wuhan 2009 Workshop.

UV-VIS, NIR AND FTIR SPECTROSCOPY OF MOON ANALOGUES. M. S. Offringa^{1,2} and B. H. Foing^{2,1},
¹Faculty of Earth and Life Sciences, Vrije Universiteit, Amsterdam, The Netherlands, ²ESA/ESTEC, Noordwijk, The Netherlands.

Introduction: A stationary laboratory test bench set-up is used to obtain reflectance spectra of lunar analogue samples, in order to create a spectral database to be used during future *in situ* measurements. Multiple spectroscopy techniques were tested to gain insight into the applicability of the spectrometers in the field. Measurements were conducted a UV-VIS and NIR reflectance as well as a Fourier Transform IR (FTIR) absorbance spectrometer.

With the FTIR absorbance spectrometer samples collected during campaigns in the Eifel, Germany in November 2015 and February 2016 were analysed, to function as reference for UV-VIS and NIR measurements. A large part of this research is focused on the calibration of the UV-VIS and NIR spectrometers in order to bridge the gap between laboratory and *in situ* measurements of Moon analogue samples. In our survey, the portable spectrometers (UV-VIS and NIR) were used in combination with the ExoGeoLab lander [1] and conducted spectral analysis in the field, during campaigns in the Eifel.

Methodology: UV-VIS and NIR reflectance measurements are performed on a test bench (figure 1) consisting of a sampling platform, an optical fiber holder, a light source and the spectrometers. Highly reflective optical PTFE was used for calibration and to acquire a reference spectrum. Multiple factors play a role in the calibration of the spectrometers, in pursuance of obtaining the best spectral signal. Calibrations in the set-up are e.g. those concerning the light source and the type of optical fibers used during the experiments as well as measurement strategies and raw data processing.

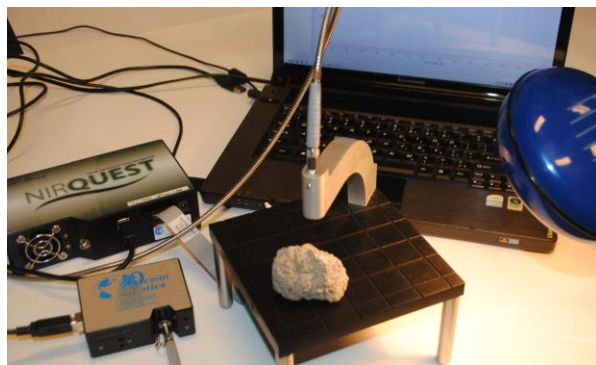


Figure 1. Test bench with UV-VIS and NIR reflectance spectrometers, optical fibers, sample platform, broad spectrum light source and sample derived from the Eifel campaign in November 2015.

During FTIR measurements a beam of light containing many frequencies of light at once is directed at a sample, while the absorbance of the light is measured. A range of wavelengths is blocked with a certain configuration of mirrors, called a Michelson interferometer. An algorithm called the ‘Fourier transform’ processes the amount of light absorption for each mirror position into the light absorbed at each wavelength. In order to perform measurements the sample is mixed with the highly transmissive powdered material KBr and pressed into a pellet that is compatible with the FTIR spectrometer.

Data: Volcanic samples derived from the previous Eifel campaign [1], Utah MDRS [2, 3], campaigns in Iceland [4] and the La Réunion campaign in France [5], were analysed together with the latest collection of Moon analogue samples from the Eifel campaigns in 2015 and 2016. The Moon analogue samples from VU University, Amsterdam, The Netherlands and standard lunar analogue reference minerals were also used for the calibration of both reflectance spectrometers.

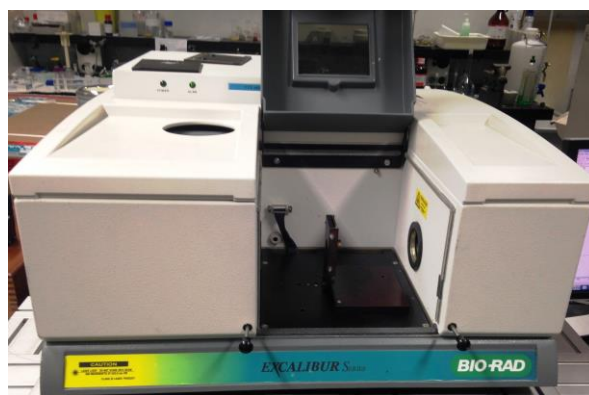


Figure 2. FTIR absorbance spectrometer at Leiden University.

The FTIR absorbance spectrometer used during this research is located at Leiden University (figure 2). It measures the absorption at wavenumbers 5000 – 400 cm^{-1} , which is translated to a wavelength range of 2–20 μm . UV-VIS and NIR reflectance spectroscopy measurements resulted in reflectance spectra covering a wavelength range from 200 – 850 nm and 900 – 2500 nm, respectively, obtained during laboratory experiments at ESTEC as well as field experiments in the Eifel.

Results: In the UV-VIS region of the electromagnetic spectrum molecules undergo electronic transitions. The reflectance in this range directly affects the colour of involved chemicals. The green colour of e.g. olivine reflectance is higher in the corresponding wavelengths between 495 – 570 nm. Moreover, we searched for transitions in Fe state that are visible with a band at 700 nm.

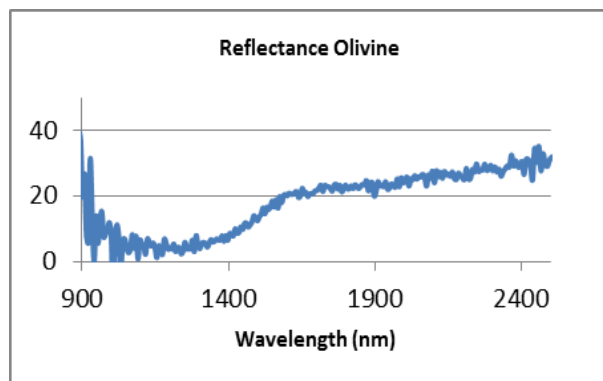


Figure 3. NIR spectrum of olivine, showing characteristic band at 1 micron. Integration time: 230 ms, scans to average: 400.

Additionally, the mineralogy of the sample (here olivine) is determined by characteristic bands in the NIR spectrum (figure 3), which is based on molecular overtone and combination vibrations.

The interpretation of the FTIR absorbance spectrum is much like that of the NIR reflectance spectra a matter of elimination. A combination of specific absorption bands results in the identification of a possible mineral composition. The absorbance spectrum of pyroxene (figure 4) is characteristic for the lunar analog mineral due to a silicate Si-O stretch broad band at 9.5 – 12 micron.

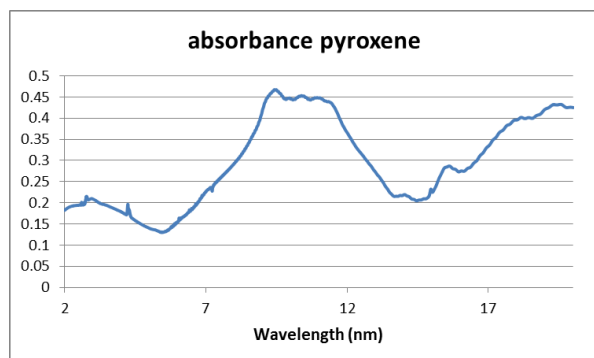


Figure 4. FTIR absorbance spectrum of pyroxene, showing characteristic silicate Si-O stretch broad band at 9.5 - 12 micron.

Discussion & conclusion: Where FTIR measurements and interpretation of obtained spectra proves to be straightforward, the set-up with the UV-VIS and especially the NIR reflectance spectrometers needs calibration. The NIR spectrometer requires recalibration of dark and flat field spectra between each sample measurement. The most suitable integration time for the UV-VIS spectrometer varies, depending on the availability of sunlight. For the NIR spectrometer the optimal integration time is dependent on the amount of light passing through the optical fiber, taking into account that longer exposure times might lead to over-saturation. Noise in the spectrum towards the edges of the covered wavelengths can be reduced by dividing the signal by a reference spectrum. Optical fibers covering a wider range of wavelengths should result in a clearer signal. Artefacts in the signal embedded in the NIR spectrometer are filtered out afterwards. The spectra obtained with the reflectance spectrometers is checked for accuracy with the use of the FTIR absorbance spectrometer.

Laboratory measurements of Moon analogue samples with UV-VIS and NIR spectrometers require specific set-up calibrations in order to attain the clearest spectra. Apart from selecting the optimal light source and optical fibers, new dark and reference spectra need to be acquired frequently in order to account for shifts in the signals caused by and during the use of the devices. An integration time to pick up a non saturated signal as well as performing enough scans to average the signal results in the clearest, noise-free spectra that can function as reference for future campaigns. FTIR data is obtained in a straightforward manner, but requires preparation of the sample by making pellets.

Acknowledgements: We thank colleagues at ESTEC and Leiden University for help with the instrumentation.

References: [1] Foing B. et al, (2010) *LPSC*, 1701. [2] Foing B. et al, (2011) *IJA*, 10, 137-139. [3] Foing B. et al, (2011) *IJA*, 10, 141-160. [4] Calzada A., Foing B., Gazeas K., Tondeur A., Iceland Campaign, private communication. [5] Pignolet et al, (2010), *GLUC*, 3, 6, 12.

NASA'S SOLAR SYSTEM EXPLORATION RESEARCH VIRTUAL INSTITUTE: MERGING SCIENCE AND EXPLORATION. Y.J. Pendleton¹, G.K. Schmidt¹, and B.E. Bailey¹, ¹NASA Ames Research Center, M/S 17-1, Moffett Field, CA 94035, Yvonne.Pendleton@nasa.gov

Abstract: The NASA Solar System Exploration Research Virtual Institute (SSERVI) is a virtual institute focused on research at the intersection of science and exploration, training the next generation of lunar scientists, and community development. As part of the SSERVI mission, we act as a hub for opportunities that engage the larger scientific and exploration communities in order to form new interdisciplinary, research-focused collaborations.

This poster will describe the research efforts of the nine domestic teams that constitute the U.S. complement of the Institute and how we are engaging the international science and exploration communities through workshops, conferences, online seminars and classes, student exchange programs and internships.

1. Introduction: NASA's Solar System Exploration Research Virtual Institute (SSERVI) represents a close collaboration between science, technology and exploration that will enable deeper understanding of the Moon and other airless bodies as we move further out of low-Earth orbit. The Institute is centered on the scientific aspects of exploration as they pertain to the Moon, Near Earth Asteroids (NEAs) and the moons of Mars. The Institute focuses on interdisciplinary, exploration-related science centered around all airless bodies targeted as potential human destinations. Areas of study reported here will represent the broad spectrum of lunar, NEA, and Martian moon sciences encompassing investigations of the surface, interior, exosphere, and near-space environments as well as science uniquely enabled from these bodies.

We will provide a detailed look at research being conducted by each of the 9 domestic US teams as well as our 7 international partners. The research profile of the Institute integrates investigations of plasma physics, geology/geochemistry, technology integration, solar system origins/evolution, regolith geotechnical properties, analogues, volatiles, ISRU and exploration potential of the target bodies.

2. Summary and Conclusions: As the new Institute's teams continue their proposed research, new opportunities for both domestic and international partnerships are being generated that are producing exciting new results and generating new ideas for scientific and exploration endeavors. SSERVI enhances the widening knowledgebase of planetary research by acting as a

bridge between several different groups and bringing together researchers from: 1) scientific and exploration communities, 2) multiple disciplines across the full range of planetary sciences, and 3) domestic and international communities and partnerships.

This poster will focus on these opportunities as well as highlights of recently published work that demonstrates the importance of interdisciplinary, collaborative research.

Acknowledgements: The authors would like to thank the hard work and dedication of all SSERVI Team members and International partners that work diligently to create an innovative and collaborative Institute.

MGM DECONVOLUTION OF ROCK SLAB SPECTRA WITH PLAGIOCLASE / OLIVINE MINERAL ASSEMBLAGES. P.C. Pinet^{1,2}, D. Glenadel-Justaut^{1,2}, Y. Daydou^{1,2}, G. Ceuleneer^{1,3}, S.D. Chevrel^{1,2}, P. Launeau⁴, S. Gou⁵, C. Carli⁶, ¹Université de Toulouse ; UPS-OMP ; IRAP ; Toulouse, France (patrick.pinet@irap.omp.eu), ²CNRS, IRAP, 14 avenue Edouard Belin, F-31400 Toulouse, France ; ³CNRS, GET, 14 avenue Edouard Belin, F-31400 Toulouse, France, ⁴LPGN, Nantes, France; ⁵Institute of Remote Sensing and Digital Earth, Beijing, China; ⁶IAPS-INAF, Roma, Italy.

Introduction: Recent observations of the lunar surface from the multiband imager and the spectral profiler onboard the Japanese SELENE spacecraft and from the Moon Mineralogy Mapper imaging spectrometer onboard the Chandrayaan mission identified in several lunar regions the unambiguous occurrence of a 1.2 - 1.25 μm spectral feature, indicative of a crystal field absorption consistent with Fe-bearing plagioclase feldspar in anorthosite [1], also confirmed by the Diviner LR Experiment onboard LRO [2]. However, advanced hyperspectral processing is needed to explore the existing variability involving plagioclase and mafic crystal field absorptions and to constrain the crustal lithology and stratigraphy of the lunar Highlands. MGM deconvolution is tested here on terrestrial mineral assemblages involving olivine and plagioclase.

Background on MGM works: The principle of the Modified Gaussian Model is to deconvolve overlapping absorptions of mafic mineral spectra into their fundamental absorption components. It has been shown that MGM is able to retrieve modal and/or chemical composition from an unknown spectrum in the case of simple mineralogical assemblages [3]. So far, situations addressing more complex mineralogies (i.e. olivine and pyroxene(s) and/or different pyroxene composition) and/or actual rock samples (e.g., [4, 5]) have been little explored by the MGM approach and little has been done in the case of plagioclase involved in mineral assemblages [5, 6].

Here, as part of an ongoing project [7, 8], we assess the capability of the MGM to realistically model complex mafic mineralogies when considering rock slab surfaces with coarse grained textures, involving plagioclase and olivine crystal field absorptions. This testing is carried out on a hyperspectral cube (8246 pixels from a scan of 28 across-track x 308 along-track pixels, measured with HYSPEX instrument) of a core section sample (271mm long x 25mm wide) collected at the Hess Deep Rift during IODP Expedition 345 in recent oceanic lower crust off the Galapagos Islands [9]. This core is mainly composed of plagioclase feldspar Pl, clinopyroxene cpx (gabbroic composition), olivine Ol (troctolitic layer) and orthopyroxene Opx, and gives access to a variety of mafic mineralogical assemblages.

MGM modeling results: Four examples of mineral detections, addressing olivine and plagioclase

monomineralic cases, and polymineralic assemblages are shown below (Fig. 1) and compared to the available groundtruth in terms of petrography and mineral composition determined by electron microprobe.

First, the overall blue slope (characteristic of slab spectra) is rather well modelled by the second-order polynomial adjusted on the local maxima along the spectra and used to handle the continuum. The thin hatched line in red corresponds to the initial settings and the solid hatched line shows the MGM modelled continuum after deconvolution; they do overlap pretty well.

Figure 1.b demonstrates that the MGM plagioclase configuration performs well on spectra acquired on pure plagioclase crystals, with a band center at nearly 1.25 μm .

Figure 1.c highlights that the spectrum associated with pixel (X37 Y155) is very ol-rich, with Mg#80, as established from the band center positions (rms: 0.008). It agrees with the core composition [9]. The 0.65 μm band absorption reveals the presence of Ni.

Figure 1.d points at two pixels located in a troctolitic layer of the core [9]. Interestingly, for both red and magenta spectra, the MGM deconvolution approach returns two possible configurations, i.e. Ol and Pl ones. Though the modeling performance is excellent in terms of residuals (see rms), one notes that for both pixels, the Gaussians associated with Ol and Pl absorptions are distorted, namely in terms of band center and/or width. Complexity arises from the well-known overlap of absorption features in this spectral domain and more work is needed along with [6] as a function of the relative abundances.

Conclusions and perspectives: With some care, results highlighted here show that Pl and Ol minerals can be detected from MGM modeling even in the case of mineral assemblages with variable proportion. We are currently in the process of generating a systematic mapping of the mineralogical variability found along the core section. It opens the path to document with an MGM approach lunar crustal mixed lithologies from the orbital study of specific units such as exposed outcrops in impact craters (central peaks, inner walls and rims).

References : [1] Ohtake, M. et al. (2009), *Nature*, 461, 236-240 ; Pieters, C.M. et al. (2009), *Curr. Sci*, 96 (4), 500-505. [2] Donaldson Hanna et al. (2014), *JGR-Planets*, 119, DOI: 10.1002/2013JE004476. [3] Sunshine, J. et al. (1990), *JGR* 95, 6955-696 ; Sunshine, J. and Pieters, C. (1993), *JGR*, 98(E5), 9075-9087. [4] Pompilio, L. et al. (2007), *JGR*, 112, E01004 ; Pompilio, L. et al. (2009),

Icarus, 201, 781-794. [5] Clenet et al. (2011), *Icarus* 213, 404-422. [6] Serventi, G. et al. (2015), *Icarus*, 254, pp. 34–55 ; Carli, C. et al. (2014), *Am. Mineral.*, 99, pp. 1834-1848. [7] Pinet, P.C. et al. (2016) *Whispers*, abstract. [8] Gou, S. et al. (2015), European Lunar Symp. 3rd, abstract book, pp.77-78 and poster, Frascati, Italy. [9] Gillis, K.M. et al. (2014) *Nature*, 505, pp. 204-207.

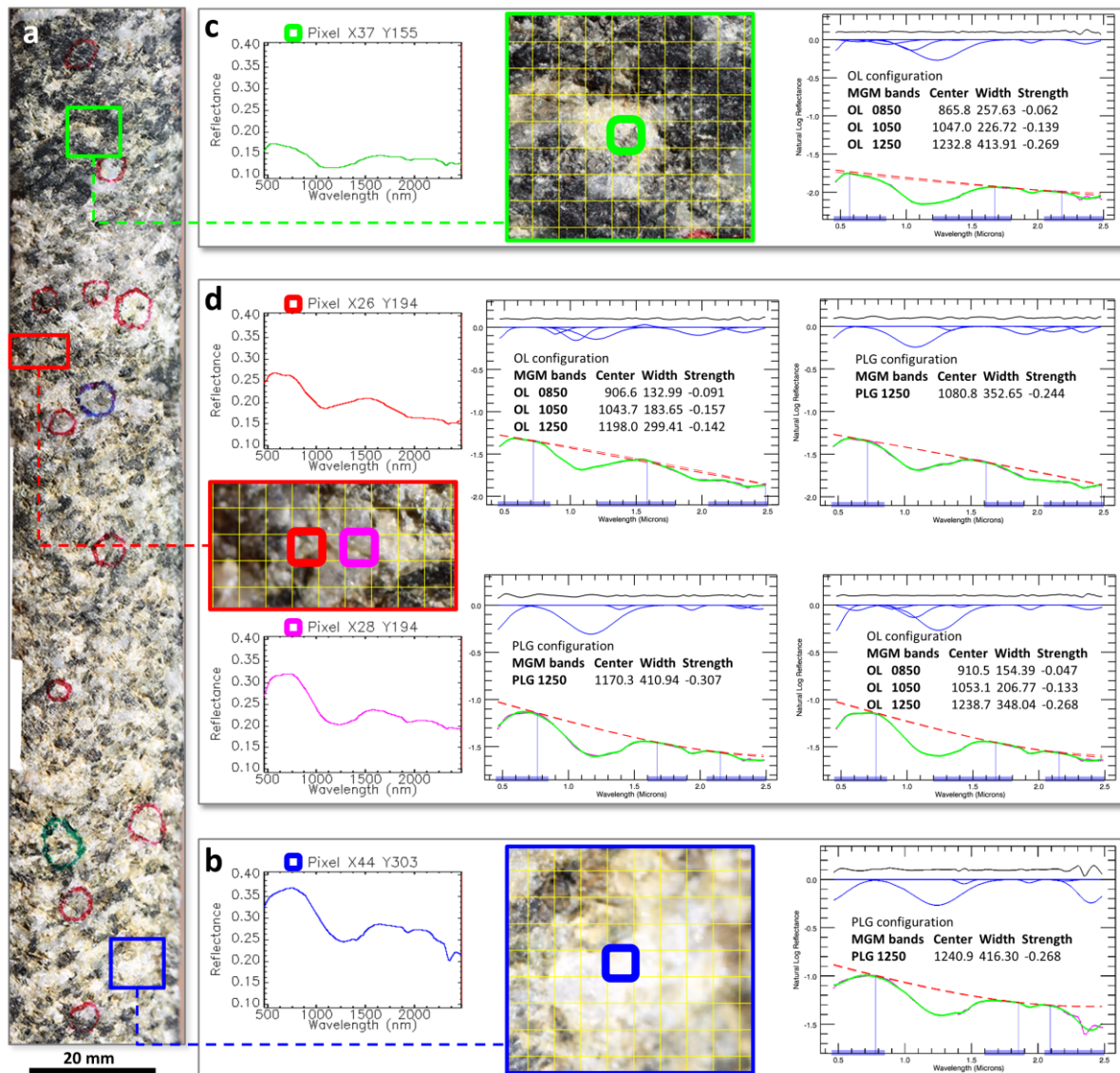


Figure 1. (a) Image of a part (145mm long) of the core with the location of the 4 spectra discussed and of related macropictures (colored rectangles). (b) the spectrum in blue (pixel X44 Y303 located at the center of blue frame) is properly modeled as an hydrated plagioclase (rms: 0.0014 is slightly increased due to unperfect hydration modeling at 2.3 μ m), in agreement with the mineral characterization from the macropicture (blue frame). (c) modeling of green spectrum (pixel X37 Y155) and associated macropicture framed in green reveal the presence of Ol mineral (rms: 0.008). (d) Spectra in red (X96 Y194) and in magenta (X98 Y194), located in the red frame, are modeled with Ol and Plg MGM configurations (red spectrum: Ol configuration rms: 0.006; Pl configuration rms: 0.007 and magenta spectrum: Pl configuration rms: 0.008; Ol configuration rms: 0.005).

PROMOTING A LOW FREQUENCY RADIO OBSERVATORY ON THE FAR SIDE OF THE MOON.

J. S. Ping¹, Y. H. Ji², M. H. Huang¹, Y. H. Jan¹, G. Y. Fang², M. Zhang¹, M. Y. Wang¹, L. J. Chen¹, H. B. Zhang¹, C. L. Li¹, and X. L. Chen¹, ¹National Astronomical Observatories of Chinese Academy of Sciences, Datun Rd. 20A, 100012, Beijing, China, jsping@bao.ac.cn, ²Electronic Research Institute of Chinese Academy of Sciences, Zhongguancun, Haidian, 100080, Beijing, China.

Abstract: Following the development of the Chinese lunar exploration program, astronomical facilities have been planned to set on the surface of the Moon so as to obtain new sciences from the Moon. The Chang'E 4 explorer (including a relay satellite, a lander and a rover, etc.) is a mission to the lunar far side, designed, assembled, and tested by CNSA. In Chang'E-4 lunar lander mission, a low frequency radio astronomical detector will be firstly settled on the far side surface of the Moon to detect the solar burst, and to investigate the lunar ionosphere. Additionally, it will be tested technically as a pathfinder mission for the future lunar surface low frequency radio observatory.

Low Frequency Detector of Chang'E-4 Lander: After ~10 years preparation of a radio astronomical team from National Astronomical Observatory of Chinese Academy of Science, a very low frequency radio astronomical detector will be settled on the far side surface of the Moon[1], in Chinese Chang'E-4 lunar lander mission. The 3 monopole detector of 5 meter long each will mainly investigate the type II and type III solar burst, and will also to investigate the possible lunar ionosphere above the landing site[2], by means of taking the advantage of radio quiet environment of lunar far side. Figure 1 shows the concept of the lander with radio astronomical payload.

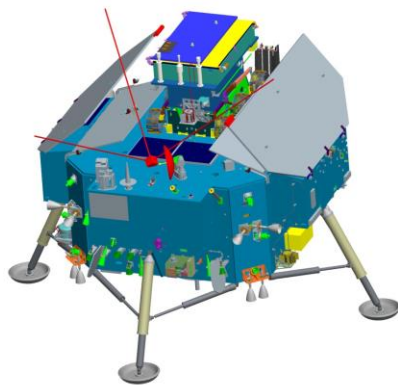


Fig.1 Three monopole HF antenna onboard lander.

After the successful Chang'E-3 lunar nearside landing mission, the backup mission of Chang'E-4 with an identified lander platform and the same designed rover as YUTU has been planned to launch and land to the lunar far side in a couple of years by CNSA. A relay communication satellite will operate

in the orbit around the Earth-Moon Lagrange point L2.

Due to the geometric limitation and the data link limitation from the lunar far side to the Earth, two ultra-violet optical payloads have been removed from the lander. The saved installing space, launch mass, and power consuming of the lander makes a unique chance for testing some advanced payload techniques of the science from the Moon. Very low frequency (of 100KHz~40MHz) radio astronomical payload becomes one of the leading choices.

However, due to the absorption by the Earth's ionosphere and hampered by the man-made low frequency signals (RFI), the radio sky below ~15 MHz cannot be viewed from earth-based facilities. In fact, up to date the range from several kHz to 15-30 MHz remains the least explored electromagnetic frequency range and is expected to conceal many scientific discoveries. Hence, the future advent in radio astronomy is expected by the realization of low-frequency radio space-based facilities to open up this frequency domain for astronomical exploration.

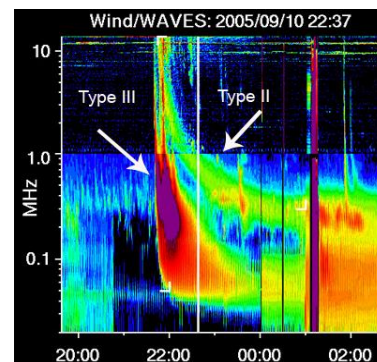


Fig.2 Type II and III solar burst measured by the Wind/WAVES instrument (credit: NASA)

In Chang'E-4 mission, considering EMC control not being carefully designed for the lander platform, and considering that a long-time working low frequency GPR on board the rover will give serious effect to HF band, the mission team has lease chance of using the radio payload to detect the sky background for cosmological observation. During the 6 months nominal mission of the lander, the low frequency payload will focus on the solar burst so as to follow CMEs out to 1 AU, and will study the possible lunar ionosphere simultaneously with the solar activity [2]. The lunar ionosphere was 1st reported by Luna missions [3]. Also below 2MHz, the payload will monitor the possible Jupiter burst, which may be

used to explain the planetary radio burst in other solar planetary system.

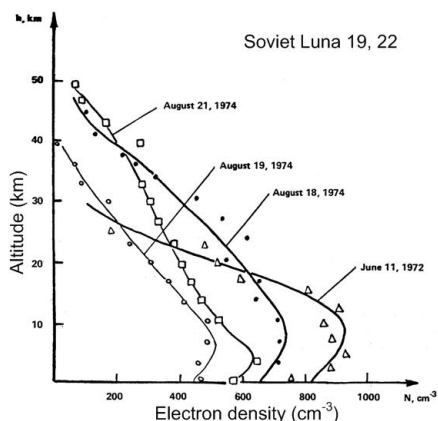


Fig.3 Ionospheric profile of the Moon by Luna 19, 22 (credit: Vyshlov, 1976)

VLBI or Not: Many limitations of nature or artificial are blocking the interferometric observation between the lander and the Earth ground, as well as between the lander and the relay satellite, where a joint Dutch and Chinese low frequency receiver installed [4]. The nature limitations include: (1) not easy to find a compact HF radio source in the space; (2) HF signal from radio source to the receiver(s) may be totally scattered or blown away by the interplanetary plasma or by the solar wind [5]. The artificial limitations includes: (1) range and range rate link between lander-relay satellite-ground station has not been required and designed from very beginning;(2) only the optical image match method will be applied to find the position of lander in the lunar coordinate frame with large systematical biases; (3) OCXO of payload with enough stability and perfect time synchronization to UT1 has lease chance; (4) only up to ~90Kbps low data rate link downlink to the Earth.

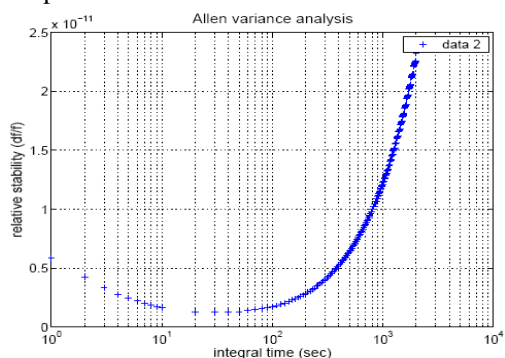


Fig.4 The Allen variance analysis for a selected space qualified ultra-stable oscillator.

Mission team are trying the best to solve above limitations, so as to find a route to test the interferometric observatory between the lander and other possible low frequency unites. Among them, the most important ones are developing a time synchronization

method among the lander, a relay satellite and the Earth ground UT1, and a 4-way range & range rate link between lander-relay satellite and the ground tracking station. Also, several kinds of OCXO of space qualified or military qualified have been selected. The Allen deviation analysis of a best stability USO is shown in Figure 4. Mission team are still working on the choice of OCXO now.

Additionally, with the possible 4-way link, lander positioning and POD of relay satellite can be done at the same time. After that, with the relay communication link, a reasonable time synchronization can be carried out.

The payload may using the lander bus information and tag two layers time signal on the recording data, one from the lander and another from the payload OCXO time counter. A short period linear model of time drift between them will be retrieved for correlation analysis.

Jupiter may be a reasonable candidate compact radio source at HF band. However, even after above solutions being applied in the mission development, there will still be some large blocks for space VLBI. We will use the payload as a pathfinder radio observatory, to test and to find the new techniques for the future special designed lunar far side low frequency mission.

Acknowledgement: This study is supported by a NSFC grant (No. 41590851), by the National Key Basic Research and Development Plan (Grant No. 2015CB857101), and by the State Key Laboratory of Astronautic Dynamics and by Chinese Chang'E-4 exploration lunar project.

References: [1]Zhang M.,(2014) Ph.D. Thesis, [2]Wang M. et al., (2016) this meeting. [3]Vyshlov A. S.(1976) Spacecraft, Space Res., 16, 945-949. [4]Wolt M. W. et al., (2016) this meeting. [5] Barrow C.H. et al. (1999) A&Ap. 344, 1001–1013.

DEVELOPMENT OF SAMPLE HANDLING SYSTEMS AT OHB MUNICH. Lutz Richter¹, Janos Biswas², Robert Paul³, Quirin Muehlbauer⁴, Daniel Redlich⁵, Wolfgang Shulte⁶, Fabio Musso⁷, Stephen Durrant⁸, Luke Fowler⁹, Andrea Jaime¹⁰; ^{1-6,10}OHB System AG, Manfred-Fuchs Straße 1, Weßling, Germany; ⁷Thales Alenia Spazio, Str. Antica di Collegno, Torino Italy; ⁸European Space Agency, Keplerlaan 1, Noordwijk, The Netherlands; ⁹Primech Ltd, Price Crescent, Auckland, New Zealand.
E-mail of main author: Lutz.Richter@ohb.de

Introduction: The Moon has been one of OHB's strategic objectives since the inception of the company, as a life-long passion of the founder, Manfred Fuchs. Following his vision, OHB System AG has been working on Lunar projects for many years, including lunar lander and payload studies, lunar power and communications, as well as In-Situ Resource Utilization technology development, among many other.

In fact, Space Robotics is a major line of projects at OHB Munich, formerly Kayser-Threde GmbH, comprising planetary exploration robotics and orbital robotics. OHB has been assuming a leading role in a number of studies addressing this area, with lunar exploration applications, ranging from vision systems, manipulation systems and active space debris removal (e.g. the ADRS and e.Deorbit studies) to mechanical subsystems for the ESA-Roscosmos 2018 ExoMars rover mission.

This paper describes OHB's ongoing activities related to automated sample handling and sample distribution for planetary or lunar landing, roving and sample return missions.

First, it provides a progress report on the ongoing development of the Sample Processing and Distribution Subsystem (SPDS) for the 2018 ExoMars rover, and later, focuses on the related development activities of sample handling mechanisms and instruments targeted to lunar polar missions.

SPDS for the 2018 ExoMars Rover: The ExoMars rover sample handling subsystem (SPDS) is being developed by OHB under direct subcontract to TAS-I to supply the scientific instruments of the ExoMars rover with granular Mars rock and soil samples of a specific particle size distribution. This is achieved through a set of mechanisms making up the SPDS which receive the samples from the rover drill, crush, meter ('dose') and distribute them. Between 2007 and 2013, ever more sophisticated breadboards and engineering models of the SPDS mechanisms have been developed and tested, culminating in the successful "end-to-end" test campaign of breadboards of the mechanisms in correct relative positions in simulated Mars atmosphere and temperature in early 2013. Meanwhile, the SPDS flight design has been finalized, in particular related to static and dynamic pressure seals (the latter with minimized parasitic torque) needed to ensure the required contamination levels within

the ExoMars rover Analytical Laboratory Drawer (ALD) which is pressurized until arrival on Mars. Moreover, complex questions on the SPDS mechanisms' materials coatings driven by both tribology and the need to sustain the ExoMars 2018 sterilisation and ultra cleaning processes have been solved. The Qualification Models (QM's) of the individual SPDS mechanisms have been manufactured and integrated. At the time of this writing, qualification testing on three of the four mechanisms is on-going, with one of the QM's having recently been delivered to the customer. Concurrently, fabrication of parts for the SPDS flight models is on-going, as permitted by the successful progress of testing the QM's.

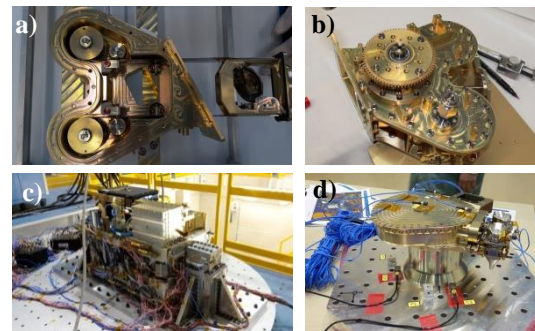


Figure 1. a) Core Sample Transfer Mechanism (CSTM) Sample Acceptance Mechanism QM; b) Same as a) but with Blank Sample Dispenser mounted on the top; c) ALD structure during vibration qualification testing; d) Powered Sample Dosing and Distribution System (PSDDS) Sample Metering Mechanism QM.

Since mid 2013, OHB Munich have also been developing the structure of the ExoMars rover analytical laboratory (ALD) which houses the SPDS sample handling system. The ALD incorporates a pressurized Ultra Clean Zone (UCZ) surrounding the sample path.

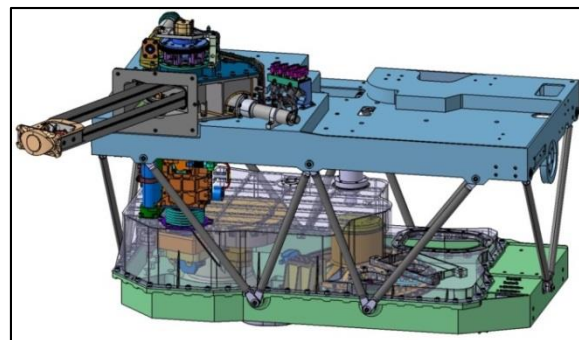


Figure 2. SPDS mechanisms in the ALD

Lunar Applications: Concepts as well as technologies developed for the SPDS can be applied to sample handling for upcoming lunar surface missions, such as the planned ESA-Roscomos collaboration targeted to lunar polar regions with subsurface sampling and analysis of volatile-enriched regolith down to 2 metres depth.

First, the SPDS “end-to-end” breadboard has been successfully tested with icy regolith samples in 2013, crushing and metering the resultant powder under vacuum conditions. Secondly, OHB Munich have been involved in two different, ESA-funded, preparatory studies – L-GRASP (Lunar Generic Regolith Acquisition/Sampling Paw) and ProsPA (Lunar Polar Prospecpecting: Processing and Analysis) – related to the planned “PROSPECT” lunar drilling and analysis package as a potential ESA contribution to the upcoming Russian lunar lander missions to polar sites.

L-GRASP developed a prototype of a sample acquisition mechanism for a lunar icy regolith drill, and ProsPA has been a Phase A on a volatile detection and analysis instrument including a sample positioning carousel and oven sealing mechanism conceptually designed by OHB. In ProsPA, the key design driver has been to achieve exceptionally low leak rates on the sample ovens situated on the carousel which was solved by OHB through a lead-screw driven oven sealing mechanism. Both the carousel and the sealing mechanism have been inherited from OHB’s SPDS design.

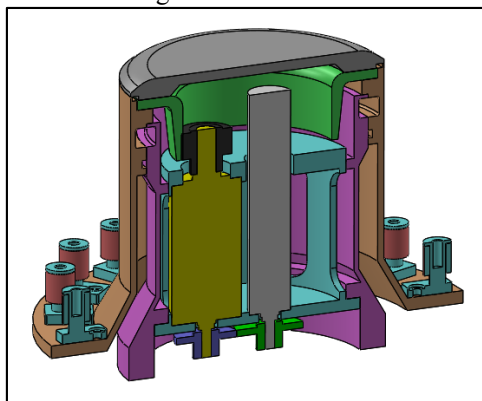


Figure 3. Conceptual design of the ProsPa carousel wheel (inherited from SPDS PSHS)

An additional, recent activity of OHB Munich related to lunar polar sampling has been the “LUISE” concept study of a volatile detection payload. “LUISE” does not strictly do sampling but emplaces an electrical heating rod into icy regolith by way of a coring drill, in order to mobilise embedded volatiles in situ that are then routed to a miniature mass spectrometer for detection and identification. A demonstrator of the instrument mechanical assembly has been developed by OHB and recently successfully completed functional testing.

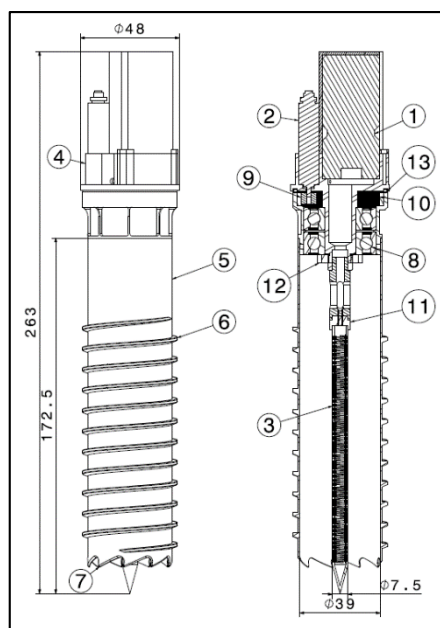


Figure 4. LUISE Instrument demonstrator

For details, see the abstract “Subsurface Thermal Extraction of Lunar Volatiles with the LUVOS Instrument” to this same conference.

References: [1] Richter, L., Hofmann, P., Mühlbauer, Q., T. C. Ng, Paul, R., Schulte, W. (2015), *Progress report on Development of the ExoMars 2018 Sample Processing and Distribution Subsystem (SPDS) and Related OHB Sample Handling Studies*, ASTRA 2015, May 11-13, The Netherlands.

THE LYNCH 002 LUNAR METEORITE REVISITED. K. L. Robinson^{1*}, C. L. Smith², A T. Kearsley², A. W. R. Bevan³, and M. Anand^{1,2}. ¹Dept. of Physical Sciences, The Open University, Walton Hall, Milton Keynes, MK7 6AA UK. ²Dept. of Earth Sciences, The Natural History Museum, Cromwell Road, London, SW7 5BD UK. ³Dept. of Earth and Planetary Sciences, Western Australian Museum, Locked Bag 49, Welshpool DC, Western Australia 6986, Australia. *katie.robinson@open.ac.uk.

Introduction: Lunar regolith breccia Lynch 002 was discovered in Western Australia in 2010 [1]. It is relatively Fe-rich for a brecciated lunar meteorite [2] and contains a mixture of feldspathic material, basalt fragments, KREEP-rich material, glass spherules, agglutinates, and melt veins [1]. Lynch 002 has undergone some terrestrial alteration [1,2] and is notably enriched in light rare earth elements [2]. It may also contain a chondrule fragment [3]. Apart from three conference abstracts [1-3], Lynch 002 is largely undescribed.

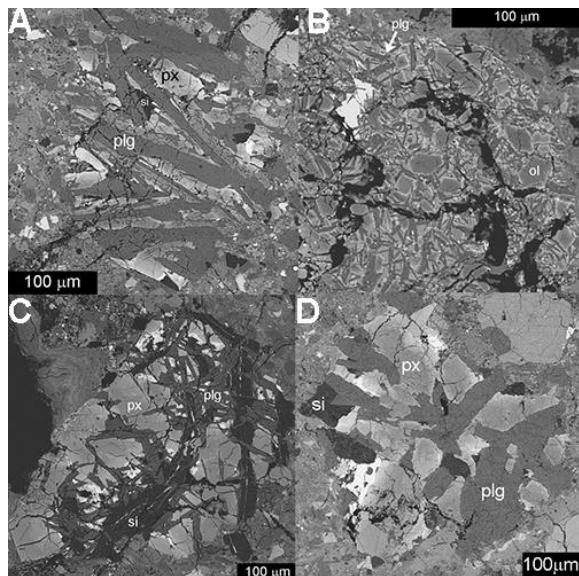


Fig. 1. Textural diversity of basalt clasts in Lynch 002. ol=olivine, px=pyroxene, plg=plagioclase, si=silica. Scale bars are all 100 μm . (A) Feldspathic basalt Lithic 4. (B) Olivine-phyric lithic 12. (C) Silica-rich basalt Lithic 1. (D) Lithic 11 is the coarsest grained basalt in Lynch 002.

Basalt clasts: Lynch 002 contains many basalt fragments of diverse sizes and textures (Fig. 1). They are all small ($< 500 \mu\text{m}$), consistent with the fine-grained nature of the meteorite. They are commonly subophitic with strongly zoned pyroxenes (Figs. 1, 2), though two fragments (Lithics 12 and 17) are olivine-phyric. All contain varying amounts of silica, though Lithic 1 is unusually silica-rich. Olivine in Lithics 12 and 17 is Mg-rich, with narrow Fe-rich rims (Fo_{60-86}). Accessory phases include ilmenite and FeS.

Lunar basalts are classified according to their TiO_2 content. We classify the basalts found in Lynch 002 by comparing the molar $\text{Fe}/(\text{Mg}+\text{Fe})$ versus molar $\text{Ti}/(\text{Ti}+\text{Cr})$ of their pyroxenes with similar data

from different types of Apollo basalts [after 4-6; Fig. 3]. All of the basaltic clasts identified so far plot in the low-Ti field or between the low-Ti and very low Ti (VLT) fields.

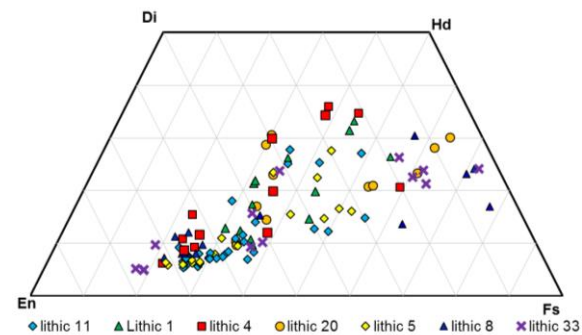


Fig. 2. Pyroxene compositions for 7 basalt fragments in Lynch 002.

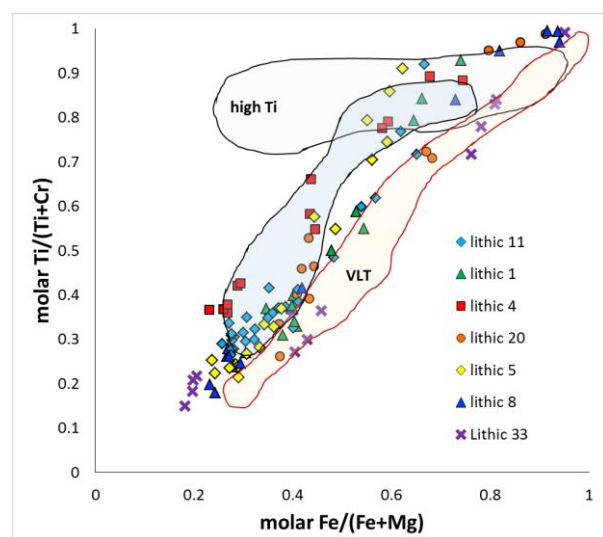


Fig. 3. Molar $\text{Ti}/(\text{Ti}+\text{Cr})$ vs. molar $\text{Fe}/(\text{Fe}+\text{Mg})$ plot for 7 basalts in Lynch 002. Apollo data [7-9] are shown as fields.

TiO₂ abundance of parental lava flows. We can model the bulk TiO_2 content of the parental magma of the basaltic fragments using the distribution coefficient $D(\text{TiO}_2)(\text{px}/\text{bas})$ and the TiO_2 abundance of the earliest formed (most magnesian) pyroxene [3,4] from each fragment. The equation used (defined in [4]) is:

$$D(\text{TiO}_2)(\text{px}/\text{bas}) = [0.0148 \times (\text{CaO}_{\text{pxx}}) + 0.09 \pm 0.05 (2\sigma)]$$

The TiO_2 contents of inferred parent magmas for Lynch 002 basaltic clasts range from ~ 1.5 to ~ 4 wt. %. The magmas sampled by Lithics 5, 8, and 33

have similar TiO_2 content of ~ 1.5 wt. %. Given where Lithic 33 plots on Fig.3, we have tentatively classified it as a VLT basalt. The parental magmas for Lithics 1, 11, and 20 have TiO_2 contents between 2-3 wt. %, while the source of Lithic 4 has the highest inferred TiO_2 abundance at ~ 4 wt. %. Based on the feldspar content of Lithic 4, we have tentatively classified it as a feldspathic basalt. Lynch 002 thus appears to have sampled multiple basalt flows.

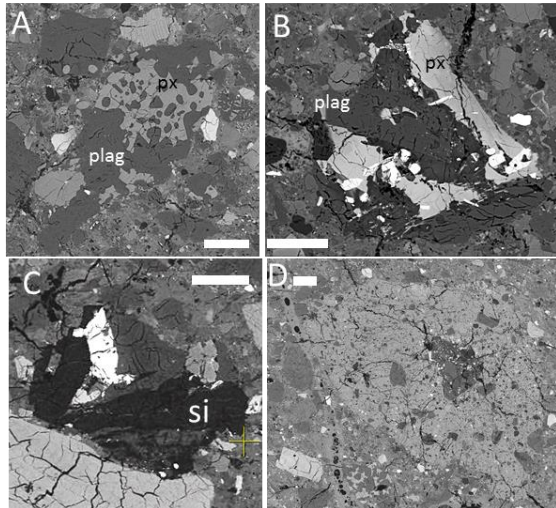


Fig. 4. Other lithologies in Lynch 002. Scale bars are 50 μm . (A). Lithic 6, possible FAN fragment? (B) KREEP-rich Lithic 7. The darkest areas are K-rich glass. The tabular grain in the center is Na-rich plagioclase, while the long gray grains are pyroxenes. (C). Lithic 23, a possible QMD fragment? (D) Lithic 9 with surrounding breccia. The fragment in the center contains K-rich glass.

Other lithologies: Lynch 002 contains many non-basaltic fragments including KREEP-rich material [1,2] and remnants of pyroxferroite [1]. We have identified several KREEP-rich clasts with diverse textures. Lithics 7 and 9 contain K-rich (6-9 wt. % K_2O) glass, as well as sodic feldspars ($\text{An}_{80}\text{Ab}_{18}\text{Or}_2$ - $\text{An}_{68}\text{Ab}_{29}\text{Or}_3$; Figs. 4B, D, 5). Lithic 16, which consists mostly of broken-down pyroxferroite, also contains K-rich glass. Lithic 23 might be a poorly-sampled quartz monzodiorite fragment, based on the texture of the silica grains (Fig. 4C). A plot of mafic mineral Mg # versus plagioclase An # can be used to distinguish between alkali, magnesian, and ferroan anorthosite (FAN) suite rocks. Lithics 23, 34, 9, and 7 all fall in or near the alkali-suite field, and thus might be alkali-suite rocks.

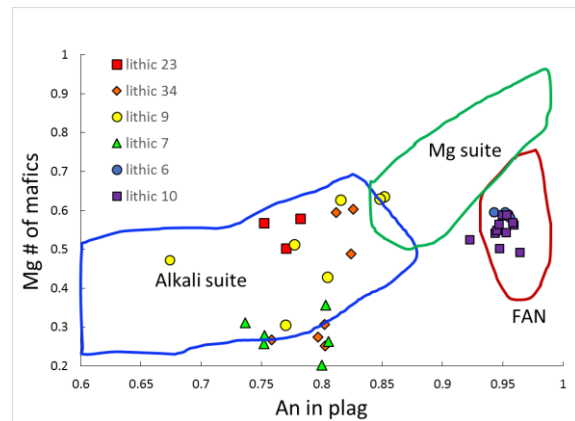


Fig. 5. Mg# of mafic minerals versus An# of plagioclase for non-basaltic lithologies in Lynch 002.

Another set of clasts (Lithics 6 and 10, Fig. 5), consisting of plagioclase enclosed by pyroxene (Fig.4A), plots in the ferroan anorthosite field on the mafic Mg # vs. Plag An # plot, but their source is unclear, as they contain proportionally too much pyroxene to be FAN. Could they be poorly sampled ferroan anorthosite, or products of impact melt? No magnesian suite clasts have yet been identified.

Preliminary conclusions: Lynch 002 is a remarkably diverse regolith breccia, containing basaltic and KREEP-rich fragments, as well as a possible chondrule fragment [3]. Basalt fragments identified so far include low-Ti, VLT, and feldspathic basalts, which likely originated from multiple lava flows. The presence of KREEP-rich clasts [1] indicates that Lynch 002 probably originated from the near side, somewhere within the Procellarum KREEP Terrane.

References: [1] Smith C.L. et al. (2012) *75th Met. Soc.*, Abstract #5137. [2] Korotev R.L. (2013) *76th Met. Soc.*, Abstract #5021. [3] Robinson K.L. et al. (2016) *47th LPSC*, Abstract #1470. [4] Robinson K.L. et al. (2012) *Meteor. Planet. Sci.* 47, 387-399. [5] Nielsen R.L. & Drake M.J. (1978) in *Mare Crisium: The View from Luna 24*, 419-428. [6] Arai T. et al. (1996) *GCA* 70, 877-892. [7] Bence A.E. & Papike J.J. (1972) *Proc. LS III*, 431-469. [8] Dymek R.F. et al. (1975) *Proc. LS VI*, 49-77. [9] Vaniman D.T. & Papike J.J. (1977) *Proc. LS VIII*, 1443-1471.

Acknowledgements: This research was partially supported by grants from UK STFC (# ST/L000776/1 to M.A. and I.A.F) and the Open University.

FLEXIBLE TO FOCUSED: THE PATH TO EXTEND HUMAN PRESENCE BEYOND LOW EARTH ORBIT. M. S. Robinson¹, ¹Arizona State University, School of Earth and Space Exploration, Tempe AZ, USA, robinson@ser.asu.edu

Introduction: Developing a sustainable long-term architecture to move humans out of low Earth orbit and into the Solar System requires a *focused path* built around a series of achievable objectives within a structured time frame. Early milestones can be accomplished through a series of robotic and crewed missions culminating in human activities on the Moon (Stage 1). While learning to live and work on another world (the Moon) development can begin on the next set of tasks focused on initiating human activities on Mars (Stage 2), and beyond. Key Stage 1 tasks include (but not limited to):

1. Test and perfect *automated pinpoint landing* (first robotic, then crewed)
2. Test and perfect *automated hazard avoidance* (first robotic, then crewed)
3. Test and perfect *autonomous roving*
4. Characterize surface radiation environment and test efficacy of mitigation strategies (robotic)
5. Characterize deep space radiation environment and test efficacy of mitigation strategies (robotic)
6. Investigate time sequence of key lunar events (robotic then crewed; critical to determining chronology of martian terranes)
7. Determine presence and location of lunar resources (robotic)
8. Determine grade and tonnage of exploitable lunar resources (robotic then crewed)
9. Test ISRU hardware (robotic)
10. Test advanced ISRU and utilize generated product for lunar surface exploration (robotic and crewed)
11. Test human support systems on lunar surface (crewed)
12. Initiate long term sustained human presence on the surface to learn to live and work on another world: exploit resources, explore, undertake scientific activities (crewed and robotic)
13. Collect and transport materials from one point on the Moon to another point on the Moon (robotic and crewed)
14. Transport materials off the Moon (robotic and crewed)

A mix of robotic and crewed missions should be implemented to accomplish these tasks to minimize risk and cost (**Table 1, Fig. 1**). What is the optimal mix? What is a realistic schedule? Which objectives can be addressed in parallel and which are serial? Beyond technical considerations the answers to these

questions depend on the level of funding, international partnerships, and long-range political goals.

Many of the key technology development tasks critical to human landing on the Moon (and Mars) can be tested on small robotic craft that are also retiring other objectives. For example *automated pinpoint landing* could be tested on a small vehicle designed to answer a specific resource or science question (i.e. viability of pits for exploitation). A second test of *automated pinpoint landing* augmented with *automated hazard avoidance* system ensures safe landing of a long-range rover designed to characterize surface properties (geology, resources, radiation environment). As these two related, yet distinct, technologies mature they can be deployed on a larger crewed vehicle with confidence. The long-range rover addresses key science and engineering objectives while testing *automated hazard avoidance* and opportunistic *automated data acquisition and onboard analysis*. Both technologies are key to human and robotic exploration of both the Moon and Mars.

Within NASA's current human space flight program the Asteroid Redirect Mission (known as ARM [1]) can *address* some of the Step 1 objectives and make incremental progress on others. However, what is missing is a meaningful (in an architecture sense) plan for follow-on missions after ARM that ultimately result in lunar exploration and a clear path forward to Mars.

Meeting the national goal of placing humans on Mars [2] requires a detailed understanding of the scope of the technology and expertise development needed, and the order in which to complete tasks. The challenge is to realistically determine required tasks and design cost effective missions that retire one or more tasks. A decadal plan (or longer) with key milestones accomplished at a frequent pace will keep public and political stakeholders attention, and give a real and meaningful sense of accomplishment to all involved. For example, the Stage 1 tasks outlined above could consist of twenty robotic and two crewed missions (mission costs spanning \$10M to \$2000M) spread across 10 years (**Fig. 1**).

The *focused path* invites international cooperation by laying out a key set of objectives with plausible focused mission scenarios; interested nations can negotiate a logical division of responsibility to divide costs and increase the political payoff (critical to sustainability). Along the *focused path*, mission returns will in many cases directly address key NSF decadal goals [3,4,5] further strengthening science community, lawmaker, and public support (*Science Enables Exploration, Exploration Enables Science* [6]). Pos-

sibly the most difficult aspect is starting on a focused path - a process that requires political vision and leadership.

Turning the so-called *flexible path* [7] into a *focused path* is simply a process of mapping out the required technical objectives with actionable tasks implementable through a series of focused missions. Each mission retires one or more milestones, each of which represents a stepping-stone to larger goals and objectives (ultimately completing Stage 1 and moving to Stage 2). Soon enough, such a sustained *focused*

path will extend human presence to Mars and beyond.

References: [1] Gates et al. (2014), IAC 14.A5.1.1, 65th Int. Astron. Con. [2] <http://mars.nasa.gov/programmissions/science/goal/> [3] NSF SSB (2013), ISBN 978-0-309-22464-2. [4] NSF SSB (2010), ISBN 978-0-309-15802-2 [5] NSF SSB (2012), ISBN 978-0-309-16428-3 [6] <http://lroc.sese.asu.edu/about/patch>. [7] Korsmeyer et al. (2010), Space Ops 2010, AIAA 2010-2272.

Class	Objective	Target	Cost	Objectives
Cubesat	Multiple low altitude flyovers of poles to inventory volatiles (4)	S. Pole, N. Pole	4 x \$10M	7
Cubesat	Multiple low altitude flyovers of localized magnetic anomaly (2)	Reiner Gamma	2 x \$10M	4, 7
Orbiter	Communication relay and radiation monitoring	Lunar Orbit	\$300M	Enable other missions
Rover	Explore at least four geologic terrains providing ground truth for orbital remote sensing observations, collect samples for return	Oc. Proc., Marius Hills, Aristarchus plateau	\$500M	1, 2, 3, 4, 6, 7
Lander	Explore viability of pits for exploitation (2)	Tranq., King crater	2 x \$125M	1, 2, 3, 4
Lander	In-situ measure of polar volatiles (2)	Shoemaker and Cabeus craters	2 x \$350M	1, 2, 4
Lander	Sample return of late Eratosthenian mare basalt	Oc. Proc.	\$600	1, 2, 6, 14
Cubesat	Measure key deep space radiation parameters (3)	Earth L1, etc	3 x \$10M	4
Rover	Follow on in-situ measure of polar volatiles	Determined by new observations	\$600M	1, 2, 7
Lander	In-situ measure of volatiles	Aristarchus plateau	\$350M	1, 2, 7
Lander	Sample return of late Copernican basalt	Ina	\$600	1, 2, 6, 14
Lander	Test in-situ resource extraction (2)	Poles, Aristarchus plateau	2 x \$350M	1, 2, 9
Crewed Lander	Advanced test of in-situ resource extraction, investigate geologic context of key resource	Poles or Aristarchus plateau	\$2500M	4, 6, 8, 10, 11, 14
Rover	Autonomously collect and transport materials (science and resources) for crewed pick-up	TBD from above exploration results	\$600M	6, 8, 13
Crewed Lander	Investigate geologic terrain investigation key basin age relation, receive materials from rover, exploit resources	TBD from above exploration results	\$2500M	4, 6, 8, 10, 11, 12, 14

Table 1. *Notional* missions comprising a focused lunar exploration program completing Stage 1 objectives. Number in parentheses indicates number of missions in that category. Costs predicated on shared technology development.

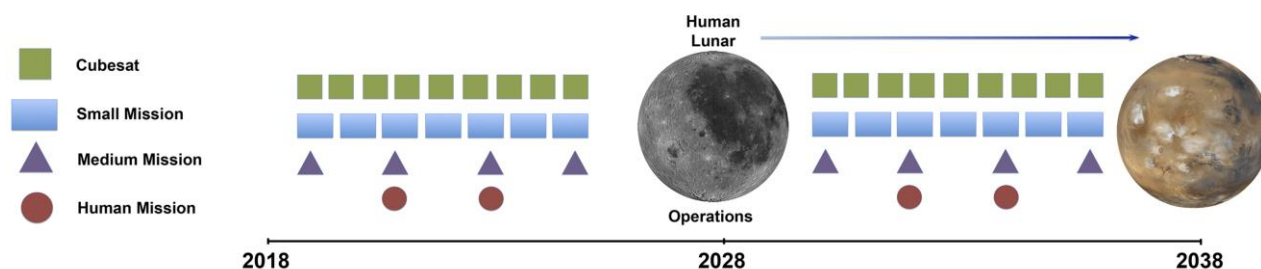


Figure 1. *Notional* number of missions required to meet key objectives on focused path to fulfilling national goal of humans on Mars (Table 1). Stage 1 is to the left of the Moon, and Stage 2 is to the right.

THE DESERT FIREBALL NETWORK. Gregory Schmidt¹, Phil Bland², Brian Day¹, Yara Al-Rajeh¹.
¹NASA Solar System Exploration Virtual Institute, ²Curtin University, Western Australia.

Meteorites, including those of lunar origin, offer a great opportunity for study of the solar system in many ways. The Desert Fireball Network, originally developed by Professor Phil Bland of Curtin University and currently being extended worldwide with the help of NASA's SSERVI, offers the capability of tracking bright fireballs as they fall through multiple-camera systems, as well as via crowdsourced data available from smartphone apps. This data allows development of the path of a meteor through the atmosphere, which allows both an estimate of its orbit and indications of its origins, as well as an estimate of its potential landing site; a quick retrieval of the meteorite will allow certain analyses not possible with old falls. Extension of this system, initially to desert areas in the world (initially targeting SSERVI international partners) will allow a great deal more data and samples to be taken into the global archive, and will further serve as an excellent citizen science opportunity through easy to use and widely available apps.

INITIAL OBSERVATION OF THE LUNAR IONOSPHERE FROM RADIO OCCULTATION BASED ON THE SERVICE MODULE OF THE CIRCUMLUNAR RETURN AND REENTRY SPACECRAFT.

M. Y. Wang¹, S. T. Han², J. S. Ping¹, G. S. Tang² and Q. Zhang², ¹National Astronomical Observatories, Chinese Academy of Sciences, 20A DaTun Road, 100012, Beijing, China, wangmy@nao.cas.cn, ²National Key Laboratory of Science and Technology on Aerospace Flight Dynamics, Beijing, China, justdoit_doing@126.com.

Introduction: Since 1960s, radio occultation has been used in planet exploration to detect vertical changing of temperature, pressure and electron density of atmosphere and ionosphere. In 1966, the radio occultation experiment of Pioneer-7 proved the existence of Lunar ionosphere which is very thin (electron density is about $4 \times 10^4 \text{ el/cm}^3$)^[4]. In Apollo 14 mission, the electron density detected by the Charged Particle Lunar Environment Experiment (CPLEE) was 10^4 el/cm^3 at several hundred meters high during lunar day time^[5]. In Luna-19 & 22 mission, the electron density profiles were detected and the peak densities were about 10^3 el/cm^3 ^[7]. In the last decade, European mission SMART-1 and Japanese mission SELENE also performed radio occultation experiment for Lunar ionosphere^[1-3,8].

The circumlunar return and reentry spacecraft (Fig 1.) is a Chinese precursor mission for the Chinese lunar sample return mission. It was launched into type lunar free-return orbit and loop behind the Moon once to test the high speed atmospheric reentry of a capsule returning from the moon. The circumlunar return and reentry spacecraft was launched on 23 October 2014 and nine days later the return vehicle landed at Inner Mongolia successfully. The service module performed a divert maneuver to avoid re-entry and to go to the Earth-Moon L2 (EML2) point. The service module stayed at EML2 until 4 January 2015 and then conducted a departure maneuver to leave EML2 and begin a transition into a Lunar Orbit. It arrived on 11 January 2015 in a $200 \times 5300 \text{ km}$ lunar orbit. Finally its orbit would be lower to $\sim 100 \text{ km}$ to image the target landing zone for the Chinese lunar sample return mission which has not yet been disclosed. During this period, we performed the radio occultation experiment to detect the Lunar ionosphere.



Fig 1. The illustration of the service module of the circumlunar return and reentry spacecraft.

Radio experiment of the service module of the circumlunar return and reentry spacecraft: With the radio occultation technique, electromagnetic waves are transmitted from the spacecrafts to the Earth, passing through the atmosphere (either during a rise event or a set event as seen from the receiver), are refracted at an angle that is determined by the refractivity gradients along the path. The refractivity variation depends on the gradients of air density, water vapour and electron density (in this case, only electron density counts).

As seen in Fig 2, the signal transmitted from the spacecraft in S and X band passed through Lunar ionosphere, interplanetary plasma, Earth ionosphere and atmosphere, finally received by the station. A hydrogen maser in the receiving station is used as the frequency reference source for open-loop radio experiments.

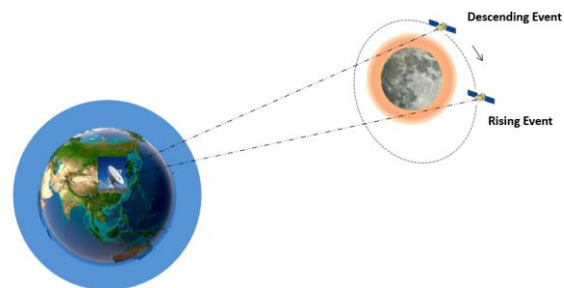


Fig 2. The illustration of the service module of the circumlunar return and reentry spacecraft radio occultation experiment.

Data Processing: How to extract the carrier phase in high precision is very important for radio experiment. Our team developed a local correlation processing method to extract frequency and carrier phase information, which is useful for inhibiting the interference caused by the stability properties of the spaceborne crystal oscillator to other extraction method in traditional time domain or frequency domain. The core of the local correlation processing technology is to reconstruct the accurate model of the received signal at the data receiving terminal.

Earth's atmosphere and ionosphere is the main source of the noise. In the observed link along the line of sight, the earth's ionosphere, the interplanetary plasma and the thin lunar ionosphere influence the signal in a similar way and change the TEC together. In this paper, we use the extrapolation algorithm to deduct the interference error of the earth ionosphere

and the interplanetary plasma^[8]. The basic idea of trend extrapolation algorithm is choosing the proper observation period which only contains the information of earth's ionosphere and interplanetary plasma first. In this period, the TEC of earth's ionosphere and interplanetary plasma alone the sight is considered changing linearly and can be predicted by polynomial fitting. Then using this information from the first step to extrapolate the TEC of earth's ionosphere and interplanetary plasma when the occultation occurs, so that we could separate lunar ionosphere from all the information.

Discussion: Fig 4 shows the phase difference of an radio occultation event on Oct 27, 2015. The result was in agreement with the result of CPLEE of the US Apollo missions^[4], was slightly higher than the results of the Soviet Luna19/22 detection results^[6], and was nearly one order higher than the result of SELENE.

This observation confirms the presence of a larger ionosphere TEC is highly likely. In the future, we will perform more observation and work on the lunar ionosphere and its distribution characteristics.

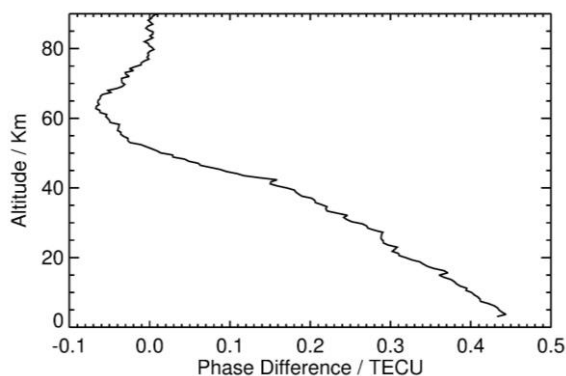


Fig 3. The phase difference of an radio occultation event on Oct 27, 2015.

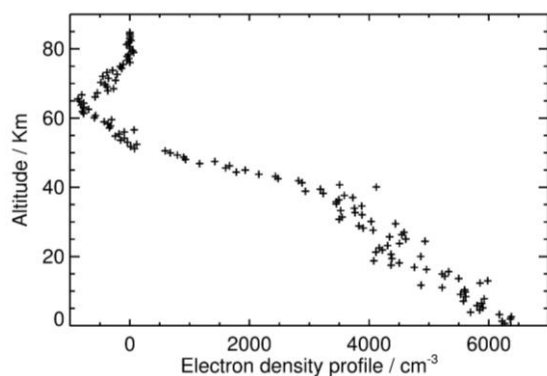


Fig 4. The electron profile density of an radio occultation event on Oct 27, 2015.

Acknowledgement: This work was supported in by the NSFC No.41590851.

References:

- [1] Goto Y. et al. (2011) *Earth Planets & Space*, 63, 47-56.
- [2] Imamura T. et al. (2008) *Earth Planets Space*, 60, 387-390.
- [3] Imamura T. et al. (2010) *Space Science Reviews*, 154, 305-316.
- [4] Pluchino S. et al. (2008) *Memorie Della Società Astronomica Italiana Supplement*, 12, 53-59.
- [5] Reasoner D.L. and Burke W.J. (1973) Springer Netherlands, 369-387.
- [6] Stubbs T. J. et al. (2011) *Planetary & Space Science*, 59, 1659-1664.
- [7] Vyshlov A.S. (1976) *Space Res*, 01, 945-949.
- [8] Wang Z. et al. (2015) *Research in Astronomy and Astrophysics*, 15, 753-763.

HOW DOES OBLIQUITY AFFECT DIURNAL TIDAL STRESSES ON THE MOON? M. Wüsthoff^{1,2} (martin.wuesthoff@dlr.de) and F. Sohl² (frank.sohl@dlr.de), ¹Institute of Physics and Astronomy, University Potsdam, ²Institute of Planetary Research, German Aerospace Centre (DLR).

Introduction: In the present study, we examine possible consequences of the significant tilt of the lunar spin axis relative to the pole of the orbital plane for diurnal tidal stresses on the Moon. For example, even small obliquities of less than 0.5° could substantially influence the characteristic pattern of diurnal tidal stresses, as recently demonstrated for the Jovian icy satellite Europa [1]. Though the tidal environments and tidally effective rigidities of the Moon

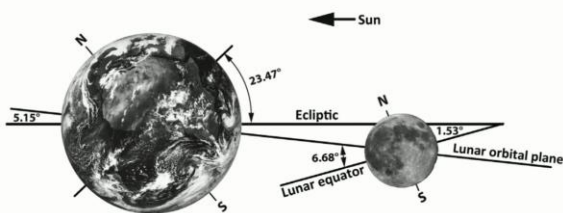


Figure 1. The equatorial plane of the Moon is inclined by 6.7° relative to its orbital plane. Adapted from [2].

and Europa differ from each other, the lunar spin axis tilt, illustrated in Figure 1, is more than one order of magnitude larger than Europa's obliquity, thereby substantially affecting the diurnal variation of tide-induced global surface stress pattern on the Moon.

Model: The modelling of stresses due to eccentricity tides as outlined in Wahr et al. (2009) [3] is expanded with respect to non-zero obliquity. The extended tidal potential possesses an additional obliquity term and is based on the work by Jara-Oru e and Vermeersen (2011) [1]. For the calculation of the time-variable global surface stress pattern, the Python package *satstress* [4] was used. It requires a

Table 1. Structural model and physical material properties of the lunar interior [5,6].

	inner core	outer core	mantle	Crust
thickness [km]	90.0	235.0	1372.4	40.0
ρ [kg/m ³]	8000.0	7000.0	3375.0	2550.0
η [10 ²¹ Pas]	1	0	1	1 10 ⁶
μ [10 ⁹ Pa]	42	0	68	35
λ [10 ⁹ Pa]	50	112	63	35

four-layered structural model input for the computation of body tide Love numbers assuming a Maxwell rheology for solids. Density models of the lunar inte-

rior are based on inferred values of the mean density, mean moment-of-inertia factor and crustal density of the Moon [6]. The reference model used in the present study is subdivided into a small solid inner core, a fluid outer core, and a solid silicate mantle overlain by a crust layer. The material properties for each layer are summarized in Tab. 1. The resultant moment-of-inertia factor is 0.3931 (measured 0.3932 ± 0.0002 [7]), and mean density is 3343.0 (measured 3344.0 ± 3.0 [2]). The calculated body tide Love numbers are $h_2 = 0.0563$ (measured 0.0371 ± 0.0033 [8]) and $k_2 = 0.0245$ (measured 0.02405 ± 0.00018 [9]; 0.024615 ± 0.0000914 [10]) and are slightly outside or sufficiently close to the corresponding error margins of the measurements.

Results: Shown in Figure 2 are global surface stress pattern at orbital longitude 90° due to (top) eccentricity tides alone (i.e., zero obliquity) and (bottom) eccentricity and obliquity tides combined. The colour coding indicates the magnitude of the most

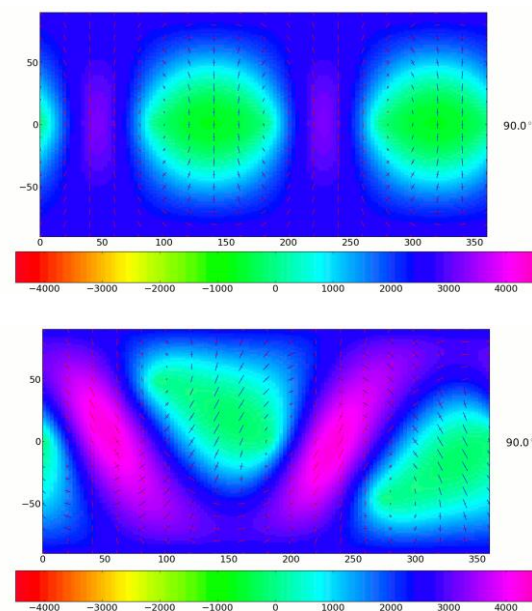


Figure 2. Comparison of global surface stress pattern at orbital longitude 90° (top) without and (bottom) with lunar spin axis tilt of 6.7° accounted for. Orbital eccentricity is taken as 0.0549 [2].

tensile of the two principal components of the stresses at the lunar surface. Whereas positive values represent tension, negative values indicate compression. The tick marks indicate the direction and magnitude of the principal components. It is seen that the global surface stress field would change from (top) symmetrical to (bottom) asymmetrical if the tilt of the lunar spin axis is accounted for. Because of the asymmet-

rical character of the tide-induced surface stresses, the global stress maxima will follow different pathways from perigee to apogee. As shown in Figure 3, the corresponding orbital positions at which global maximum tension and compression are attained will change by about 10° and are situated closer

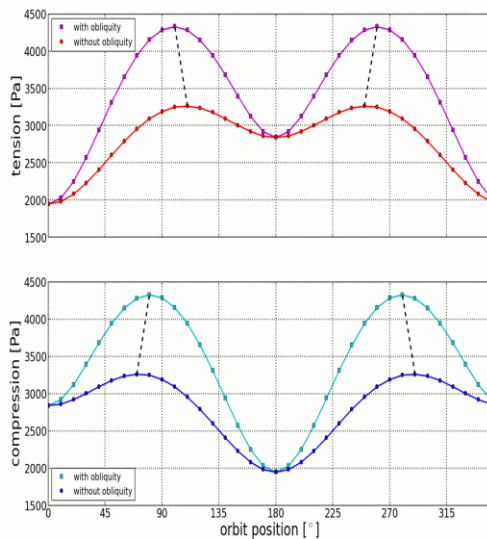


Figure 3. Global maximum (top) tension and (bottom) compression as a function of orbital longitude with and without lunar spin axis tilt accounted for.

together. In both cases, the global maximum tension and compression have the same magnitude and shape but are shifted by about 180° . Furthermore, it is seen that the maximum stress values of compression and tension are 30% larger when the lunar spin axis tilt is taken into account.

Conclusions: We show that the lunar spin axis tilt substantially affects the diurnal variation of tide-induced global surface stress pattern on the Moon. Tidal stresses attain larger values between perigee and apogee and follow sinusoidal pathways around the equator, thereby reaching higher latitudes compared to pure eccentricity tides. Thus, if one is interested in the diurnal global surface stress field not only the eccentricity but also the obliquity has to be taken into account. This could have important implications for the role tide-induced stresses play for triggering co-seismic slip events on currently active thrust faults on the Moon.

Acknowledgments: We thank Amanda Nahm and Alexander Stark for helpful discussions and gratefully acknowledge the support of the Helmholtz Alliance Robotic Exploration of Extreme Environments (ROBEX).

References: [1] Jara-Oru  H. M. and Vermeersen B. L. A. (2011) *Icarus*, 215, 417-438. [2] Hiesinger H. and Jaumann R. (2014) The Moon. In T. Spohn, D. Breuer, and T. Johnson (Eds.), *Encyclopedia of*

the Solar System, 493-538. Elsevier. [3] Wahr J. et al. (2009) *Icarus*, 200, 188-206. [4] Selvens Z.A.: Package satstress, released under GNU General Public License V.3, <http://code.google.com/p/satstress>. [5] Harada Y. et. al. (2014), *Nature Geoscience*, 7, 569-572. [6] Wieczorek M. A. et al. (2013), *Science*, 339, 671-675. [7] Konopliv A. S. et al. (2001), *Icarus*, 150, 1-18. [8] Mazarico E. et. al. (2014), *Geophys. Res. Lett.*, 41, 2282-2288. [9] Konopliv A. S. et. al. (2013), *J. Geophys. Res. Planets*, 118, 1415-1434. [10] Lemoine F. G. et al. (2013) *J. Geophys. Res. Planets*, 118, 1676-1698.

<u>Author</u>	<u>Title of contribution</u>	<u>Page</u>
Alexander, L.	Examining the History of the Solar System and the Galaxy through Cosmogenic Isotopes in Lunar Samples	79
Allouis, E.	Lunar Volatile Prospector Rover – Exploring the Lunar South Pole and the Permanently Shaded Regions	15
Arnold, J.A.	Modelling Thermal Infrared Spectra in a Lunar-Like Environment	52
Barber, S.J.	ProSPA: the Chemical Laboratory for In-Situ Assessment of Lunar Volatile Resources within ESA’s Prospect Package	7
Barnes, J.J.	Determining the Source(S) of H ₂ O in the Lunar Interior	62
Biggio, A.	Lunar Volatile Prospector Mission	13
Bussey, D.B.J.	The ISECG Science White Paper – A Scientific Perspective on the Global Exploration Roadmap	2
Canup, R. M.	Incomplete Lunar Accretion and the Depletion of Volatile	58
Carpenter, J.	Building ESA’s Lunar Exploration Mission Capabilities	3
Carpenter, J.	Challenges and Opportunities of Lunar Resource Prospecting	86
Chevrel, S.D.	Challenges in Robotic and Human Geological Field Work in Lunar Craters	87
Cowley, A.	Spaceship EAC – Enabling Activities Relevant to Lunar Exploration and 3D Printing ISRU	89
Crockett, M.	Metal-Silicate Partitioning of Siderophile Elements in the Moon: the effects of Oxygen Fugacity and Carbon.	90
Currie, D.G.	Science, Design and Flight Status of the Next Generation Retroreflector for Lunar Laser Ranging	30
Czelusckhe, A.	Re-examination of Apollo 17 Lunar Seismic Profiling Experiment Data.	29
Day, B.H.	Extending NASA’s Lunar Mapping and Modelling Portal: Enhancements for a New Era of Lunar Exploration	23
de Vera J.-P.	Astrobiology and Life Sciences on the Moon	92
Denevi, B.W.	Exploring the Effects of Space Weathering at Ultraviolet Wavelengths with the LROC Wide Angle Camera	48
Diedrich, T.	Prospecting and Returning Lunar Surface Samples with Volatiles.	14
Donaldson-Hanna, K.	Investigation of Young (<100 Million Years) Lunar Surface Features: Evidence for Outgassing or Basaltic Volcanism?	43
Durst, S.M.	International Lunar Observatory Association: 21st Century Education, Exploration and Enterprise	94
Ferri, A.	Lunar Polar Sample Return Mission	12

<u>Author</u>	<u>Title of contribution</u>	<u>Page</u>
Flahaut, J.	Candidate Landing Sites Near the Lunar Poles: A European Perspective	19
Foing, B.	Highlights From Moon Village Workshops and Studies	95
Ghafoor, N.	Small Mission Challenges and Developments in Advance of a Lunar Village	26
Glaser, P.	Lunar Polar Illumination and Implications for Future Landing Sites	97
Greenhagen B.T.	The Diviner Lunar Radiometer: Cornerstone to thermal Infrared Studies of Airless Bodies.	47
Greenwood, J.P.	Water and Volatiles in Apollo Rocks: New Results from Sapporo and Connecticut	68
Guinet, V.	Preparation of Human-Telerobotics Operations Using EAC & ESTEC Facilities	99
Hausmann, G.	Moon-Based Plasma, Dust and Radio Science: Essentials for Preparation of Future Exploration and Scientific Breakthroughs	101
Hiesinger, H.	Recent Advancements in Lunar Impact Cratering	81
Houdou, B.	Building ESA's Lunar Exploration Mission Capabilities	3
Jonglez, C.	Mineral Spectrometry & Remote Control of Exogeolab Lander Instruments	102
Kamps, O.M.	Exogeolab Moon Analogue Field Activities In Eifel, Germany	103
Kelderman, E.	Compressibility and Density of Hydrous High-Ti Lunar Red and Black Glass	71
Klima, R.L.	Integrating Remote Sensing Observations to Assess the Diversity of Intrusive Magmatism on the Moon	37
Kring, D	An Impact-Generated Lunar Magmatism Hypothesis	83
Kruijer, T.S.	Constraining the Origin and Differentiation of the Moon Using Tungsten Isotopes	73
Lavagna, M.	Drill-Terrain Energy Exchange Model to Assess Moon Subsurface Icy Samples Specimen thermo-Physical Properties Preservation During the Acquisition Phases	11
Lin, Y.H.	Hydrous Early Moon? Constraints from Hydrous Lunar Magma Ocean Solidification Experiments	64
Litvak, M.L.	Search for Lunar Water: From Current Lunar Reconnaissance Orbiter Global Mapping to the Sample Analysis at Surface onboard future Russian Lunar Landers	54

<u>Author</u>	<u>Title of contribution</u>	<u>Page</u>
Maccone, C.	Protected Antipode Circle (PAC) with a “Moon Village” to its South	105
Makaya, A.	3D Printing Technologies for Enabling Human Exploration and Human Settlement on the Moon: The Viewpoint of ESA Materials Scientists	106
Marco Figuera, R.	Water Ice Characterization near Candidate Landing Sites at the Lunar South Pole.	107
Martinot, M.	Characterizing the Lunar Crust-Mantle Transition with the Moon Mineralogy Mapper (M ³)	39
Messina, P.	Moon Village	1
Meurisse, A.	Solar 3D Printing of Lunar Regolith	34
Meyer, H.M.	The Origins of Lunar Light Plains: Implications for Exploration	50
Mitrofanov, I. G.	Landing Sites Selection for the Russian Polar Lander Luna-25	18
Morbidelli, A.	The Timeline of the Lunar Bombardment	85
Nahm, A.L.	Relative Ages of Graben and Wrinkle Ridges on the Nearside of the Moon Reveal Contradictory Relationships	41
Oberst, J.	Lunar Geodesy, Cartography, and Current Coordinate Knowledge	80
Offringa, M.S.	UV-VIS, NIR and FTIR Spectroscopy of Moon Analogues	109
Patterson, G.W.	Mini-RF On LRO and Arecibo Observatory Bistatic Radar Observations of the Moon	55
Pendleton, Y.J.	NASA’s Solar System Exploration Research Virtual Institute: Merging Science and Exploration	111
Pike, W.T.	A Silicon Seismic Package (SSP) for Lunar Seismology	27
Pinet, P.C.	MGM Deconvolution of Rock Slab Spectra with Plagioclase/Olivine Mineral Assemblages	112
Ping, J. S.	Promoting a Low Frequency Radio Observatory on the Farside of the Moon	114
Potts, N.J.	Experimental Constraints on Volatile Partitioning Between Apatite and Silicate Melt under Lunar Conditions	69
Povilaitis, R.Z.	Global Crater Density: Equilibrium in the Lunar Highlands	56
Reiss, P.	In-Situ thermal Extraction and Analysis of Lunar Volatiles with the Lunar Volatiles Scouting Instrument	9
Richter, Lutz	Development of Sample Handling Systems at OHB Munich	116
Robinson, K.L.	Connecting Hydrogen and Chlorine Isotopes in Evolved Lunar Rocks	66

<u>Author</u>	<u>Title of contribution</u>	<u>Page</u>
Robinson, K.L.	The Lynch 002 Lunar Meteorite Revisited	118
Robinson, M.S.	Lunar Reconnaissance Orbiter Camera: Exploring the Moon.	45
Robinson, M.S.	Flexible to Focused: the Path to Extend Human Presence Beyond Low Earth Orbit.	120
Rommel, D.	Petrological Map of the South Pole-Aitken Basin	21
Saunders, C.	Solving Communications and Navigation Requirements for Small Lunar Missions	25
Savoia, M.	Prospect: Key Aspects of Drilling and Collecting Samples at Moon South Pole for Luna Resurs Mission	6
Schlacht, I.L.	Walking on the Moon	35
Schmidt, G.	The Desert Fireball Network	122
Snape, J.F.	Pb Isotope Analyses of Lunar Samples: Implications for the Evolution of Major Lunar Silicate Reservoirs	75
Steenstra, E.S.	Metal-Silicate Partitioning of Volatile Siderophile Elements suggests Volatiles were not lost during Lunar Formation	60
Taylor, L.A.	Complexities of Lunar Soil: Need for Proper Simulants	32
Visscher, C. (Canup, R.M.)	Incomplete Lunar Accretion and the Depletion of Volatile Elements in the Moon	58
Wang, M.Y.	Initial Observation of the Lunar Ionosphere from Radio Occultation based on the Service Module of the Circumlunar Return and Re-entry Spacecraft	123
Wong, N.P.	Status of the Google Lunar XPRIZE	4
Wüsthoff, M.	How does Obliquity affect Diurnal Tidal Stresses on the Moon?	125
Zeigler, R. A.	MOONRISE: Sampling the South Pole-Aitken Basin to Address Problems of Solar System Significance	16
Zhao, Y.	Influence of Variable thermal Conductivity On the thermal Evolution of the Moon.	77
Zou, Y.L.	An Introduction: Scientific Objectives and its Possible Instruments of CE-4 Mission	5